Multifunctional hydrophobic nanomedicine delivery/release system: preparation and evaluation

UNIVERSITY OF LIVERPOOL

Thesis submitted in accordance with the requirements of the University of Liverpool for the degree of Doctor in Philosophy

by

Ulrike Wais

March 2018

Dedicated to

Domenico, Elisabeth, Roland, Ulrich
and my Grandmother

I declare that this thesis was composed by myself, that the work contained herein is my own except where explicitly stated otherwise in the text, and that this work has not been submitted for any other degree or processional qualification except as specified.

Liverpool, the

Ulrike Wais

Abstract

In this thesis branched/hyperbranched polymers were synthesised and used for the formulation of drug nanoparticles *via* bottom-up techniques as well as for the encapsulation and release of water-insoluble drugs. In the first Chapter current bottom-up techniques and encapsulation techniques are reviewed. A special focus was put on polymer architectures used for drug release and encapsulation and their synthesis.

In Chapter 2, branched polymers have been synthesised by conventional radical polymerisation. Three different core forming monomers and cross-linkers were used and the branched polymer products were tested for their ability to stabilise emulsions for emulsion freeze-drying. Nanoparticles of two model water-insoluble drugs were successfully produced and the optimal polymer and set-up was ascertained and used to form nanoparticles of triclosan, an antimicrobial agent. Enhanced activity was subsequently tested against *Candida albicans*. The influence of core composition on the emulsion freeze-drying process *i.e.* stability, nanoparticle yield and size, was investigated as well by varying the cross-linkage ratio. Drug nanoparticles with narrow particle size distribution, small uniform sizes and long storage stability could successfully be obtained using emulsion freeze-drying under with different branched polymers.

In Chapter 3, these polymers were tested for a simple solvent evaporation technique to obtain drug nanoparticles. Drug nanoparticles of below 250 nm with narrow particle size distribution and long storage stability were obtained, by simply evaporating an ethanolic solution of branched polymers and drugs in ratios as high as 1:1. The obtained drug nanoparticles exhibited very favourable dissolution behaviour compared to non-processed drugs.

Atom-transfer radical-polymerisation, a reversible-deactivation radical polymerisation technique was used in Chapter 4 to afford better polymerisation control and thermoresponsive polymers were synthesised. These polymers were tested for their ability to form and stabilise drug nanoparticle suspensions in dependence of core compositions. Nanosuspensions with high drug to polymer ratios of 1:1, high nanoparticle yields, and small particle sizes could be obtained.

In Chapter 5 reversible addition-fragmentation chain transfer polymerisation was used to synthesise star hyperbranched polymers by a ‘core-first’ approach with

a pH responsive core and thermoresponsive arms. The influence of core composition on pH and temperature responsive behaviour was systematically investigated. The polymer with the most favourable core composition was chosen and investigated for drug encapsulation and release. A higher encapsulation efficiency as well as prolonged and continues release was found in comparison to a diblock analogue. Z-group reduction *via* aminolysis to a thiol was used for post-polymerisation surface modifications. A fluorescent dye was successfully 'clicked' on by thiol-ene 'click' chemistry. The thiol end-group was subsequently used for gelation *via* the formation of disulphide bonds.

In the following work it was possible to successfully show the versatility of branched polymers for the use in different bottom-up techniques, as well as nanocarriers for biomedical applications. Due to their better encapsulation efficiency and favourable release profiles, as well as their ability to be form and stabilise drug nanoparticles, making further additives redundant, the use of branched polymers for biomedical application is a favourable alternative to what is currently found on the market.

Acknowledgment

I first want to thank the University of Liverpool and A*Star for making this research possible. “You just have to have the guidance to lead you in the direction until you can do it yourself.” (Tina Yothers). For all the guidance, I want to thank Dr Haifei Zhang for his supervision and open-door policy, and Dr Alexander Jackson for teaching me so much in such a short time and for always taking the time to answer my questions. I want to thank my colleagues, Ahmed Adham, Richard Hayes and Yonghong Yang for all the interesting discussions we had and for making my time in Liverpool unforgettable. Special thanks go to Alex Ho for not only the time we spend in Liverpool, but first and foremost for all the time she let me drag her around in Singapore and for her constant support on the other side of the world. I also want thank Bryony Ashford for the evenings we spend in Blue Jazz and Olessya Loiko for making me laugh and for being my fume hood buddy, as well as all the friends I made in Singapore. “If he is indeed wise he does not bid you enter the house of his wisdom, but rather leads you to the threshold of your own mind.” (Kahlil Gibran), as such I am deeply grateful to Dr Katharina Edkins for pushing me towards my potential, lighting the spark for my love of research and for straightening me out when I needed it. A ship cannot sail if it does not know to which harbour to return to. For this reason, I want to thank my family; Gabriel, Iris, Constanze, Jonas, Sebastian, Karolina, Konrad, Julia, Damian, Johanna, Karol and Alexandra for being my harbour when I needed an anchor. As well as Andreas and Deliah Rosenboom for the weekends spend at their house. I will be forever indebted to my Uncle Roland for his continues interest in my work and life, his care packages full of yellow press journals and all the hour-long phone calls. I also want to thank my late Grandmother for making me the women I am today and teaching me tenacity in the face of frustration. I also want to thank Christine Behling, the one friend that has been in my life longer than not, for all her support throughout my studies. I am more grateful than I can ever put in words to Elisabeth Friedhoff for being the best friend I could ask for. Because of her, I laugh a little harder, cry a little less and smile a lot more. One of my favourite poets, Kahlil Gibran, once said: “Ever has it been that love knows not its own depth until the hour of separation”. In this spirit I am deeply grateful to my boyfriend Domenico Tallarico for building me up when I was at my lowest, for sharing my laughter at my happiest and for everything in between.

TABLE OF CONTENT

Chapter 1. Drug nanoparticles by bottom-up techniques and encapsulation of poorly water-soluble drugs by polymeric nanoparticles

LIST OF FIGURES

Chapter 1. Drug nanoparticles by bottom-up techniques and encapsulation of poorly water-soluble drugs by polymeric nanoparticles

Chapter 2. Formulation of nanoparticles by emulsion-freeze-drying

Chapter 5. Solubilisation of hydrophobic drugs facilitated by pH-responsive hyperbranched polymers

LIST OF TABLES

Chapter 1. Drug nanoparticles by bottom-up techniques and encapsulation of poorly water-soluble drugs by polymeric nanoparticles

Chapter 2. Formulation of nanoparticles by emulsion-freeze-drying

Chapter 3. Formation of hyperbranched polymer stabilised drug nanoparticles *via* solvent evaporation

Chapter 4. Solubilisation of hydrophobic drugs facilitated by thermoresponsive hyperbranched polymers

Chapter 5. Solubilisation of hydrophobic drugs facilitated by pH-responsive hyperbranched polymers

LIST OF SCHEMES

Chapter 1. Drug nanoparticles by bottom-up techniques and encapsulation of poorly water-soluble drugs by polymeric nanoparticles

Chapter 2. Formulation of nanoparticles by emulsion-freeze-drying

Chapter 3. Formation of hyperbranched polymer stabilised drug nanoparticles *via* solvent evaporation

Chapter 4. Solubilisation of hydrophobic drugs facilitated by thermoresponsive hyperbranched polymers

LIST OF SYMBOLS AND ABBREVIATIONS

ADHD	Attention deficit hyperactivity disorder
AIBN	Azobis(isobutyronitrile)
ATRP	atom transfer radical polymerisation
B	branching units
BMA	butyl methacrylate
BSC	Biopharmaceutics Classification System
C. albicans	Candida albicans
CMC	critical micelle concentration
CO_2	Carbon dioxide
Conv.	Conversion
CRP	controlled/living polymerisation
Cryo-TEM	Cryo-transmission electron microscopy
CSIRO	Commonwealth Scientific and Industrial Research Organisation
CTA	chain transfer agent
DB	diblock
DCM	dichloromethane
DEAEMA	N,N-diethylaminoethyl methacrylate
DEGDMA	diethylene glycol dimethacrylate3
D_h	hydrodynamic diameter
DI water	deionized water
DLS	dynamic light scattering
DMF	N,N-Dimethylformamide
DMM	double-monomer
DMSO	dimethyl sulfoxide
DNA	Deoxyribonucleic acid
DP	degree of polymerisation
DVB	divinyl benzene
EBriB	ethyl α-bromoisobutyrate
EDAm	ethylene diacrylamide
EGDMA	ethylene glycol dimethylacrylate

EPR	enhanced permeability and retention
EtOH	ethanol
FRET	Fluorescence resonance energy transfer
GAS	Gas antisolvent
GPC	Gel permeation chromatography
HBP	Hyperbranched polymers
HCl	hydrochloride acid
HGRP	high gravity reactive precipitation
HIV	human immunodeficiency virus
IC	Invasive candidiasis
ICH	International conference on harmonization of technical requirements for registration of pharmaceuticals for human use
IMC	Indomethacin
IPA	isopropanol
IUPAC	International Union of Pure and Applied Chemistry
kDa	Kilodalton
L	linear units
LALS	Low angle light scattering
LCST	lower critical solution temperature
LP	linear polymer
MeOH	methanol
mg	milligram
ml	millilitre
MMA	Methyl methacrylate
M_n	number average molar mass
M_w	mass average molar mass
NaOH	sodium hydroxide
*n*BMA	n-butyl methacrylate
NFC	Nanofibre cellulose
NIPAm	*N*-isopropylacrylamide
nm	nanometre
NMR	Nuclear magnetic resonance

O/W	oil-in-water emulsion
OEGMA	oligo(ethylene glycol) methyl ether methacrylate
OR	Oil Red O
PAMAM	Polyamidoamine
PBMA	poly(butyl methacrylate)
PCA	Precipitation with a compressed fluid
PDE	permitted daily exposure
PDI	polydispersity index
Pe	Péclet number
PEG	poly(ethylene glycol)
pL	picolitre
PLA	polylactic acid
PLG	Poly(Lactide-co-Glycolide)
PLGA	poly(lactic-*co*-glycolic acid)
PLM	polarised light microscope
PNIPAm	poly(*N*-isopropylacrylamide)
ppm	parts per million
PS	poly styrene
PSD	Particle size distribution
PTP	proton-transfer polymerisation
PVA	Poly(vinyl alcohol)
PXRD	Powder X-ray diffraction
R	R-Group
RAFT	reversible addition-fragmentation chain-transfer polymerisation
RALS	Right angle light scattering
RB	average repeat units per branch
RDP	Reversible-deactivation radical polymerisation
RESOLV	Rapid expansion of supercritical solutions into a liquid solvent
RESS	Rapid expansion of supercritical solution
RI	Refractive Index
RP	Free radical/conventional polymerisation

RPB	Rotating packed bed
RX	alkyl halides
SAS	Supercritical antisolvent precipitation
SCROP	self-condensing ring-opening polymerisation
SCVP	self-condensing vinyl polymerisation
SDS	Sodium dodecyl sulphate
SEC	size exclusion chromatography
SEDDS	Self-emulsifying drug delivery systems
SEM	Scanning electron microscope
SFD	spray freeze drying
SHB	star hyperbranched polymers
SLS	static light scattering
SMEDDS	Self-microemulsifying drug delivery systems
SMM	single-monomer
T	terminal units
TDA	Triple Detector Array
TEM	transmission electron microscopy
THF	Tetrahydrofuran
Tris	tris(hydroxymethyl)aminomethane
UCST	upper critical solution temperature
UV/Vis	Ultraviolet–visible spectroscopy
W/O	water-in-oil emulsion
W/O/W	water-in-oil-in-water emulsion
Wt %	weight percentage
YEPD	Yeast Extract-Peptone-Dextrose medium
Z	Z-Group

PUBLICATIONS AND PRESENTATIONS

U. Wais, A. W. Jackson, T. He and H. Zhang, "Nanoformulation and encapsulation approaches for poorly water-soluble drug nanoparticles." *Nanoscale*, 2016, **8**, 1746-1769.

U. Wais, A. W. Jackson, Y. Zuo, Y. Xiang, T. He and H. Zhang, "Drug nanoparticles by emulsion-freeze-drying via the employment of branched block copolymer nanoparticles." *J. Control. Release*, 2016, **222**, 141-150.

J.-H. Liu, **U. Wais**, Y.-M. Zuo, Y. Xiang, Y.-H. Wang, A. W. Jackson, T. He and H. Zhang, "Unimolecular branched block copolymer nanoparticles in methanol for the preparation of poorly water-soluble drug nanoparticles" *J. Mater. Chem. B*, 2017, **5**, 423-427.

U. Wais, J. Liu, T. He and H. Zhang, "Micellar and emulsion-assisted drug delivery comparison of miktoarm star polymers and block copolymers" in Miktoarm Star Polymers: From Basics of Branched Architecture to Synthesis, Self-assembly and Applications, ed. Ashok Kakkar, Royal society of chemistry, Cambridge, 2017, ch. 5, pp. 116-149.

U. Wais, A. W. Jackson, T. He and Z. Zhang, "Formation of Hydrophobic Drug Nanoparticles via Ambient Solvent Evaporation Facilitated by Branched Diblock Copolymers", *Int. J. Pharm.*, 2017, 533, 245-253.

U. Wais, M. M. Nawrath, H. Zhang and A. W, Jackson. "Triclosan nanoparticles via emulsion-freeze-drying for enhanced antimicrobial activity" *submitted to Colloid and Polymer Science*

U. Wais, H. Zhang and A. W. Jackson. "Star polymers possessing pH-responsive hyperbranched cores via RAFT polymerisation" *under preparation*

U. Wais, "Nanoformulation of poorly water-soluble drugs with aid of branched polymers" British society for nanomedicine young researcher meeting, University of Liverpool, UK, *Oral presentation*, 2015

U.Wais, "Nanoformulation of poorly water-soluble drugs with aid of branched polymers", 5th International Conference on Multifunctional, Hybrid and Nanomaterials, Lisbon, Portugal, *Poster presentation*, 2017

Chapter 1

Drug nanoparticles by bottom-up techniques and encapsulation of poorly water-soluble drugs by polymeric nanoparticles

This Chapter is based on the publications

U. Wais, A. W. Jackson, T. He and H. Zhang, "Nanoformulation and encapsulation approaches for poorly water-soluble drug nanoparticles." *Nanoscale*, 2016, **8**, 1746-1769

and

U. Wais, J. Liu, T. He and H. Zhang, "Micellar and emulsion-assisted drug delivery: comparison of miktoarm star polymers and block copolymers" in Miktoarm Star Polymers: From Basics of Branched Architecture to Synthesis, Self-assembly and Applications, ed. Ashok Kakkar, Royal society of chemistry, Cambridge, 2017, ch. 5, pp. 116-149

1.1. Introduction

A survey done in 1988 over a period of 20 years demonstrated that 40 % of all pharmaceutical drugs produced in major companies in the United Kingdom showed low bioavailabilty.[1] Bioavailability is defined as the fraction of an administered drug that reaches systematic circulation.[2] Drugs with low bioavailability are prone to either accumulate in tissue due to their high lipophilicity or be eliminated via a first-pass metabolism in the intestines or liver, due to low solubility and inability to pass the intestinal walls. Hence, many water-insoluble drugs need to be administered intravenously and in high quantities to reach target sites in suitable concentrations, which often goes hand in hand with discomfort for patients. Estimation in 2000 put the cost of drug development, from first discovery to approval for a single drug at 800 million[3, 4], with one of the reasons being that only one in ten developed drugs achieve final approval.[5] Methods like high-throughput screening,[6] computer-aided and structure-based drug design [7] as well as fragment-based lead discovery [8] increased the rate of success in pharmaceutical research. Due to the adoption of these methods, drugs showing low bioavailability may be identified early on. Hence, the percentage of drugs not passing Phase I testing because of low bioavailability decreased from 40 % to 10 % between 1991 and 2000.[5] However, 40 % of approved drugs as well as an estimate of 90 % of developed drugs in the pipeline still exhibit poor water solubility[9] and highly efficient drugs are still being abandoned early on because of low solubility. As an example of this, a list of essential drugs compiled by the world health organisation in 2004 cited that only 23.6 % of the listed drugs were Biopharmaceutics Classification System (BCS) Class I drugs (high solubility and high permeability, Figure 1.1.), as defined by Amidon,[10] and thus showed high bioavailability.[11] Over the past years, much research efforts went into tackling the poor water solubility problem. Various methods have been

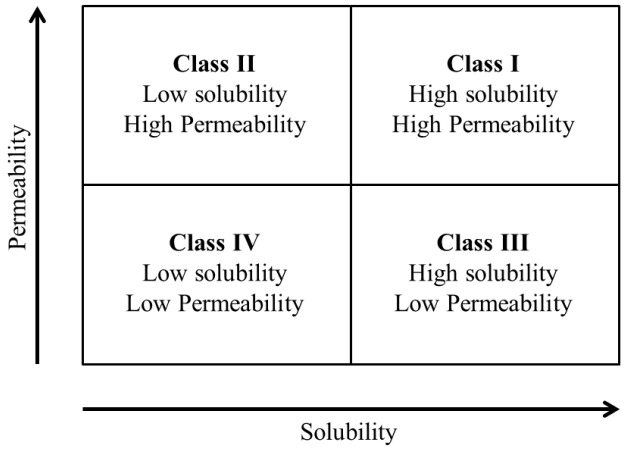

Figure 1.1. Biopharmaceutics Classification System

developed, for example, cyclodextrin complexation[12], crystal modification,[13] solid dispersions,[14] polymeric micelles,[15] lipid-based delivery,[16] and hot melt extrusion.[17]

Another highly researched topic is the prodrug design approach, where the drug is kept in an inactive state exhibiting better solubility or permeability. However, this approach relies on specific metabolic mechanisms to change the inactive prodrug to an active one.[18] Prodrugs can either consist of a drug linked to a carrier or antibody that is cleaved off by a metabolic mechanism or be a precursor that is turned into the active form by hydrolyses, oxidation or other metabolic reactions.[19-22] In addition to the difficulty in synthesis, in-vitro testing is done in rodents and other animals, which exhibit slightly different metabolistic conditions compared to humans, *e.g.*, enzymes or level of transporters, metabolites from carriers, or metabolic intermediates during activation.[23] Another highly researched area is the formulation by nanotechnology, where the size of drug particles is decreased to the nanometre range. By downsizing the poorly water-soluble drug particles, thermodynamic and kinetic characteristics change, giving rise to new attributes like water solubility and applications such as dry powder inhalation. [24,25] Solubility is increased based on the Ostwald-Freundlich equation (1.1) [26-28]:

$$\log\frac{c_S}{c_\infty} = \frac{2\sigma V}{2.303RT\rho r} \qquad (\mathbf{1.1})$$

With c_S = saturation solubility, c_∞ = solubility of large particles, σ = interfacial tension, V = atomic volume, R = gas constant, T = absolute temperature, ρ = density of the solid, r = radius.

The dissolution rate increases at the same time due to the decrease in size and subsequent increase in surface area as shown in the Noyes-Whitney equation (1.2) [29]:

$$\frac{dc}{dt} = D \times A\left(\frac{c_s - c_x}{h}\right) \qquad (\mathbf{1.2})$$

With D = diffusion coefficient, A = surface area of the particle, c_S = saturation solubility, c_x = bulk concentration and h = diffusional distance.[30]

There are two major strategies in nanoparticle formulation: top-down and bottom-up approaches. That is, the drug material can either function as a nanoparticle by being downsized from large particles (top-down) or grown from molecules in solution (bottom-up). Drugs may be also encapsulated in nanoparticle forming material (*e.g.*,

liposomes, dendrimers, polymers). These encapsulation methods may be classified in the bottom-up category.

In this Chapter, the working principles and recent development of various methods developed for bottom-up techniques and encapsulation in nanoparticles will be reviewed. Due to recent excellent reviews on top-down approaches,[31,32] we focus on bottom-up techniques (particularly the novel cryogenic methods, supercritical fluid-related methods) and encapsulation approaches, discuss how solvents and additives may be selected to achieve stable and uniform nanoparticles dispersions, and also describe the applications of such poorly water-soluble drug nanoparticles. Another focus will be on encapsulation techniques using polymeric nanoparticles. A brief overview will be given of structures being used for encapsulation and polymerisation techniques. We conclude the review with a summary and perspective on the development and challenges of nanoformulation techniques.

1.2. Bottom-up techniques

Methods starting from solutions to afford nanoparticles are categorized as bottom-up techniques. In the following section, different approaches are described, and an overview of advantages and disadvantages is given in Table 1.1.

1.2.1. Nanoparticle formation by precipitation techniques

1.2.1.1. Solvent anti-solvent precipitation

Solvent anti-solvent precipitation is the most straight forward bottom-up technique for producing nanoparticles. In the solvent anti-solvent process a water insoluble drug is dissolved in an organic solvent. The solution is then mixed with a solvent in which the drug is not soluble (antisolvent), containing stabilisers. The chosen solvents need to be miscible with each other. Precipitation of nanoparticle sized drug is immediate.[33] Formation of nanoparticles is due to the Marangoni effect and directly dependent on interfacial turbulence of the phase interface and flow, diffusion and surface tension.[34] These are influenced by the speed of mixing, solvent, stabiliser, and temperature. Studies on mixing have shown that an increase of mixing speed decreases particle size. Higher mixing speed leads to greater micromixing *i.e.* the mixing on molecular level, between two phases. As a result, mass transfer and diffusion from one phase to the other increases and a higher supersaturation of drug in the antisolvent

phase is reached. This causes faster nucleation and subsequently a narrower particle size distribution (PSD). [35]

Stabilisers prevent Ostwald ripening by covering the surface of the formed nanoparticles. Surfactants can also be used as surface wetting agents for orally administered drugs to make them more bioavailable.[36] Generally, an increase in surfactant concentration leads to a decrease in particle size, till a plateau is reached where the size does not change anymore. In certain cases, it has been found that stabilisers were more effective when dissolved in the solvent phase. Although the particle size was slightly bigger it was possible to use less stabiliser since being dissolved in the same medium as the drug made the stabiliser more readily available.[37] Another factor determining size is temperature. Lower temperatures in general lead to smaller sizes. At lower temperatures, the solubility of drug decreases and the metastable zone gets narrower. Simultaneously an increase in nucleation can be observed since nucleation is a process of free energy and heat release.[38]

In the solvent anti-solvent process the obtained nanoparticles need to be dried immediately to prevent crystal growth. Due to this, research has focused on combining different bottom-up techniques. Hu *et al.*[38] presented an industrially applicable process which combined the solvent anti-solvent precipitation followed by a freeze-drying step for continuous and scalable nanosizing of fenofibrate. It was found that short stirring time in the Solvent anti-solvent step and immediate freeze drying minimized the Ostwald ripening and led to faster dissolution in water. Homayouni and colleagues [39] incorporated a high-pressure homogenizing step between Solvent anti-solvent precipitation and freeze drying. With Soluplus as stabiliser, celecoxib nanoparticles around 440 nm were produced with a 4 times higher solubility than raw celecoxib. Unexpectedly, crystalline samples dissolved better than amorphous samples, which could be attributed to the devitrification of amorphous celecobix when in contact with water. Using only the solvent anti-solvent technique, Zu *et al.* [40] produced taxifolin nanoparticles, a water insoluble antioxidant. By reducing the size to 24.6 nm, they found that the solubility increased two times compared to the raw material, as well as the bioavailability and antioxidative ability. Another approach using ionic liquids as antisolvent and phosphate buffer as solvent was done by Viçosa *et al.* [41], producing amorphous rifamipicin particles with a mean size of 280-360 nm at room temperature.

A variation of the solvent anti-solvent precipitation process is high gravity reactive precipitation (HGRP). On the basics of the Higee technology,[42] a rotating packed bed (RPB) [43, 44] is used to form nanoparticles. Solvent and antisolvent are added to the rotating RBP. Centrifugal forces and high gravity in the chamber generate a thin liquid film or fine droplets. This in turn intensifies micromixing as well as mass transfer.[45,46]

1.2.1.2. Sonoprecipitation

Most solvent anti-solvent processes struggle with poor micromixing. This problem may be solved by the use of ultrasonic waves in a sonoprecipitation process. This process leads to rapid and more thorough mixing. Consequently, maximal supersaturation and crystal growth arrest are reached faster. Initial cavitation and size reduction occur during the negative period of the sound wave, which generates cavitation bubbles. Implosion of bubbles results in localized spikes in temperature and pressure, leading to the creation of shock waves. The consequence for crystallisation is immediate formation of primary nucleation, reduction in crystal size, and inhibition of agglomeration.[47,48] Particle size, particle size distribution, and particle morphology are dependent on duration of sonication. Dhumal and colleagues [49] prepared amorphous cefuroxime axetil particles by sonoprecipitation. It was observed that by lowering the temperature, cefuroxime axetil precipitated faster with a higher yield and a smaller size. The same result was obtained when increasing the sonication amplitude. A comparison study for cefuroxime axetil nanoparticles produced by spray drying and sonoprecipitation demonstrated similarity in both lower yields, decreased size and broader particle size distribution for both processes. With sonoprecipitation it is possible to not only influence size but also morphology of particles, which has an impact on dissolution. Tran *et al.*[50] studied the influence of three polymer types and ultrasonication conditions on the shape and size of curcumin nanoparticles. It was found that by changing drug to polymer ratio and reaction conditions the molecular interaction of the curcumin hydroxyl groups changed and subsequent size and dissolution rate could be modulated.

1.2.1.3. Supercritical fluid precipitation

Most drugs produced by precipitation techniques employing organic solvents show trace amounts of solvents even after purification. Using supercritical fluids as

solvents could overcome this issue. Supercritical fluids, where both the temperature and pressure of the fluids are higher than the critical temperature and pressure respectively, exhibit the density of a liquid but the mass transfer ability between gas and liquid, making them ideal candidates to be used as solvents for precipitation processes.[51] The supercritical fluid can be removed from the nanoparticles simply by depressurisation. Due to its mild critical points, non-toxicity and non-flammability, CO_2 has been the most widely used supercritical fluid.[52] When a low temperature is favoured (*i.e.* < 31 ºC), compressed CO_2 can be also used as solvent or medium for reaction or processing.[53] The major techniques to produce drug nanoparticles utilizing supercritical fluids are rapid expansion of supercritical solution (RESS), rapid expansion of supercritical solutions into a liquid solvent (RESOLV), supercritical antisolvent precipitation (SAS), gas antisolvent (GAS), and precipitation with a compressed fluid (PCA).

Supercritical fluid acting as a solvent

In the RESS and RESOLV processes, the supercritical fluid acts as a solvent. In the RESS process a supercritical liquid with dissolved drug passes through a thin nozzle into a low pressure vessel, where the drug precipitates.[54] The rapid expansion of the supercritical fluid via the reduction in pressure leads to a high supersaturation of drug in the fluid droplets and the subsequent homogenous nucleation. The size of the particles depends on expansion temperature, pressure, nozzle geometry and lengths, solute-solvent interaction, and solubility of compound in supercritical liquid. Most RESS processes employ supercritical CO_2 as solvent. Although there are examples for nanosized particles, the RESS process produced mainly particles in the micrometre range.[55] To overcome this problem, the RESS process was extended by expansion of supercritical fluid into a liquid solvent rather than air. This process is called RESOLV. It is rationalized that the liquid solvent inhibits crystal growth in the expansion jet. The nanoparticles may be further prevented from accumulating by adding stabiliser to the solvent phase. For example, using the RESOLV process, Pathak *et al.*[55] prepared ibuprofen nanoparticles at 40 nm.

Supercritical fluid as an antisolvent

Supercritical fluids can be introduced as anti-solvent for the SAS, GAS, and PCA processes. The common feature is that the drugs are dissolved in organic solvents

(usually CO_2-miscible) and then precipitate as a result of anti-solvent impact from the introduced compressed or supercritical fluid. For example, in the SAS process, the supercritical fluid is introduced into a high-pressure vessel which already contains a liquid solution, like in the common SAS precipitation technique (see 1.2.1.1.). However, the high diffusion ability of the supercritical fluid leads to rapid diffusion/mixing at the interface and hence rapid supersaturation and precipitation. The supercritical fluid acts as an anti-solvent as well as a 'spray enhancer'. The homogeneity of the precipitated particles may be tuned by flow rate, temperature and pressure of the system.

In contrast to the SAS process in the GAS process, a supercritical gas (the temperature is higher than the critical temperature, but the pressure is lower than the critical pressure) is introduced instead of a supercritical fluid into the liquid solution. Quite often, the SAS and GAS process are not distinguished clearly during applications. Yeo and colleagues[56] utilised the GAS technique to downsize macromolecules, such as insulin, showing that the conditions of this process were mild enough to downsize complex biological structures. The same was shown on insulin and catalase by Tom and co-workers.[57] They micronized both proteins for the formation of drug-polymer microspheres for controlled release.

The PCA process is similar to SAS in that a compressed fluid (usually higher than the critical pressure but lower than the critical temperature) is introduced into a drug solution. The solution may also be sprayed into the compressed fluid for the solute precipitation to occur. The compressed fluid is miscible with the solvent, but functions as an anti-solvent to the solute. It can diffuse into the solution and increase the supersaturation whereupon the solute precipitates.[58-60] Gentamicin-loaded bioadhesive microspheres were produced using compressed CO_2. In addition to high entrapment efficiency, homogeneous distribution of drug within polymer microspheres and continuous release of the drug were achieved.[61] In a recent study, aerogel silica particles with loaded drug were coated with polymer by the PCA process, which slowed down the release of the loaded drug.[62] The PCA process could also be applied to precipitate lysozyme in reverse micelles by introducing compressed CO_2 into the reverse micellar solution.[63]

1.2.1.4. Spray drying

Spray drying is a one-step solvent evaporation process directly from liquid solution to powder. The process can be divided into four steps. In the first step, a substance is dissolved in an organic solvent, which is then pumped through a nozzle and atomized into hot air in the second step. Thirdly the solvent evaporates and a dry powder forms. The last step is the separation of dried product from gas.[64] Atomization of solution is achieved using pressure, rotating, or two fluids nozzle. Higher atomization pressure leads to smaller droplets and hence smaller particles. A high ratio of surface to volume favours rapid and effective drying. With regard to the spray from the nozzle, there are three different air current systems (Figure 1.2.). If hot air is flowing in the same direction of the feed, it is termed co-current. The advantages and disadvantages of co-current lie in the short contact between substance and hot air, since the air cools down rapidly further down in the chamber. Although not the whole chamber is used for drying, thermo sensitive substances have minimal heat contact. Most food powders are produced using co-current spray drying. If air is let into the systems from the sides or from below it is called mixed flow and counter-current, respectively. In both processes the whole chamber is used for drying.[65,66]

Size is directly proportional to feed rate and not concentration, although higher concentrated solutions can lead to higher viscosity and slower feed rate. Particle morphology and size are dependent on the drying conditions and solvent evaporation rate. The Péclet number (Pe) is the ratio between convection time for drying and diffusion coefficient in the solid and can give a trend for morphology and size. For Pe < 1, small and dense particles can be expected. Fast drying can lead to large and hollow particles, while slow drying may result

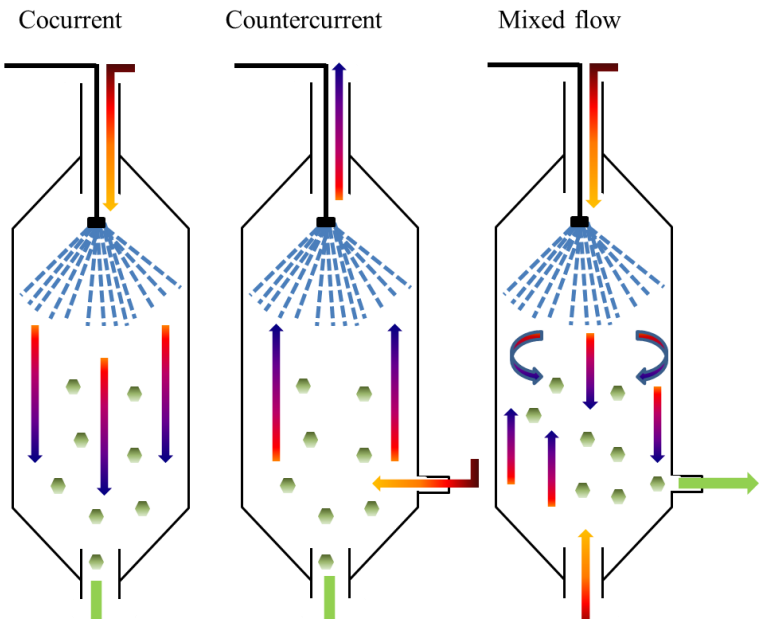

Figure 1.2. Schematic representation of spray drying apparatus with different currents.

in small and dense particles.[67] In spite of a continuous, potentially easily scalable and fast process, there are some drawbacks and limitations to the spray drying technique. One is that thermolabile substances are difficult to process, due to the potential of decomposition or change in property. Another factor is the poor thermal efficiency of the process which leads to a low cost-efficiency.[64,68] Despite these limitations spray drying is widely used in food production and in the pharmaceutical industry. This is mainly due to the possibility of adding additives to the feed mixture. Hence it is possible to produce encapsulated microparticles for release or better storage in one-step, by adding polymers to the feed solution. Another possibility is adding agents to tune particle size and shape, as well as ease the granulation.[69] The spray drying technique is often used for encapsulation in particles. For example, Rizi and co-workers[70] investigated the encapsulation of three model drugs in the pH-responsive polymer Eudragit L100. Similar drug encapsulation and drug release effects were observed by Kolakovic *et. al.*[71]. They produced microparticles with nanofibre cellulose (NFC) and could form a tight fibre network with amorphous drug present in the matrix. Sustained drug release was dependent on the substance used and, on its solubility, and affinity for NFC under the same experimental conditions. Another interesting study was done by Al-Qadi and co-workers,[72] who produced insulin-loaded chitosan nanoparticles for inhalation into deep lung tissue as an alternative absorption route into systematic circulation. *In vivo* tests in rats showed an increased and prolonged hypoglycaemic effect.

1.2.2. Cryogenic Methods

1.2.2.1. Freeze-drying

In a freeze-drying process, a solution (or suspension) is frozen and the solvent is sublimated under reduced pressure and low temperatures. Freeze drying on its own is mainly used to achieve more stability in storage, since dry powder formulations tend to exhibit longer shelf lives and the freeze-drying process does not cause shrinkage or toughening and leaves micropores in the material behind, which makes rehydration easier.[72-76] Nanosuspensions produced by other top-down or bottom-up techniques can be freeze-dried into more stable powders without the risk of agglomeration as is often encountered in other drying methods. Protective agents such as cryoprotectants like sugars can be added to avoid possible decomposition or loss of activity

during the freezing stage.[77] For example, fenofibrate dissolved in tertiary butyl alcohol, was mixed with a water solution of mannitol. The resulting solution was immediately frozen and freeze-dried. Mannitol functioned as a nucleation seed in this case. After freeze drying, dispersions of the crystalline drug nanoparticles could be obtained, which showed an increase in dissolution behaviour [78]. In recent years, ice crystals formed during the freezing stage have been explored as templates to produce porous polymers and ceramics.[79,80] In the case of porous polymers, the concentration of the solution had a significant impact on pore morphology, *i.e.* by freeze-drying diluted aqueous polymer solutions, polymer nanofibers could be readily formed.[81] Incorporation of small molecules or proteins could easily be achieved by simply mixing them with the initial aqueous solution.[82] In a more complicated procedure, curcumin and curcumin-loaded silica microspheres were incorporated via freeze-drying into porous chitosan scaffolds with varied morphologies. A dual-tuned drug release profile was achieved with fast initial release and sustainable release at later stage.[83] Freeze-dried porous materials from polyvinyl alcohol (PVA), poly(ethylene glycol) (PEG) and surfactant sodium dodecyl sulphate (SDS) could be used as scaffold to form poorly water-soluble drug nanoparticles. By soaking the porous materials in organic drug solution and subsequent evaporation of the solvent, drug nanoparticles formed within the porous material, which could be re-dissolved in water to give aqueous nanoparticle dispersion.[84]

1.2.2.2. Spray freeze-drying

In a spray freeze drying (SFD) process, a drug or more often a protein solution is sprayed through a thin nozzle into a vessel containing liquid nitrogen at its bottom. The nozzle types used are the same as used in spray drying. Nucleation starts while the solution droplets are travelling through the cold nitrogen gas phase to the liquid phase, where they freeze. After recovery of the frozen droplets with a thin sieve, the solvent is removed by lyophilisation. Because of the freeze-drying process, in contrast to air drying, the obtained particles are porous while maintaining the droplet size and shape. SFD is a popular method for downsizing protein powders for inhalation since the low processing temperature thwarts denaturation.[24,85] As with other processes it is possible to add stabilisers, although a slight increase in size as well as some loss of activity for proteins can be the consequence.[86,87] The main difference between spray drying and spray freeze drying is the drying process. A comparison study of the spray

drying, and spray freeze drying processes for the production of lipid-polymer hybrid nanoparticles made from PVA, lecithin and levofloxacin for inhalation was conducted. It was found that particles produced by SFD were superior in terms of flowability, physical handling and yield.[88] Although the particle size and shape mainly depended on droplet size and solution concentration, the use of additives during the process was found to have an impact. This was improved by utilising a thermal-ink-jet printer as head of a spray freeze dry apparatus. Droplets with volumes as low as 2 – 180 pL could be continuously formed. The resulting particles showed good stability in storage even without any excipients.[89,90] Murugappan *et al.*[91] reported the preparation of dry powder for inhalation by immobilizing live influenza virus on inulin, dextran or dextran/trehalose. Activity tests showed that storage at 30 °C for up to three months after the SFD did not influence the receptor binding properties or biochemical integrity while the activity of unprocessed live vaccination decreased by 100-fold.

An extension of SFD is spraying directly into the liquid nitrogen by submerging the nozzle into the nitrogen, rather than across the cold nitrogen gas. In this process, an insulated nozzle is submerged, and the solution is sprayed directly into liquid nitrogen. The solution gets atomized by passing through a small nozzle at high pressure.[92-94] High atomization rate is furthermore a consequence of high Weber and Reynolds numbers at liquid-liquid collision.[95] The rapid freezing of solvent droplets leads to fast nucleation with arrested crystal growth. For proteins, the rapid freezing and hence fast passing of the critical temperature (the temperature between crystallisation and glass transition of the solution) can avoid the formation of large ice crystals which leads to denaturisation. Rapid freezing limits the time available for the drug molecules to crystallize, thus leading to the formation of amorphous drug particles.

1.2.2.3. Emulsion freeze-drying

Emulsions are mixtures of two immiscible liquids, with one droplet phase dispersed in a continuous phase, stabilised by a surfactant. Emulsions usually consist of a water phase and an oil phase. When the oil phase is emulsified as droplets in aqueous phase, the formed emulsion is called an oil-in-water (O/W) emulsion. Vice versa, a water-in-oil emulsion (W/O) can be formed.[96]

In an emulsion-freeze-drying process (Figure 1.3.), a poorly water-soluble drug is dissolved in an organic solvent (oil phase) which is then dispersed into an aqueous polymer/surfactant solution (usually by stirring or homogenization) to form

an O/W emulsion. The whole emulsion is frozen in liquid nitrogen and then freeze-dried to remove both water and the organic solvent. During the freeze-drying process, drug nanoparticles are formed in situ in the porous polymer scaffold. Entrapment of nanoparticles in the porous polymer structure prevents nanoparticle aggregation, which enables easy handling, transport, and storage of the nanoparticles composites. More importantly, the highly porous nature of the hydrophilic polymer scaffold ensures the fast re-dissolution in water when required and produce stable aqueous nanoparticle dispersions.[97]

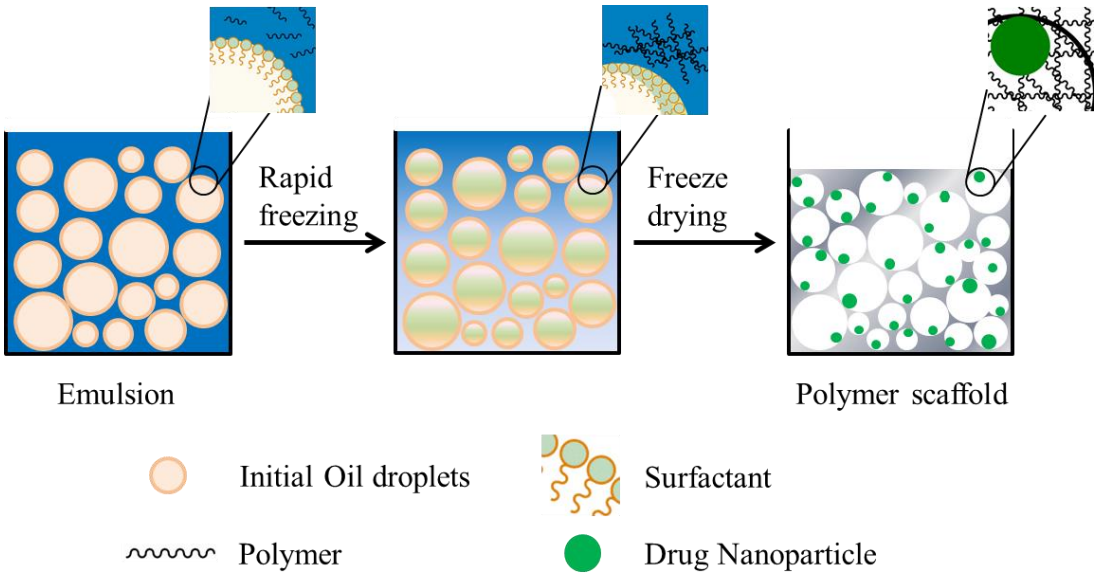

Figure 1.3. Schematic representation of the emulsion freeze-drying process.

In an emulsion, the number of droplets or the volume percentage can be varied. A high internal phase emulsion is formed when the volume percentage of the internal phase is greater than 74.05 %. These can be used as templates to prepare highly interconnected porous polymers.[96,98] Additives such as surfactants to stabilise the droplet phase can decrease the droplet size and hence pore size and narrower pore size distribution.[99,100] An increase in polymer concentration generally leads to a decrease in porosity.[101] Pore morphology and pore size can also be tuned by varying the freezing rate. Rapid freezing in liquid nitrogen for instance produces smaller pores and higher order, whilst slower freezing rate favours disordered structures with larger pores.[99] Wang and co-workers[102] formed emulsions containing sucrose in the aqueous phase and phospholipids and PEG in the oil phase. After lyophilisation and re-suspension in water, liposomes formed with a mean size smaller than 200 nm that showed high en-

trapment efficiency for selected water insoluble drugs. Grant *et al.*[103] produced amorphous indomethacin nanoparticles below 300 nm within porous PVA. Size and loading of indomethacin nanoparticles could be tuned by varying the emulsion compositions. Furthermore, a one-step procedure was developed to generate protein-encapsulated poly(lactide-*co*-glycolide) (PLGA) microspheres in chitosan by freeze drying a W/O/W double emulsion, where previously a two-step method consisting of a microsphere preparation step followed by incorporating in a pre-formed scaffold had to be employed. Due to the mild processing conditions and non-chemistry specificity, this method may be applied to a wide variety of proteins and polymers. Porosity and morphology, both crucial factors for release profiles, can easily be tuned by changing stirring time and concentration.[104] Mc Donald *et al.*[105] produced efavirenz particles with sizes of around 300 nm by the emulsion-freeze-drying approach. These particles showed reduced cytotoxicity, increased in vitro transport and a fourfold higher pharmacokinetic exposure in vivo. Giardiello and colleagues [106,107] presented the formation of two and three component nanoparticles. The two component particles were made up of FRET dyes and subsequently used for better cell imaging. For the three component particles it was possible to combine polymer, drug and magnetic nanoparticles, giving rise to the possibility of tracing and sensing particles to enhance targeted drug delivery.

1.2.3. Emulsion/Microemulsion

Emulsions are formed from two immiscible phases by energy input (*i.e.*, stirring, homogenization) in the presence of surfactants to reduce surface tension and stabilise the droplets. Emulsions are thermodynamically unstable. As such, phase separation occurs in emulsions to revert back to two immiscible phases. This happens via flocculation, creaming, coalescence or Ostwald ripening.[108,109] Surfactants and co-surfactant are added to increase kinetic stability. One way to prepare drug particles is by solvent extraction of an emulsion. Usually, a drug is dissolved in a non-polar solvent and is emulsified into an aqueous continues phase containing polymers or

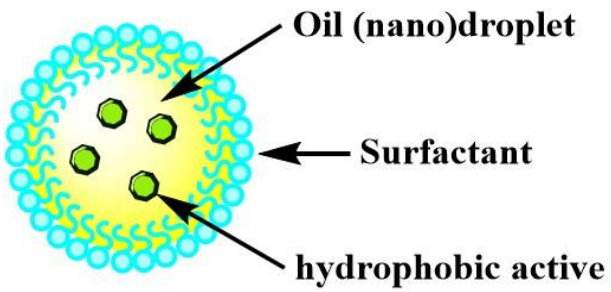

Figure 1.4. Schematic representation of an emulsion droplet with dissolved drug molecules

surfactants (Figure 1.4.). The emulsion is then quenched with water. After stirring, the resulting particles can be filtered out. A second method is by single emulsion solvent evaporation. After an O/W emulsion is formed, the volatile oil phase is evaporated to produce aqueous nanoparticle dispersions. Final particle size may be controlled via droplet size and use of suitable surfactants.[110,111]

Microemulsions form a sub-class of emulsions with droplets in the nanometer range (< 100 nm). Schuman and colleagues[112,113] first observed the formation of microemulsions in 1943 by titrating a milky emulsion with hexanol and subsequently coined the term microemulsion in 1959. Although many definitions of microemulsions can be found, the most commonly used is by Danielsson.[114] He defined a microemulsion as 'a system of water, oil and amphiphile which is a single optically isotropic and thermodynamically stable liquid solution.' Because of their liquid form and their sub-micron droplet sizes microemulsions are ideal candidates for the transdermal delivery of drugs.[115-117] Due to the nature of microemulsions, dermal and oral drug deliveries are the two most favoured delivery routes. High solubility potential in the oil droplet phase resulting in high drug concentration in microemulsion can be beneficial for potential therapeutic treatment. High concentration of surfactants and co-surfactants contained in the emulsion may enhance permeation by reducing the diffusional barrier of the stratum corneum.[118-120] For example, cyclosporin A, an immunosuppressant,[121] docetaxel,[122] an anti-cancer drug and biphenyl dimethyl dicarboxylate,[123] a treatment drug for liver diseases, have been investigated for microemulsion delivery. Microemulsions for oral delivery are usually encapsulated to prolong storage. Mostly this is done in gelatine capsules. However, due to the hydrophilic nature of gelatine, water containing formulations cannot be filled into a gelatine capsule, without change in emulsion composition.[124] Self-microemulsifying drug delivery systems (SMEDDS) present a solution. The basic principle of SMEDDS is the ability of an oil, surfactant, co-surfactant and drug to form spontaneous emulsions under gentle agitation and dilution with water. The gastrointestinal tract provides aqueous medium and sufficient agitation.[125,126] By virtue of high bioavailability, direct formation in the gastrointestinal tract, and prolonged storage, current research in emulsion drug delivery focuses more on SMEDDS and SEDDS (Self-emulsifying drug delivery systems) for industrial production.

Table 1.1. gives an overview of the advantages and disadvantages of the discussed bottom-up techniques

Table 1.1. Bottom-up methods with advantages and disadvantages

Method	Advantages	Disadvantages
Solvent Antisolvent precipitation (SAS)	• Cost and energy efficient • Straight forward production conditions [33]	• Particle agglomeration if not immediately worked-up[38] • Not below specific size plateau • High concentrations of surfactants needed[36] • Drugs needs to be soluble in one solvent • Solvent and anti-solvent need to be miscible • Organic solvent residue
High gravity Reactive precipitation (HGRP)	• Intensified micromixing[45] • Smaller particles and narrower size distribution	• Drugs needs to be soluble in one solvent • Solvent and anti-solvent need to be miscible • Not below specific size plateau[43] • Organic solvent residue • Additives
Rapid expansion of supercritical solution (RESS)/ Rapid expansion of supercritical solutions into a liquid solvent (RESOLV)	• Green chemistry[52] • Non-toxic, no solvent residue[52] • Formation of Nanoparticles possible in RESOLV[55]	• Expensive machinery and material • Many AIPs cannot dissolve in $scCO_2$ and need an organic co-solvent • Microparticles in RESS[55] • Additives

Supercritical Antisolvent precipitation (SAS)	• mild conditions • AIP does not need to be miscible with supercritical fluid, giving way to a broad range of materials • Recrystallization can be controlled leading to either smaller or larger particles of a desired morphology	• Solvent residue • Solvent needs to miscible with super critical fluid • Immediate work up required, otherwise particle can change morphology
Gas antisolvent (GAS)	• mild conditions allowing the handling of proteins[57] • AIP does not need to be miscible with supercritical fluid • Broad range of materials • Very small particles possible and easy particle size control • Recrystallization can be controlled leading to either smaller or larger particles of a desired morphology	• Solvent residue, which is difficult to strip • Batch technique, difficult to scale-up • Difficult separation of gas and solvent stream
Spray drying	• One –step processes[64] • Continuous and fast[64] • Additives can be mixed in with feed solution making encapsulation possible in a one-step process[68]	• Efficiency loss when milder conditions are needed[65,66] • Energy and thermal inefficient[65,66]
Spray freeze drying	• Mild conditions[24,84] • No agglomeration, due to immediate freezing of particles • Lyophilisation leads to enhanced characteristics, like wettability, storage and handling[114-117]	• Expensive equipment • Freeze-drying process is time and energy consuming • Solvent residue[118]

Emulsion freeze-drying	• Mild conditions • Particles stabilised against agglomeration even after prolonged storage[73-76] • Lyophilisation leads to enhanced characteristics, like wettability, storage and handling[73-77]	• Additives [99,100] • Freeze-drying process is time and energy consuming • Expensive equipment
Emulsions /microemulsions	• Dermal application possible[115-117] • High solubility and high drug concentration[118-120] • High affinity to the internal emulsion phase, can be modified to increase transdermal flux[118-120] • high concentration of surfactants and cosurfactants enhance permeation to the stratum corneum[118-120] • SMEDDS make it possible to form emulsions directly in the intestines[125,126]	• High concentrations of additives[118-120] • difficult to achieve long time stability[125,126]

1.3. Nanocarriers for encapsulation

1.3.1. Liposomes

Liposomes are stable microscopic vesicles of natural or synthetic lipids (usually phospholipids), first observed in 1964 by Bangham *et al.* [127-129] Liposomes are formed when amphipathic lipids spontaneously assemble in layer form in aqueous medium.[130] Depending on the conditions multilayer or monolayer vesicles are formed (Figure 1.5.).

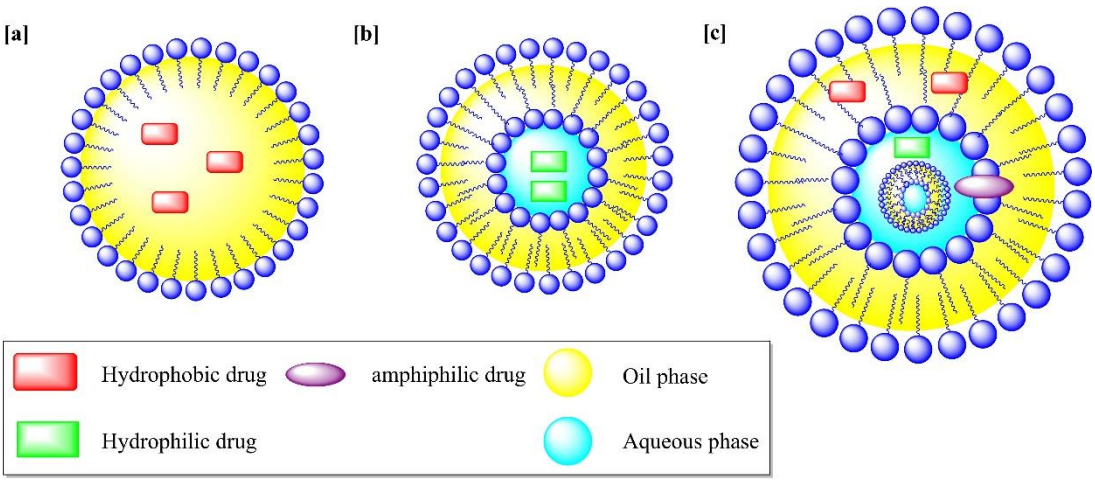

Figure 1.5. Schematic representation of a) monolayer liposomes; b) bilayer liposomes and c) multilayer liposomes.

In multilayer vesicles lipids are either ordered in circular rings with a head to tail structure with aqueous compartments in between or in a tail to tail arrangement with an aqueous internal department. The ability to enclose water soluble and entrap lipophilic drugs in the lipid layers as well as encompassing drugs with intermediate logP makes liposomes ideal candidates for drug delivery.[131] Liposomes cannot enter the cell *via* plasma clearance or tissue disposition, but by fusion or endocytosis, which increases the success rate of drug delivery to cells.[132] This trait makes liposomes highly attractive not only for drug delivery but also as carriers for enzymes and other proteins into the inner part of the cell.[133-135] Surface charge, hydrophobicity, size, fluidity and packing of lipid layers heavily influence the stability and type of proteins for binding of liposomes.[136,137] Changes in these parameters can be used for fine tuning of liposome properties. However, liposomes tend to be sensitive to fast elimination from the bloodstream as well as accumulation in tissue especially in the liver.[138] To prevent accumulation, different strategies may be applied. For example, liposomes can be formed with pH sensitive materials which pass into the cell as a whole and release their drug load triggered by the change in pH [139] or modified with suitable ligands for targeted delivery.[140,141] Different methods have been developed to circumvent fast clearance. One of the most successful is the employment of 'stealth' liposomes. These liposomes are linked to PEG which decreased the aggregation between the liposomes and particle-protein interaction.[143]

1.3.2. Dendrimers

Dendrimers belong to the family of branched polymers. Polymer arms are radiating in a highly ordered fashion from a core, reminiscing of a tree. The first reports about dendrimers were published in the late 70s early 80s by the groups of Buhleier ,[143] Denkewalter,[144] Newkome,[145] and Tomalia.[146] Tomalia and co-workers reported the formation of polymers with 'controlled occupation of space in three-dimensions as a function of size, shape and disposition of desired organic functionality'. These differed from classic monomers and oligomers in their higher degree of symmetry, higher branching and a maximized density in reactive end groups. A dendrimer includes three structural components. An initiator core, an interior layer (made up of repeating units radially attached to the core and an exterior) and functionalised end groups (attached to the outermost interior layer) (Figure 1.6.). By removing the central core, identical dendrons can be obtained. These branched polymer arms are again constructed from the above described three structural elements.

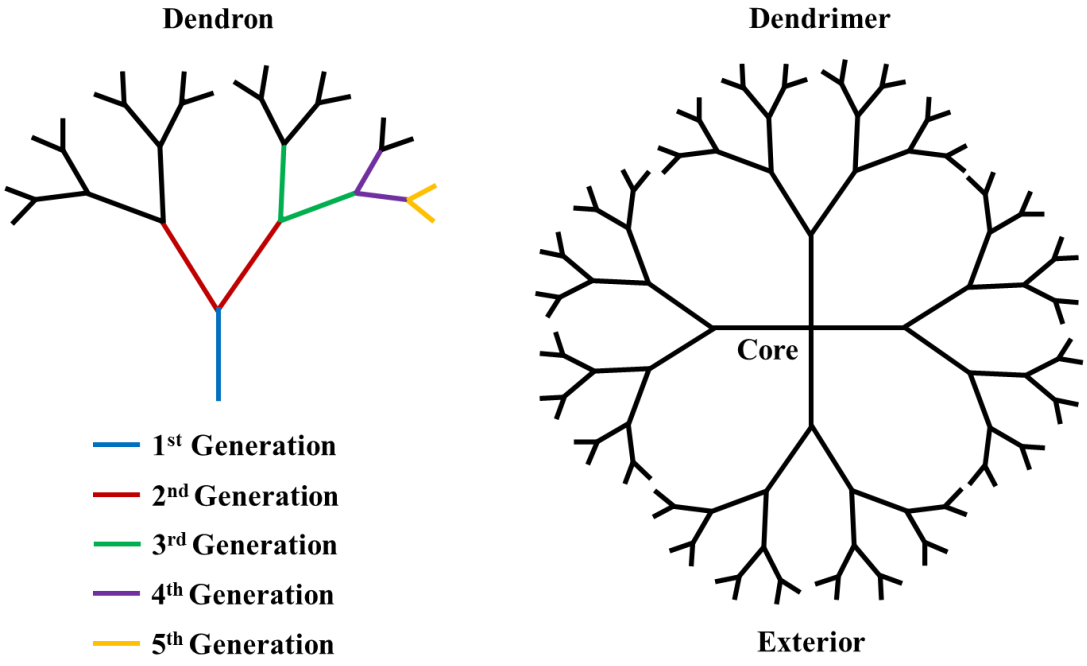

Figure 1.6. Schematic representation of a dendron and dendrimer

The number of dendrons is dependent on the multiplicity of the central core. Further away from the core a dendron possesses more and more branch points. Every branch points represents one generation. Higher generations are more branched and have more end groups. Synthesis of dendrimers is a stepwise process, which can either start from the central core outwards, in which case the growth is exponentially,[147] or

by synthesising dendrons, which are then coupled to a central core.[148] Both cases lead to a high degree of monodispersity in contrast to classical polymers, where growth is statistical, and the end product is polydisperse.[149] Like classical polymers, a wide variety of materials can be used as starting materials, even DNA.[150] Dendrimers of different generations are commercially available. Polyamidoamine (PAMAM) is commonly selected as starting material.[147] With a size between 2 and 10 nm dendrimers possess the favourable characteristics of nanoparticles. Depending on the number of generations the shape of dendrimers can change from small and floppy disks (up to generation 4) to spherical, three dimensionally defined and densely packed particles (generation 5 and up). The dense packaging can be used to achieve more concentrated drug loading. End groups can be changed to obtain hydrophilic or hydrophobic dendrimers with a hydrophobic or hydrophilic core respectively and to facilitate higher binding affinities to target sites.

1.3.3. Polymers

Polymeric nanocarriers have been gaining more and more interest in recent years, because of their favourable characteristics compared to liposomes and dendrimers. Liposomes have a few inherent problems, *i.e.* drug encapsulation is usually low and water-soluble drugs have been known to leak out prematurely, as well as a poor storage stability.[151] Dendrimers are synthetically challenging to produce. For this reason, different polymeric structures capable of encapsulation will be discussed in the following section. Figure 1.7. gives an overview over the structures under discussion.

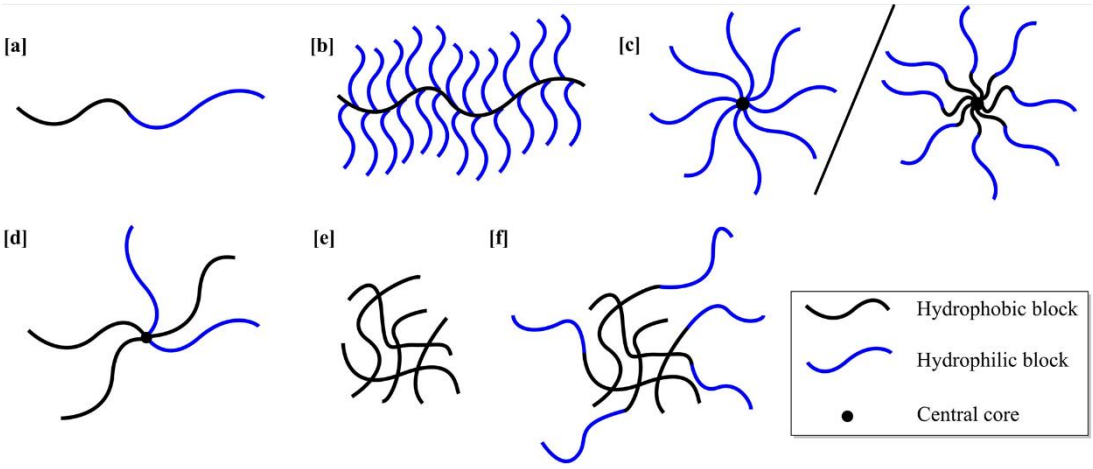

Figure 1.7. Schematic representation of a) linear block polymers; b) graft polymers; c) star polymers; d) Miktoarm polymers; e) Hyperbranched polymers and f) star-hyperbranched polymers.

1.3.3.1. Linear block polymers

A Block copolymer (Figure 1.7.a.) is according to IUPAC 'a copolymer that is a block polymer. In the constituent macromolecules of a block copolymer, adjacent blocks are constitutionally different, *i.e.* adjacent blocks comprise constitutional units derived from different species of monomer or from the same species of monomer but with a different composition or sequence distribution of constitutional units.'[151] Three basic structural types of block copolymers can be defined. The first is the A-B structure, so called diblock, with A and B being two different repeating units. A block of repeating unit A is thereby connected to a block of unit B. The second type is an A-B-A or A-B-C structure, called triblock. A block of B is enclosed between blocks of A on either side or three different block (A, B and C) are connected to form a linear block polymer- The third type is a multiblock in the style of $(A\text{-}B)_n$, where blocks of A and B are repeated to form areas of repeating unit A and B. In comparison to random copolymers, block copolymers exhibit well defined structures and their synthesis requires sequential addition of each monomer. Since the two repeating units are different in chemical and physical properties, a two-phase morphology on a micro-scale level can be observed for block copolymers.[152] This gives rise to the spontaneous formation of micelles in certain solvents, where one of the blocks is insoluble. The insoluble block forms a core, while the soluble block forms the corona. This behaviour can be further favoured by repulsive forces between blocks A and B.[153] Linear block polymers have been widely studied and manifold applications in cosmetics, stabilisation of insoluble materials, and drug delivery can be found. Drugs can be incorporated in the core chemically (covalent) and/or physically (electrostatic interactions; H-bonding).[154-156] The aggregation number, *i.e.*, the number of molecules needed to form a stable micelle, is closely relevant to the critical micelle concentration (CMC) *i.e.* the concentration 'below which virtually no micelles are detected and the limit above which virtually all additional surfactant molecules form micelles'.[156] For linear block copolymers, the aggregation number and CMC are relatively high. Hence, formed micelles will easily dissociate in the blood stream due to increased dilution. To prevent this happening cross-linked branches are introduced to enhance micelle stability below the CMC,[158] which in turn means additional synthetic steps.

1.3.3.2. Graft polymers

Graft polymers consists of a linear backbone from which a large number of polymer side arms of a different kind are chemically attached (Figure 1.7.b). In comparison to linear block polymers this gives rise to greater possibilities of fine-tuning the characteristics *e.g.* amphiphilicity, by adjusting the lengths of the arms and backbone as well as the grafting density.[159] In some instances, more stable micelles could be obtained in comparison to linear block polymer analogues and the use of graft polymers for drug encapsulation has been researched.[160-164] Graft polymers are often used in the formation of hydrogels, highly absorbent polymeric networks, where drugs can be incorporated into the network and depending on the constitution of the graft- polymers, released by pH or other stimuly.[165]

1.3.3.3. Star and Miktoarm polymers

Star polymers are a type of branched polymer where linear 'arms' radiate from a central branching point or 'core' (Figure 1.7.c and d). Star-homo or block polymers can be synthesised using the 'core first' method where multifunctional initiators propagate the polymerisation of arm A onto the core. Arm B is subsequently either added as a pre-existing block or the polymerisation is initiated by the living chain of A. However, to form uniform arms all sites need to be equally reactive, have the same initiation rate, which must be higher than the propagation rate with steric hindrance and repulsions kept at a minimum. The other option is to synthesis star polymers by an 'arm first' strategy. These can be further subcategorized according to procedure used.[166] Either the arms are polymerised as already described for linear di- and triblock polymers and subsequently added *via* coupling reactions to a core, *i.e.* 'grafted' onto a central core. In this case the core and arms can be synthesised and characterised independently before the star is formed.[167] The other option is to chain extend linear arms with multivinyl crosslinking agents. The 'arms' can either be linear homo or hetero block polymers, which greatly influences their ability to encapsulate actives *i.e.* homo star polymers seldom form micelles for encapsulation because of their tendency to be either hydrophilic or hydrophobic and they are more often used for the formation of hydrogels and subsequent drug encapsulation into gels.[168] However, homostars possessing longer arms and slightly bigger cores, or hetero block polymer

stars, may entrap molecules in their corona, forming unimolecular micelles, with a hydrophobic core and a hydrophilic corona.[169]

Miktoarm polymers (Figure 1.7.d) are a class of star polymers, where at least two chemically different arms emit from a common core, and are also sometimes called heterostar polymers.[170] Miktoarm polymers show smaller aggregation number compared to linear polymers, while maintaining the same hydrodynamic radii due to the greater difficulty of arms to be accommodated into a micelle.[171] Miktoarms are able to self-assemble and transform into very interesting structures by adjusting the lengths of one or more arms *e.g.* transformation of a hamburger like structure to a worm like structure,[170] and are also able to form multicompartment micelles due to the possibility of forming structures of three mutually immiscible arms connected via a central point.[172]

1.3.3.4. Branched/Hyperbranched polymers

Branched or Hyperbranched polymers (HBP) are similar in build to dendrimers, however in contrast to dendrimers these macromolecules have a high dispersity and show defects from build in linear segments. Hence, while they are still highly branched and possess a large number of end groups, the branching is imperfect (Figure 1.7.e).[173,174] In comparison to dendrimers, hyperbranched polymers are not as synthetical challenging while still maintaining most of the favourable characteristics such as solubility and reactivity (Table 1.2.).[175] Hyperbanched polymers can be synthesised by either single-monomer (SMM) or double-monomer (DMM) methodology, whereby either an AB_n monomer (SMM) or two momoners directly (DMM) are polymerised. There are four main sub-categories of SMM; polycondensation of AB_n Monomer,[176] self-condensing vinyl polymerisation (SCVP),[177] self-condensing ring-opening polymerisation (SCROP) [178] and proton-transfer polymerisation (PTP).[179] The synthesis of hetero star block polymers, as mentioned before, is challenging. Hyperbranched polymers on the other hand can easily be grown out (graft from) to obtain 'star hyperbranched polymers' (Figure 1.7.f) with a core-shell architecture. Depending on the monomers used amphiphilic character or an abundance of other features can easily be incorporated.[180]

Table 1.2. Comparison between linear, hyperbranched and dendrimeric polymers. Adapted with permission from Ref. 175 © 2015 Royal Society of Chemistry

Polymer	**Linear**	**Hyperbranched**	**Dendrimer**
Structure		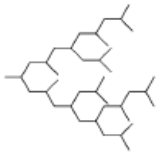	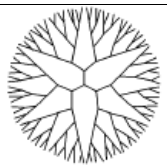
Topology	1D, linear	3D, irregular	3D, regular
Synthesis	One-step, facile	One-step, relatively facile	Multi-step, laborious
Purification	Precipitation	Precipitation or classification	Chromatography
Scaling-up	Already, easy	Already, easy	Difficult
M_w	Discrepant	Discrepant	Identical
PDI	>1.1	>1.1	1.0 (<1.05)
DB	0	0.4–0.6	1.0
Entanglement	strong	weak	Very weak or no
Viscosity	High	Low	Very low
Solubility	Low	High	High
Functional group	At two ends	At linear and terminal units	On periphery (terminal units)
Reactivity	Low	High	High
Strength	High	Low	Very low

Hyperbranched polymers possess spatial cavities in comparison to star polymers, whose tightly cross-linked core does not allow for cavities. In comparison to all other polymeric structures described before *e.g.* star polymers, linear block polymers or graft polymers, hyperbranched polymers, especially star hyperbranched polymers, do not need to self-assemble to stabilise themselves in unfavourable conditions. Hence, when used for encapsulation and release in the bloodstream no concerns of CMC values arise and no premature disassembly, triggered by outside factors, is possible. These, as well as the enhanced solubility, and easy manipulation of the many end-groups make hyperbranched polymers favourable materials for encapsulation and targeted delivery for drugs and genes,[181,182] mostly *via* the formation of core-shell particles. Encapsulation and release are directly influenced by the core, which determines the shape of the hyperbranched polymer, the internal structure which deter-

mines the internal dimensions and guest-host interactions and the outer-shell that governs the solubility and accessibility of the core region.[183] Core-Shell particles can easily be obtained by modifying the many end-groups. End-group modifications can be divided in four major categories which all give rise to interesting new polymers; End-capping with short chains or molecules,[183] terminal grafting, which affords core-shell multi-arm star polymers or hyperstars,[184,185] surface growing to fabricate inorganic/organic-hyperbranched polymer hybrid materials [186,187] and hypergrafting *i.e.* grafting hyperbranched macromolecules to a multifunctional polymeric core to obtain hypergrafted polymers.[188,189]

1.4. Polymer synthesis

As has been mentioned before, one major benefit of using polymeric nanocarriers is the ability to easily modify every component. Be that either by changing the monomers and hence changing the encapsulation ability, size or amphiphilicity, or by modifying the outer periphery of a nanocarrier with targeting ligands. This has mainly been made possibly by the discovery of a wide range of polymerisation techniques. For this reason, the following segment will give a brief overview of frequently used polymerisation techniques, which were also used in the following work.

1.4.1. Free radical ('conventional') polymerisation (RP)

Synthesis by free radical polymerisation accounts for roughly 45 % of all industrially produced synthetic polymers (~100 mt in 2009).[190] In the following segment, free and controlled radical polymerisation techniques will be described and compared as well as considered for their application in drug encapsulation.

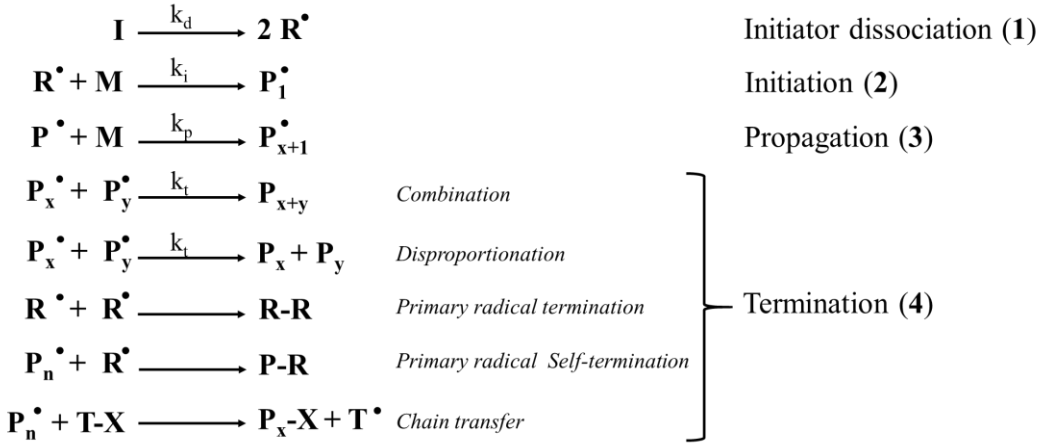

Scheme 1.1. Mechanism of free radical polymerisation.

Free radical polymerisation, sometimes also called conventional radical polymerisation has been known since the 1940s and is one of the most applied polymerisation techniques in industry,[191] because of a high tolerance for functional monomers as well as being synthetically straightforward *i.e.* tolerant of protic solvents and trace impurities of oxygen and monomer stabilisers. Furthermore, reactions can be done in aqueous medium (emulsion polymerisation).

Scheme 1.1. shows the mechanism of RP, which consists of four major steps, *i.e.* initiator dissociation, initiation, propagation and termination. In the first step, a radical is generated from a non-radical species. Radical initiators are molecules that exhibit a labile bond. Stimuli such as temperature or light lead to the decomposition of these molecules and subsequent radical formation. The two most prominent representatives of these class of molecules are azoinitiators and peroxides.[190] After the generation of the primary radicals the addition of monomer molecules leads to an initial short polymer chain which is called the initiation radical. This step is generally much faster than the dissociation of the initiator ($k_i > k_d$). This step is followed by the chain growths *i.e.* propagation, with a rate in the order of $k_p \sim 10^2–10^4\ M^{-1}\ s^{-1}$. Termination of the reaction is possible in manifold ways. Generally, it is either possible that radicals can become inactive by radical-radical recombination with an initiator molecule *i.e.* primary radical (self-) termination or growing polymer chains can be terminated by atom transfer and atom abstraction reactions *i.e.* combination, disproportionation or chain transfer. However, these manifold termination reactions as well as the fast chain growths lead to broad dispersity, low reaction control and the possibilities of introducing structural irregularities.[190,192,193] The poor reaction control also leads to difficulties in the preparation of di- and multiblock polymers.[192] The preparation of these structures is often only possible if one block is first synthesised by a different polymerisation technique and then grown out [194] by RP. However, RP can be used to graft polymer chains onto an inorganic surface *e.g.* silica or titanium, by modifying the surface to carry a radical initiator.[195,196] To encapsulate hydrophobic actives and release them in aqueous medium amphiphilic characteristics need to be incorporated into the polymer, which is difficult using RP. However, it is possible to synthesise polymer capsules by miniemulsion polymerisation, which can be used to incorporate actives [197, 198] or form nanocomposite hydrogels for encapsulation and release or biomedical implants.[199]

1.4.2. Reversible-deactivation radical polymerisation (RDP)

In RP, the initiator dissociation is slower than the chain growths. Polymers formed at the beginning of the reaction are longer then the polymers formed later in the reaction (Figure 1.8.a), resulting in broad dispersity (Figure 1.8.b). By using Reversible-deactivation radical polymerisation (RDP) methods, previously known as controlled/living radical polymerisation (CPR), this can be avoided.[200,201] At the same time RDP gives rise to the synthesis of many interesting structures *e.g.* stars or hyperbranched polymers, which could not be obtained *via* RP. The basic principal of any RDP is an equilibrium between a minimal amount of growing free radicals and a majority of a dormant species.[202] Much research has been done in the development of RDPs in the last decades and an in-depth discussion of the different methods is beyond the scope of this work. As such the focus is put on atom transfer radical polymerisation (ATRP) developed in 1995 by Wang et. al.[203] and reversible addition-fragmentation chain-transfer polymerisation (RAFT) established in 1998 at the Commonwealth Scientific and Industrial Research Organisation (CSIRO) [204].

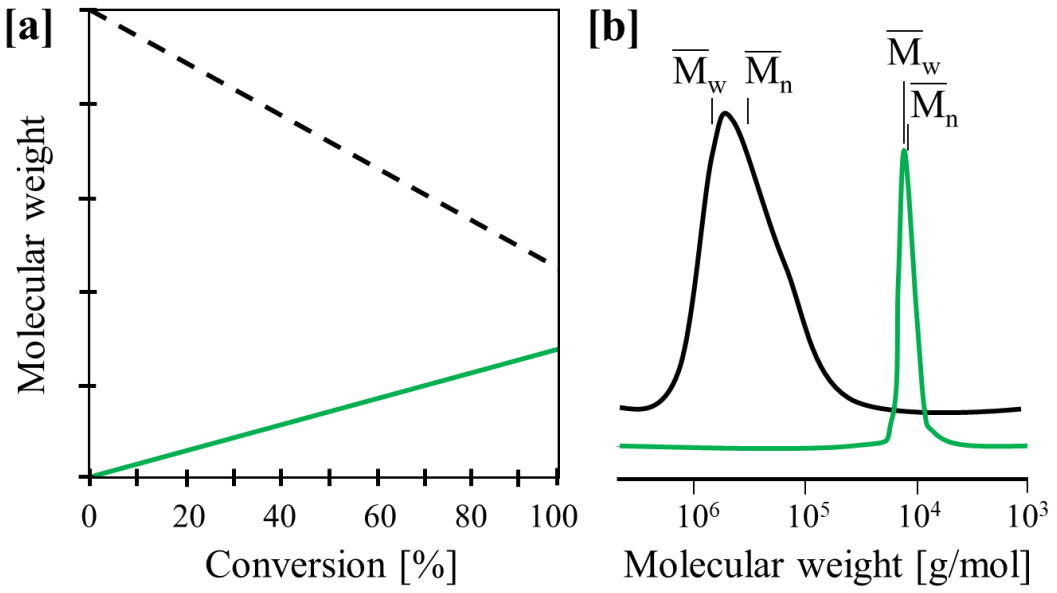

Figure 1.8. a) Evolution of molecular weight with monomer conversion for a conventional radical polymerisation with constant rate of initiation (dotted line) and a living radical polymerisation (green line). Reproduced from Ref. 200 with permission from CSIRO Publishing and b) Typical molecular weight distributions for a conventional (black line) and living radical polymerisation (green line). Data shown are from GPC analysis of polystyrene prepared by thermal polymerisation of styrene at 110◦C for 16 h (M_n 324000, M_w/M_n = 1.74, 72 % conversion) and a similar polymerisation in the presence of cumyl dithiobenzoate (0.0029 M) (M_n 14400, M_w/M_n = 1.04, 55 % conversion). Adapted with permission from Ref. 201 © 2000 Wiley.

1.4.2.1. Atom transfer radical polymerisation (ATRP)

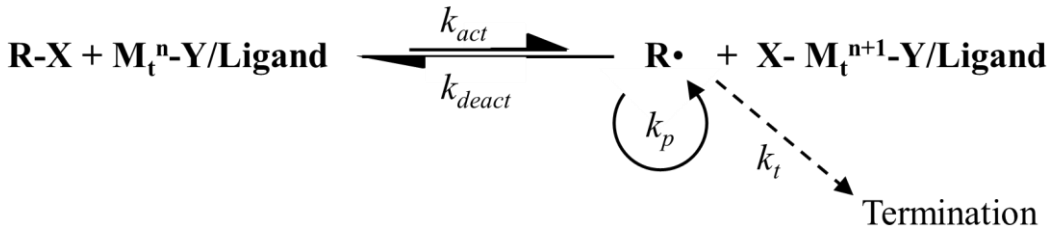

Scheme 1.2. Mechanism of ATRP as proposed by Matyjaszewski et. al.

In ATRP an active species is generated through a reversible redox process catalysed by a transition metal on the radical (monomer) and the dormant species (Scheme 1.2.). To that end alkyl halides (RX) are used as initiators. For the polymerisation of well-defined polymers with narrow size distribution the halide group has to selectively and rapidly migrate between the growing chain and the metal complex. Initiation needs to be fast and quantitative to avoid the uncontrolled growth of longer chains at the start of the reaction. Fast initiation also assures that transfer and termination reactions are negligible, and the number of growing chains is constant. The metal catalyst determines the position of the equilibrium. It has to have two readily accessible oxidation states separated by one electron, an affinity for halides and has to be able to accommodate an incoming halide in its coordination sphere. A ligand (Y) is added to solubilise the metal salt in organic solvent and adjust the redox potential of the metal centre. The equilibrium constant ($K_{eq} = k_{act}/k_{deact}$) determines the polymerisation rate. If the constant is too small ATRP will not occur or occur very slowly, if however, the constant is too large a large amount of termination reaction will occur. To achieve controlled polymerisation the equilibrium has to lay on the side of the dormant species to assure that at any given time only a small number of free radicals are able to grow and then get 'capped' again after a short amount of time by the halide to avoid the formation of long polymer chains.

As with RP, ATRP can be done in bulk, in solution or in emulsion polymerisation, however by using ATRP it is possible to easily synthesise complex polymer architectures such as stars, comb polymers or multiblock polymers [202,205,206] as well as functionalise the polymer by nucleophilic substitution, radical or electrophilic addition of the end-chain halide post polymerisation or pre-polymerisation by using a

monofunctional ATRP initiator [206,207]. ATRP has since been used in a plethora of biomedical applications from direct synthesis of polymer bioconjugates,[208,209] polymer dug-conjugates,[210,211] micelles,[211,212] cross-linked nano- and microgels [214,215] and vesicles [216,217] to name just a few and an excellent review can be found about the application of ATRP in biomedical applications by Siegwarta et. al. [218]

1.4.2.2. Reversible addition−fragmentation chain-transfer polymerisation (RAFT)

While in ATRP the dormant species is also the source of the radical, a radical initiator is needed to start the reaction in RAFT. Hence, the first step of a RAFT polymerisation (Scheme 1.3.) is the dissociation of the initiator and subsequent addition of monomers to the initiator radical.

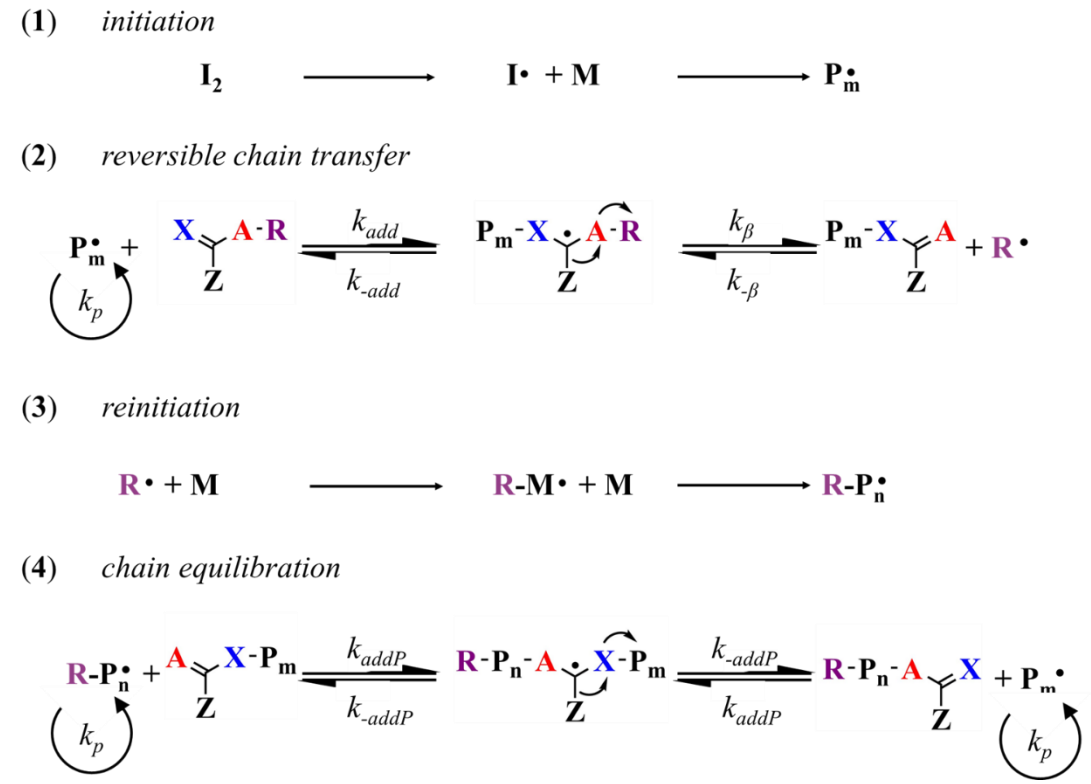

Scheme 1.3. RAFT mechanism as proposed by the CSIRO group

The same as in a conventional polymerisation (**1**). However, shortly after initiation the propagating radical (P_m•) reacts with a thiocarbonylthio compound (RC(=X)AZ with A, X = S), or chain transfer agent (CTA). The instable intermediate radical then gives rise *via* fragmentation to a new radical (R•) (**2**). This radical is then free to react with monomers to form a new propagating radical (P_n•) (**3**). Chain equi-

librium is reached by the addition of the propagating radical (P_n•) back onto the thiocarbonyl compound thereby 'capping' its growth and releasing previously dormant chains (P_m•) to grow further (**4**). This equilibrium between active propagating radicals (R-$P_{n/m}$ •) and dormant thiocarbonlythio compound (Z(A=)CX-$P_{m/n}$•) affords equal opportunity for all chains to grow at equal rates.

In ATRP controlled polymerisation comes from a reversible activation *via* atom transfer, this equilibrium also determines the rate of polymerisation. In RAFT however, deactivation and activation are chain-transfer reactions *i.e.* radicals are neither formed nor destroyed. To assure that mostly dormant polymers are present in the reaction a higher amount of CTA is present than initiator. After the polymerisation is stopped most chains retain the thiocarbonylthio end group and can be obtained as stable materials, which allows for re-initiation of the polymerisation to afford complex polymer architectures.[199,203,218] The CTA must fulfil the following criteria to guarantee an efficient polymerisation; it needs to have a reactive C=S double bond (high k_{add}) and a weak S-R bond for rapid fragmentation (high k_β). The R group should furthermore be a good leaving group ($k_\beta \geq k_{-add}$) and should efficiently re-initiate polymerisation. The addition and fragmentation step are directly influenced by the Z and R-group respectively and careful consideration when selecting a CTA has to be made in respect to the chosen monomers [200].

RAFT synthesis, as ATRP, allows for easy pre- and post-polymerisation functionalisation. Pre-functionalisation can be done by modification of either Z or R group. Since in RAFT the chain is growing from the R group, functionalities on the R group affords α-functionalised polymers, while ω-functionalised polymers are obtained by modifying the Z group. These modifications can range from proteins, to ligands for targeted delivery to functional groups such as -N_3 or -COOH, which can be used to react with sensitive targeting moieties post polymerisation.[220] Post-polymerisation modification is also possible by converting the Z group into a thiol which is then readily available to react *via* thiol-ene chemistry.[221] As with ATRP, RAFT polymerisation opens the door to the synthesis of manifold complex polymer structures [219,222-224] as well as the possibility of a wide variety of biomedical applications whose discussion is beyond the scope of this work. However, excellent reviews can be found in literature.[225-227]

1.5. Solvents and additives used in the formulations

1.5.1. Solvents

Although the use of organic solvents in general is unfavourable, for some techniques the use of such solvents is inevitable. For the production of pharmaceutical drugs some consideration has to be made before choosing a solvent, *i.e.,* toxicity and production method. A guideline on toxicity of organic solvents and their residue limit was proposed at the second international conference on harmonization of technical requirements for registration of pharmaceuticals for human use (ICH) and subsequently published as Guidance for Industry Q3C.[228] In this guideline, commonly used organic solvents are sorted into three categories. Class 1 solvents are known or strongly suspected of human carcinogens and environmental hazards and should be avoided. If avoidance is not possible their use needs to be strongly justified and solvent residue needs to be highly restricted. Examples are benzene (residue limit 2 ppm) and carbon tetrachloride (residue limit 4 ppm). Class 2 solvents are non-genotoxic animal carcinogens, or solvents that can possibly cause irreversible toxicity such as neurotoxicity or teratogenicity, as well as solvents with reversible toxicity. The use of these solvents should be limited. Residue limits can be calculated as either parts per million (ppm) or as a permitted daily exposure (PDE) in gram per day (milligram per day), which takes the maximal administered mass of drug per day into account. Examples for such solvents are chloroform (limit 0.6 mg/day and 60 ppm), methanol (limit 30 mg/day and 3000 ppm), acetonitrile (limit 4.1 mg/day or 410 ppm) and cyclohexane (limit 38.8 mg/day and 3880 ppm). Class 3 solvents have a low toxic potential and no exposure limit is needed. They generally have PDEs above 50 mg per day. Such solvents include acetone, DMSO, and ethanol. Complete classification of the most commonly used organic solvents can be found in the Guidance for Industry Q3C [228] and in specific reviews.[229,230]

Other considerations, as already mentioned, are challenges related to the preparation methods. Many of these have already been described with the corresponding techniques, therefore only some general requirements are described here. Techniques such as SAS and HGRP require organic solvents to function as solvent to the drugs and as anti-solvent to water, another organic solvent or a supercritical fluid, while being simultaneously miscible with the antisolvent. Whereas in methods related to emulsion and emulsion-freeze-drying, solvents need to be immiscible with water, or

at least partially immiscible for the formation of emulsions. If the solvent is removed by freeze-drying, the melting points of the selected solvents has to be taken into account. The solution made from the solvents should have a melting point above the lowest temperature in the chamber of the freeze-dryer, although it is still possible to freeze dry a small volume frozen solution with a lower melting point with high capacity vacuum. When the melting point is low and the frozen sample melts in the freeze dryer, the porous structure and the quality of the nanoparticles can be compromised.

1.5.2. Additives

Nanoparticle formation is a rapid process where nucleation is induced by a drastic increase of supersaturation or by downsizing microparticles with mechanical force. In both cases, particle agglomeration or further particle crystallisation needs to be suppressed. Additives, mainly surfactants, are usually added in the processing step to address the aggregation problem. Surfactants are amphiphilic molecules consisting of a hydrophobic part and a hydrophilic part. Surfactants can be classified according to the charge of the hydrophilic part of the molecule as anionic, cationic, zwitterionic, or non-ionic. Adsorption of surfactants on surface or surrounding droplets is driven by the decrease in free energy at the phase interface. Surfactants can form micelles with a hydrophobic core in aqueous medium. The hydrophilic part of the molecule interacts strongly with the surrounding water and hence well dispersed.[231] An increase of surfactant concentration usually leads to a decrease in particle size due to enhanced adsorption on the surface, however if the concentration is above the critical micelle concentration, the molecules will exist in micelle form and interaction with the drug molecules is limited.[232] Length and charge of surfactants play another important role for stabilization. Longer hydrophobic chains can cover more surface area and the required amount would be lower. Particles with charged surfactants on the other hand show greater electrical repulsion due to the resulting surface charge.[233] One major concern in using surfactants is the impact that surfactants may have for biomedical application and on the environment. Studies show that surfactants can accumulate in water and may be toxic to marine life.[234,235] Elevated levels of surfactants are also known to lead to irritation of the human skin due to changes in the stratum corneum.[236,237]

1.5.3. Polymers

There are two main routes polymers can be used in nanoparticle formulation, either as stabilisers or in drug encapsulation which has already been discussed. Some polymers can stabilise nanoparticles by adsorption on the surface in the same way as surfactants, although in contrast to surfactants polymers can agglomerate in the hydrodynamic layer between particles and prevent particle collision and agglomeration .[238] Depending on the techniques applied, polymers can form scaffolds in the dried state, which prolongs the shelf life of nanoparticles.[84,103] To address toxicology concerns, recent research has focused on the synthesis of biodegradable polymers and polymers made from materials native or similar to the human body, which may also increase the cellular uptake. Typical examples of such polymers include poly(lactic acid) (PLA),[239] poly(lactide-co-glycolide) (PLG) [240] and chitosan.[241]

1.6. Applications

Table 1.3 shows a selection of approved nanodrug products on the market and the administrations achieved by drug nanoformulations.[245-271] Most of these nanomedicines are either produced by top-down processes or encapsulation. The only industrially applied bottom-up technique is spray drying, since it is possible to mix additives in the feed solution and achieve encapsulation in one-step. All the drugs produced by spray drying listed in Table 1.3. have utilised polymers. Encapsulation in liposomes and drug delivery *via* emulsions are well established methods especially in cancer and HIV treatment. Dendrimers are not as well established, which may in part be due to the difficulty in synthesising such polymers and also the possible toxicity. To the best of our knowledge, the first dendrimer-nanomedicine containing the dendrimer SPL7013, an antiviral agent, is VivaGel™ by Starpharma. The drug may be applied for topical use to prevent infection with HIV and other sexual transmitted diseases. At this time, it is still in Phase III testing.[242] The similar limited use has been noticed for block copolymer micelles. Genexol®-PM by Samyang Biopharmaceuticals, a polymeric micelle formulation of paclitaxel, is currently undergoing Phase II and III tests. Other cancer drugs, SP1049C (a doxorubicin polymer micelle conjugate) and NC-6004 (a cisplatin micelle conjugate) have also been tested.[244,245]

Table 1.3. Selected marketed nanodrugs.

Name	Active Ingredient	Dosage form	Application	Method	Company
Pletal	Cilostazol	oral	peripheral vascular disease	Wet pearl/ball milling (NanoCrystal™)	Otsuka Pharmaceutical Co.[245]
Rapamune®	Sirolimus	oral	Immunosuppressant	Wet pearl/ball milling (NanoCrystal™)	Pfizer [246]
Emend®	Aprepitant	oral	Suppresses nausea and vomiting	Wet pearl/ball milling (NanoCrystal™)	Merck [247]
Megace® ES	Megestrol acetate	oral	Breast cancer	Wet pearl/ball milling (NanoCrystal™)	Par Pharmaceuticals Inc. [248,249]
Tricor®	Fenofibrate	oral	Reductionof cholesterol levels	Wet pearl/ball milling (NanoCrystal™)	Abbott Laboratories [250]
Avinza®	Morphine Sulphate	oral	Severe pain treatment	Wet pearl/ball milling (NanoCrystal™)	King Pharmaceuticals [251]
Focalin®	Dexmethylphenidate hydrochloride	oral	Attention deficit hyperactivity disorder (ADHD)	Wet pearl/ball milling (NanoCrystal™)	Novartis [252]
Ritalin LA®	Methylphenidate hydrochloride	oral	Attention deficit hyperactivity disorder (ADHD)	Wet pearl/ball milling (NanoCrystal™)	Novartis [253]
Triglide®	Fenofibrate	oral	Reduction of cholesterol levels	High pressure homogenization (IDD-P Skyepharma)	Sciele Pharma Inc.[254]
Abraxane®	Albumin-bound paclitaxel	i.v.	Cancer treatment	High pressure homogenization	Abraxis BioScience [255]
Sporanox®	Itraconazole	oral	Antifungal agent	Spray drying	Janssen Pharmaceutica[256]

Prograf®	Tacrolimus	oral	Immunosuppressant	Spray drying	Atellas [257]
Cesamet®	Nabilone	oral	Suppresses nausea and vomiting	Spray drying	Meda Pharmaceuticals [258]
Intelence®	Etravirine	oral	HIV treatment	Spray drying	Janssen Pharmaceutica[259]
Diprivan®	Propofol	i.v.	Anaesthetic	Microemulsion	Fresenius Kabi[260]
Neoral®	Cyclosporine	oral	Immunosuppressant	SMEDDS	Novartis[261]
Norvir®	Ritonavir	oral	HIV treatment	SMEDDS	Abbott Laboratories[262]
Fortovase®	Saquinavir	oral	HIV treatment	SMEDDS	Roche[263]
Restasis®	Cyclosporine A	Ophthalmic	Dry eye syndrome	Lipid emulsion	Allergan[264]
Durezol®	Difluprednate	Ophthalmic	Eye inflammation	Lipid emulsion	Alcon Pharmaceuticals[265]
Doxil®	Doxorubicin	i.v.	Treatment of Kaposi's sarcoma	PEGylated liposomes	Janssen PharmaceuticaN.V. [266,267]
Myocet®	Doxorubicin	i.v.	Breast cancer	liposomes	Enzon Pharmaceuticals[268]
DepoCyt®	Cytarabine	i.v.	Leukaemia and non-Hodgkin lymphoma	liposomes	Pacira pharmaceuticals[269]
DaunoXome®	Daunorubicin citrate	i.v.	Leukaemia	liposomes	Galen[270]
LMX®-4	Lidocaine	topical	Local anesthetic	liposomes	Ferndale Laboratories
Epaxal	Inactivated hepatitis A virus	parenteral	Hepatitis A vaccine	liposomes	Crucell[271]

1.7. Summary and perspective

Nanomedicine has shown to be an answer to many problems in pharmaceutical applications, particularly in addressing the poor water-soluble problem. A wide range

of techniques, including top-down method, bottom-up method, or various encapsulation approaches, have been developed to make drug nanoparticles. Reducing the drug particles to nanoscale can enhance dissolution rates and increase water solubility. Furthermore, the decrease in size and functionalisation of the particle surface can facilitate the sustainable, targeted, and responsive drug delivery and release. Due to the tendency of drug nanoparticles aggregation, the preparation methods have been improved to produce stable aqueous nanoparticle dispersions or prevent nanoparticles aggregation by efficient use of stabilisers or dry porous scaffolds.

Because of the easy control in fabrication process, top-down approaches such as wet-milling and high-pressure homogenization have been mostly used by industry for nanoformulated drugs on the market. Spray drying is also a technique that has been employed industrially. However, it is generally very difficult to produce small, uniform, and non-aggregated nanoparticles by the top-down methods. There are also limits for soft compounds or temperature-sensitive drug compounds to be processed by milling or homogenization. Various bottom-up processes have been developed and investigated to address different aspects of drug nanoformulations, for example, spray drying, sonoprecipitation, use of supercritical fluids, emulsions, cryogenic methods, and different encapsulation techniques. The results are highly promising. However, the cost of production, quality control in different production batches, and meeting the regulation requirements, have to be considered carefully before adopting these techniques industrially for marketing nanodrug formulations.

For poorly water-soluble drugs with different properties, a suitable preparation technique should be selected to match the compound property and the requirement for the targeted application. In terms of producing drug nanoparticles, the challenge is how to produce drug nanoparticles with controlled sizes, narrow particle size, and control the shape of the nanoparticles. When the nanoformulations have been made for potential treatment, a reasonably long shelf life with non-aggregated nanoparticles is required, which can be normally met by use of surfactants and/stabiliser. However, in terms of treatment, a high ratio of drug to stabiliser is required for therapeutic efficacy, not to mention the potential toxicity or side effects of the stabilisers. When it comes to in vivo test or clinical use, the surface of the drug nanoparticles should be properly functionalised, binding with multiple modalities (e.g., imaging modality), to allow sufficient circulation time in bloodstream, to deliver to the targeted sites, and to

release the drug payload on demand by triggers. Imaging techniques could be employed to tract where the drug nanoparticles are and to better understand the treatment outcome and hence to help develop more efficient drug formulations. Overall, nanoformulations for poorly water-soluble drugs are highly promising and fast growing pharmaceutical sector. Great efforts are required from researchers and industries to develop and optimize different nanoformulation techniques to achieve the best possible results in healthcare.

1.8. Project aims and plans

The following thesis will focus on the use of branched/hyperbranched polymers to obtain drug nanoparticles by two different bottom-up techniques as well as the direct use as drug nanocarriers. The polymers used in Chapter 2 and 3 will be synthesised *via* free radical polymerisation, while the polymers used in Chapter 4 and 5 will be synthesised by RDP techniques (ATRP and RAFT). Thereby making the direct comparison between branched systems obtained by 'controlled' and 'uncontrolled' polymerisation techniques possible.

In Chapter 2, 3 and 4 emulsion-freeze drying, and a simple solvent evaporation technique will be employed to afford drug nanoparticles and drug nanosupensions of water insoluble drugs. These two bottom-up techniques were chosen for their mild conditions and hence broad applicability for sensitive actives. The (hyper) branched polymers were designed to be amphiphilic to avoid any further use of additives. Drug nanoparticles obtained by emulsion-freeze drying will furthermore be tested for their enhanced antimicrobial activity. Drug nanoparticles formed by solvent evaporation will be tested for enhanced dissolution. Chapter 4 will focus on the use of temperature responsive polymer nanoparticles for the formation of drug nanosuspensions *via* solvent evaporation and the changed behaviour facilitated by changing the hydrophilic arms from linear to branched PEG will be investigated.

In Chapter 5 pH responsive, hyperbranched polymers will be designed and synthesised by RAFT as a platform for encapsulation and release of water insoluble actives. Besides passive targeting the polymers will be surface modified for active targeting and tested for the possibility of using the polymers for the formation of hydrogels.

The focus will be on hyperbranched polymers because of their excellent solubility in most media, easy synthesis and no need to self-assemble as well as the resulting longer blood-circulation. The overall aim will be to investigate the possibility to develop different multifunctional, stable platforms for drug delivery that are easy to synthesis, cost-efficient, highly reproducible and have a long shelf live.

1.9. References

1. R. A. Prentis, Y. Lis and S. R. Walker, *Br. J. Clin. Pharmacol.*, 1988, **25**, 387-396.
2. J. P. Griffin, J. Posner and G. R. Barker, eds., *The textbook of pharmaceutical medicine*, Blackwell Publishing Ltd., Oxford, 2013.
3. J. A. DiMasi, R. W. Hansen and H. G. Grabowski, *J. Health Econ.*, 2003, **22**, 151-185.
4. B. Munos, *Nat. Rev. Drug Discov.*, 2009, **8**, 959-968.
5. I. Kola and J. Landis, *Nat. Rev. Drug Discov.*, 2004, **3**, 711-716.
6. A. Persidis, *Nat. Biotechnol.*, 1998, **16**, 488.
7. G. R. Marshall, *Annu. Rev. Pharmacool. Toxicol.*, 1987, **27**, 193-213.
8. D. C. Rees, M. Congreve, C. W. Murray and R. Carr, *Nat. Rev. Drug Discov.*, 2004, **3**, 660-672.
9. T. Loftssona and M. E. Brewsterb, 2010, *J. Pharm. Pharmaco.*, **62**, 1607–1621
10. G. Amidon, H. Lennernäs, V. Shah and J. Crison, *Pharm. Res.*, 1995, **12**, 413-420.
11. N. A. Kasim, M. Whitehouse, C. Ramachandran, M. Bermejo, H. Lennernäs, A. S. Hussain, H. E. Junginger, S. A. Stavchansky, K. K. Midha, V. P. Shah and G. L. Amidon, *Mol. Pharm.*, 2004, **1**, 85-96.
12. Y. Kawabata, K. Wada, M. Nakatani, S. Yamada and S. Onoue, *Int. J. Pharm.*, 2011, **420**, 1-10.
13. R. Thakuria, A. Delori, W. Jones, M. P. Lipert, L. Roy and N. Rodríguez-Hornedo, *Int. J. Pharm.*, 2013, **453**, 101-125.
14. C. L.-N. Vo, C. Park and B.-J. Lee, *Eur. J. Pharm. Biopharm.*, 2013, **85**, 799-813.
15. Y. Lu and K. Park, *Int. J. Pharm.*, 2013, **453**, 198-214.
16. H. Mu, R. Holm and A. Müllertz, *Int. J. Pharm.*, 2013, **453**, 215-224.

17. M. Lu, Z. Guo, Y. Li, H. Pang, L. Lin, X. Liu, X. Pan and C. Wu, *Curr. Pharm. Des.*, 2014, **20**, 369-387.
18. A. Albert, *Nature*, 1958, **182**, 421.
19. B. Testa and J. M. Mayer, *in Hydrolysis in Drug and Prodrug Metabolism: Chemistry, Biochemistry, and Enzymology*, Verlag Helvetica Chimica Acta, Zurich, 2003.
20. V. J. Stella and K. W. Nti-Addae, *Adv. Drug Del. Rev.*, 2007, **59**, 677-694.
21. R. Duncan, *Anti-Cancer Drugs*, 1992, **3**, 175-210.
22. G. M. Dubowchik and M. A. Walker, *Pharmacol. Ther.*, 1999, **83**, 67-123.
23. B. Testa, *Biochem. Pharmacol.*, 2004, **68**, 2097-2106.
24. Y.-F. Maa, P.-A. Nguyen, T. Sweeney, S. J. Shire and C. C. Hsu, *Pharm. Res.*, 1999, **16**, 249-254.
25. A. Chawla, K. M. G. Taylor, J. M. Newton and M. C. R. Johnson, *Int. J. Pharm.*, 1994, **108**, 233-240.
26. G. Kaptay, *Int. J. Pharm.*, 2012, **430**, 253-257.
27. W. Ostwald, *Z. Phys. Chem.*, 1900, **34**, 795-503.
28. A. T. Florence and D. Attwood, *Physicochemical principles of pharmacy*, pharmaceutical press, London, 5th edn., 2011.
29. A. A. Noyes and W. R. Whitney, *J. Am. Chem. Soc.*, 1897, **19**, 930-934.
30. M. Kakran, N. Sahoo, I. L. Tan and L. Li, *J. Nanopart. Res.*, 2012, **14**, 1-11.
31. E. Merisko-Liversidge and G. G. Liversidge, *Adv. Drug Del. Rev.*, 2011, **63**, 427-440.
32. C. Brough and R. O. Williams Iii, *Int. J. Pharm.*, 2013, **453**, 157-166.
33. M. R. Violanto and H. W. Fischer, *US Pat.*, US4826689 A, 1989.
34. U. Bilati, E. Allémann and E. Doelker, *Eur. J. Pharm. Sci.*, 2005, **24**, 67-75.
35. J.-Y. Zhang, Z.-G. Shen, J. Zhong, T.-T. Hu, J.-F. Chen, Z.-Q. Ma and J. Yun, *Int. J. Pharm.*, 2006, **323**, 153-160.
36. N. Rasenack and B. Müller, *Pharm. Res.*, 2002, **19**, 1894-1900.
37. M. E. Matteucci, M. A. Hotze, K. P. Johnston and R. O. Williams, *Langmuir*, 2006, **22**, 8951-8959.
38. J. Hu, W. K. Ng, Y. Dong, S. Shen and R. B. H. Tan, *Int. J. Pharm.*, 2011, **404**, 198-204.

39. A. Homayouni, F. Sadeghi, J. Varshosaz, H. Afrasiabi Garekani and A. Nokhodchi, *Colloids Surf. B. Biointerfaces*, 2014, **122**, 591-600.
40. Y. Zu, W. Wu, X. Zhao, Y. Li, W. Wang, C. Zhong, Y. Zhang and X. Zhao, *Int. J. Pharm.*, 2014, **471**, 366-376.
41. A. Viçosa, J.-J. Letourneau, F. Espitalier and M. Inês Ré, *J. Cryst. Growth*, 2012, **342**, 80-87.
42. R. Fowler, *Chemical Engineer*, 1989, 35-37.
43. *US Pat.*, US4283255 A, 1981.
44. *European Pat.*, EP0002568 B1, 1979.
45. H. Zhao, L. Shao and J.-F. Chen, *Chem. Eng. J.*, 2010, **156**, 588-593.
46. Z.-L. Zhang, Y. Le, J.-X. Wang, H. Zhao and J.-F. Chen, *Drug Dev. Ind. Pharm.*, 2012, **38**, 1512-1520.
47. Z. Guo, M. Zhang, H. Li, J. Wang and E. Kougoulos, *J. Cryst. Growth*, 2005, **273**, 555-563.
48. M. D. Luque de Castro and F. Priego-Capote, *Ultrason. Sonochem.*, 2007, **14**, 717-724.
49. R. S. Dhumal, S. V. Biradar, S. Yamamura, A. R. Paradkar and P. York, *Eur. J. Pharm. Biopharm.*, 2008, **70**, 109-115.
50. T. T.-D. Tran, K. A. Tran and P. H.-L. Tran, *Ultrason. Sonochem.*, 2015, **24**, 256-263.
51. A. I. Cooper, *Adv. Mater.*, 2003, **15**, 1049-1059.
52. M. Türk and D. Bolten, *J. Supercrit. Fluids*, 2010, **55**, 778-785.
53. H. Zhang, J. Long and A. I. Cooper, *J. Am. Chem. Soc.*, 2005, **127**, 13482-13483.
54. B. Helfgen, M. Türk and K. Schaber, *Powder Technol.*, 2000, **110**, 22-28.
55. P. Pathak, M. J. Meziani, T. Desai and Y.-P. Sun, *J. Am. Chem. Soc.*, 2004, **126**, 10842-10843.
56. S.-D. Yeo, G.-B. Lim, P. G. Debendetti and H. Bernstein, *Biotechnol. Bioeng.*, 1993, **41**, 341-346.
57. J. W. Tom, G.-B. Lim, P. G. Debenedetti and R. K. Prud'homme, in *Supercritical Fluid Engineering Science*, eds. E. Kiran and J. F. Brennecke, American Chemical Society, Washington DC, 1992, vol. 514, ch. 19, pp. 238-257.

58. J. Bleich, B. W. Müller and W. Waßmus, *Int. J. Pharm.*, 1993, **97**, 111-117.
59. D. J. Dixon and K. P. Johnston, *J. Appl. Polym. Sci.*, 1993, **50**, 1929-1942.
60. D. J. Dixon, K. P. Johnston and R. A. Bodmeier, *AlChE J.*, 1993, **39**, 127-139.
61. E. Elizondo, S. Sala, E. Imbuluzqueta, D. González, M. Blanco-Prieto, C. Gamazo, N. Ventosa and J. Veciana, *Pharm. Res.*, 2011, **28**, 309-321.
62. N. Murillo-Cremaes, P. Subra-Paternault, J. Saurina, A. Roig and C. Domingo, *Colloid. Polym. Sci.*, 2014, **292**, 2475-2484.
63. H. Zhang, J. Lu and B. Han, *J. Supercrit. Fluids*, 2001, **20**, 65-71.
64. J. Broadhead, S. Edmond Rouan and C. Rhodes, *Drug Dev. Ind. Pharm.*, 1992, **18**, 1169-1206.
65. K. Masters, *Spray drying handbook*, John Wiley and Sons, New York, 3rd edn., 1979.
66. B. Bhandari and M. W. Woo, in *Handbook of Food Powders: Processes and Properties*, eds. B. Bhandari, N. Bansal, M. Zhang and P. Schuck, Woodhead Publishing, Camebridge, 2014.
67. A. Bohr, C. A. Ruge and M. Beck-Broichsitter, *Nanomaterial*, 2014, 183.
68. J. Salazar, R. H. Müller and J. P. Möschwitzer, *J. Pharm. Sci.*, 2013, **102**, 1636-1649.
69. C. Arpargaus, D. Rütti and M. Meuri, in *Drug Delivery Strategies for Poorly Water-Soluble Drugs*, eds. D. Douroumis and A. Fahr, John Wiley & Sons, Ltd., 2013, pp. 551-585.
70. K. Rizi, R. J. Green, M. Donaldson and A. C. Williams, *J. Pharm. Sci.*, 2011, **100**, 566-579.
71. R. Kolakovic, T. Laaksonen, L. Peltonen, A. Laukkanen and J. Hirvonen, *Int. J. Pharm.*, 2012, **430**, 47-55.
72. S. Al-Qadi, A. Grenha, D. Carrión-Recio, B. Seijo and C. Remuñán-López, *J. Control. Release*, 2012, **157**, 383-390.
73. B. Van Eerdenbrugh, L. Froyen, J. A. Martens, N. Blaton, P. Augustijns, M. Brewster and G. Van den Mooter, *Int. J. Pharm.*, 2007, **338**, 198-206.
74. A. K. Konstantinidis, W. Kuu, L. Otten, S. L. Nail and R. R. Sever, *J. Pharm. Sci.*, 2011, **100**, 3453-3470.
75. A. Saez, M. Guzmán, J. Molpeceres and M. R. Aberturas, *Eur. J. Pharm. Biopharm.*, 2000, **50**, 379-387.

76. J. Lee and Y. Cheng, *J. Control. Release*, 2006, **111**, 185-192.
77. C. Schwarz and W. Mehnert, *Int. J. Pharm.*, 1997, **157**, 171-179.
78. H. de Waard, W. L. J. Hinrichs and H. W. Frijlink, *J. Control. Release*, 2008, **128**, 179-183.
79. L. Qian and H. Zhang, *Journal of Chemical Technology & Biotechnology*, 2011, **86**, 172-184.
80. S. Deville, *Adv. Eng. Mater.*, 2008, **10**, 155-169.
81. L. Qian, E. Willneff and H. Zhang, *Chem. Commun.*, 2009, DOI: 10.1039/B905130A, 3946-3948.
82. L. Qian and H. Zhang, *Green Chem.*, 2010, **12**, 1207-1214.
83. A. Ahmed, J. Hearn, W. Abdelmagid and H. Zhang, *J. Mater. Chem.*, 2012, **22**, 25027-25035.
84. A. D. Roberts and H. Zhang, *Int. J. Pharm.*, 2013, **447**, 241-250.
85. H. Costantino, L. Firouzabadian, K. Hogeland, C. Wu, C. Beganski, K. Carrasquillo, M. Córdova, K. Griebenow, S. Zale and M. Tracy, *Pharm. Res.*, 2000, **17**, 1374-1382.
86. H. R. Costantino, L. Firouzabadian, C. Wu, K. G. Carrasquillo, K. Griebenow, S. E. Zale and M. A. Tracy, *J. Pharm. Sci.*, 2002, **91**, 388-395.
87. W. S. Cheow, M. L. L. Ng, K. Kho and K. Hadinoto, *Int. J. Pharm.*, 2011, **404**, 289-300.
88. Y. Wang, K. Kho, W. S. Cheow and K. Hadinoto, *Int. J. Pharm.*, 2012, **424**, 98-106.
89. G. Sharma, W. Mueannoom, A. B. M. Buanz, K. M. G. Taylor and S. Gaisford, *Int. J. Pharm.*, 2013, **447**, 165-170.
90. W. Mueannoom, A. Srisongphan, K. M. G. Taylor, S. Hauschild and S. Gaisford, *Eur. J. Pharm. Biopharm.*, 2012, **80**, 149-155.
91. S. Murugappan, H. P. Patil, G. Kanojia, W. ter Veer, T. Meijerhof, H. W. Frijlink, A. Huckriede and W. L. J. Hinrichs, *Eur. J. Pharm. Biopharm.*, 2013, **85**, 716-725.
92. Z. Yu, K. P. Johnston and R. O. Williams Iii, *Eur. J. Pharm. Sci.*, 2006, **27**, 9-18.
93. T. Rogers, A. Nelsen, M. Sarkari, T. Young, K. Johnston and R. Williams, III, *Pharm. Res.*, 2003, **20**, 485-493.

94. T. L. Rogers, A. C. Nelsen, J. Hu, J. N. Brown, M. Sarkari, T. J. Young, K. P. Johnston and R. O. Williams Iii, *Eur. J. Pharm. Biopharm.*, 2002, **54**, 271-280.
95. J. Hu, T. Rogers, J. Brown, T. Young, K. Johnston and R. Williams Iii, *Pharm. Res.*, 2002, **19**, 1278-1284.
96. H. Zhang and A. I. Cooper, *Soft Matter*, 2005, **1**, 107-113.
97. H. Zhang, D. Wang, R. Butler, N. L. Campbell, J. Long, B. Tan, D. J. Duncalf, A. J. Foster, A. Hopkinson, D. Taylor, D. Angus, A. I. Cooper and S. P. Rannard, *Nature Nanotechnology*, 2008, **3**, 506-511.
98. S. D. Kimmins and N. R. Cameron, *Adv. Funct. Mater.*, 2011, **21**, 211-225.
99. L. Qian, A. Ahmed, A. Foster, S. P. Rannard, A. I. Cooper and H. Zhang, *J. Mater. Chem.*, 2009, **19**, 5212-5219.
100. W. Abdelwahed, G. Degobert and H. Fessi, *Int. J. Pharm.*, 2006, **309**, 178-188.
101. N. Sultana and M. Wang, *J. Mater. Sci. Mater. Med.*, 2008, **19**, 2555-2561.
102. T. Wang, N. Wang, T. Wang, W. Sun and T. Li, *Chem. Phys. Lipids*, 2011, **164**, 151-157.
103. N. Grant and H. Zhang, *J. Colloid Interface Sci.*, 2011, **356**, 573-578.
104. L. Qian and H. Zhang, *Chem. Commun.*, 2013, **49**, 8833-8835.
105. T. O. McDonald, M. Giardiello, P. Martin, M. Siccardi, N. J. Liptrott, D. Smith, P. Roberts, P. Curley, A. Schipani, S. H. Khoo, J. Long, A. J. Foster, S. P. Rannard and A. Owen, *Adv. Healthc. Mater.*, 2014, **3**, 400-411.
106. M. Giardiello, T. O. McDonald, P. Martin, A. Owen and S. P. Rannard, *J. Mater. Chem.*, 2012, **22**, 24744-24752.
107. M. Giardiello, T. O. McDonald, J.-S. Lee, A. D. Roberts, A. Owen and S. P. Rannard, *Green Chem.*, 2013, **15**, 1590-1599.
108. D. J. McClements, *Food Emulsions: Principles, Practices, and Techniques*, CRC Press, 2nd edn., 2004.
109. C. Washington, *Adv. Drug Del. Rev.*, 1996, **20**, 131-145.
110. M. Trotta, M. Gallarate, F. Pattarino and S. Morel, *J. Control. Release*, 2001, **76**, 119-128.
111. H. Sah, *J. Control. Release*, 1997, **47**, 233-245.

112. J. H. Schulman, W. Stoeckenius and L. M. Prince, *J. Phys. Chem.*, 1959, **63**, 1677-1680.
113. T. Hoar and J. Schulman, *Nature*, 1943, **152**, 102-103.
114. I. Danielsson and B. Lindman, *Colloids and Surfaces*, 1981, **3**, 391-392.
115. L. Djordjevic, M. Primorac, M. Stupar and D. Krajisnik, *Int. J. Pharm.*, 2004, **271**, 11-19.
116. M. Kreilgaard, E. J. Pedersen and J. W. Jaroszewski, *J. Control. Release*, 2000, **69**, 421-433.
117. A. C. Sintov and L. Shapiro, *J. Control. Release*, 2004, **95**, 173-183.
118. U. Schmalfuß, R. Neubert and W. Wohlrab, *J. Control. Release*, 1997, **46**,279-285.
119. Y.-S. Rhee, J.-G. Choi, E.-S. Park and S.-C. Chi, *Int. J. Pharm.*, 2001, **228**, 161-170.
120. M. B. Delgado-Charro, G. Iglesias-Vilas, J. Blanco-Méndez, M. A. López-Quintela, J.-P. Marty and R. H. Guy, *Eur. J. Pharm. Biopharm.*, 1997, **43**, 37-42.
121. Z.-G. Gao, H.-G. Choi, H.-J. Shin, K.-M. Park, S.-J. Lim, K.-J. Hwang and C.-K. Kim, *Int. J. Pharm.*, 1998, **161**, 75-86.
122. Y.-M. Yin, F.-D. Cui, C.-F. Mu, M.-K. Choi, J. S. Kim, S.-J. Chung, C.-K. Shim and D.-D. Kim, *J. Control. Release*, 2009, **140**, 86-94.
123. C.-K. Kim, Y.-J. Cho and Z.-G. Gao, *J. Control. Release*, 2001, **70**, 149-155.
124. G. W. Mark, W. P. Colin, J. M. Brian and S. M. Frank, in *Phenomena in Mixed Surfactant Systems*, ed. J. F. Scamehorn, American Chemical Society, Washington DC, 1986, vol. 311, ch. 18, pp. 242-255.
125. H. Shen and M. Zhong, *J. Pharm. Pharmacol.*, 2006, **58**, 1183-1191.
126. B. K. Kang, J. S. Lee, S. K. Chon, S. Y. Jeong, S. H. Yuk, G. Khang, H. B. Lee and S. H. Cho, *Int. J. Pharm.*, 2004, **274**, 65-73.
127. R. W. Horne, A. D. Bangham and V. P. Whittaker, *Nature*, 1963, **200**, 1340-1340.
128. A. D. Bangham and R. W. Horne, *Nature*, 1962, **196**, 952-953.
129. A. D. Bangham and R. W. Horne, *J. Mol. Biol.*, 1964, **8**, 660-IN610.
130. R. Fielding, *Clin. Pharmacokinet.*, 1991, **21**, 155-164.

131. M. Gulati, M. Grover, S. Singh and M. Singh, *Int. J. Pharm.*, 1998, **165**, 129-168.
132. R. L. Juliano and D. Stamp, *Biochem. Pharmacol.*, 1978, **27**, 21-27.
133. K. Iwanaga, S. Ono, K. Narioka, M. Kakemi, K. Morimoto, S. Yamashita, Y. Namba and N. Oku, *J. Pharm. Sci.*, 1999, **88**, 248-252.
134. D. Stanimirovic, M. Markovic, D. Micic, M. Spatz and B. Mrsulja, *Neurochem. Res.*, 1994, **19**, 1473-1478.
135. M. M. Gaspar, R. Perez-Soler and M. E. M. Cruz, *Cancer Chemother. Pharmacol.*, 1996, **38**, 373-377.
136. C. D. Oja, S. C. Semple, A. Chonn and P. R. Cullis, *Biochim. Biophys. Acta*, 1996, **1281**, 31-37.
137. A. Chonn, S. C. Semple and P. R. Cullis, *J. Biol. Chem.*, 1992, **267**, 18759-18765.
138. G. L. Scherphof, J. A. N. Dijkstra, H. H. Spanjer, J. T. P. Derksen and F. H. Roerdink, *Ann. N.Y. Acad. Sci.*, 1985, **446**, 368-384.
139. M. J. Turk, J. A. Reddy, J. A. Chmielewski and P. S. Low, *Biochim. Biophys. Acta*, 2002, **1559**, 56-68.
140. A. N. Lukyanov, T. A. Elbayoumi, A. R. Chakilam and V. P. Torchilin, *J. Control. Release*, 2004, **100**, 135-144.
141. J. W. Park, D. B. Kirpotin, K. Hong, R. Shalaby, Y. Shao, U. B. Nielsen, J. D. Marks, D. Papahadjopoulos and C. C. Benz, *J. Control. Release*, 2001, **74**, 95-113.
142. T. M. Allen, C. Hansen, F. Martin, C. Redemann and A. Yau-Young, *Biochim. Biophys. Acta*, 1991, **1066**, 29-36.
143. E. Buhleier, W. Wehner and F. Vögtle, *Synthesis*, 1978, 155–158
144. *US Pat.*, US4360646 A, 1982.
145. G. R. Newkome, Z. Yao, G. R. Baker and V. K. Gupta, *J. Org. Chem.*, 1985, **50**, 2003-2004.
146. D. A. Tomalia, H. Baker, J. Dewald, M. Hall, G. Kallos, S. Martin, J. Roeck, J. Ryder and P. Smith, *Polym. J.*, 1985, **17**, 117-132.
147. D. A. Tomalia, A. M. Naylor and W. A. Goddard, *Angew. Chem. Int. Ed.*, 1990, **29**, 138-175.

148. E. M. M. de Brabander-van den Berg and E. W. Meijer, *Angew. Chem. Int. Ed.*, 1993, **32**, 1308-1311.
149. C. J. Hawker and J. M. J. Frechet, *J. Am. Chem. Soc.*, 1990, **112**, 7638-7647.
150. Y. Li, Y. D. Tseng, S. Y. Kwon, L. d'Espaux, J. S. Bunch, P. L. McEuen and D. Luo, *Nat. Mater.*, 2004, **3**, 38-42.
151. K. S. Soppimath, T. M. Aminabhavi, A. R. Kulkarni, W. E. Rudzinski, *J. Control. Release*, 2001, **70**, 1-20.
151. IUPAC. Compendium of Chemical Terminology, 2nd ed. (the "Gold Book") https://goldbook.iupac.org/html/B/B00683.html, (accesed August 2017).
152. A. Noshay and J. E. McGrath, *Block Copolymers Overview and Critical Survey*, Academic Press, New York, 1977.
153. S. E. Webber, P. Munk and Z. Tuzar, eds., *Solvents and self-organization of polymers*, Springer Science & Business Media, Netherlands, 2012.
154. M. Yokoyama, T. Okano, Y. Sakurai, H. Ekimoto, C. Shibazaki and K. Kataoka, *Cancer Res.*, 1991, **51**, 3229-3236.
155. M. Yokoyama, G. S. Kwon, T. Okano, Y. Sakurai, T. Seto and K. Kataoka, *Bioconjugate Chem.*, 1992, **3**, 295-301.
156. M. Yokoyama, S. Inoue, K. Kataoka, N. Yui and Y. Sakurai, *Makromol. Chem., Rapid Commun.*, 1987, **8**, 431-435.
157. A. Wilkinson, *IUPAC. Compendium of Chemical Terminology*, Blackwell Scientific Publications, Oxford, 2 edn., 1997.
158. A. Rösler, G. W. M. Vandermeulen and H.-A. Klok, *Adv. Drug Del. Rev.*, 2012, **64, Supplement**, 270-279.
159. C. Feng, Y. Li, D. Yang, J. Hu, X. Zhang and X. Huang, *Chem. Soc. Rev.*, 2011,**40**, 1282-1295.
160. J. Rzayev, *Macromolecules*, 2009, **42**, 2135-2141.
161. Y. Zhang, Q. Yin, H. Lu, H. Xia, Y. Lin and J. Cheng, *ACS Macro Letters*, 2013, **2**, 809-813.
162. A. Cambón, A. Rey-Rico, D. Mistry, J. Brea, M. I. Loza, D. Attwood, S. Barbosa, C. Alvarez-Lorenzo, A. Concheiro, P. Taboada and V. Mosquera, *Int. J. Pharm.*, 2013, **445**, 47-57.

163. T.-H. Tran, C. T. Nguyen, L. Gonzalez-Fajardo, D. Hargrove, D. Song, P. Deshmukh, L. Mahajan, D. Ndaya, L. Lai, R. M. Kasi and X. Lu, *Biomacromolecules*, 2014, **15**, 4363-4375.
164. L. Y. Qiu and Y. H. Bae, *Biomaterials*, 2007, **28**, 4132-4142.
165. A. M. Lowman, M. Morishita, M. Kajita, T. Nagai and N. A. Peppas, *J. Pharm. Sci.*, 1999, **88**, 933-937.
166. J. M. Ren, T. G. McKenzie, Q. Fu, E. H. H. Wong, J. Xu, Z. An, S. Shanmugam, T. P. Davis, C. Boyer and G. G. Qiao, *Chem. Rev.*, 2016, **116**, 6743–6836.
167. H. Gao and K. Matyjaszewski, *Macromolecules*, 2006, **39**, 4960–4965.
168. W. Wu, J. Liu, S. Cao, H. Tan, J. Li, F. Xu and X. Zhang, *Int. J. Pharm.*, 2011, **416**, 104-109.
169. M. A. R. Meier, J.-F. Gohy, C.-A. Fustin and U. S. Schubert, *J. Am. Chem. Soc.*, 2004, **126**, 11517-11521.
170. K. Khanna, S. Varshney and A. Kakkar, *Polymer Chemistry*, 2010, **1**, 1171-1185.
171. S. Pispas, N. Hadjichristidis, I. Potemkin and A. Khokhlov, *Macromolecules*, 2000, **33**, 1741-1746.
172. Z. Li, E. Kesselman, Y. Talmon, M. A. Hillmyer and T. P. Lodge, *Science*, 2004, **306**, 98-101.
173. C. Gao and D. Yan, *Prog. Polym. Sci.*, 2004, **29**, 183-275.
174. A. Hult, M. Johansson and E. Malmström, in *Branched Polymers II*, ed. J. Roovers, Springer Verlag, Berlin, 1999, ch. 1, pp. 1-34.
175. Y. Zheng, S. Li, Z. Weng and C. Gao, *Chem. Soc. Rev.*, 2015, **44**, 4091-4130.
176. Y. H. Kim and O. W. Webster, *Polym. Prepr.*, 1988, **29**, 310-311.
177. J. M. J. Fréchet, M. Henmi, I. Gitsov, S. Aoshima, M. Leduc and R. B. Grubbs, *Science*, 1995, **269**, 1080-1083.
178. M. Suzuki, A. Li and T. Saegusa, *Macromolecules*, 1992, **25**, 7071-7072.
179. H. T. Chang and J. M. J. Fréchet, *J. Am. Chem. Soc.*, 1999, **121**, 2313-2314.
180. H. Sun, C. P. Kabb and B. S. Sumerlin, *Chem. Sci.*, 2014, **5**, 4646-4655.
181. A. M. Caminade, D. Yan and D. K. Smith, *Chem. Soc. Rev.*, 2015, **44**, 3870-3873.
182. I. N. Kurniasih, J. Keilitz and R. Haag, *Chem. Soc. Rev.*, 2015, **44**, 4145-4164.

183. C. Gao and D. Yan, *Chin. Sci. Bull.*, 2000, **45**, 1760-1764.
184. A. Sunder, R. Hanselmann and H. Frey, *Macromolecules*, 2000, **33**, 309-314.
185. S. Maier, A. Sunder, H. Frey and R. Müllhaupt, *Macromol. Rapid Commun.*, 2000, **21**, 226-230.
186. M. Okazaki, M. Murato, Y. Kawaguchi and N. Tsubokawa, *J. Appl. Polym. Sci.*, 2001, **80**, 573-579.
187. H. J. Kim, J. H. Moon and J. W. Park, *J. Cooloid Interface Sci.*, 200, **227**, 247-249.
188. H. M. Weimer, J. M. J. Fréchet and I. Gitsov, *J. Polym. Sci, Part A: Polym. Chem.*, 1998, **36**, 955-970.
189. C. Lach, R. H. Hanselmann, H. Frey and R. Müllhaupt, *Macromol. Rapid Commun.*, 1998, **19**, 461-465.
190. P. Nesvadba, in *Encyclopedia of Radicals in Chemistry, Biology and Materials*, ed. C. Chatgilialoglu and A. Studer, John Wiley and Sons, Inc, New Jersey, US, 2012, pp 1-36.
191. H. Morawetz, Polymers – The Origins and Growth of a Science, John Wiley & Sons, New York, 1985.
192. J. P. A. Heuts, in *Handbook of Radical Polymerisation*, ed. K. Matyjaszewski and T. P. Davis, John Wiley & Sons, Inc., Hoboken, 2003, Chapter 1, pp 1-76.
193. G. Moad and D. H. Solomon, *The Chemistry of Radical Polymerisation*, Elsevier science, Oxford, 2006.
194. J. L. Eguiburu and M. J. Fernandez-Berridi, *Polymer*, 1996, **37**, 3615-3622.
195. Y. Shiraia, K. Kawatsuraa and N. Tsubokawab, *Prog. Org. Coat.*, 1999, **36**, 217-224.
196. G. K. Raghuraman, J. Rühe and R. Dhamodharan, *J. Nanopart. Res*, 2008, **10**, 415-427.
197. J. M. Asua, *Prog. Polym. Sci.*, 2002, **27**, 1283-1346.
198. K. Landfester, *Angew. Chem. Int. Ed.*, 2009, **48**, 4488 – 4507.
199. K. Haraguchi, *Curr. Opin. Solid State Mater. Sci.*, 2007, **11**, 47-54.
200. G. Moad, E. Rizzardo and S. H. Thang, *Aust. J. Chem.*, 2005, **58**, 379–410.
201. G. Moad, J. Chiefari, J. Krstina, A. Postma, R. T. A. Mayadunne, E. Rizzardo, S. H. Thang, *Polym. Int.* 2000, **49**, 993-1001.

202. K. Matyjaszewski and J. Xia, *Chem. Rev.*, 2001, **101**, 2921-2990.
203. J.-S. Wang and K. Matyjaszewski, *J. Am. Chem. Soc*., 1995, **117**, 5614–5615.
204. J. Chiefari , Y. K. Chong , F. Ercole , J. Krstina , J. Jeffery , T. P. T. Le , R. T. A. Mayadunne , G. F. Meijs , C. L. Moad , G. Moad , E. Rizzardo and S. H. Thang, *Macromolecules*, 1998, **31,** 5559–5562.
205. K. Matyjaszewski, *Macromolecules*, 2012, **45**, 4015–4039.
206. K. Matyjaszewski and N. V. Tsarevsky, *Nat. Chem.*, 2009, **1**, 276-288.
207. V. Coessens, T. Pintauer and K. Matyjaszewski, *Prog. Polym. Sci.*, 2001, **26**, 337–377.
208. D. Bontempo, R. C. Li, T. Ly, C. E. Brubaker and H. D. Maynard, *Chem. Commun.* ,2005 , **37** , 4702-4704.
209. D. Bontempo and H. D. Maynard, *J. Am. Chem. Soc.*, 2005, **127**, 6508-6509.
210. J. Khandare and T. Minko, *Prog. Polym. Sci.*, 2006, **31**, 359-397.
211. M. J. Vicent, F. Greco, R. I. Nicholson, A. Paul, P. C. Griffiths and R. Duncan, *Angew Chem Int Edit*, 2005, **44**, 4061-4066.
212. Y. Bae, S. Fukushima, A. Harada and K. Kataoka, *Angew. Chem. Int. Ed.*, 2003, **42**, 4640-4643.
213. A. Harada and K. Kataoka, *Prog Polym Sci*, 2006, **31**, 949-982.
214. J. Oh, R. Drumright, D. Siegwart and K. Matyjaszewski, *Prog Polym Sci*, 2008, **33**, 448-477
215. J. K. Oh, D. I. Lee and J. M. Park, *Prog Polym Sci*, 2009, **34**, 1261-1282.
216. J. Wu and A. Eisenberg, *J Am Chem Soc*, 2006, **128**, 2880-2884.
217. V. Buetuen, S. Liu, J. V. M. Weaver, X. Bories-Azeau, Y. Cai, S. P. Armes, *React Funct Polym*, 2006, **66**, 57-165.
218. D. J. Siegwarta., J. K. Oh and K. Matyjaszewski, *Prog Polym Sci*, 2012, **37**, 18-37.
219. C. Barner-Kowollik, T. P. Davis, J. P. A. Heuts, M. H. Stenzel, P. Vana and M. Whittaker, *J. Polym. Sci. Part A: Polym. Chem.*, 2003, **41**, 365-375.
220. M. A. Tasdelen, M. U. Kahveci and Y. Yagci, *Prog Polym Sci*, 2011, **36**, 455-567.
221. P. J. Roth, C. Boyer, A. B. Lowe and T. P. Davis, *Macromol. Rapid Commun.*, 2011, **32**, 1123-1143.
222. A. Gregory and M. H. Stenze, *Prog Polym Sci*, 2012, **37**, 38-105.

223. G. Moad, R. T. A. Mayadunne, E. Rizzardo, M. Skidmore and S. H. Thang, *Macromol Symp*, 2003, **192**, 1-12.
224. C. Barner-Kowollik, T. P. Davis and M. H. Stenzel, *Aust. J. Chem*, 2006, **59**, 719-727.
225. B. D. Fairbanks, P. A.Gunatillake and L. Meagher, *Adv. Drug Deliv. Rev.*, 2015, **91**, 141-152.
226. A. W. York, S. E. Kirkland and C. L. McCormick, *Adv. Drug Deliv. Rev.*, 2008, **60**, 1018-1036.
227. M. H. Stenzel, *Chem. Comm.*, 2008, **30**, 3486-3503.
228. ICH, ICH Harmonised Tripartite Guideline-Impurities: guideline for residual solvents Q3C (R5), http://www.ich.org/fileadmin/Public_Web_Site/ICH_Products/Guidelines/Quality/Q3C/Step4/Q3C_R5_Step4.pdf, (accessed September, 2015).
229. C. Witschi and E. Doelker, *Eur. J. Pharm. Biopharm.*, 1997, **43**, 215-242.
230. K. Grodowska and A. Parczewski, *Acta Pol. Pharm.*, 2010, **67**, 3-12.
231. T. F. Tadros, *Applied surfactants: principles and applications*, WILEY-VCH Verlag GmbH & Co. KGaA, Weinheim, 2005.
232. J. Deng, L. Huang and F. Liu, *Int. J. Pharm.*, 2010, **390**, 242-249.
233. S. V. Dalvi and R. N. Dave, *Ind. Eng. Chem. Res.*, 2009, **48**, 7581-7593.
234. S. S. Talmage, *Environmental and human safety of major surfactants: alcohol ethoxylates and alkylphenol ethoxylates*, CRC Press, Boca Raton, Florida, 1994.
235. M. A. Lewis, *Ecotoxicol. Environ. Saf.*, 1990, **20**, 123-140.
236. J. K. Lee, D. B. Kim, J. I. Kim and P. Y. Kim, *Toxicol. In Vitro*, 2000, **14**, 345-349.
237. H. E. J. Hofland, J. A. Bouwstra, M. Ponec, H. E. Boddé, F. Spies, J. C. Verhoef and H. E. Junginger, *J. Control. Release*, 1991, **16**, 155-167.
238. S. L. Raghavan, A. Trividic, A. F. Davis and J. Hadgraft, *Int. J. Pharm.*, 2001, **212**, 213-221.
239. Y. Dong and S.-S. Feng, *Biomaterials*, 2004, **25**, 2843-2849.
240. K. A. Woodrow, Y. Cu, C. J. Booth, J. K. Saucier-Sawyer, M. J. Wood and W. Mark Saltzman, *Nat. Mater.*, 2009, **8**, 526-533.

241. Y. Hu, X. Jiang, Y. Ding, H. Ge, Y. Yuan and C. Yang, *Biomaterials*, 2002, **23**, 3193-3201.
242. R. Rupp, S. L. Rosenthal and L. R. Stanberry, *Int. J. Nanomedicine*, 2007, **2**, 561-566.
243. A. Hafner, J. Lovrić, G. P. Lakoš and I. Pepić, *Int. J. Nanomedicine*, 2014, **9**, 1005-1023.
244. Y. Matsumura and K. Kataoka, *Cancer Sci.*, 2009, **100**, 572-579.
245. N. Okamoto, Y. Ito, Y. Kawakami, T. Kurimoto, N. Nagai and T. Yamashita, *WO Pat.*, WO2009017259 A1, 2009.
246. A. S. Nagi, *US Pat.*, US5989591, 1999.
247. C. P. Dorn, J. J. Hale, M. Maccoss, S. G. Mills, T. Ladduwahetty and S. K. Shah, *WO Pat.*, WO1994000440 A1, 1994.
248. S. Anker and J. Springer, *WO Pat.*, WO2009056256 A1, 2009.
249. D. Hovey, J. Pruitt and T. Ryde, *US Pat.*, US7101576 B2, 2006.
250. T. A. Ryde, E. E. Gustow, S. B. Ruddy, R. Jain, R. Patel, M. J. Wilkins and N. P. Ryde, *US Pat.*, US20080241070 A1, 2008.
251. P. Stark, S. Cunningham and J. Moodley, *CA Pat.*, CA2558783 A1, 1999.
252. A. L. Zeitlin, M. M. Darian and D. L. Stirling, *US Pat.*, US20130109719 A1, 2013.
253. A. M. Mehta, A. L. Zeitlin, M. M. Dariani, *US Pat.*, US7431944 B2, 2008.
254. G. W. Pace, A. K. Mishra, R. A. Snow, I. Parikh, P. W. Guivarch, *US Pat.*, US6696084 B2, 2004.
255. N. P. Desai, A. Yang, S. X. Ci, T. De, V. Trieu, P. Soon-Shiong, G. B. Beals and Q. Yao, *CA Pat.*, CA2509365 C, 2012.
256. W.-T. Bae, S.-W. Jang, J.-H. Kim, J.-W. Kwon and H.-S. Wang, *WO Pat.*, WO2001041765 A1, 2001.
257. R. D. Gordon, P. Holm, A.-M. Lademann and T. Norling, *US Pat.*, US8685998 B2, 2014.
258. H. Viernstein, S. Toegel and R. Schueller, *European Pat.*, EP2643022 A1, 2013.
259. B. De Corte, M. R. De Jonge, J. Heeres, C. Y. Ho, P. A. J. Janssen, R. W. Kavash, L. M. H. Koymans, M. J. Kukla, D. W. Ludovici, K. J. A. Van Aken and K. J. L. M. Andries, *US Pat.*, US8530655 B2, 2013.

260. C. B. Jones and J. H. Platt, *US Pat.*, US5908869 A, 1999.
261. W. Brox, A. Meinzer and H. Zande, *US Pat.*, US7078054 B2, 2006.
262. D. J. Kempf, D. W. Norbeck, J. W. Erickson, L. M. Codacovi, H. L. Sham and J. J. Plattner, *European Pat.*, EP0402646 B1, 1998.
263. O. Pacheco, E. Russo and V. Russo, *WO Pat.*, WO2005007069 A2, 2005.
264. A. Acheampong, D. D. Tang-Liu, J. N. Chang, D. F. Power, *US Pat.*, US8633162 B2, 2014.
265. M. Kimura, S. Yasueda, M. Yamaguchi and K. Inada, *US Pat.*, US6114319, 2000.
266. A. H. Huang and S. Krishnan, *US Pat.*, US4927571, 1990.
267. B. Schoentjes, S. Descamps, N. C. I. Amblard, *WO Pat.*, WO2010089327 A2, 2010.
268. A. F. Vikbjerg, S. A. Petersen, F. Melander, J. R. Henriksen and K. Jorgensen, *US Pat.*, US20120009243 A1, 2012.
269. S. Kim and S. B. Howell, *US Pat.*, US5723147, 1998.
270. C. A. Presant, R. T. Proffitt, R. L. Teplitz, L. E. Williams and G. W. Tin, *US Pat.*, US5441745, 1995.
271. R. Gluck and R. Mischler, *US Pat.*, US5565203, 1996.

Chapter 2

Formulation of drug nanoparticles via emulsion-freeze-drying

This Chapter is based on the publications

U. Wais, A. W. Jackson, Y. Zuo, Y. Xiang, T. He and H. Zhang, "Drug nanoparticles by emulsion-freeze-drying via the employment of branched block copolymer nanoparticles." *J. Control. Release*, 2016, **222**, 141-150.

and

U. Wais, M. M. Nawrath, A. W. Jackson and H. Zhang, "Triclosan nanoparticles via emulsion-freeze-drying for enhanced anti-microbial activity" *submitted to Colloid and Polymer Science*

2.1. Introduction

The formulation of nanoparticles by bottom-up techniques is nowadays well established and applied in industry *e.g.* solvent-antisolvent precipitation (SAS),[1-3] high gravity reactive precipitation (HGRP),[4,5] supercritical fluid precipitation [6-9] and spray drying.[10-12] However, most bottom-up techniques suffer from poor particle stabilisation and undesirable Ostwald-Ripening. An established way to prevent this is to use stabilising agents *i.e.* surfactants, that carry the risk of being potentially harmful to the body and toxic to the environment.[13,14] As an alternative to surfactants, amphiphilic polymers can be used to stabilise particles. These polymers can, due to modern polymerisation techniques, be synthesised with high structural precision and be composed of biocompatible monomers like PLA, PLG or chitosan.[15-17] Polymers, in contrast to surfactants, who form a charged layer around the particles *i.e.* ionic stabilisation, prevent collision and agglomeration by steric stabilisation [18] and can also be used to form scaffolds to stabilise nanoparticles when dried, which leads to prolonged shelf life.[19,20]

Our group previously reported the use of emulsion freeze-drying to form organic or drug nanoparticles *in situ* in water-soluble porous polymer.[20] Emulsions were successfully stabilised by polymers and surfactants. The polymer scaffold obtained after freeze-drying prevents the nanoparticles from aggregating in the solid state, ensuring a long storage time. The nanoparticles could readily be released by re-suspending the polymer scaffold in water to produce aqueous nanoparticle dispersion.[20,21] Both polymer (*e.g.*, poly(vinyl alcohol)) and surfactant (*e.g.*, sodium dodecyl sulphate) were required to form the emulsions, produce the porous scaffold, and stabilise the nanoparticles in aqueous suspensions. It was furthermore possible to a generate porous polymer scaffold by freeze drying and then employ a solvent evaporation approach to form organic/drug nanoparticles directly in the porous polymeric scaffold.[19,22] Aqueous nanoparticles dispersion could be prepared similarly. In both approaches, the use of both polymer and surfactant was important in forming stable aqueous nanoparticle dispersions. This, however, can result in low loading of drug compounds in the formulations. A formulation that utilises a biocompatible polymer acting both as scaffold and surfactant would be advantageous in improving drug loading and reducing the formulation complexity.

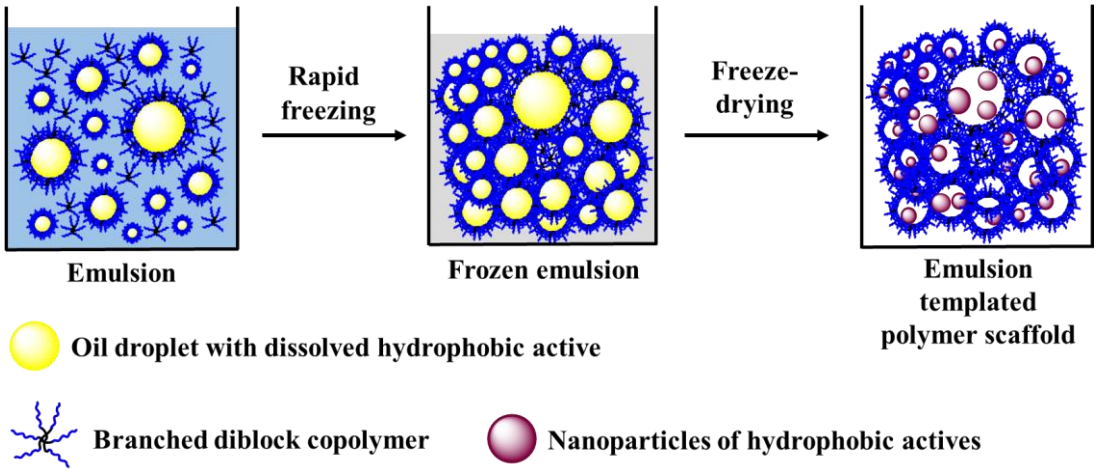

Scheme 2.1. Schematic representation of the emulsion freeze-drying process using branched diblock copolymers.

This Chapter describes the formation of hydrophobic drug nanoparticles *via* emulsion freeze-drying (Scheme 2.1.). The emulsions were initially formed using different amphiphilic branched polymers of different cores, short PEG arms and two different solvents, cyclohexane and *o*-xylene. The emulsions were subsequently freeze-dried to obtain nanoparticles of two different hydrophobic active, Oil Red O (OR), an organic dye and indomethacin (IMC). After isolating the best polymer and conditions, this method was used to form triclosan nanoparticles, which could readily be re-suspended in aqueous medium and tested on *Candida albicans* for enhanced microbial activity. Afterwards a series using PNIPAm, with varying cross-linkage equivalences and longer PEG chains was produced to investigate the influence of cross-linkage on emulsion stability and particle size. To that end nanoparticle of IMC and OR using *o*-xylene and cyclohexane respectively as oil phase, were formed and evaluated.

2.2. Experimental

2.2.1 Chemicals and reagents

Deionized water was prepared using an AquaMAX-Basic 321 DI water purification system. Oil Red O (OR) dye content ≥ 75 %, ketoprofen ≥ 98 % (TLC), ibuprofen ≥ 98 % (HPLC), indomethacin ≥ 99 % (TLC), triclosan, *o*-xylene ≥ 98 % (GC), sodium acetate, *N*-isopropylacrylamide (NIPAm, 97 %), styrene (S), divinyl benzene (DVB), butyl methacrylate (BMA), di(ethylene glycol) dimethacrylate (DEGDMA) and dodecanethiol (DDT, 98 %) were purchased from Sigma-Aldrich. Macro-azo poly(ethylene glycol) initiator was obtained from Wako Pure Chemical Industries Ltd

(Osaka, Japan). Cyclohexane (extra pure), dimethylformamide (DMF, HPLC grade) and *o*-xylene were purchased from Fisher scientific and VWR international respectively. All other solvents were reagent grade and purchased from Sigma-Aldrich. All chemicals were used as received.

2.2.2. Characterisation

The emulsions were imaged on an Olympus CX41 microscope with Plan magnifying lenses. CellSens entry imaging software by Olympus was used for size measurements. ^{1}H NMR spectra were recorded on Bruker 400 Ultra Shield spectrometer. GPC was conducted on a Viscotek TDAmax consisting of a GPCmax integrated solvent and sample delivery module, a TDA 302 Triple Detector Array, and OmniSEC software. 2 x PLgel 5 µm Mixed-C (200-2,000,000) columns were applied in sequence for separation. DMF was used as the eluent at 0.8 mL/min with column and detector temperature at 50 °C, molecular weight values were determined against poly(styrene) standards. Particle size was measured by dynamic laser scattering (DLS) analysis on a Malvern Zetasizer Nanoseries at 25 °C from Malvern Instruments. Cryo-Transmission Electron Microscopy (Cryo-TEM). Cryo-TEM to investigate size of the obtained nanoparticles was carried out using a vitrification robot (FEI Vitrobot MARK IV). All samples were prepared at room temperature and 100 % humidity with blotting time of 2 and blot force of 1. The samples (5 µL) were applied onto a grid (Quantifoil, R2/2, Holey carbon film, freshly glow-discharged prior to use at 20mA for 30 sec. without dilution. Excess sample was blotted away with filter paper to leave a thin film on the grid before being vitrified in liquid ethane. Cryo TEM measurements were performed on FEI Titan Krios equipped with automated sample loader and Field Emission Gun (FEG) operating at 300 kV. Images were recorded with Falcon II camera (4X4) with magnification of 29000 and pixel size of 2.873. Scanning electron microscope (SEM) images were obtained using a Hitachi S-4800 SEM. The samples were coated with gold prior to imaging on an Emitech K550X Automated Sputter Coater. The freeze-dried samples were cut into thin slices and carefully mounted to the SEM stud using double adhesive carbon tape. For aqueous nanoparticles suspension, a drop of the suspension was deposited on a clean SEM stud and the solvent was left to evaporate before coating with gold. The cyro-transmission electron microscopic (cryo-TEM) analysis was performed on Tecnai G2 Spirit - T12 with 120 kV

acceleration made by FEI, Hillsboro, USA. Powder x-ray diffraction (PXRD) data was collected on a PanalayticalX'Pert Pro Multi-Purpose Diffractometer in high-throughput transmission geometry. Cu Kα Radiation was used with Λ=1.541 Å and a divergence slit of 0.76 mm. Samples were pressed in a well of an aluminium plate and scanned at 40 kV and 40 mA over 5-50 ° 2θ with a scan time of 60 min and a step size of 0.0131°.

*2.2.3. Synthesis of branched poly(ethylene glycol)-b-Poly(N-isopropylacrylamide) (PEG_{45}-b-($PNIPAm_{60}$-co-$EDAm_{0.8}$)-b-PEG_{45}) (**1**)*

Typically, the radical macro-initiator poly(ethylene glycol) dimer (4 kDa, 2 g, 0.5 mmol, 1 eq), *N*-isopropylacrylamide (3.4 g, 30 mmol, 30 eq per PEG chain), ethylene diacrylamide (67 mg, 0.4 mmol, 0.4 eq per PEG chain) and dodecanethiol (40.5 mg, 0.2 mmol, 0.2 eq per PEG chain) were transferred into a schlenk tube fitted with a magnetic stirrer bar and *N*,*N*-dimethylformamide (DMF,20 mL) added. The reaction mixture was degassed by three freeze-pump thaw cycles and the vessel was backfilled with N_2. The reaction mixture was then placed in an oil bath at 70 °C and the polymerisation was quenched by rapid cooling after 16 h. The reaction mixture was dissolved in a minimal amount of tetrahydrofuran (THF) and added dropwise to a large excess of ice-cold diethyl ether. The precipitation was repeated once more before the desired branched copolymer was obtained as a white solid (2.7 g, theoretical M_w = 10900 g/mol). Yield = 50 %. ^{1}H-NMR were measured in $CDCl_3$ (400 MHz): 1.19 ppm (s, 3H, HN-C<u>H</u>$_3$), 1.21 – 1.60 ppm (m, 2H, PEG-C<u>H</u>$_2$), 1.66 – 2.13 ppm (m, 1H, PEG-CH$_2$-C<u>H</u>-C=O), 3.64 ppm (s, 4H, PEG), 4.03 ppm (s, 1H, -N<u>H</u>).

*2.2.4. Synthesis of branched poly(ethylene glycol)-b-poly(butyl methacrylate) (PEG_{45}-b-($PBMA_{50}$-co-$DEGDMA_{0.7}$)-b-PEG_{45}) (**2**)*

Typically, the radical macro-initiator poly(ethylene glycol) dimer (4 kDa, 2 g, 0.5 mmol, 1 eq), *n*-Butyl methacrylate (4.2 g, 30 mmol, 30 eq per PEG chain), Diethylene Glycol Dimethacrylate (96 mg, 0.4 mmol, 0.4 eq per PEG chain) and dodecanethiol (40.5 mg, 0.2 mmol, 0.2 eq per PEG chain) were transferred into a schlenk tube fitted with a magnetic stirrer bar and *N*,*N*-dimethylformamide (DMF, 20 mL) added. The reaction mixture was degassed by three freeze-pump thaw cycles and the vessel was backfilled with N_2. The reaction mixture was then placed in an oil bath at 70 °C

and the polymerisation was quenched by rapid cooling after 16 h. The reaction mixture was dissolved in a minimal amount of tetrahydrofuran (THF) and added dropwise to a large excess of ice-cold petroleum ether (60/80). The precipitation was repeated once more before the desired branched copolymer was obtained as a white solid (3.9 g, theoretical M_w = 11270 g/mol). Yield = 70 %. ^{1}H-NMR were measured in $CDCl_3$ (400 MHz): 0.83 ppm (s, 3H, O=C-C-C<u>H</u>$_3$), 0.91 ppm (s, 3H, O=C-CH$_2$-CH$_2$-CH$_2$-C<u>H</u>$_3$), 1.36 ppm (d, 2H, O=C-CH$_2$-CH$_2$-C<u>H</u>$_2$-CH$_3$), 1.57 ppm (d, 2H, O=C-CH$_2$-C<u>H</u>$_2$-CH$_2$-CH$_3$), 1.78 ppm (m, 2H, PEG-C<u>H</u>$_2$-CH$_3$), 3.61 ppm (s, 4H, PEG), 3.90 ppm (d, 2H, O=C-C<u>H</u>$_2$-CH$_2$-CH$_2$-CH$_3$).

*2.2.5. Synthesis of branched poly(ethylene glycol)-b-poly(styrene) (PEG$_{45}$-b-(PS$_{46}$-co-DVB$_{0.6}$)-b-PEG$_{45}$) (**3**)*

Typically, the radical macro-initiator poly(ethylene glycol) dimer (4 kDa, 2 g, 0.5 mmol, 1 eq), Styrene (3.1 g, 30 mmol, 30 eq per PEG chain), divinylbenzene (52 mg, 0.4 mmol, 0.4 eq per PEG chain) and dodecanethiol (40.5 mg, 0.2 mmol, 0.2 eq per PEG chain) were transferred into a schlenk tube fitted with a magnetic stirrer bar and *N*,*N*-dimethylformamide (DMF,20 mL) added. The reaction mixture was degassed by three freeze-pump thaw cycles and the vessel was backfilled with N_2. The reaction mixture was then placed in an oil bath at 70 °C and the polymerisation was quenched by rapid cooling after 16 h. The reaction mixture was dissolved in a minimal amount of tetrahydrofuran (THF) and added dropwise to a large excess of ice-cold diethyl ether. The precipitation was repeated once more before the desired branched copolymer was obtained as a white solid (1.9 g, theoretical M_w = 8870 g/mol). Yield = 45 %. ^{1}H-NMR were measured in $CDCl_3$ (400 MHz): 1.21 – 1.60 ppm (m, 2H, PEG-C<u>H</u>$_2$), 1.66 – 2.13 ppm (m, 1H, PEG-CH$_2$-C<u>H</u>-C=O), 3.64 ppm (s, 4H, PEG), 6.57 ppm (m, 2H, Ar), 7.04 ppm (m, 3H, Ar).

2.2.6. Formation of polymer nanoparticle dispersions

Corresponding nanoparticles aqueous suspension can be prepared by a simple solvent-removal process. Typically, 10 mg of branched block copolymer was dissolved in 5 mL of acetone, followed by addition of 5 mL of water and stirred for 0.5 h at room temperature. Acetone was removed by evaporation at room temperature, and final transparent nanoparticles aqueous suspension was obtained.

Triclosan particle size measurements were performed on nanoparticles suspensions in YPD medium with concentrations of 0.5 mg/ml. Measurements were performed after vigorously shaking the solution for 30 seconds by hand to disperse the material. The suspensions were put in a +4 °C fridge for 15 minutes to settle any formed foam and larger particles.

*2.2.7. Synthesis of branched poly(ethylene glycol)-b-Poly(N-isopropylacrylamide) (PEG_{135}-b-($PNIPAm_{50}$-co-EDA_{2n})-b-PEG_{135}) (**4-6**) and the corresponding nanoparticle dispersions.*

Typically, the radical macro-initiator poly(ethylene glycol) dimer (12 kDa, 1.2 g, 0.1 mmol, 1 eq), *N*-isopropylacrylamide (0.56 g, 5 mmol, 25 eq per PEG chain), ethylene diacrylamide (10.1 mg, 0.06 mmol, 0.3 eq per PEG chain) and dodecanethiol (10.1 mg, 0.05 mmol, 0.25 eq per PEG chain) were transferred into a small schlenk tube fitted with a magnetic stirrer bar and *N*,*N*'-dimethylformamide (DMF,7 mL) added. The reaction mixture was degassed and the vessel was backfilled with N_2. The reaction mixture was then placed in an oil bath at 70 °C and the polymerisation was quenched by rapid cooling after 16 h. The reaction mixture was dissolved in a minimal amount of tetrahydrofuran (THF) and added dropwise to a large excess of ice-cold diethyl ether. The precipitation was repeated once more before the desired branched copolymer was obtained as a white solid (0.94 g). The molar ratio of ethylene diacrylamide per PEG chain was varied as n = 0.3 (**4**), 0.6 (**5**), and 0.9 (**6**) eq per PEG change for the PEG-PNIPAM branched block copolymers, while the equivalents per PEG chain of *N*-isopropylacrylamide and dodecanethiol were kept at 25 and 0.25 respectively. Corresponding nanoparticles aqueous suspension can be prepared by a simple solvent-removal process. Typically, 10 mg of branched block copolymer was dissolved in 5 mL of acetone, followed by addition of 5 mL of water and stirred for 0.5 h at room temperature. Acetone was removed by evaporation at room temperature, and final transparent nanoparticles aqueous suspension was obtained.

2.2.8. Formulation of nanoparticles by emulsion-freeze-drying approach

Typically, stock solutions of 0.5 wt % Oil Red O (indomethacin, ibuprofen, ketoprofen and triclosan) in cyclohexane (*o*-xylene) and 2 wt % branched block copolymers **1-6** in deionized water were prepared. To that end polymers were dissolved

in acetone and water was added dropwise. Acetone was then evaporated off at room temperature under constant stirring. Although pharmaceutical Class 2 solvents, cyclohexane and *o*-xylene were chosen because of the good solubility for Oil red O (triclosan) and indomethacin respectively as well as their tendency to form stable emulsions. A high melting point of 6 °C and -24 °C respectively and high vapour pressure make them furthermore ideal for the freeze-drying process. A study [23] measuring solvent residues after lyophilisation showed that after freeze drying solvents with similar vapour pressures had solvent residues well within the limit as defined by the International Council for Harmonization of Technical Requirements for Pharmaceuticals for Human Use (ICH).[24] Under vigorous stirring with an overhead stirrer the cyclohexane solution was added dropwise over a period of 2 minutes to the aqueous polymer solution of PEG_{45}-$PNIPAM_{30}$ and PEG_{45}-BMA_{30} at room temperature. PEG_{45}-Sty_{30} could not be dissolved in high concentration in water and was therefore added directly into *o*-xylene with indomethacin. Emulsions with the volume ratios of aqueous phase to organic phase (W/O) of 1:4 and 1:1 were prepared. After stirring for 2 minutes with an overhead stirrer at 1000 rpm, the emulsions were homogenised for another 2 minutes using a Power Gen 1000 homogenizer by Fischer Scientific on setting 3. The emulsion was rapidly frozen in liquid nitrogen and placed in a CoolSafe freeze dryer by Scanvac at a condensing temperature of -90 °C and lyophilised for two days to produce dry porous polymer containing organic nanoparticles. After which the water to oil ratio was chosen that produced the most stable emulsion for polymers **1-3**.

2.2.9. Determination of the nanoparticles yields in the formulations

5 mg of freeze dried material was dispersed in 10 mL deionized water and centrifuged at 3000 rpm for 3 minutes and another minute at 3600 rpm with an Eppendorf Centrifuge 5415 D. This was to precipitate micronsized particles by centrifuging while nanosized particles stay in the supernatant. The precipitant was re-dissolved in ethanol. The concentrations of Oil Red O (OR) or other drug compounds were determined by UV/Vis absorption on a µQuant spectrometer by Northstar Scientific. Ethanol was added to the aqueous supernatant and water was then added to the ethanol solution of precipitation to achieve a 1:1 v/v ethanol/water mixture. The measured absorption was compared to a standard curve of OR (or indomethacin) in the 1:1 v/v ethanol/water medium. Yield of ketoprofen and ibuprofen was measured

on a 1200 series HPLC (because of no UV absorbance on the UV-Vis spectrum) from Agilent, comprising a vacuum degasser, quaternary pump, ALS auto-sampler, heated column compartment and UV-Vis detector. A 300 mm by 4.6 mm phase symmetry silica column with a particle diameter of 5 µm and a pore size of 120 Å was used. A flow rate of 1 ml/min was set. The mobile phase was a mixture of hexane and isopropyl alcohol with 70 % hexane for ketoprofen and 90 % hexane for ibuprofen. All tests were carried out at 20 °C. All signals were UV detected at 254 nm. Data analysis was performed using Agilent Chemstation software, version B.02.01 (Agilent Technologies, USA).

Nanoparticle yield was calculated as follows. Microparticles and aggregates were removed by centrifugation. The yield of suspended drug/dye in water was calculated as described below:

$$\boldsymbol{Yield} = \frac{\boldsymbol{m_{NP}}}{\boldsymbol{m_T}} \times \mathbf{100} = \frac{\boldsymbol{m_S}}{\boldsymbol{m_S + m_P}} \times \mathbf{100} \quad (\mathbf{1.1.})$$

Where m_{NP} is the mass of drug/ dye suspended in water and m_T is the total initial mass of drug/ dye. m_S is the mass of drug/ dye in the suspension after centrifugation and m_P is the mass of precipitated drug/ dye after centrifugation. To determine the mass in suspension, 1.5 ml sample was added to 1.5 ml ethanol and measured by UV/Vis. The centrifugation precipitant was re-dissolved in 3 mL ethanol. 1,5 ml of this solution was then added to 1.5 ml DI water and measured by UV/Vis. Quantities of drug/ dye were determined against calibration curves of known concentrations in ethanol.

2.2.10. Antimicrobial activity of triclosan nanoparticles

The efficacy of the nanoparticles was tested on opportunistic fungal pathogen *Candida albicans* in formulation with the broad-spectrum antimicrobial agent Triclosan. Growth kinetics of *C. albicans* exposed to different dilutions of stock solutions of 2 mg/ml of PEG_{45}-*b*-($PNIPAm_{60}$-*co*-$EDAm_{0.8}$)-*b*-PEG_{45} stabilised triclosan nanoparticles, triclosan and 10 mg/ml of PEG_{45}-*b*-($PNIPAm_{60}$-*co*-$EDAm_{0.8}$)-*b*-PEG_{45}. Cell growth was monitored by optical density at 600 nm (OD_{600}) over a period of 5 h incubation at 37°C, 150 rpm. *C. albicans* was first grown aerobically at 37°C, 200 rpm in a 100 mL- Erlenmeyer flask with 40 mL YEPD (10 g/L Yeast Extract (Fisher BioReagents), 20 g/L Bacteriological Peptone (Oxoid), 20 g/L Dextrose (Sigma-

Aldrich) media overnight. Overnight culture was inoculated into fresh YEPD media in NUNC 96-well plates containing dilutions of polymer stabilised triclosan nanoparticles, triclosan and PEG_{45}-$PNIPAM_{30}$ respectively with a final volume of 200 µL per well. OD_{600} measurements were taken in triplicate using a Varioskan™ Flash spectral scanning multimode reader (Thermo Scientific, Singapore).

2.3. Results and discussion

2.3.1. Synthesis of PEGylated hyperbranched block copolymers

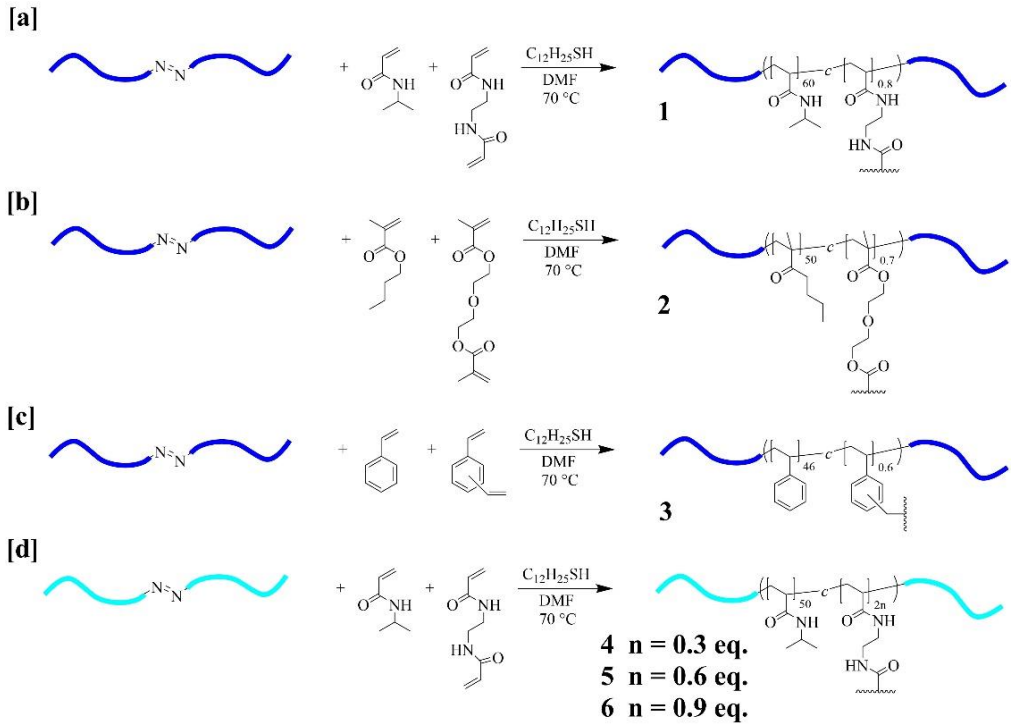

Scheme 2.2. Schematic representation of the synthesis of a) PEG_{45}-*b*-($PNIPAm_{60}$-*co*-$EDAm_{0.8}$)-*b*-PEG_{45} (**1**); b) PEG_{45}-*b*-($PBMA_{50}$-*co*-$DEGDMA_{0.7}$)-*b*-PEG_{45} (**2**); c) PEG_{45}-*b*-(PS_{46}-*co*-$DVB_{0.6}$)-*b*-PEG_{45} (**3**) and d) PEG_{135}-*b*-($PNIPAm_{50}$-*co*-$EDAm_{2n}$)-*b*-PEG_{135} with varying cross-linked equivalences

Branched diblock copolymers were synthesised using a macro-initiator PEG azo-dimer with a molecular weight of 4000 g/mol and three core-forming monomers *N*-isopropylacrylamide, *n*-butyl methacrylate and styrene. To form lightly branched copolymers these were copolymerised with the cross-linkers ethylene diacrylamide (EDAm) (synthesised by Dr A. Jackson in ICES), diethylene glycol methacrylate (DEGDMA) and divinyl benzene (DVB), respectively (**1-3**). Next, branched block copolymers of a PEG macro-azo initiator with a molecular weight of 12000 g/mol and PNIPAm with cross-linkage equivalences of 0.3, 0.6 and 0.9 (**4-6**) were synthesised. Scheme 2.1 shows a schematic representation of the synthesis of polymer **1-6**.

Table 2.1. Synthesis of branched polymers 1-6 with different core monomers and varying amounts of cross-linker and nanoparticles size. M_W 4 kDa = PEG_{45}-N=N-PEG_{45} and M_W 12 kDa = PEG_{135}-N=N-PEG_{135}.

Polymer	PEG dimer	Monomer	Cross-linker	DDT	DMF	T	t	Yield	size (D_h)
-	eq.				wt%	°C	h	%	nm
1	1 (M_w = 4 kDa)	60 PNIPAm (30 eq./ PEG chain)	0.8 EDAm (0.4 eq / PEG chain)	0.4	22	70	16	50	33
2	1 (M_w = 4 kDa)	60 *n*BMA (30 eq. / PEG chain)	0.8 DVB (0.4 eq / PEG chain)	0.4	22	70	16	70	64
3	1 (M_w = 4 kDa)	60 Styrene (30 eq./ PEG chain)	0.8 DEGDMA (0.4 eq / PEG chain)	0.4	22	70	16	45	38
4[+]	1 (M_w = 12 kDa)	50 PNIPAm (25 eq. / PEG chain)	0.6 EDAm (0.3 eq / PEG chain)	0.5	22	70	16	-[+]	70
5[+]	1 (M_w = 12 kDa)	50 PNIPAm (25 eq. / PEG chain)	1.2 EDAm (0.6 eq / PEG chain)	0.5	22	70	16	-[+]	81
6[+]	1 (M_w = 12 kDa)	50 PNIPAm (25 eq. / PEG chain)	1.8 EDAm (0.9 eq / PEG chain)	0.5	22	70	16	-[+]	96

[+] synthesis was carried out by Dr. Alexander Jackson in ICES.

Table 2.1. shows the synthetic parameters used in the synthesis of polymers **1-6**. For polymers **1-3** a (hydrophobic to hydrophilic) ratio of 0.66:1 units was chosen to obtain lightly cross-linked, amphiphilic polymer nanoparticles. All polymers were synthesised using the same parameters. The obtained polymers were characterised using ^{1}H-NMR (Figure 2.2.), DLS (Table 2.1. and Figure 2.1. d-f) and GPC (Figure 2.1.a-c and Table 2.2). Gel permeation chromatography (GPC) analysis of branched macromolecules does not yield accurate molecular weights when compared to linear calibration standards. However, GPC analysis (Figure 2.1.) confirmed the successful consumption of the PEG azo-dimer and the high dispersity values obtained are typical of branched macromolecules. Aqueous nanosuspensions for DLS were prepared by dissolving polymer **1-3** in acetone and adding water dropwise. Acetone was evaporated off under constant stirring and the obtained suspension were used to measure particle size. Sizes obtained by DLS in aqueous medium of 33, 64 and 38 nm for polymers **1-3** respectively, showed that unimolecular branched block copolymers were obtained and not linear block copolymers.

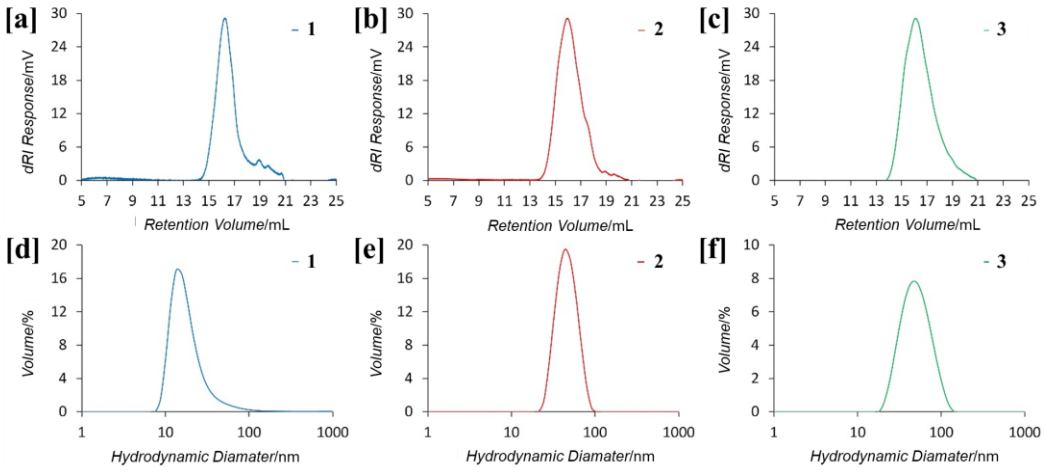

Figure 2.1 Characterisation of branched diblock copolymers PEG_{45}-*b*-($PNIPAm_{60}$-*co*-$EDAm_{0.8}$)-*b*-PEG_{45} (**1**), PEG_{45}-*b*-($PBMA_{50}$-*co*-$DEGDMA_{0.7}$)-*b*-PEG_{45} (**2**) and PEG_{45}-*b*-(PS_{46}-*co*-$DVB_{0.6}$)-*b*-PEG_{45} (**3**) via gel permeation chromatography in THF (a-c) and dynamic light scattering (d-f) in H2O.

Table 2.2. GPC data of polymers **1-3**

Branched copolymer	Conv.	M_n[a] (kDa)	M_w[a]	PDI[a] (M_w/M_n)
	%	kDa		-
1	99	8,400	16,200	1.93
2	83	8,000	22,300	2.79
3	77	3,900	20,000	5.26

[a] Determined by GPC in THF. [b] Determined by DLS analysis in H_2O (0.1 wt %).

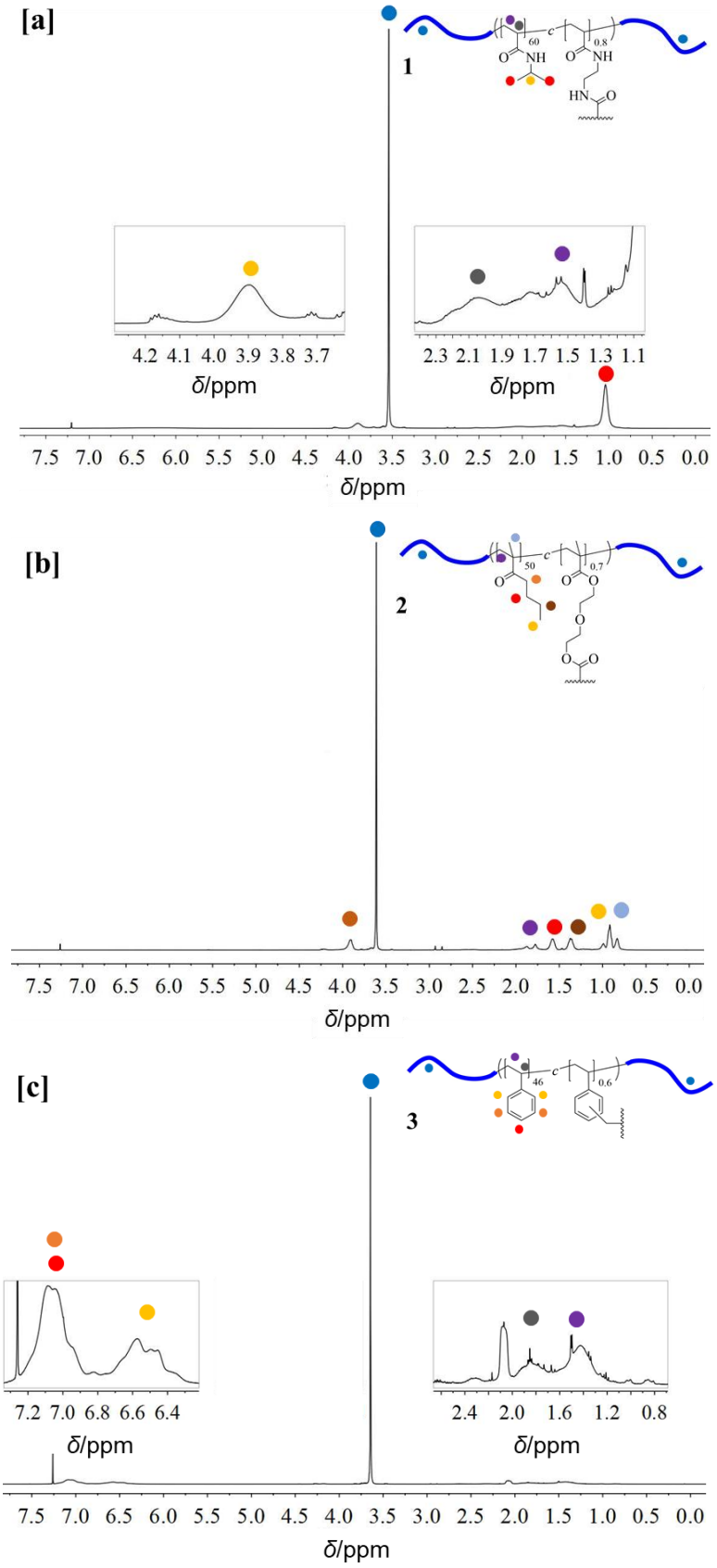

Figure 2.2. ^{1}H-NMR in $CDCl_3$ of of a) PEG_{45}-*b*-($PNIPAm_{60}$-*co*-$EDAm_{0.8}$)-*b*-PEG_{45} (**1**); b) PEG_{45}-*b*-($PBMA_{50}$-*co*-$DEGDMA_{0.7}$)-*b*-PEG_{45} (**2**) and c) PEG_{45}-*b*-(PS_{46}-*co*-$DVB_{0.6}$)-*b*-PEG_{45} (**3**).

Figure 2.2 shows the ^{1}H-NMR measured in $CDCl_3$ after purification by precipitation of the polymer into petroleum ether (60/80) three times. The peak at 3.61 ppm can be assigned to the ethylene group of PEG. These signals were integrated and compared to the signals of the core forming monomers to obtain the degree of polymerisation. In figure 2.2.a the signals at 3.9 ppm (s, 1H, -NC<u>H</u>) and 1.04 (s, 6H, -NC<u>H</u>$_3$) were chosen because they are specific to PNIPAm. Integration shows that a conversion of 99 % was reached and PEG_{45}-*b*-($PNIPAm_{60}$-*co*-$EDAm_{0.8}$)-*b*-PEG_{45} was obtained. In Figure 2.2.b *n*BMA signals at 1.36 ppm (d, 2H, -C<u>H$_2$</u>CH_3), 1.57 (d, 2H, -CH_2C<u>H$_2$</u>CH_2-) and 3.91 ppm (d, 2H, -COC<u>H$_2$</u>CH_2-) were chosen. Integration showed that the conversion was 83 % and that PEG_{45}-*b*-($PBMA_{50}$-*co*-$DEGDMA_{0.7}$)-*b*-PEG_{45} was obtained. Figure 2.2.c shows the NMR spectra of PEG_{45}-*b*-(PS_{46}-*co*-$DVB_{0.6}$)-*b*-PEG_{45}. The integration of signals at 6.58 ppm (m, 2H, Ar, -C<u>H</u>) and 7.07 ppm (m, 3H, Ar, -C<u>H</u>) show that the conversion was 77 %. The trend in conversion from NIPAm > *n*BMA > Styrene is due to the different reactivity's of the chosen monomers.[25]

The ability to form nanoparticles by emulsion freeze-drying and stabilisation was further investigated in dependency of cross-linkage. To that end, branched copolymer of PEG_{135}-*b*-($PNIPAm_{50}$-*co*-$EDAm_{2n}$)-*b*-PEG_{135} with varying cross-linkages of n = 0.3, 0.6 and 0.9 (**4-6**) were synthesised by Dr A. Jackson in ICES, Singapore. A longer PEG chain of a molecular weight of 12000 g/mol was chosen, because a longer PEG chain was believed to lead to an increased ability to form emulsions with higher oil phases. DLS data (Table 2.1.) shows that the obtained polymers **4-6** were branched block copolymers of 70, 81 and 96 nm. The increased sizes reflect the use of the longer PEG chains. With increasing cross-linker equivalences the particle size increased. More cross-link equivalences could lead to the incorporation of more linear polymer chains into a unimolecular branched polymer, which would increase the size.

2.3.2. Hydrophobic dye and drug nanoparticles by emulsion freeze-drying effect of core forming monomer

Polymers **1**, **2** and **3** were used to form emulsions with two organic solutions of indomethacin in *o*-xylene and oil red in cyclohexane, which were subsequently lyophilised to generate nanoparticles, which could be re-suspended to form nanosuspensions. The nanoparticles were investigated using DLS to obtain size data. UV/Vis

was used to calculate nanoparticle yield. The best conditions, *i.e.* polymer, o/w ratio and oil phase solvent were identified and used for further tests.

2.3.2.1. Emulsion freeze-drying of Indomethacin

Emulsions were formed with aqueous dispersions of polymers **1** and **2**. To that end 2 wt % aqueous stock solutions of **1** and **2** were obtained by dissolving the polymers in acetone and evaporating into water to assure that well dispersed polymer nanosupensions were obtained. These were emulsified using a homogenizer with a 0.5 wt % indomethacin solution in *o*-xylene in a ratio of o/w 4:1 (80 % oil phase). Polymer **3** could not be dissolved in water in such high concentrations and was subsequently added to *o*-xylene directly with the indomethacin and homogenised with pure water in the same ratio. Figure 2.3. shows microscope pictures of the obtained emulsions. Figure 2.3. a, c, and e show emulsions formed from **1**, **2** and **3** respectively with 80 % oil phase. None of the emulsions were stable for longer than a few minutes and separation could be observed under the microscope. Although, emulsions formed from polymer **1** were slightly more stable than their counterparts. We ascribed this to be a result of the high oil content. Consequently, emulsions were formed with 50 % oil phase (o/w 1:1) (Figure 2.3. b, d and f). This led to the formation of stable emulsions for **1** with uniform droplet sizes between 10 and 20 µm (Figure 2.3.b). Emulsions formed with **3** were also slightly more stable with less oil phase, however a broad distribution of droplet sizes could be found ranging from as small as 5 µm to almost 100 µm (Figure 2.3. f). Emulsion formed from polymer **2** on the other hand, could not be stabilised even with a lesser oil content (Figure 2.3. d). The reason for that might be that *o*-xylene is a poor theta solvent for the BMA core and as such the ability to stabilise even lower oil phase emulsions is diminished. All emulsions were rapidly frozen in liquid nitrogen and lyophilised. All obtained emulsions were oil-in-water emulsions.

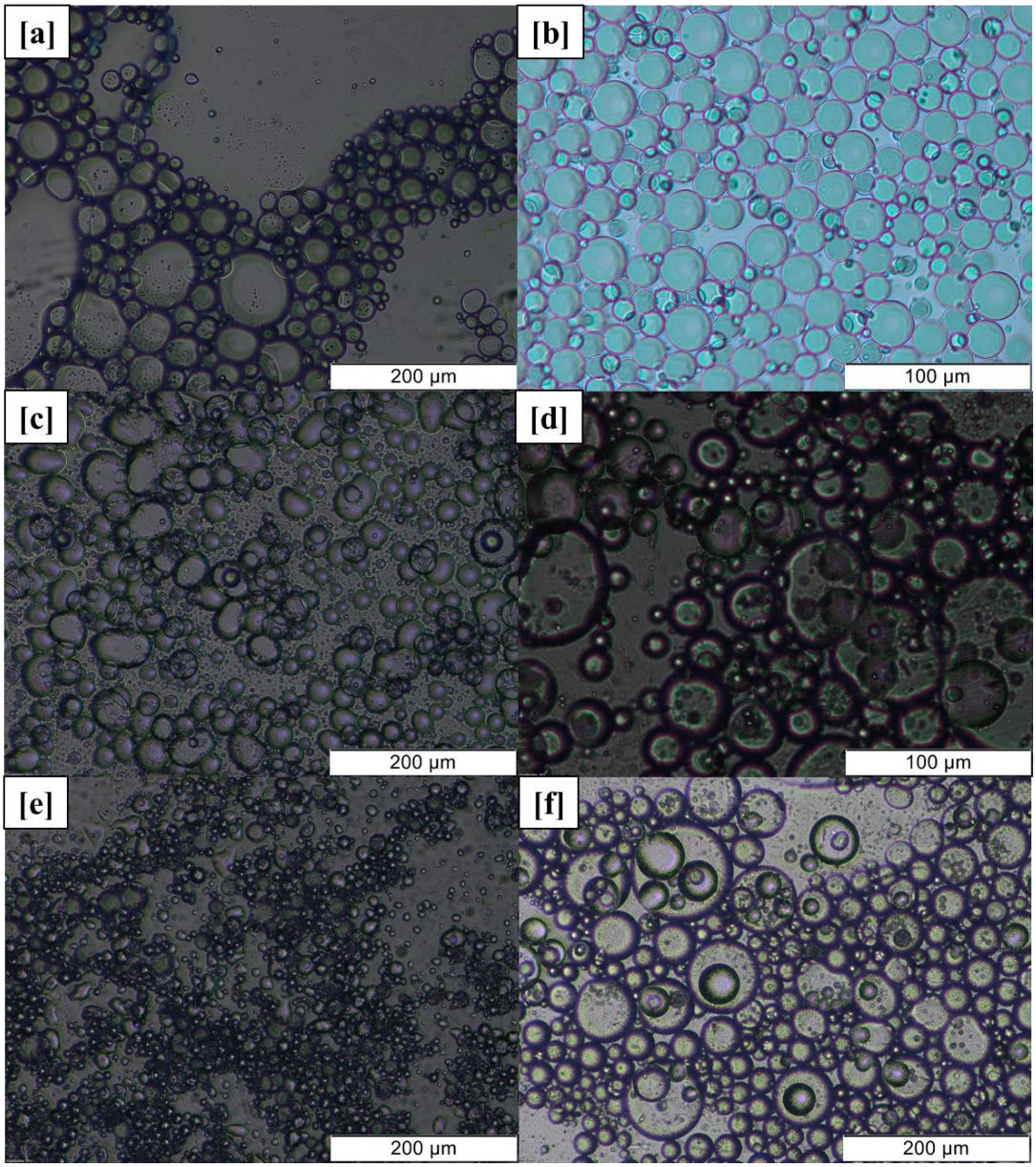

Figure 2.3. Emulsions formed from stock solutions of 0.5 wt % indomethacin in *o*-xylene and 2 wt % stock solutions of a) Polymer PEG_{45}-*b*-($PNIPAm_{60}$-*co*-$EDAm_{0.8}$)-*b*-PEG_{45} (**1**) with 80 % oil phase; b) Polymer PEG_{45}-*b*-($PNIPAm_{60}$-*co*-$EDAm_{0.8}$)-*b*-PEG_{45} (**1**) with 50 % oil phase; c) Polymer PEG_{45}-*b*-($PBMA_{50}$-*co*-$DEGDMA_{0.7}$)-*b*-PEG_{45} (**2**) with 80 % oil phase; d) Polymer PEG_{45}-*b*-($PBMA_{50}$-*co*-$DEGDMA_{0.7}$)-*b*-PEG_{45} (**2**) with 50 % oil phase; e) Polymer) PEG_{45}-*b*-(PS_{46}-*co*-$DVB_{0.6}$)-*b*-PEG_{45} (**3**) with 80 % oil phase; and f) Polymer) PEG_{45}-*b*-(PS_{46}-*co*-$DVB_{0.6}$)-*b*-PEG_{45} (**3**) with 50 % oil phase.

Figure 2.4. shows SEM pictures of the polymer **1** scaffold obtained after emulsion freeze-drying emulsions of 80 % and 50 % oil phase. All other samples containing polymer **2** and **3** had collapsed after two days *i.e.* the sample shrunk and lost its porosity. Due to that reason, no images were taken. In Figure 2.4. a clear difference between the scaffold formed from an emulsion of 80 % oil (Figure 2.4.a) and 50 %

oil (Figure 2.4.b) can be observed. While the scaffold of 50 % oil phase shows clear emulsion templating *i.e.* emulsion droplets can still be observed as spheres, the scaffold from 80 % more closely resembles a reef, a possible result of the more unstable emulsion.

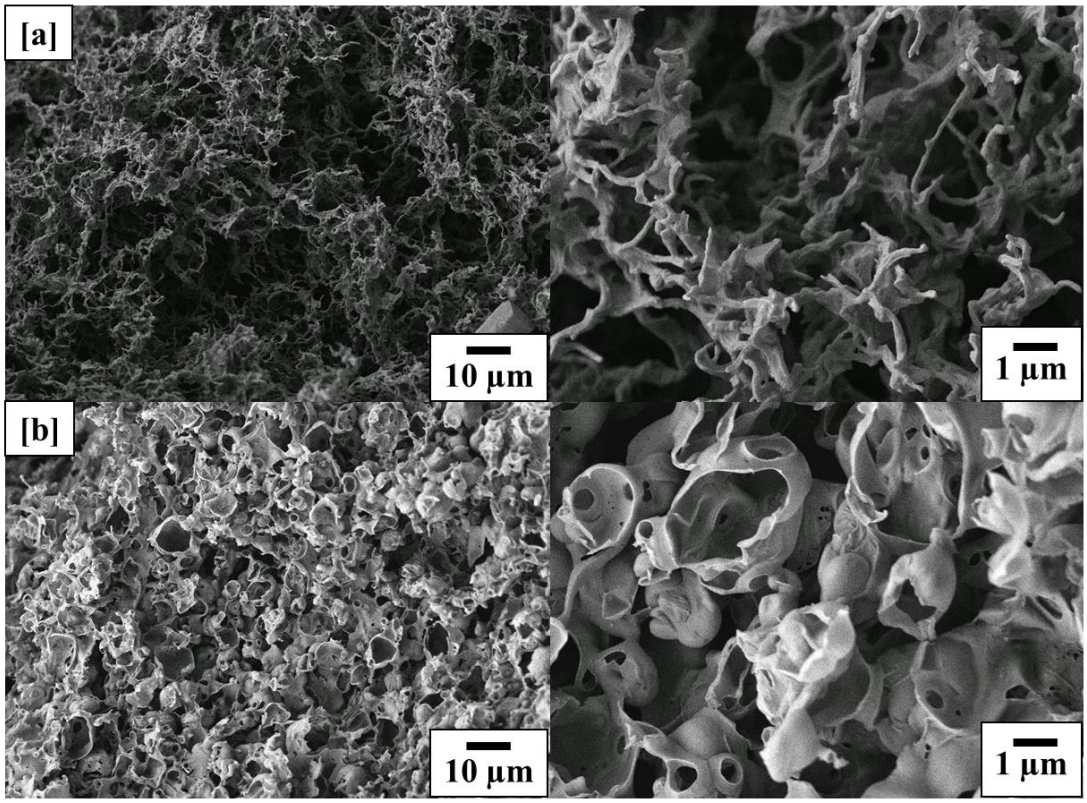

Figure 2.4. SEM pictures of a) IMC nanoparticles stabilised by a polymer PEG_{45}-*b*-($PNIPAm_{60}$-*co*-$EDAm_{0.8}$)-*b*-PEG_{45} (**1**) Matrix after emulsion freeze-drying of an *o*-xylene/water emulsion with 80 % oil phase and b) indomethacin nanoparticles stabilised by a polymer PEG_{45}-*b*-($PNIPAm_{60}$-*co*-$EDAm_{0.8}$)-*b*-PEG_{45} (**1**) Matrix after emulsion freeze-drying of an *o*-xylene/water emulsion with 50 % oil phase. Magnified 1000 times (left) and 5000 times (right).

The obtained polymer scaffolds containing indomethacin nanoparticles were re-suspended in DI water, however no stable nanosuspension for DLS measurements could be obtained. Therefore, Yeast Extract-Peptone-Dextrose (YEPD) medium was used, because it had been shown before that in growths medium PEGylated particles did not agglomerate.[26] Table 2.3. shows the obtained DLS data as well as the nanoparticles yields.

Table 2.3. DLS data in YEPD medium and nanoparticles yield from indomethacin nanoparticles obtained by forming emulsions of water/*o*-xylene stabilised by polymer PEG_{45}-*b*-($PNIPAm_{60}$-*co*-$EDAm_{0.8}$)-*b*-PEG_{45} (**1**)

Oil phase	Polymer	D_h Z-Average	PDI	D_h Int. %	Yield
%		nm	-	nm	%
80	1	749 ± 297	0.8	1209 ± 297 208 ± 40	59
50	1	657 ± 297	0.9	910 ± 154 131 ± 52	74

No DLS data of samples using polymers **2** and **3** could be obtained because not enough could be re-dispersed in water or medium after the scaffold had collapsed. Nanoparticles formed from higher oil phase emulsions produced bigger particles, then when less oil was used *e.g.* 749 nm compared to 657 nm. This, as well as the lower yield of 54 % was ascribed again to a more unstable emulsion. Figure 2.5. shows the samples re-dispersed in water. None of the samples could be completely re-dispersed to obtain a nanoparticle yield of 100%.

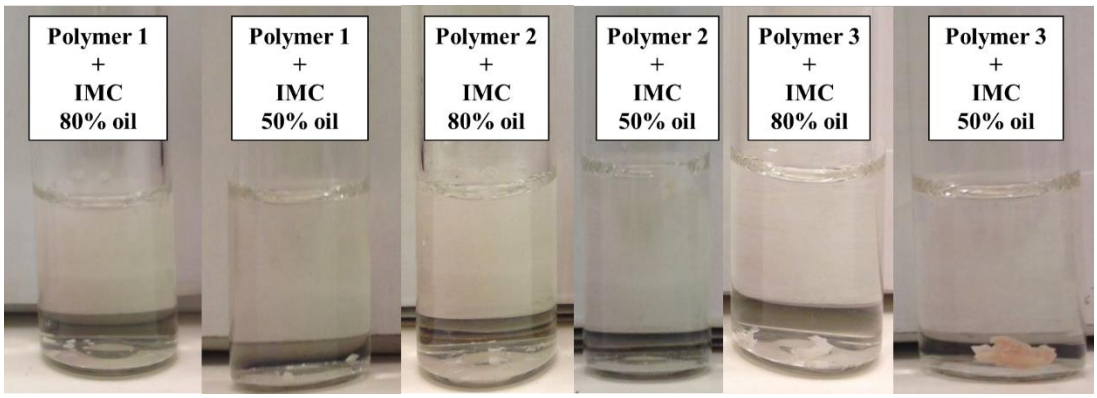

Figure 2.5. Nanosuspensions of indomethacin (IMC) nanoparticles obtained by emulsion freeze-drying after re-suspension in DI water stabilized by PEG_{45}-*b*-($PNIPAm_{60}$-*co*-$EDAm_{0.8}$)-*b*-PEG_{45} (**1**), PEG_{45}-*b*-($PBMA_{50}$-*co*-$DEGDMA_{0.7}$)-*b*-PEG_{45} (**2**) and PEG_{45}-*b*-(PS_{46}-*co*-$DVB_{0.6}$)-*b*-PEG_{45} (**3**)

2.3.2.2. Emulsion freeze-drying of Oil Red O

Cyclohexane is a good solvent for freeze-drying and emulsion formation. For that reason, it was investigated if changing the oil phase solvent to cyclohexane would improve the nanoparticles formation. Stock solutions of polymer **1** and **2** were created as has been described before and emulsified with a 0.5 wt % oil red/cyclohexane

solution. No stock solution of **3** could be obtained because the polymer could not be dissolved in cyclohexane or water.

Figure 2.6. shows the microscope pictures of emulsions formed after homogenisation. In the case of **1** it was observed that emulsions formed with 80 % oil (Figure 2.6. a) were not stable while emulsions formed with 50 % oil were stable (Figure 2.6. b) with oil droplet sizes between 20 and 50 µm. When stock solutions of **2** were emulsified with cyclohexane stable emulsions with small droplets could be obtained regardless of oil content (Figure 2.6. c and d). All obtained emulsions were oil-in-water emulsions.

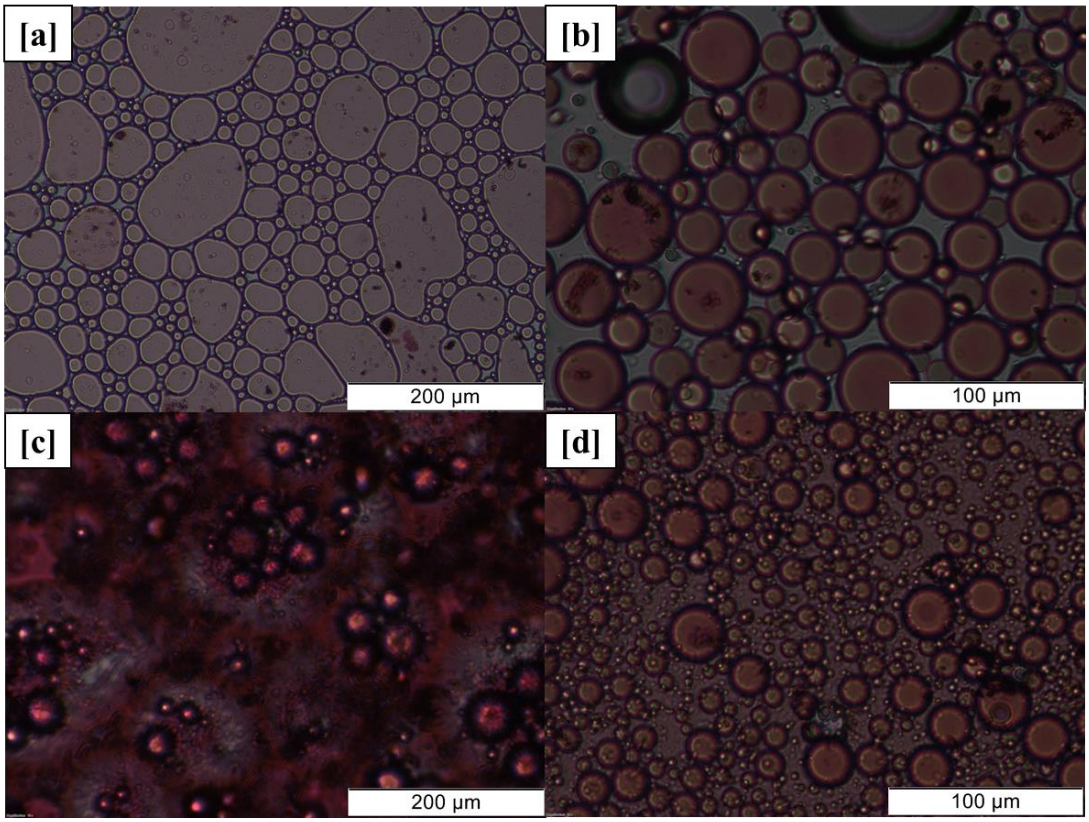

Figure 2.6. Emulsions formed from stock solutions of 0.5 wt % oil red in cyclohexane and 2 wt % stock solutions of a) Polymer PEG_{45}-*b*-($PNIPAm_{60}$-*co*-$EDAm_{0.8}$)-*b*-PEG_{45} (**1**) and 80 % oil; b) Polymer PEG_{45}-*b*-($PNIPAm_{60}$-*co*-$EDAm_{0.8}$)-*b*-PEG_{45} (**1**) and 50 % oil; c) Polymer PEG_{45}-*b*-($PBMA_{50}$-*co*-$DEGDMA_{0.7}$)-*b*-PEG_{45} (**2**) and 80 % oil and d) Polymer PEG_{45}-*b*-($PBMA_{50}$-*co*-$DEGDMA_{0.7}$)-*b*-PEG_{45} (**2**) and 50 % oil.

After lyophilisation red powders were obtained and imaged using SEM. Figure 2.7. shows the results. All samples, except for polymer **2** emulsified with 50 % oil phase, produced stable scaffolds. This might be a result of the increased hydrophobicity of *n*BMA which led to higher oil phase emulsions being more stable. While the

emulsion templating in scaffolds produced from **1** and 50 % oil phase is clearly discernible (Figure 2.6. b), scaffolds using higher oil content *i.e.* 80 % formed from **1** and **2** exhibited fibre like structures (Figure 2.6. a and b).

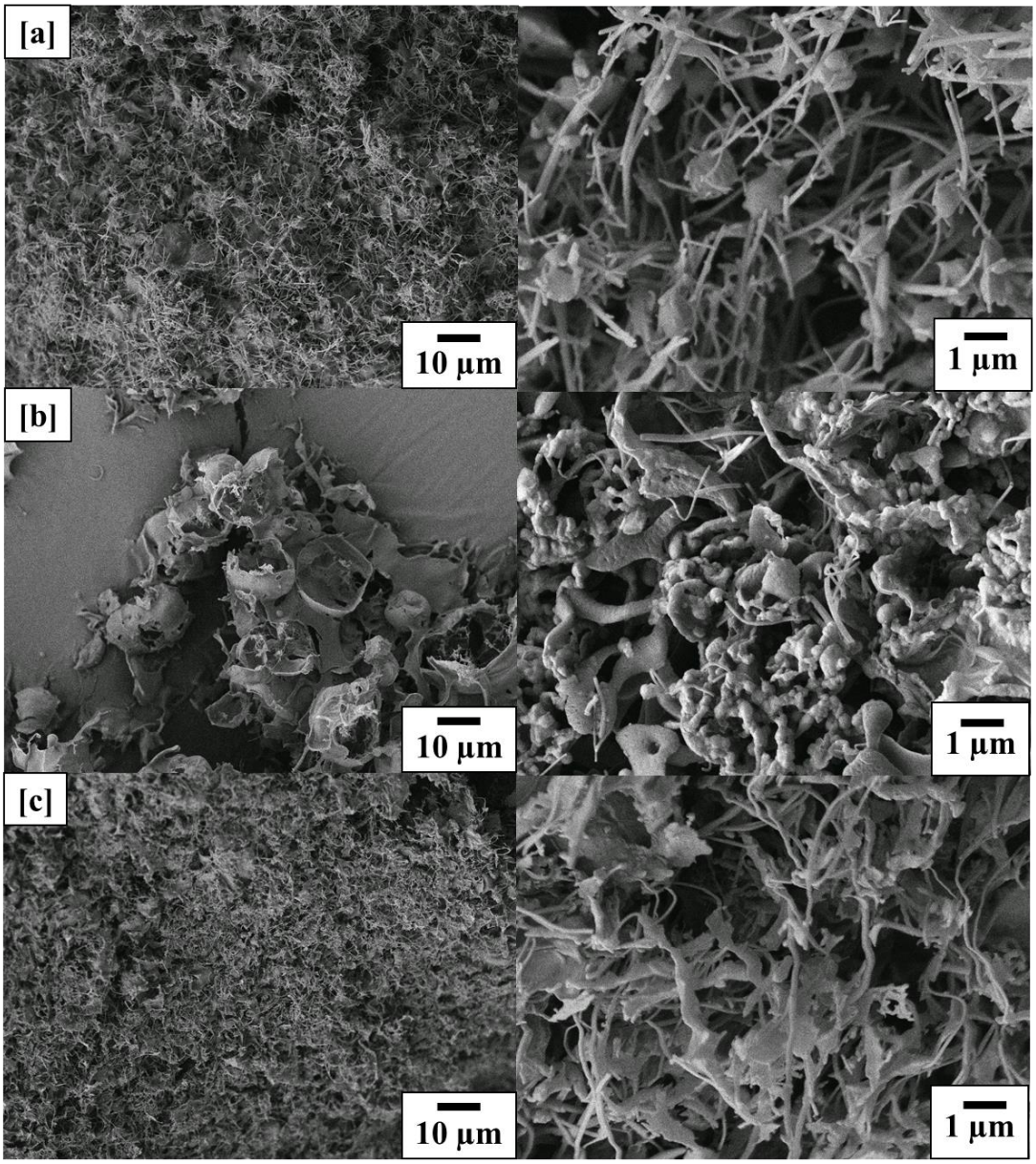

Figure 2.7. SEM pictures of oil red nanoparticles stabilised by a polymer scaffold after emulsion freeze-drying of a) Polymer PEG_{45}-*b*-($PNIPAm_{60}$-*co*-$EDAm_{0.8}$)-*b*-PEG_{45} (**1**) and 80 % oil; b) Polymer PEG_{45}-*b*-($PNIPAm_{60}$-*co*-$EDAm_{0.8}$)-*b*-PEG_{45} (**1**) and 50 % oil and c) Polymer PEG_{45}-*b*-($PBMA_{50}$-*co*-$DEGDMA_{0.7}$)-*b*-PEG_{45} (**2**) and 80 % oil. 1000 times magnified (left) and 10000 times magnified (right).

The three samples were subsequently re-suspended in water (Figure 2.8.). Nanosuspensions of emulsions with 50 % oil phase could be formed in the case of polymer **1**, while 80 % oil phase failed. Polymer **2** with 80 % oil could form nanosuspensions of OR. Scaffolds which had collapsed already, were not re-suspended

because it had been shown before (Figure 2.5.) that these would not be able to form suspensions. As had already been done for indomethacin, DLS data and yield were measured in YEPD medium. Table 2.4. shows the data obtained.

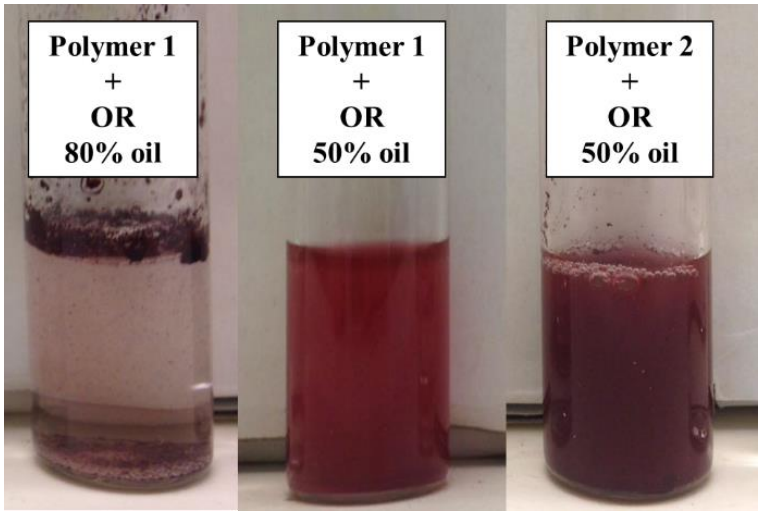

Figure 2.8. Nanosuspensions of oil red nanoparticles obtained by emulsion freeze-drying OR with polymers PEG_{45}-*b*-($PNIPAm_{60}$-*co*-$EDAm_{0.8}$)-*b*-PEG_{45} (**1**) and PEG_{45}-*b*-($PBMA_{50}$-*co*-$DEGDMA_{0.7}$)-*b*-PEG_{45} (**2**).

All OR nanoparticle formed *via* emulsion freeze-drying showed large sizes of 1366 and 859 nm as well as high PDIs of 0.5 and 0.6. However, using polymer **1** led to a high yield of 99 % nanoparticles in solution.

Table 2.4. DLS data in YEPD medium and nanoparticles yield of OR nanoparticles obtained by forming emulsions of water/cyclohexane stabilised by PEG_{45}-*b*-($PNIPAm_{60}$-*co*-$EDAm_{0.8}$)-*b*-PEG_{45} (**1**) and PEG_{45}-*b*-($PBMA_{50}$-*co*-$DEGDMA_{0.7}$)-*b*-PEG_{45} (**2**).

Oil phase	Polymer	D_h Z-Average	PDI	D_h Int. %	Yield
%		nm	-	nm	%
80	**2**	1366 ± 48	0.5	2089 ± 1094 506 ± 191	70
50	**1**	859 ± 36	0.6	1043 ± 225 375 ± 208	99

Table 2.5. gives a summarized overview of all conditions used in the screening process, as well as nanoparticle yield, PDI and DLS size data. Due to the favourable emulsion, scaffold and nanoparticle stability as well as nanoparticle yield and DLS size data, polymer **1** and cyclohexane/water with 50 % oil phase (entry 4) were utilised to prepare triclosan nanoparticles.

Table 2.5 Screening of branched diblock copolymers as stabilisers during the emulsion-freeze-drying approach, dynamic light scattering analysis of successful nanoparticle preparation including nanoparticle size, PDI and yield of suspended active molecule.

Entry	Branched Diblock Copolymer	Active	Solvent	Oil phase [%]	Emulsion Stability	Scaffold Stability	Nanoparticle Stability	Nanoparticle D_h [nm]	PDI	Nanoparticle Yield [%]
	-	-	-	%	-	-	-	nm	-	%
1	**1**	IMC	*o*-xylene	80	✓	✓	✓	208	0.82	59
2	**1**	IMC	*o*-xylene	50	✓	✓	✓	131	0.90	74
3	**1**	OR	cyclohexane	80	✓	✓	✗	-	-	-
4	**1**	OR	cyclohexane	50	✓	✓	✓	375	0.62	99
5	**2**	IMC	*o*-xylene	80	✗	✗	✗	-	-	-
6	**2**	IMC	*o*-xylene	50	✓	✗	✗	-	-	-
7	**2**	OR	cyclohexane	80	✓	✓	✓	506	0.53	70
8	**2**	OR	cyclohexane	50	✓	✗	✗	-	-	-
9	**3**	IMC	*o*-xylene	80	✗	✗	✗	-	-	-
10	**3**	IMC	*o*-xylene	50	✓	✗	✗	-	-	-

2.3.3. Activity of triclosan nanoparticles against Candida albicans

After having investigated the best possible parameters to form nanoparticles by emulsion freeze-drying using branched block copolymers we used the following parameters, 50 % cyclohexane and polymer **1**, to form triclosan nanoparticles. Figure 2.9. show emulsions formed from a 2 wt % aqueous polymer **1** solution and a 0.5 wt % triclosan cyclohexane solution (Figure 2.9. a) and a control emulsion of 2 wt % aqueous polymer **1** solution and cyclohexane without triclosan (Figure 2.9. b).

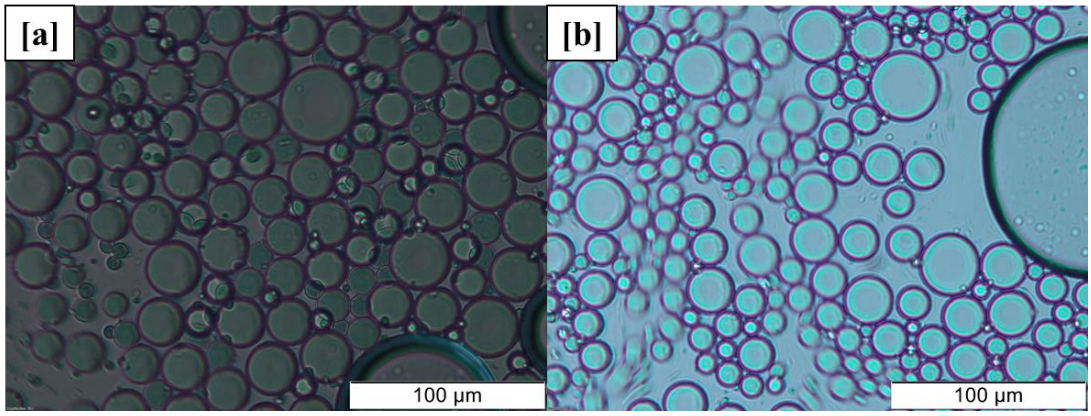

Figure 2.9. Microscope imagines of emulsions of cyclohexane/water in a ratio of 1:1 with a) 2 wt % aqueous polymer PEG_{45}-*b*-($PNIPAm_{60}$-*co*-$EDAm_{0.8}$)-*b*-PEG_{45} (**1**) solution + 0.5 wt % triclosan and b) 2 wt % aqueous polymer PEG_{45}-*b*-($PNIPAm_{60}$-*co*-$EDAm_{0.8}$)-*b*-PEG_{45} (**1**) solution.

Stable oil in water emulsions with small and uniform droplets of between 20 to 30 µm could be obtained (Figure 2.9. a). The control emulsion also formed stable o/w emulsion and showed, in average, smaller droplet sizes of around 10 µm, which is likely a result of the changed viscosity of cyclohexane without the dissolved triclosan (Figure 2.9. b).

After freeze-drying white powders were obtained that could be readily re-dissolved in water to form nanosuspensions with no discernible precipitant. The dried powders also exhibited storage stability over several months. SEM pictures of the obtained powder showed emulsion templated scaffolds for both emulsions (Figure 2.10). Upon closer inspection, spherical protrusions of around 200 to 300 nm could be observed for the scaffold containing triclosan (Figure 2.10.a). These could be the triclosan nanoparticles however, the low contrast between organic compounds makes it difficult to make this assertion with full certainty. DLS data in YPED medium gave the size of triclosan nanoparticles as 280 ± 12 nm (Z-Average), 260 ± 15 nm (Intensity %) and 148 ± 9 nm (Number %) with a low PDI of 0. 36 (Figure 2.11.b). Comparison

with the freeze-dried material obtained of emulsions formed with only polymer **1** showed significant less, as well as smaller spherical protrusions, which were presumably formed by rapid freezing (Figure 2.10.b).

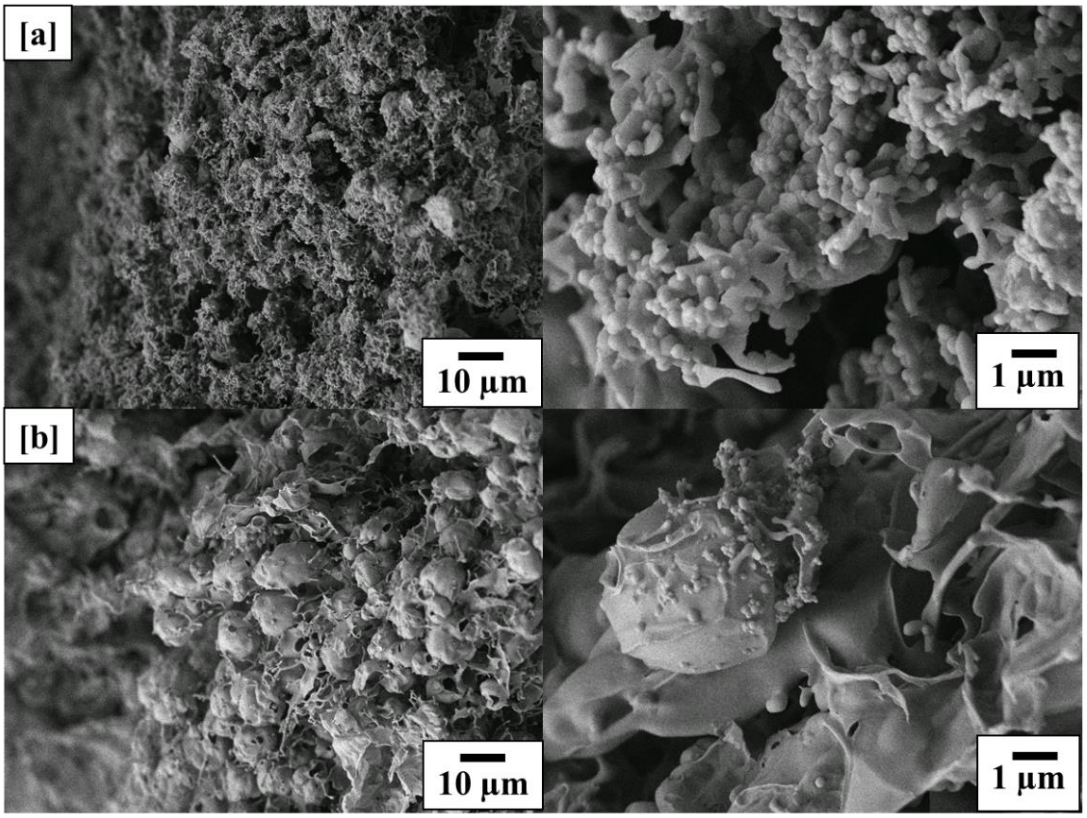

Figure 2.10. SEM imagines of polymer scaffolds after emulsion freeze-drying of emulsions of cyclohexane/water in a ratio of 1:1 with a) 2 wt % polymer PEG_{45}-*b*-($PNIPAm_{60}$-*co*-$EDAm_{0.8}$)-*b*-PEG_{45} (**1**) + 0.5 wt % triclosan and b) 2 wt % polymer PEG_{45}-*b*-($PNIPAm_{60}$-*co*-$EDAm_{0.8}$)-*b*-PEG_{45} (**1**).

Cryo-TEM of triclosan nanoparticles suspended in YEPD Medium (Figure 2.11.a) was measured to obtain a more accurate picture of the size and shape. The obtained pictures show spherical particles between 150 and 300 nanometre, confirming the DLS data. Studies have shown previously that the cell uptake of spherical shaped nanoparticles compared to rod-shaped particles of the same size increased by up to 500 %. This was attributed to an increase in membrane wrapping time needed for non-spherical particles.[27] Hence, the triclosan nanoparticles obtained from emulsion freeze-drying exhibit a favourable shape for cell uptake.

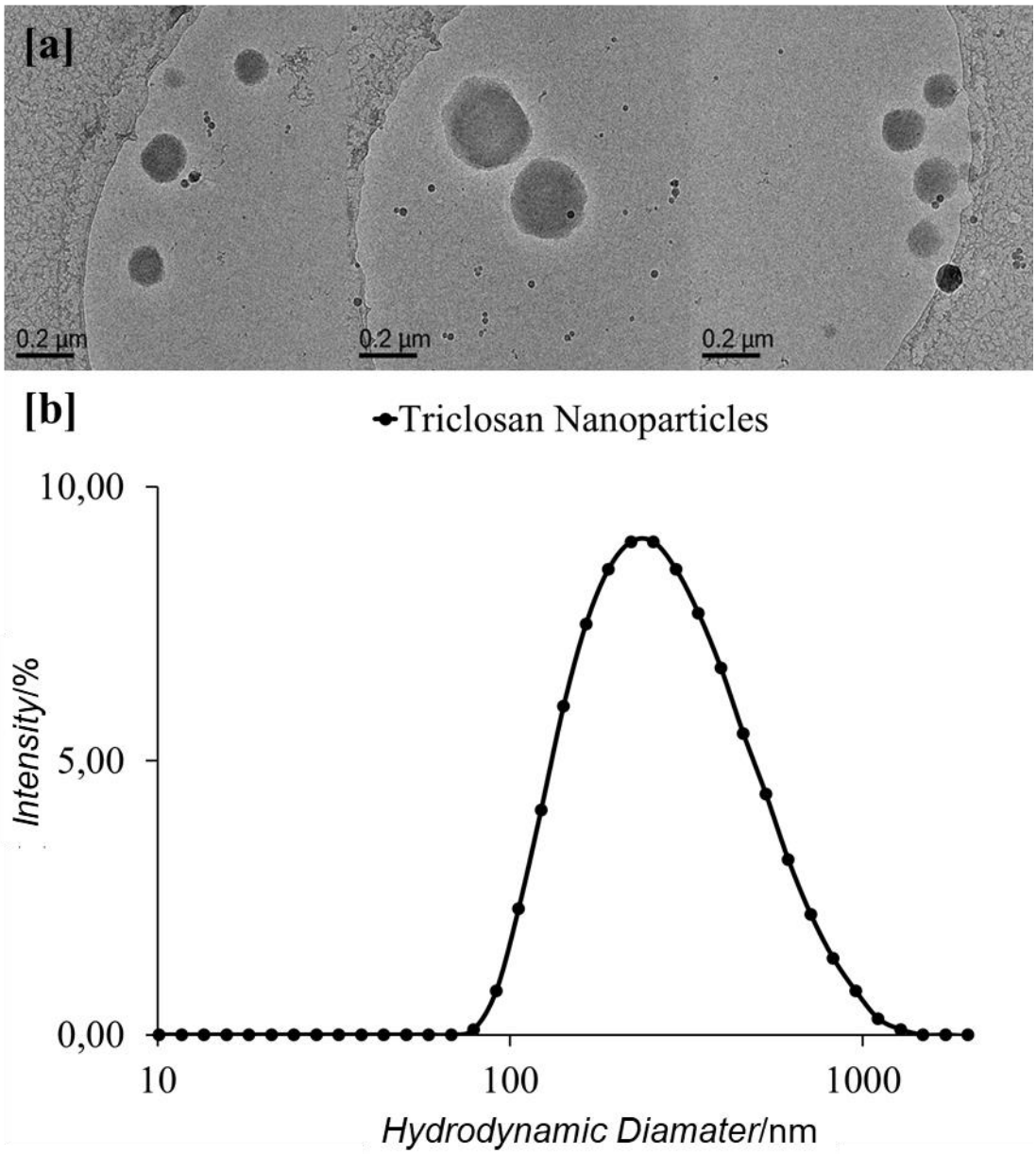

Figure 2.11. a) Cryo-TEM images of triclosan nanoparticles in YEPD medium obtained by emulsion freeze-drying and b) DLS data of triclosan nanoparticles in YEPD medium obtained by emulsion freeze-drying.

Nanoparticles of triclosan were used to test their antimicrobial activity against *Candida albicans*. *C. albicans* was chosen as a model organism because it is well adapted to laboratory testing and because it is the leading cause for Invasive candidiasis (IC), accounting for 40 % of all IC cases. IC is a leading cause of nosocomial blood stream infections in hospitals in the USA with a high mortality rate of 40 %.[28,29] Triclosan was chosen because of its very low water solubility of only about 10 µg/ml.[30] Triclosan as received and triclosan nanoparticles formed by emulsion freeze-

drying stabilised by polymer **1** were added to *C. albicans* in concentrations of 6 to 1 µg/ml in steps of 1 µg/ml and incubated till optical density of 1 was reached. Optical density at 600 nm was measured every half hour by our collaborator M. Nawrath in Industrial biology in ICES. The nanoparticles could be re-dispersed directly into DI water to form a stock solution of 2 mg/ml. For comparison, a triclosan stock solution of 2 mg/ml and polymer stock solution of 10 mg/ml were made. Triclosan as received could not be dissolved directly into water in such high concentrations and had to be dissolved in methanol and then added to medium. Figure 2.12. shows the growth curves of *Candida albicans* incubated with the highest and lowest concentrations of triclosan as received, triclosan nanoparticles and polymer **1**.

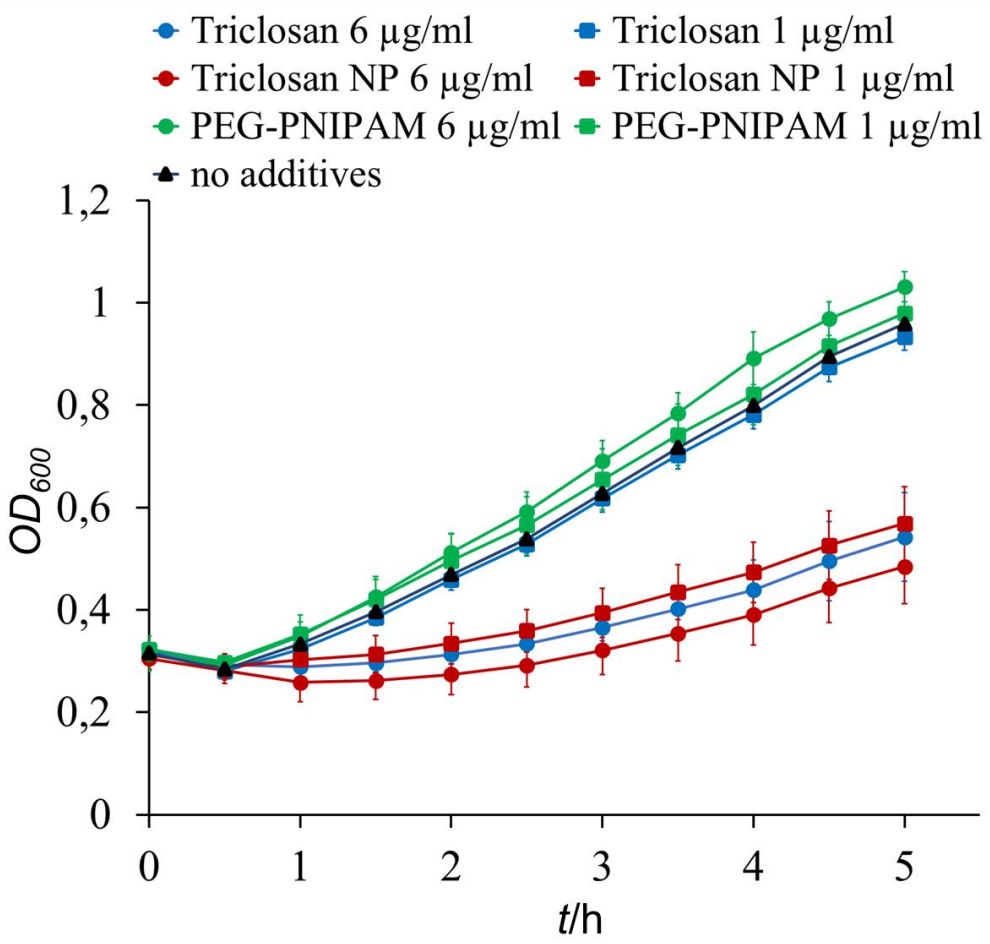

Figure 2.12. Growths curves of *Candida albicans* after the addition of triclosan (blue) methanolic solutions in YEPD medium, triclosan nanoparticles and polymer PEG_{45}-*b*-($PNIPAm_{60}$-*co*-$EDAm_{0.8}$)-*b*-PEG_{45} (**1**) (red) re-suspended in YEPD medium and polymer PEG_{45}-*b*-($PNIPAm_{60}$-*co*-$EDAm_{0.8}$)-*b*-PEG_{45} (**1**) re-suspended in YEPD medium (green) as well as *Candida albicans* without any additives (black).

The black curve in Figure 2.12. shows the growth of *C. albicans* without any additives over a period of 5 hours. For direct comparison, the green curve shows the growths of cells after the addition of polymer **1**. No inhibition could be observed, proving that there is no influence of polymer on the growths inhibition of *C. albicans*. The inhibition of *C. albicans* with triclosan as received (blue) was highly dependent on the concentration used. As such, low concentrations of 1 µg/ml had almost no effect on the cells, while 6 µg/ml significantly slowed down the cell growths. Using triclosan nanoparticles (red) showed that even at low concentrations the growths was stunted almost as much as when the highest concentration of triclosan as received was used. Previous studies of triclosan nanosuspensions tested on *E.coli* and *S. Aureus* had already shown that nanosizing greatly improved the activity of triclosan by up to 10 times and up to 8 times against *Corynebacterium*.[23,31] However, no studies on *C. albicans* had been done up to this point. Differences in activity enhancement between these organisms are likely a result of the difference in cell wall composition and as such a direct comparison is not possible.

Figure 2.13 shows the obtained data of growths curves for triclosan as received (Figure 2.13.a) and triclosan nanoparticle (Figure 2.13.b) concentrations of 1, 2, 3, 4, 5 and 6 µg/ml. For triclosan as received, the inhibitory activity significantly depends on the concentration, while triclosan nanoparticles seem to inhibit growths in almost the same manner independent of concentration. To illustrate this better, the OD_{600}, *i.e.* the optical density measured at 600 nm, after 5 h incubation was plotted against the concentration (Figure 2.13.c). It could clearly be observed that triclosan as received showed a decrease in growths with increasing concentration as was expected. However, when triclosan nanoparticles were used, it was observed that the OD_{600} after 5 h was only slightly higher for the lowest concentration compared to the highest *i.e.* 0.57 to 0.48.

This can be explained by the higher dissolution rate as well as higher availability of nanosized particles. Higher dissolution rate according to the Noyes-Whitney equation is a direct consequence of an increased surface area brought on by a decreased size,[32-34] which has been proven repeatedly for different water insoluble actives.[35,36] Studies with gold and silver nanoparticles have shown that nanoparticles, because of their decreased size, can be taken up by cells via endocytosis. One study found that nanoparticles anchored onto the cell walls, where they were able to form

pits where more nanoparticles could agglomerate and taken into the cell by endocytosis.[37-40] Both effects favour the cell intake and as such even at small concentration enough active. *i.e.* triclosan, can reach the cells to stop the population from growing compared to non-processed triclosan. Therefore, lower amounts of drugs are sufficient to reach the same therapeutic efficacy.

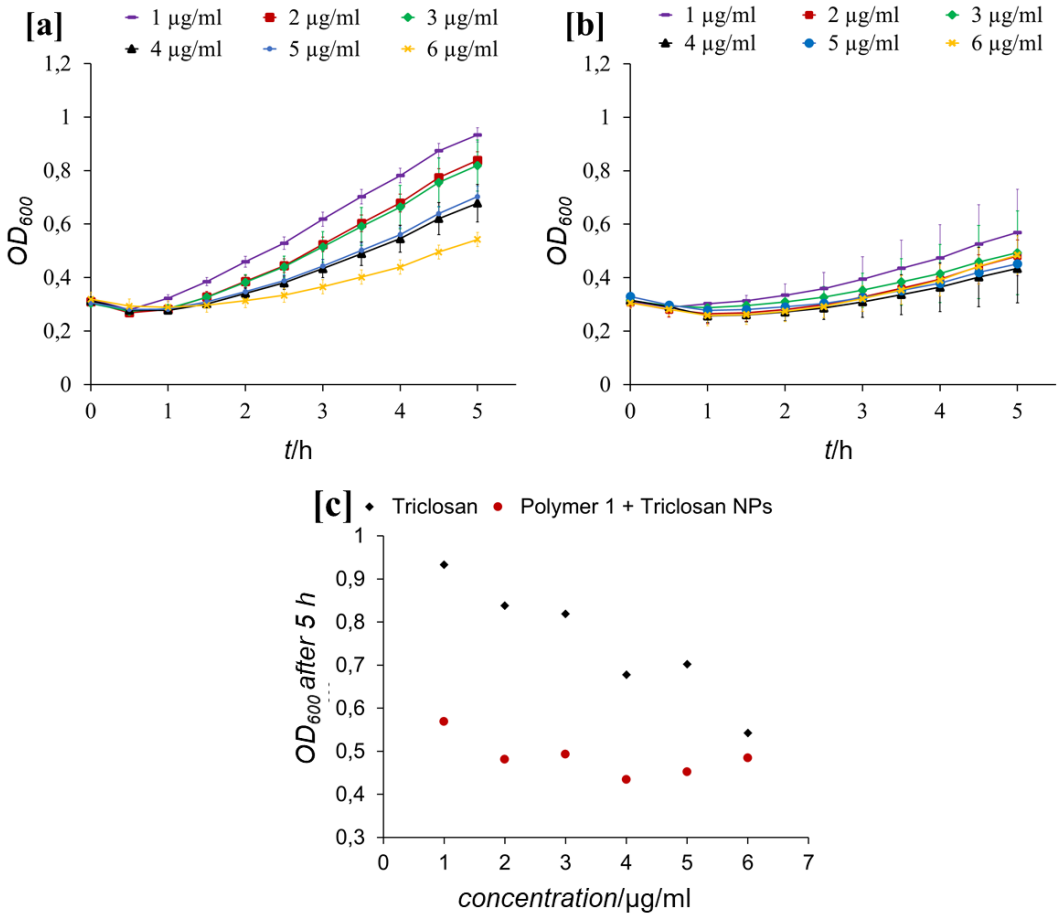

Figure 2.13. Growths curves of *Candida albicans* after the addition of different concentrations of a) triclosan; b) triclosan nanoparticles and c) OD_{600} after 5h of *C. albicans* incubated with triclosan and triclosan nanoparticles against concentration.

2.3.4. Hydrophobic dye and drug nanoparticles by emulsion freeze-drying in dependence of cross-linking

The influence of cross-linking density of the polymers on nanoparticle size and emulsion stabilisation was investigated as well. To that end, a series of PEG_{135}-*b*-($PNIPAm_{50}$-*co*-$EDAm_{2n}$)-*b*-PEG_{135} with cross-linker equivalences of n = 0.3, 0.6 and 0.9 (**4-6**) was synthesised by Dr A. Jackson in ICES. A PEG-dimer with a higher molecular weight of 12000 g/mol was chosen, because it was theorised that a higher

M_w would lead to emulsions with better stability and the ability to obtain emulsions with higher percentage oil, which would in turn mean higher loading. The synthesis has been discussed in 2.3.1 and will, for that reason, not be discussed here. As had already been done before, cyclohexane/oil red and *o*-xylene/indomethacin solutions were used to form emulsions and subsequently nanoparticle.

2.3.4.1 Emulsions freeze drying of Oil Red O

Emulsions of 2 wt % aqueous polymer stock solutions and 0.5 wt % oil red (OR) in cyclohexane were formed. Oil phase percentages were chosen as 66 % (o/w = 2/1), 75 % (o/w = 3/1) and 80 % (o/w = 4/1). It was observed that emulsions formed by polymer **4** were stable over all percentages of oil, while emulsions of polymer **5** became more unstable when less oil was used *i.e.* 66 % oil phase failed to form a stable emulsion. The trend continued with polymer **6** where only 80 % oil phase emulsions were stable enough to be lyophilised. This may be a result of higher cross-linking producing particles with tighter cores and more polymer chains, which in turn leads to more PEG arms on the surface of the particle. These particles are then increasingly more hydrophilic and the wettability by water is higher,[22] up to the point where adsorption at the oil/water interface is not possible anymore. Increasing the percentage of oil could have forced the adsorption.

Figure 2.14. shows SEM pictures of OR nanoparticles and the polymer scaffolds obtained after emulsion freeze-drying of emulsions stabilised by polymer **5** and **6** with 80 % oil phase content. Figure 2.14. a and b show the emulsion templated scaffolds of polymer **5** and **6** of emulsion formed with 80 % oil respectively. Both scaffolds show the structure associated with an emulsion. Scaffolds formed from **5** however show slightly smaller spheres *i.e.* droplets pre-lyophilisation, than scaffolds of polymer **6**. This corresponds well with the observation that increased cross-linkage led to destabilisation of the emulsions. Figure 2.14. b and d show SEM images of nanoparticles obtained after re-dispersion of OR nanoparticles stabilised in the polymer scaffolds in water. Nanoparticles of around 200 to 300 nm were obtained.

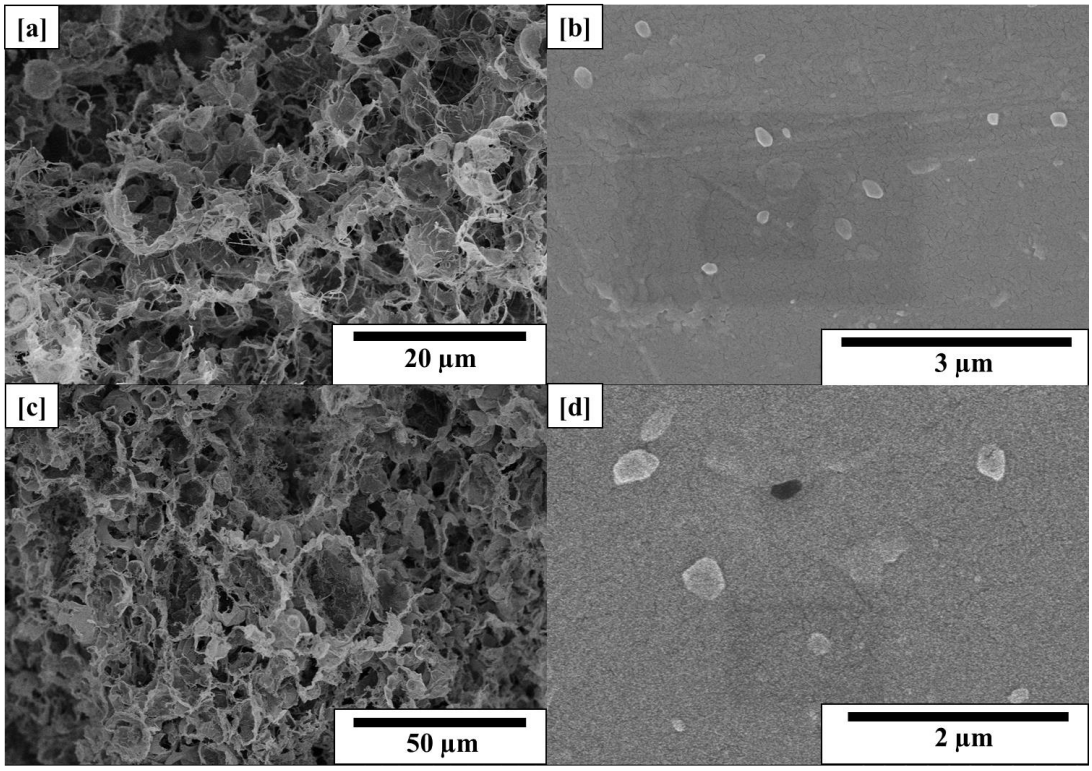

Figure 2.14. SEM pictures of a) Scaffold of an 80 % oil phase emulsions after emulsion freeze-drying of 2 wt % polymer PEG_{135}-*b*-($PNIPAm_{50}$-*co*-$EDAm_{1.2}$)-*b*-PEG_{135} (**5)** + 0.5 wt % oil red; b) Nanoparticles of oil red after resuspension of a; c) Scaffold of a 80 % oil phase emulsions after emulsion freeze-drying of 2 wt % polymer PEG_{135}-*b*-($PNIPAm_{50}$-*co*-$EDAm_{1.8}$)-*b*-PEG_{135} (**6)** + 0.5 wt % oil red and d) Nanoparticles of oil red after resuspension of c.

The obtained powders could readily be re-suspended in water to form nanosuspensions. Figure 2.15.c shows the obtained nanosuspensions as well as OR dissolved in cyclohexane (Figure 2.15.a) and unprocessed, undissolved OR in water (Figure 2.15.b) for comparison.

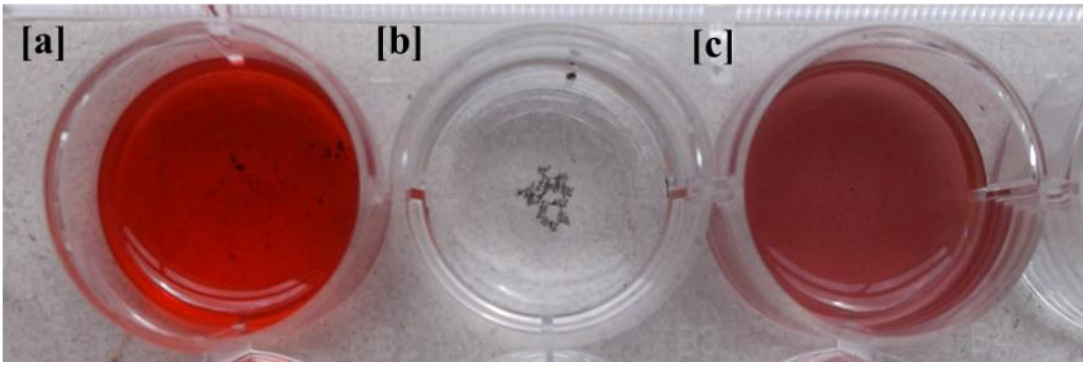

Figure 2.15. a) Oil Red O dissolved in cyclohexane; b) Oil Red O as received dissolved in water and c) Oil Red O nanoparticles produced by emulsion freeze-drying in water.

Nanosuspensions were measured by DLS and UV/Vis to acquire size and nanoparticle yield. The results are shown in Table 2.6. Data obtained indicated that with decreasing oil phase the nanoparticle yield increased *e.g.* from 45 to 50 % yield when the oil phase percentage decreased from 80 % to 66 % for polymer **4**, while the PDI decreased *e.g.* 0.42 to 0.35 going from 80 % to 66 %. No discernible particle size trend could be observed, indicating that by using emulsion freeze-drying with branched polymers, consistently small particles could be obtained almost independent of cross-linkage. The plotted DLS data in Figure 2.16. confirms this observation.

Table 2.6. Overview of size and yield of OR nanoparticles prepared by emulsion freeze drying stabilised by PEG_{135}-*b*-($PNIPAm_{50}$-*co*-$EDAm_{0.6}$)-*b*-PEG_{135} (**4**); PEG_{135}-*b*-($PNIPAm_{50}$-*co*-$EDAm_{1.2}$)-*b*-PEG_{135} (**5**) and PEG_{135}-*b*-($PNIPAm_{50}$-*co*-$EDAm_{1.8}$)-*b*-PEG_{135} (**6**)

Cross linkage	**Oil Phase [%]**	**D_h Z-Average [nm]**	**D_h Int. % [nm]**	**PDI**	**Yield [%]**
	%	**——— nm ———**		**-**	**%**
0.3 (**4**)	80	395	438	0.42	45
0.3 (**4**)	75	340	980, 274	0.39	37
0.3 (**4**)	66	423	760,231	0.35	50
0.6 (**5**)	80	506	606, 115	0.29	54
0.6 (**5**)	75	298	376	0.22	67
0.6 (**5**)	66	not stable	not stable	not stable	not stable
0.9 (**6**)	80	348	456	0.33	36
0.9 (**6**)	75	not stable	not stable	not stable	not stable
0.9 (**6**)	66	not stable	not stable	not stable	not stable

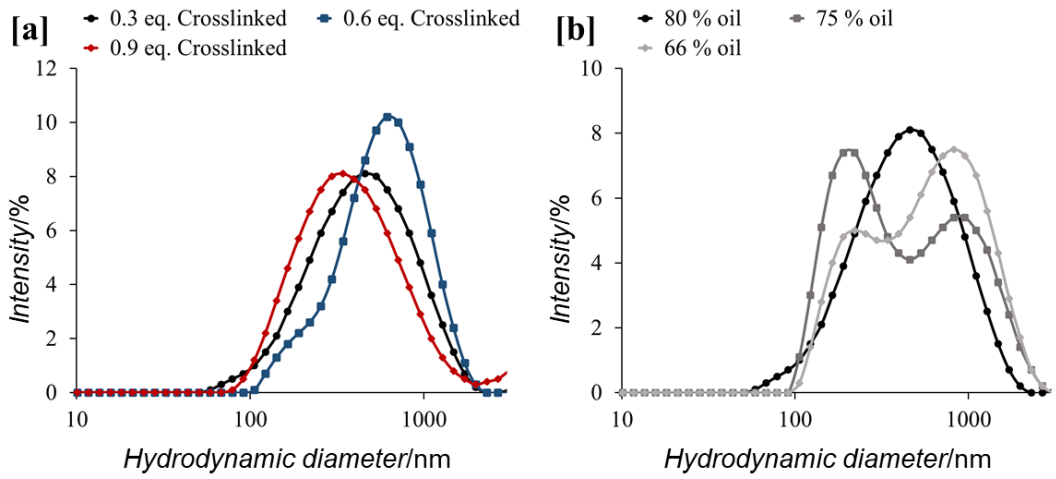

Figure 2.16. DLS data of oil red nanoparticles re-suspended in water of a) freeze-drying an 80 % emulsion stabilised by PEG_{135}-*b*-(PNIPAm$_{50}$-*co*-EDAm$_{0.6}$)-*b*-PEG_{135} (**4**); PEG_{135}-*b*-(PNIPAm$_{50}$-*co*-EDAm$_{1.2}$)-*b*-PEG_{135} (**5**) and PEG_{135}-*b*-(PNIPAm$_{50}$-*co*-EDAm$_{1.8}$)-*b*-PEG_{135} (**6**) and b) emulsions of varying oil percentages stabilised by PEG_{135}-*b*-(PNIPAm$_{50}$-*co*-EDAm$_{0.6}$)-*b*-PEG_{135} (**4**).

The emulsion freeze-drying approach also ensures long storage stability. To verify this, nanosuspensions were formed immediately after freeze-drying and after 8 and 9 months storage at room temperature. Figure 2.17. shows the plotted DLS data.

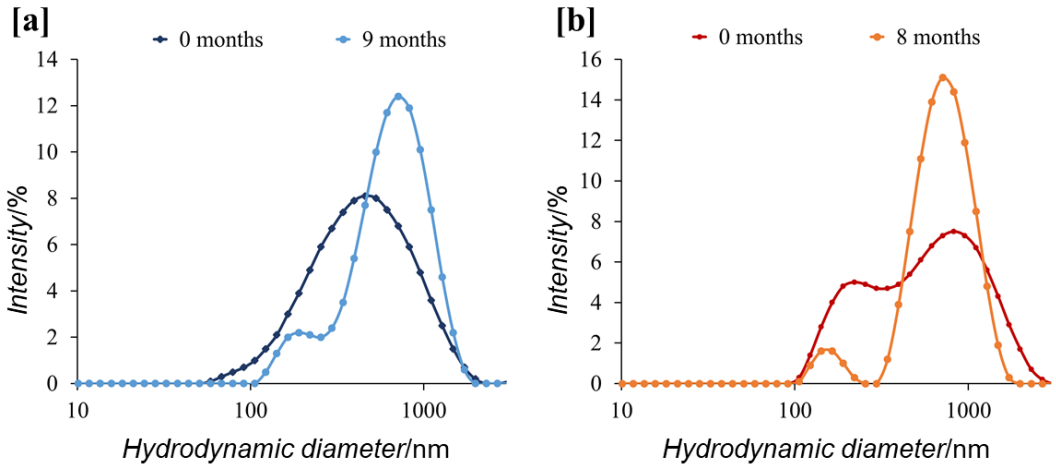

Figure 2.17. DLS data of oil red nanoparticles after resuspension in water stabilised by polymer PEG_{135}-*b*-(PNIPAm$_{50}$-*co*-EDAm$_{0.6}$)-*b*-PEG_{135} (**4**) from a) 80 % oil phase emulsion after being stored and re-suspended after 9 months and directly after freeze-drying and b) 66 % oil phase emulsion after being stored and re-suspended after 8 months and directly after freeze-drying.

Figure 2.17. shows that after 8 and 9 months the OR nanoparticles were slightly bigger than immediately after freeze-drying, hence some agglomeration

probably occurred. However, the size increase is quite small, showing that the polymer scaffold is excellent in stabilising nanoparticles against agglomeration.

2.3.4.2 Emulsions freeze drying of Indomethacin

Indomethacin was chosen as a model drug as had been done before in 2.3.2.1. Emulsions were formed by homogenizing 2 wt % aqueous solutions of **4**-**6** and 0.5 wt % indomethacin in *o*-xylene. In contrast to using cyclohexane as oil phase solvent, emulsions formed from *o*-xylene could be formed for all oil phase percentages and all cross-linkages.

Figure 2.18. shows microscope pictures of emulsions containing 75 % oil of polymer **5** and **6** respectively (Figure 2.17. a and b) and an emulsion formed using **6** and 80 % oil. All formed emulsions were oil in water emulsions. The average droplet size spanned between 3 µm and 20 µm with the average size being around 5 µm for all emulsions formed for polymers **5** and **6** using the same oil percentage. This seemed to indicate that the droplet size was independent of cross-linking when *o*-xylene was used as oil phase. However, when the oil percentage was decreased, the droplet size decreased slightly which should lead to smaller nanoparticles.

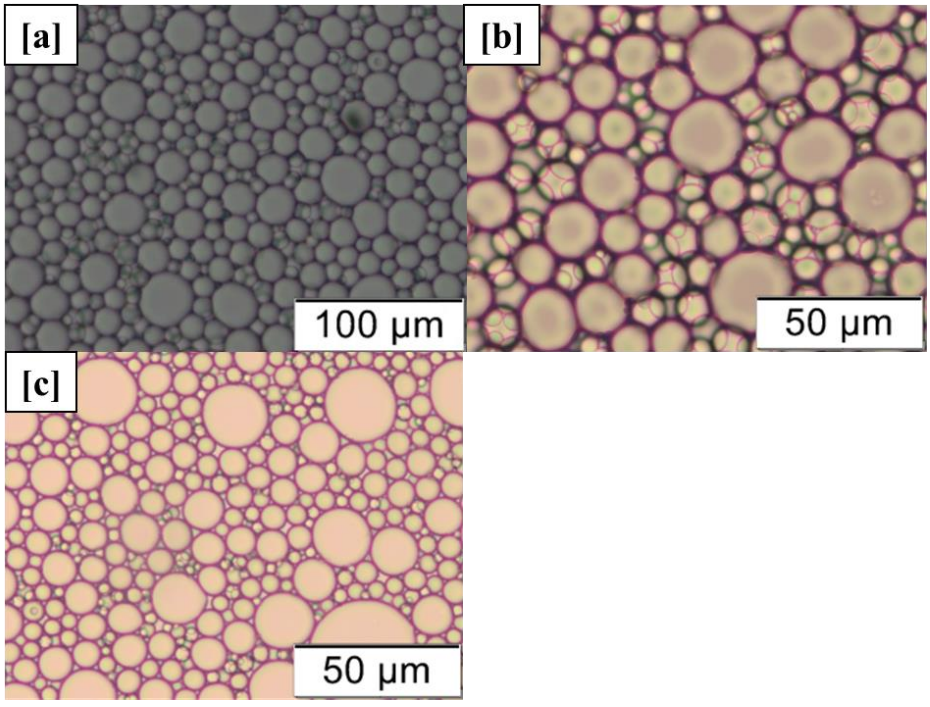

Figure 2.18. Optical microscopic images of the emulsions formed by dispersing IMC/*o*-xylene solution in aqueous polymer solution. a) PEG_{135}-*b*-($PNIPAm_{50}$-*co*-$EDAm_{1.2}$)-*b*-PEG_{135} (**5**) with 75 % oil phase; b) PEG_{135}-*b*-($PNIPAm_{50}$-*co*-$EDAm_{1.8}$)-*b*-PEG_{135} (**6**) with 75 % oil phase and c) PEG_{135}-*b*-($PNIPAm_{50}$-*co*-$EDAm_{1.8}$)-*b*-PEG_{135} (**6**) with 66 % oil phase

After freeze-drying the emulsions, SEM pictures were taken of all three variations of the cross-linked branched polymer scaffolds with 80 % oil phase (Figure 2.19.). Those were chosen because they produced the highest nanoparticle yield, which will be discussed further on. All scaffolds clearly show emulsion templating. The scaffolds of polymers **4** and **5** both showed similar sized vesicles templated by the oil droplets (Figure 2.19. a and b). Unfortunately, no high magnification SEM pictures of the scaffold of polymer **6** (Figure 2.19.c) could be obtained and as such the vesicle sizes could not be observed well enough to make any assertions about the size of the droplet templated spheres.

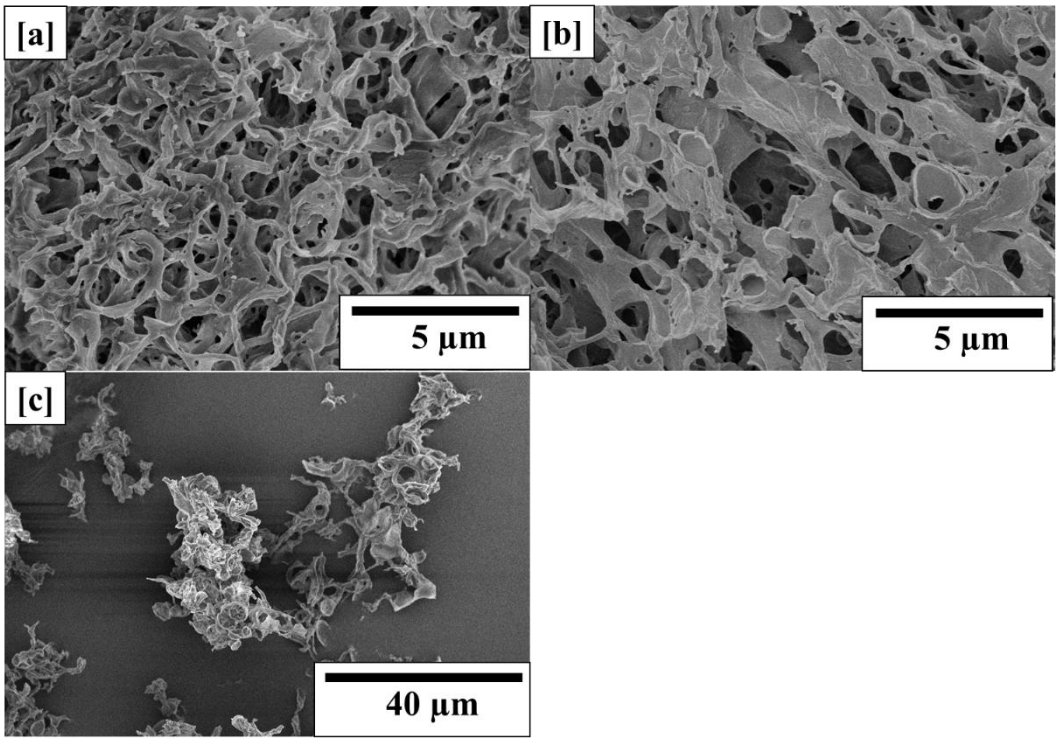

Figure 2.19. SEM pictures of scaffolds formed by emulsion freeze-drying of emulsions of 80 % oil phase and 0.5 wt % indomethacin using a) 2 wt % polymer PEG_{135}-*b*-($PNIPAm_{50}$-*co*-$EDAm_{0.6}$)-*b*-PEG_{135} (**4**);; b) 2 wt % polymer PEG_{135}-*b*-($PNIPAm_{50}$-*co*-$EDAm_{1.2}$)-*b*-PEG_{135} (**5**) and c) 2 wt % polymer PEG_{135}-*b*-($PNIPAm_{50}$-*co*-$EDAm_{1.8}$)-*b*-PEG_{135} (**6**).

The scaffolds could readily be re-suspended in water to form nanosuspensions of indomethacin. Table 2.7 shows the DLS data measured and the nanoparticles yield. All sizes were between 550 and 480 nm and no discernible size trend could be observed. However, the nanoparticle yield tended to decrease with less oil phase and lower cross-linkages of 0.3 eq (**4**) and 0.6 eq. (**5**) While the yield increased slightly for higher

oil phases when 0.9 eq. (**6**) cross-linkages were used and small PDIs of around 0.3 and under could be obtained for all samples.

To give a better insight into size changes in dependence of cross-linkage and oil phase content the size data was plotted in Figure 2.20. Data was plotted for the same oil phase percentage with varying cross-linkage (Figure 2.20 a, b and c) and for constant cross-linkage and varying the oil phase (Figure 2.20. d, e and f). The plotted data shows that while no significant difference between sizes overall could be observed, polymer **5** produced multiple peaks in the DLS *i.e.* two main particle size populations. This is also reflected in the higher PDIs as seen in Table 2.7.

Table 2.7. Overview of size and yield of indomethacin nanoparticles prepared by emulsion freeze drying stabilised by PEG_{135}-*b*-($PNIPAm_{50}$-*co*-$EDAm_{0.6}$)-*b*-PEG_{135} (**4**); PEG_{135}-*b*-($PNIPAm_{50}$-*co*-$EDAm_{1.2}$)-*b*-PEG_{135} (**5**) and PEG_{135}-*b*-($PNIPAm_{50}$-*co*-$EDAm_{1.8}$)-*b*-PEG_{135} (**6**).

Cross linkage	**Oil Phase [%]**	**D_h Z-Average [nm]**	**D_h Int. % [nm]**	**PDI**	**Yield [%]**
	%	**nm**		**-**	**%**
0.3 (**4**)	80	480	472	0.22	40
0.3 (**4**)	75	475	486	0.18	23
0.3 (**4**)	66	484	396, 192	0.36	28
0.6 (**5**)	80	551	408	0.35	46
0.6 (**5**)	75	476	492, 148	0.51	38
0.6 (**5**)	66	552	713, 219	0.43	40
0.9 (**6**)	80	454	472, 93	0.33	53
0.9 (**6**)	75	507	545, 163	0.33	43
0.9 (**6**)	66	470	484, 112	0.38	64

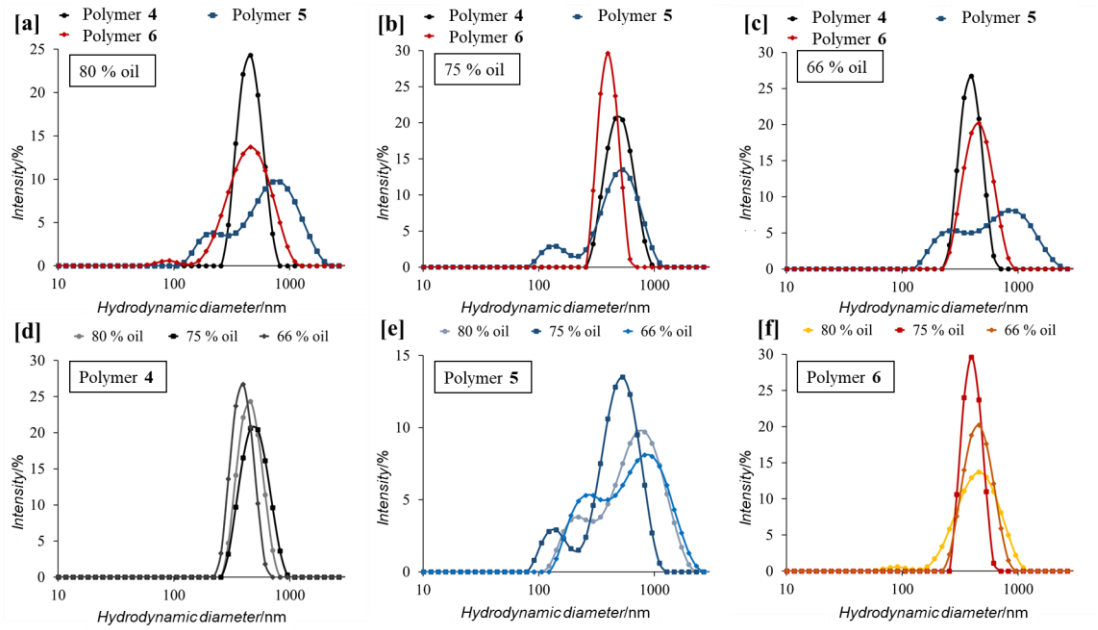

Figure 2.20. DLS data of indomethacin nanosuspensions formed by emulsion freeze drying emulsion formed with a) 80 % oil phase with different cross-linkages; b) 75 % oil phase with different cross-linkages; c) 66 % oil phase with different cross-linkages; d) 2 wt % of polymer PEG_{135}-*b*-($PNIPAm_{50}$-*co*-$EDAm_{0.6}$)-*b*-PEG_{135} (**4**) with different oil phase percentages e) 2 wt % of polymer PEG_{135}-*b*-($PNIPAm_{50}$-*co*-$EDAm_{1.2}$)-*b*-PEG_{135} (**5**) with different oil phase percentages; and f) 2 wt % of polymer PEG_{135}-*b*-($PNIPAm_{50}$-*co*-$EDAm_{1.8}$)-*b*-PEG_{135} (**6**) with different oil phase percentages.

Generally, amorphous drugs exhibit higher solubility and dissolution rate, which is favourable for clinical applications.[41] The crystallinity of indoemthacin nanoparticles was therefore examined by PXRD. Figure 2.21 shows the measured data of as received indomethacin (Figure 2.21 a), nanoparticles of indomethacin formed after emulsion freeze-drying in the presence of **4**-**6** (Figure 2.21 b, d and f), pure polymer **6** and centrifugated nanosuspensions to obtain pure nanoparticles with the least amount of polymer (Figure 2.21 e).

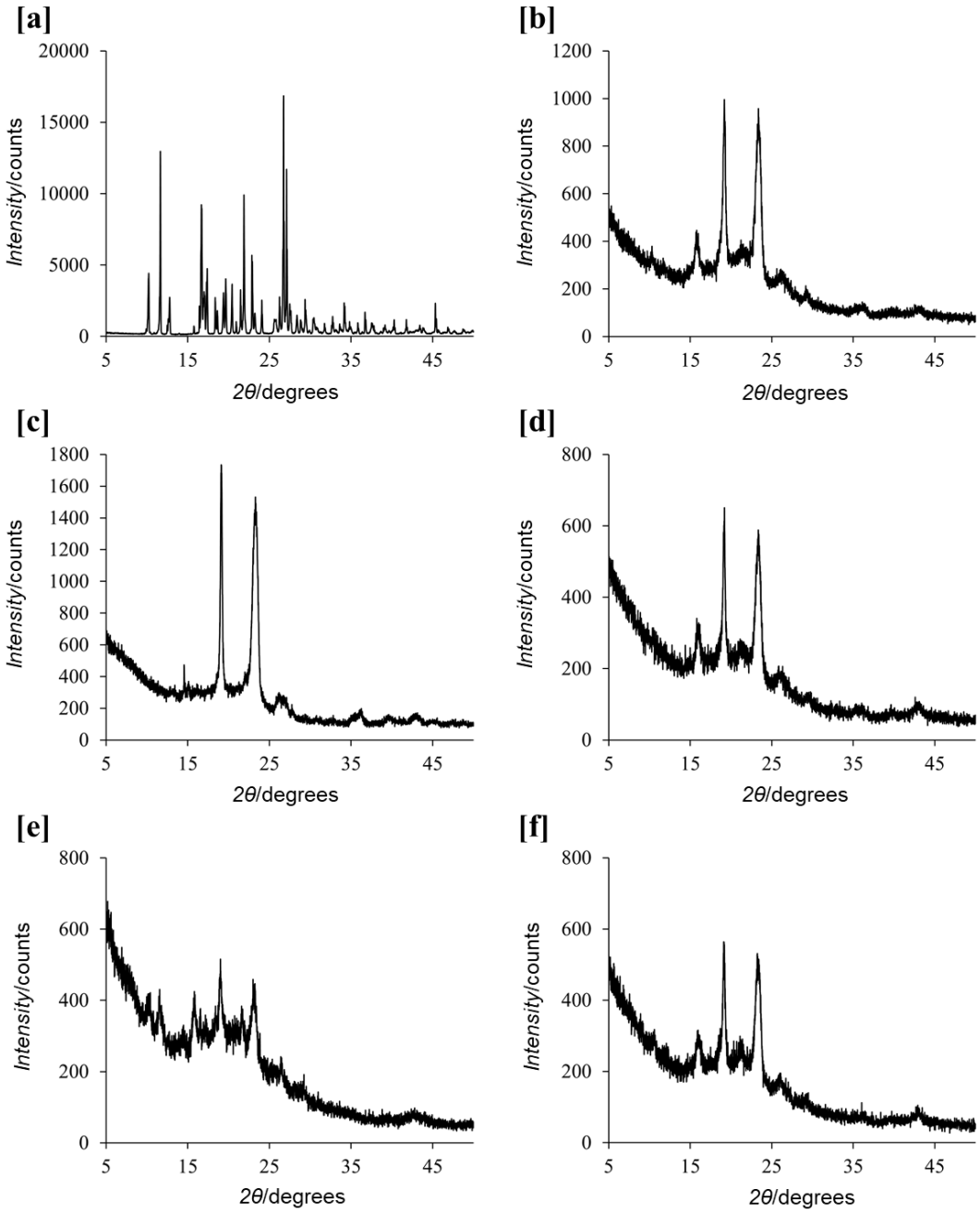

Figure 2.21. PXRD data of a) crystalline indomethacin; b) indomethacin nanoparticles in polymer PEG_{135}-*b*-($PNIPAm_{50}$-*co*-$EDAm_{0.6}$)-*b*-PEG_{135} (**4**) scaffold; c) polymer PEG_{135}-*b*-($PNIPAm_{50}$-*co*-$EDAm_{1.8}$)-*b*-PEG_{135} (**6**); d) indomethacin nanoparticles in polymer PEG_{135}-*b*-($PNIPAm_{50}$-*co*-$EDAm_{1.2}$)-*b*-PEG_{135} (**5**) scaffold; e) Nanoparticles of indomethacin after centrifugation of indomethacin nanosuspension and f) indomethacin nanoparticles in polymer PEG_{135}-*b*-($PNIPAm_{50}$-*co*-$EDAm_{1.8}$)-*b*-PEG_{135} (**6**) scaffold.

Sharp peaks could clearly be seen for crystalline indomethacin (Figure 2.21 a), while in the PXRDs of nanoparticles stabilised by polymer scaffolds of **4**,**5**, and **6** (Figure 2.21 b, d and f) only three peaks could be found on top of an amorphous 'halo'

between 15° to 30°. These peaks could not be assigned to indomethacin. For this reason, polymer **6** alone was measured (Figure 2.21 c) and the same signals could be detected, which are probably a result of semicrystalinity. Polymers typically form amorphous structures, however semicrystalline structures which exhibit amorphous and crystalline regions are known for polymers as well. Semicrystallinity accounts for the sharp peaks in the PXRD, as well as the broad underlying peak, the so called 'halo', from 15° to 30°. In order to identify the phase of indomethacin particles more clearly, the indomethacin nanoparticles were separated from the polymer by centrifuging at 13,000 rpm for 5 min. A control experiment with aqueous polymer solution at this speed showed no precipitation of the polymer. Figure 2.21 c shows the similar PXRD pattern as Figure 2.21 b, d and f (non-centrifuged), but with the peak intensity significantly decreased. This led us to the conclusion that these peaks were more likely the artefacts of polymer adsorbed to indomethacin particles and precipitated together. This indicated that amorphous indomethacin nanoparticles were produced by this approach.

Long term storage stability was measured by re-suspending the powders after 8 months of storage at room temperature and measuring DLS. Figure 2.22 shows these results.

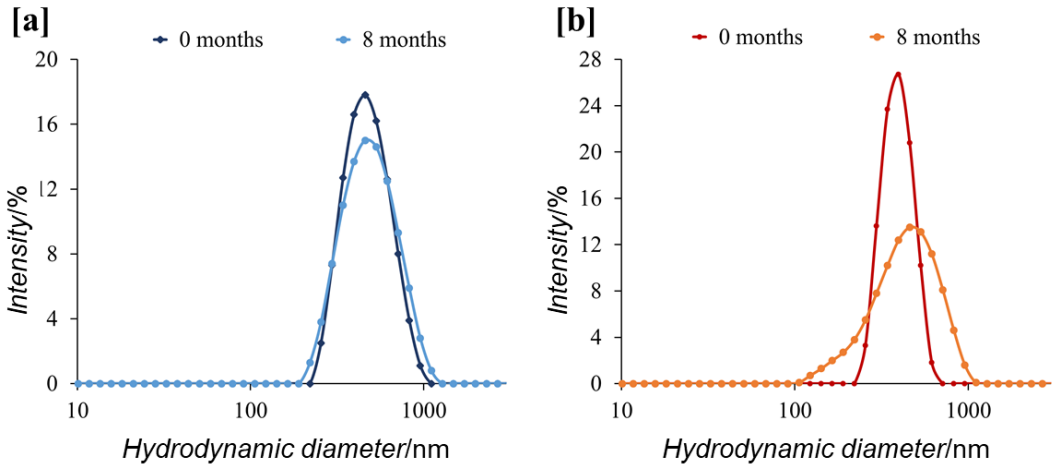

Figure 2.22. DLS data of indomethacin nanoparticles after resuspension in water stabilised by PEG_{135}-*b*-($PNIPAm_{50}$-*co*-$EDAm_{0.6}$)-*b*-PEG_{135} (**4**) from a) 80 % oil phase emulsion after 8 months and directly after resuspension and b) 66 % oil phase emulsion after 8 months and directly after resuspension.

Figure 2.22 clearly shows that sizes of indomethacin nanoparticles formed by emulsion freeze-drying stabilised in a polymer scaffold of **4** did not significantly

change over 8 months. In case of emulsions form 80 % oil the sizes did not change at all. Showing that the polymers used are excellent in stabilising against agglomeration.

2.3.4.3. Emulsions freeze drying of ketoprofen and ibuprofen

In order to demonstrate the versatility of the emulsion-freeze drying approach, two more drugs, ketoprofen and ibuprofen were processed using the same procedure. Since the highest yield for indomethacin was achieved using polymer **6** and 66 % o-xylene, these conditions were also used for ketoprofen and ibuprofen.

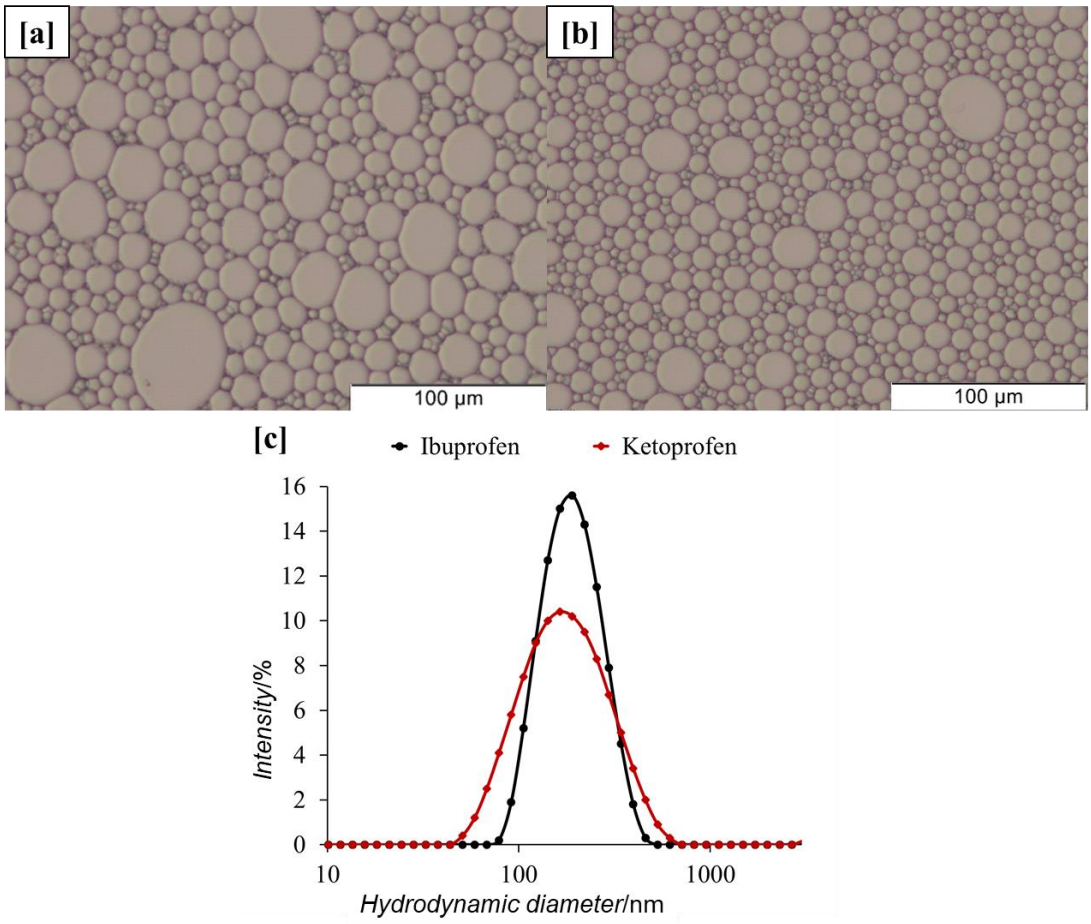

Figure 2.23. Optical microscopic images of the emulsions formed by a) polymer PEG_{135}-*b*-($PNIPAm_{50}$-*co*-$EDAm_{1.8}$)-*b*-PEG_{135} (**6**) with 66 % oil phase and 0.5 wt % ibuprofen; b) polymer PEG_{135}-*b*-($PNIPAm_{50}$-*co*-$EDAm_{1.8}$)-*b*-PEG_{135} (**6**) with 66 % oil phase and 0.5 wt % ketoprofen and c) DLS size data of ketoprofen and ibuprofen nanoparticles after resuspension in water after emulsion freeze-drying.

It was possible to form stable emulsions with droplet sizes between 5 to 25 µm (Figure 2.23. a and b) with ketoprofen being slightly smaller and more uniform. After freeze-drying, porous white powders were obtained for both ketoprofen and

ibuprofen, which were dissolved in water to produce a clear suspension without any precipitates observed. This indicates that a 100 % yield of nanoparticles for ketoprofen and ibuprofen was achieved by the emulsion-freeze-drying approach. DLS measurements were performed without any pre-treatment of the nanosuspensions. The DLS profiles by intensity (Figure 2.23 c) gave the peak size 198 nm for ibuprofen and 211 nm for ketoprofen. The particle size distribution (PDI) was calculated to be 1.32 for ketoprofen and 1.15 for ibuprofen.

2.4. Conclusions

Initially branched diblock copolymers composed of low Mw PEG (2000 kDa) arms and hydrophobic cores of PNIPAm, *n*BMA and styrene were synthesised by conventional radical polymerisation in a one-pot synthesis. These monomers were chosen because of their different hydrophobicity and solubility in organic solvents. Initially emulsions were formed using *o*-xylene with 0.5 wt % indomethacin and 2 wt % aqueous polymer solutions in ratios of 4:1 (80 % oil) and 1:1 (50 % oil), which were lyophilised to obtain indomethacin nanoparticles stabilised by a branched polymer scaffold. The obtained dry powders were re-dispersed in medium to form nanosuspensions and analysed for size and stability in dependence of branched polymer used. It was observed that only the use of PEG_{45}-*b*-($PNIPAm_{60}$-*co*-$EDAm_{0.8}$)-*b*-PEG_{45} (**1**) produced stable emulsions and nanoparticles. This was attributed to *o*-xylene being a bad θ-solvent for PEG_{45}-*b*-($PBMA_{50}$-*co*-$DEGDMA_{0.7}$)-*b*-PEG_{45} (**2**), while PEG_{45}-*b*-(PS_{46}-*co*-$DVB_{0.6}$)-*b*-PEG_{45} (**3**) was too hydrophobic to be re-dispersed at all. Changing the oil phase to cyclohexane and using the same weight percentages, nanoparticles of Oil Red O stabilised by **1** as well as **2** could be obtained. Because of the increased amphiphilic character of **2** in comparison to **1** only emulsions of o/w ratios of 4:1 (80 %) could produce nanoparticles when **2** was used, while **1** formed more stable emulsions with o/w ratios of 1:1 (50 %).

Because of the high nanoparticle yield and relatively small particle sizes polymer **1** and cyclohexane were chosen to form triclosan nanoparticles by emulsion freeze-drying which could readily be dissolved in water to form nanosuspensions. These triclosan nanoparticles showed sizes of below 300 nm. Triclosan nanoparticles were then tested for enhanced antimicrobial activity against *C. albicans.* In comparison to as received triclosan it was possible using triclosan nanoparticles formed by emulsion freeze-drying to disperse the highly hydrophobic triclosan directly into

water without the need for methanol as a co-solvent. The antimicrobial activity of aqueous nanosuspensions of triclosan compared to non-processed triclosan was found to be 6 times higher. This would be highly advantageous in a medical setting because less active needs to be administered to achieve the same results. This shows not just that nanoparticles stabilised in a branched diblock copolymer scaffold formed by emulsion freeze-drying are excellent in addressing the problem of water insolubility of drugs but are also a promising solution to the problem of emerging resistance in many bacterial and fungi strains due to over medication.[42-44] Simultaneously the decreased dosage would be greatly cost beneficial to our health care systems as well reduce the strain wide spread over use of antimicrobial agents have put on our environment.[45]

Next, the influence of cross-linking on emulsion stability and nanoparticle formation and size was studied. PEG-PNIPAm was chosen as core forming monomer for further studies. Three different equivalences of cross-linking were chosen as well as a longer PEG chain (Mw 6000 kDa), to facilitate the possibility to stabilise higher oil phase ratios and as such achieve higher drug loading. All three branched diblock copolymers (0.3, 0.6 and 0.9 eq. cross-linking (**4**-**6**)) were tested for their ability to form emulsions and nanoparticles with cyclohexane (oil red) and *o*-xylene (indomethacin) in ratios of 4:1 (80 %); 3:1 (75 %) and 2:1 (66 %). It was possible to consistently obtain drug nanoparticles with sizes of around 500 nm and smaller as well as narrow PDIs. The small PDIs were attributed to be the result of the uniform droplet sizes obtained while forming the emulsion *i.e.* similar droplets contain similar amounts of drug available to form nanoparticles, hence narrow PDIs. Furthermore, high particle yields using both *o*-xylene and cyclohexane when using lighter cross-linked branched copolymers were achieved, with high cross-linkage only producing stable emulsions in specific environments.

In summary, it was possible to synthesise and optimise a non-toxic, amphiphilic branched block copolymer to form stable emulsions that could be used to form nanoparticles *via* an emulsion freeze-drying approach by varying the core monomers used and the cross-linkage. The so obtained dry powders could be readily redispersed into water to form nanosuspensions. Dry formulations were stable against agglomeration over months.

Considering the enhanced bioavailability, easy preparation, consistent nanoparticles sizes and high yields, as well as the prolonged stability against agglomeration, the emulsion freeze-drying process presents itself as a favourable alternative to conventional bottom-up techniques like spray-drying, which is often used in the pharmaceutical industry. The spray-drying process presents a few major limitations like the difficulties in working with thermolabile substances, due to the high risk of decomposition or change in property, as well as the poor thermal efficiency of the process which leads to a low cost-efficiency and the need for addition of stabilisers.[46,47] Emulsion freeze-drying with branched block polymers would be a way to circumvent these issues.

2.5. References

1. H. Fessi, F. Puisieux, J.P. Devissaguet, N. Ammoury and S. Benita, *Int. J. Pharm.*, 1989, **55**, R1-R4.
2. H. Fessi, J.P. Devissaguet, F. Puisieux and C. Theis, *US Pat,* US5118528 A, 1992.
3. U. Bilati, E. Allémann and E. Doelker, *Eur. J. Pharm. Sci.*,2005 , **24**, 67-75.
4. R. Fowler, *Chemical Engineer*,1989, 35-37.
5. Z.-L. Zhang, Y. Le, J.-X. Wang, H. Zhao and J.-F. Chen, *Drug Dev. Ind. Pharm.*, 2012, **38**, 1512-1520.
6. E. Reverchon, I. De Marco and E. Torino, *J. Supercrit. Fluids*, 2007, **43**, 126-138.
7. M. Türk and D. Bolten, *J. Supercrit. Fluids*, 2010, **55**, 778-785.
8. J.W. Tom, G.-B. Lim, P.G. Debenedetti and R.K. Prud'homme in *Supercritical Fluid Engineering Science*, ed. E. Kiran and J.F. Brennecke, American Chemical Society, Washington DC, 1992, ch. 19, pp. 238-257.
9. P. Pathak, M.J. Meziani, T. Desai and Y.-P. Sun, *J. Am. Chem. Soc.*, 2004, **126**, 10842-10843.
10. K. Masters, *Spray drying handbook*, John Wiley and Sons, New York, 1979.
11. B. Bhandari and M.W. Woo in *Handbook of Food Powders: Processes and Properties*, ed. B. Bhandari, N. Bansal, M. Zhang and P. Schuck, Woodhead Publishing, Camebridge, 2014, ch. 2, pp. 29-51.

12. K. Rizi, R.J. Green, M. Donaldson and A.C. Williams, *J. Pharm. Sci*., 2011, **100**, 566-579.
13. S.S. Talmage, *Environmental and human safety of major surfactants: alcohol exthoxylates amd alkylphenol ethoxalates,* CRC Press, Baco Raton, Florida, 1994.
14. M. A. Lewis, *Ecotoixol. Environ. Saf.,* 1990, **20**, 123-140.
15. Y. Dong and S.-S. Feng, *Biomaterials*, 2004, **25**, 2843-2849.
16. K. A. Woodrow, Y. Cu, C. J. Booth, J. K. Saucier-Sawyer, M. J. Wood and W. Mark Saltzman, *Nat. Mater.*, 2009, **8**, 526-533.
17. Y. Hu, X. Jiang, Y. Ding, H. Ge, Y. Yuan and C. Yang, *Biomaterials*, 2002, **23**, 3193-3201.
18. S. L. Raghavan, A. Trividic, A. F. Davis and J. Hadgraft, *Int. J. Pharm.*, 2001, **212**, 213-221.
19. A. D. Roberts and H. Zhang, *Int. J. Pharm.*, 2013, **447**, 241-250
20. N. Grant and H. Zhang, *J. Colloid Interface Sci.*, 2011, **356**, 573-578
21. H. Zhang, D. Wang, R. Butler, N.L. Campbell, J. Long, B. Tan, D.J. Duncalf, A.J. Foster, A. Hopkinson, D. Taylor, D. Angus, A.I. Cooper and S.P. Rannard, *Nat. Nanotechol.,* 2008, **3**, 506-511
22. L. Qian, A. Ahmed and H. Zhang, *Chem. Commun.*, 2011, **47**, 10001-10003.
23. D. L. Teagarden and D. S. Baker, *Eur. J. Pharm. Sci.*, 2002, **15**, 115-133.
24. ICH, ICH Harmonised Tripartite Guideline-Impurities: guideline for residual solvents Q3C (R5), http://www.ich.org/fileadmin/Public_Web_Site/ICH_Products/Guidelines/Quality/Q3C/Step4/Q3C_R5_Step4.pdf, (accessed September, 2015).
25. A. Ueda and S. Nagai, in *Polymer Handbook*, ed. J. Brandrup, E. H. Immergut and E. A. Grulke, John Wiley & Sons, Inc. New York, 4th edn, 1999, ch. II/97, pp. II/97 – II/168.
26. S. Mishra, P. Webster and M. E. Davis, *Eur. J. Cell Biol.*, 2004, **83.3**, 97-111.
27. A. Verma and F. Stellacci, *small*, 2010, **6**, 12-21
28. M. A. Pfaller and D. J. Diekema, *Clin. Microbiol. Rev.*, 2007, **20**, 133–163

29. R. Singh and A. Chakrabarti, in C. albicans: Cellular and Molecular Biology, ed. R. Prasad, Springer International Publishing, Switzerland, 2017, ch. 3, pp 25-40
30. T. Loftsson, N. Leeves, B. Bjornsdottir, L. Duffy and M. Masson, *J. Pharm. Sci.*, 1999, **88**, 1254-1258.
31. T. O. McDonald, L. M. Tatham, F. Y. Southworth, M. Giardiello, P. Martin, N. J. Liptrott, A. Owen and S. P. Rannard, 2013, *J. Mater. Chem. B*, **1**, 4455-4465
32. G. Kaptay, *Int. J. Pharm.*, 2012, **430**, 253-257.
33. W. Ostwald, *Z. Phys. Chem.*, 1900, **34**, 795-503
34. A. A. Noyes and W. R. Whitney, *J. Am. Chem. Soc.*, 1897, **19**, 930-934.
35. S. Maleki Dizaj, Z. Vazifehasl, S. Salatin, K. Adibkia and Y. Javadzadeh, *Res. Pharm. Sci.*, 2015, **10**, 95–108.
36. D. Heng, D. J. Cutler, H. K. Chan and J. A. Raper, *Pharm. Res*., 2008, **25**, 1696-1701.
37. S. Prabhu and E. K. Poulose, *Int. Nano Lett.*, 2012, **2**, 32-41.
38. J. Panyam and V. Labhasetwar, 2003, *Adv. Drug Deliv. Rev*., 2003, **55**, 329-347.
39. M. P Desai, V. Labhasetwar, E. Walter, R. J. Levy, R.J. and G. L. Amidon, *Pharm. Res.*, 1997, **14**, 1568-1573.
40. M. P. Desai, V. Labhasetwar, G. L. Amidon and R. J. Levy *Pharm. Res.*, 1996, **13**, 1838-1845.
41. P. Karmwar, J.P. Boetker, K.A. Graeser, C.J. Strachan, J. Rantanen and T. Rades, *Eur. J. Pharm. Sci*., 2011, **44**, 341–350.
42. D.L. Teagarden and D.S. Baker, *Eur. J. Pharm. Sci.*, 2002, **15**, 115-133.
43. S. B. Levy and B. Marshall, *Nat. Med.*, 2004, 10, S122-129
44. T. M. Barbosa and S. B. Levy, 2000, *Drug Resist. Updat.*, **3**, 303–311.
45. A. B. Dann and A. Hontela, *J. Appl. Toxicol*., 2011, **31**, 285–311.
46. J. Broadhead, S. Edmond Rouan and C. Rhodes, *Drug Dev. Ind. Pharm*., 1992, 18, 1169-1206.
47. J. Salazar, R. H. Müller and J. P. Möschwitzer, *J. Pharm. Sci*., 2013, 102, 1636-1649.

Chapter 3

Formation of hyperbranched polymer stabilised drug nanoparticles via solvent evaporation

This Chapter is based on the publication

U. Wais, A. W. Jackson, T. He and H. Zhang, "Formation of hydrophobic drug nanoparticles via ambient solvent evaporation facilitated by branched diblock copolymers.", *Int. J. Pharm.*, 2017, **533**, 245-253.

3.1. Introduction

Chapter 2 focused on the use of different PEGylated branched diblock copolymers to form nanoparticles and to stabilise them against agglomeration *via* emulsion freeze-drying. In this Chapter, these polymers were used to form nanoparticles by a simple solvent evaporation approach.

Bottom-up methods often employ small molecule surfactants as stabilisers for drug nanoparticles, unfortunately, agglomeration is still a significant issue unless the solvent is removed quickly.[1,2] This key drawback introduces scalability issues with most bottom-up processes.

Thermodynamic crystallisation methods generally utilise mild conditions and are energy and cost efficient. Therefore, they may be ideal for industrial production. However, crystallisation methods are commonly used to obtain large single crystals, and it is desirable to obtain drug nanoparticles which are much smaller and amorphous for improved solubility.[3] Solvent mediated crystallisation studies with carbamazepine and different amino acids showed that the addition of certain surfactants (e.g. sodium lauryl sulphate, sodium taurochlorate) could prolong or even inhibit the transformation or growth of certain polymorphic forms.[4-6] One study demonstrated that polymer additives were able to delay nucleation on the basis of hydrogen-bond formation with the active ingredient.[7] It was also observed that the application of polymers could prevent the formation of crystalline materials *via* arrest of the amorphous particles, after either evaporation by spin-coating, spray drying [8, 9] or solvent casting, whereby polymeric films with incorporated drugs are produced. However, higher amounts of drug loading led to the recrystallisation of hydrophobic drug in solution. [10]

Despite these inhibitory characteristics, drug particles produced by solvent evaporation are commonly in the micron range.[10-13] Consequently, the development of thermodynamic crystallisation for drug nanoparticles facilitated by surfactants or polymers could be highly beneficial. The main goal in this area is to develop a route to nano-sized drug nanoparticles which requires mild conditions and a simple/ cost-effective process. Herein, we describe the formation of hydrophobic drug nanoparticles *via* a simple ambient solvent evaporation approach. This process employs the more benign organic solvent ethanol and simple open-air evaporation at room temperature. The yields of hydrophobic Ketoprofen drug nanoparticles in the region of

$D_h \approx 200$ nm can reach 96 % while the stability of the nanoparticles in solution reaches up to 9 months.

3.2. Experimental

3.2.1. Materials

Deionized water was prepared using an AquaMAX-Basic 321 DI water purification system. Ibuprofen ≥ 98 % (HPLC), indomethacin ≥ 99 % (TLC), Ketoprofen ≥ 98 % (TLC), Oil Red O (OR) dye content ≥ 75 %, anthracene (97 %), macro-initiator poly(ethylene glycol) dimer (12 kDa), and 1-dodecanethiol (DDT) were purchased from Sigma-Aldrich and used as received. Tetrahydrofuran (THF) from Aldrich was purified by refluxing with sodium overnight under nitrogen to remove water, then distilled prior to use. All other solvents were purchased from Sigma-Aldrich and used as received.

3.2.2. Characterisation

Particle size and Zeta-potential were measured by dynamic laser scattering (DLS) analysis on a Malvern Zetasizer Nanoseries at 25 °C from Malvern Instruments. The measurements were performed on aqueous nanoparticles suspensions with a concentration of ~ 0.2 mg/mL. Microparticles or aggregates were removed by centrifugation with an Eppendorf Centrifuge 5415 D at 3000 rpm for 3 minutes and one minute at 3600 rpm to ensure that larger particles precipitate. Cryo-Transmission Electron Microscopy (Cryo-TEM) was used to investigate the habit of the obtained nanoparticles and was carried out using a vitrification robot (FEI Vitrobot MARK IV). All samples were prepared at room temperature and 100 % humidity with blotting time of 2 and blot force of 1. The samples (5 µL) were applied onto a grid (Quantifoil, R2/2, Holey carbon film, freshly glow-discharged prior to use at 20mA for 30 sec. without dilution. Excess sample was blotted away with filter paper to leave a thin film on the grid before being vitrified in liquid ethane. Cryo TEM measurements were performed on FEI Titan Krios equipped with automated sample loader and Field Emission Gun (FEG) operating at 300 kV. Images were recorded with Falcon II camera (4X4) with magnification of 29000 and pixel size of 2.873.

3.2.3. Nanoparticle formulation by solvent evaporation

The branched block copolymer PEG_{135}-*b*-(PNIPAm$_{50}$-*co*-EDAm$_{2n}$)-*b*-PEG_{135} (**4-6**) and drug were added to a glass vial containing 6 ml of solvent (dichlormethane, acetone or ethanol) in mass ratios of 1:1, 2:1 and 3:1. The total polymer + drug concentrations were 2 mg/ml. For example, for the ratio of PEG-*b*-PNIPAm:drug at 3:1, 9 mg of PEG_{135}-*b*-(PNIPAm$_{50}$-*co*-EDAm$_{2n}$)-*b*-PEG_{135} (**4-6**) and 3 mg of drug were dissolved in 6 ml of the selected solvent under vigorous stirring. Polymer to ketoprofen ratios of 1:1 to 10:1 were tested by dissolving 5 mg 0.6 cross-linked PEG_{135}-*b*-(PNIPAm$_{50}$-*co*-EDAm$_{2n}$)-*b*-PEG_{135} (**4-6**) and 5 mg to 0.5 mg ketoprofen in 6 ml ethanol. If the materials did not dissolve quickly the mixture was gently heated to 55 °C. After an initial screening for the most suitable solvent, the solution was either left to evaporate without stirring at room temperature, 50 °C and 80 °C or was rotary evaporated under reduced pressure at 30 °C and 50 °C. The endpoint of evaporation was verified visually, *i.e.* the sample was deemed finished when no solvent could be seen anymore.

3.2.4. Determination of nanoparticle yield

Evaporated samples were dispersed into distilled water. Microparticles and aggregates were precipitated by centrifugation for 3 minutes at 3000 rpm and a further minute at 3600 rpm on an Eppendorf Centrifuge 5415 D. Particle Yield was calculated as described below.

$$\boldsymbol{Yield = \frac{m_{NP}}{m_T} \times 100 = \frac{m_S}{m_S + m_P} \times 100} \qquad (\mathbf{3.1})$$

Where m_{NP} is the mass of nanoparticles, m_T the total mass of added drug compound, m_S the mass of particles in the suspension after centrifuging, and m_P the mass of precipitated particles after centrifuging. Nanoparticle mass was measured using UV/Vis. To measure the nanoparticle mass in the nanosuspension, 100 µL sample were added to 2900 µL ethanol and measured on a UV 2700 UV/Vis from Shimadzu. Precipitant was re-dissolved in 3 mL ethanol. 60 µL of this stock solution was then added to 2940 µL ethanol and measured. The raw data was analysed using the software UV Probe 2.52.

3.2.5. Determination of dissolution rate

Dissolution rates were tested using a *Flow-Through USP IV Dissolution Apparatus* by Erweka. 2.0 mg of ketoprofen as received and 8.0 mg ketoprofen: PEG-b-PNIPAm 0.33: 1 (2.0 mg Ketoprofen + 6.0 mg PEG-b-PNIPAm) were added to glass beads and filled into the flow through cells. Membrane filters of 0.2 µm pore sizes were inserted before and after the glass beads. A flow rate of 4.15 % was chosen and the temperature was set to 37 °C. The set-up was set to close loop and 200 mL DI water was continuously passed through the flow cell. The beaker containing the medium was kept at 37 °C and stirred at 100 rpm. At specific time intervals 2.4 ml samples were withdrawn and 0.6 ml ethanol was added to ensure that all the Ketoprofen was completely dissolved for analysis. UV/Vis was employed to determine concentration.

3.3. Results and Discussion

The synthesis of PEG_{135}-*b*-($PNIPAm_{50}$-*co*-$EDAm_{2n}$)-*b*-PEG_{135} (**4-6**) with n = 0.3, 0.6 and 0.9 was described and discussed in Chapter 2 and will therefore not be discussed again. After preliminary evaluation of hydrophobic drug (Ketoprofen and Oil Red O) encapsulation by solvent evaporation, the branched copolymer with 0.3 and 0.6 cross-linking ratio showed best results in terms of nanoparticle size and stability. Presumably, a cross-linking molar ratio of 0.9 eq (**6**) relative to each PEG chain results in more tightly cross-linked branched diblock copolymers which is not favourable for good polymer to drug/ dye interactions during solvent evaporation. Therefore, polymers **4** and **5** were selected for a more systematic and detailed evaluation. PEG_{45}-*b*-($PNIPAm_{60}$-*co*-$EDAm_{0.8}$)-*b*-PEG_{45} (**1**) had also been tested for encapsulation, but low nanoparticle yields led to the abandonment of this polymer for solvent evaporation.

3.3.1. Solvent screening

Dichloromethane (DCM) a non-polar solvent, acetone a polar aprotic solvent and ethanol a polar protic solvent were initially tested for formulation of organic nanoparticles by solvent evaporation (simply leaving the solutions in open vial in a fume cupboard) at ambient temperatures. These solvents were chosen for their variety in vapour pressure, polarity and for their low toxicity (ICH class 2 or 3).[14] Oil Red

O (OR), an organic dye, was used as a model hydrophobic compound for the screening process in a mass ratio of 1:1 with polymers **4** and **5**. The use of oil red led to easy recognition of successful nanoparticle formation by visual observation and the facile determination of nanoparticle yield by UV/Vis.

Table 3.1. Yield, size and PDI of oil red nanoparticles measured by DLS, prepared from oil red and PEG_{135}-*b*-($PNIPAm_{50}$-*co*-$EDAm_{0.6}$)-*b*-PEG_{135} (**4**) and PEG_{135}-*b*-($PNIPAm_{50}$-*co*-$EDAm_{1.2}$)-*b*-PEG_{135} (**5**) (1:1) with different organic solvents.

Cross-linkage	Solvent	Z-Average	PDI	Yield
		nm	-	%
0.3 (**4**)	DCM	339 ± 8	0.41	76
0.3 (**4**)	Acetone	220 ± 2	0.26	27
0.3 (**4**)	Ethanol	145 ± 0	0.27	88
0.6 (**5**)	DCM	220 ± 2	0.26	12
0.6 (**5**)	Acetone	359 ± 18	0.07	1
0.6 (**5**)	Ethanol	315 ± 23	0.33	1

Table 3.1 shows the results for the evaporation of oil red and **4** (**5**) from different solvents at room temperature (around 25 ^{o}C). It was observed that the nanoparticle yield for the evaporation from acetone was under 30 % for both polymers. Thus, acetone was ruled out for further study due to low nanoparticle yield, although small particle sizes of around 200 nm could be achieved for polymer **4**. DCM and ethanol both gave a good nanoparticle yield of 76 % and 88 % for **4** and 12 % and 1 % for polymer **5** respectively. Particles obtained from evaporating ethanol were less than half the size of particles obtained by evaporating DCM (145 nm vs. 339 nm) in the case of **4**. For **5** the use of dichloromethane as a solvent lead to smaller sizes (220 nm) and higher particle yield. However still not as high, as was achieved using **4**. The slightly higher yield, smaller polydispersity index (PDI) of 0.27 (values greater than 0.7 would indicate a very broad particle size distribution and that the DLS technique is not suitable) and its lower toxicity led to the selection of ethanol as a solvent for further experiments. Although the results for **5** and Oil Red O were poor with each solvent it was still decided to continue with both **4** and **5** in ethanol, to see if this trend continued with different hydrophobic actives

3.3.2 Organic compounds and poorly water-soluble drugs

Subsequently the versatility of the solvent evaporation approach was investigated to form nanoparticles of three different hydrophobic actives (including two hydrophobic drugs).

Table 3.2. Size, yield, Zeta potential and PDI of oil red and poorly water-soluble drugs evaporated in the presence of PEG_{135}-*b*-($PNIPAm_{50}$-*co*-$EDAm_{0.6}$)-*b*-PEG_{135} (**4**) and PEG_{135}-*b*-($PNIPAm_{50}$-*co*-$EDAm_{1.2}$)-*b*-PEG_{135} (**5**) from ethanol.

cross-linking [eq]	drug/ dye	drug/ dye: polymer mass ratio	D_h Z-Average	PDI	Yield
			nm	-	%
0.3	Oil Red O	1: 1	146 ± 0	0.26	75
0.3	Indomethacin	1: 1	374 ± 2	0.38	35
0.3	Ketoprofen	1: 1	203 ± 5	0.32	80
0.3	Ketoprofen	0.33: 1	208 ± 5	0.22	96
0.6	Oil Red O	1: 1	315 ± 23	0.33	1
0.6	Indomethacin	1: 1	218 ± 1	0.24	15
0.6	Ketoprofen	1: 1	209 ± 2	0.25	30
0.6	Ketoprofen	0.33: 1	209 ± 2	0.23	88

Table 3.2 shows sizes, nanoparticle yield and PDI of 3 different hydrophobic compounds, which were evaporated from ethanol to form nanoparticles. Although using polymer **5** initially showed low particle yield and higher sizes when Oil Red O was evaporated from ethanol (Table 3.1.) the same procedure using ketoprofen (indomethacin) showed promising results with a particle size of 209 nm and 30 % drug loading (218 nm and 15 %), as well as narrower PDIs compared to **4**. The lower yield obtained when Oil Red O was used with higher cross-linking (**5** compared to **4**) could be a consequence of the larger size and higher hydrophobicity of Oil Red O compared to drug molecules like ketoprofen or indomethacin. It was hypothesised that good interactions between the hydrophobic active and polymer are required during solvent evaporation to allow diffusion into the branched core and increased

cross-linking density could hinder these interactions when larger and more hydrophobic actives are employed. The same effect could be observed using anthracene (a highly hydrophobic fluorescent dye) and ritonavir (an antiretroviral drug) with polymer **4**. Although the space in the core should be larger, due to lower cross-linking, no quality DLS data could be obtained. This was attributed to the increased hydrophobicity of ritonavir and anthracene as well as the higher spatial demand in the case of ritonavir. However, for a mass ratio of 1:1 of drug to polymer, nanoparticle under 400 nm could be formed for both polymers for all the drugs used. The relevant DLS profiles are shown in Figure 3.1., which also shows the afore mentioned comparison of cross-linkage and nanoparticle size using Oil Red O as well as indomethacin as model compounds (Figure 3.1.c and d).

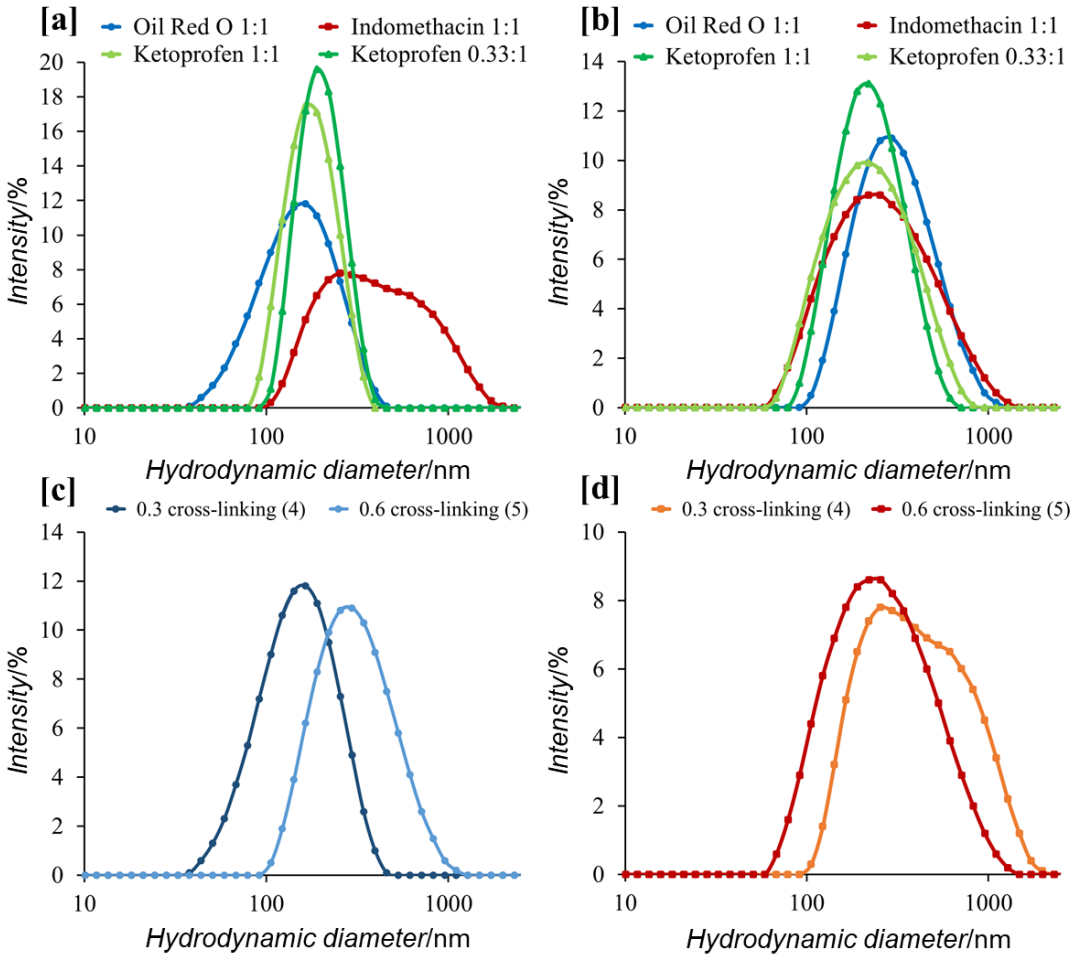

Figure 3.1. DLS profiles of different drugs and drug to polymer ratios evaporated from ethanol solutions at room temperature in the presence of a) PEG_{135}-*b*-($PNIPAm_{50}$-*co*-$EDAm_{0.6}$)-*b*-PEG_{135} (**4**); b) PEG_{135}-*b*-($PNIPAm_{50}$-*co*-$EDAm_{1.2}$)-*b*-PEG_{135} (**5**); c) Oil Red O with varied cross-linkage and d) Indomethacin with varied cross-linkages.

Figure 3.1. a and b show DLS data for all actives evaporated from ethanol in the presence of **4** and **5** respectively. It could be observed that in the case of lower cross-linking the obtained nanoparticle size varied from compound to compound *e.g.* oil red 146 nm and indomethacin 374 nm. Higher cross-linkage, although showing slightly lower drug encapsulation, gave almost the same nanoparticle sizes for all tested compounds and showed a general lower PDI (Table 3.2).

Interestingly the obtained ketoprofen nanoparticles with sizes of about 200 nm did not vary significantly independently of cross-linkage of the polymer or drug to polymer ratios. However, the PDIs and nanoparticle yields did. PDI seemed to increase with increasing drug content, more so for lower cross-linkage *e.g.* 0.22 to 0.32 for **4** compared to 0.23 to 0.25 for **5**. The percentage of drug in suspension increased with decreasing drug content, as expected. In the case of **5** a decrease of 58 % nanoparticle yield could be observed when the drug to polymer ratio was changed from 0.33:1 to 1:1, while at the same decrease in the presence of **4** only lead to a decrease of 16 %. This was because the initial nanoparticle yield was already quiet high at 80 % for a drug to polymer ratio of 1:1. As polymer **5** showed a greater dependence on the drug: polymer ratio this system was chosen for a more detailed investigation into the influence of drug to polymer ratio on nanoparticle size and yield of suspended drug.

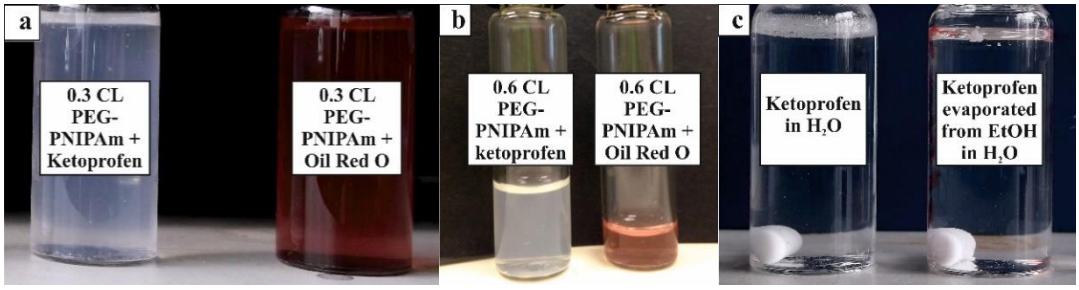

Figure 3.2. Nanosuspensions of Oil Red O and ketoprofen in the presence of a) PEG_{135}-*b*-($PNIPAm_{50}$-*co*-$EDAm_{0.6}$)-*b*-PEG_{135} (**4**) (0.3 cross-linking); b) PEG_{135}-*b*-($PNIPAm_{50}$-*co*-$EDAm_{1.2}$)-*b*-PEG_{135} (**5**) (0.6 cross-linking) and c) control experiments using ketoprofen.

Photographs of the obtained nano-suspensions of ketoprofen and Oil Red O using polymer **4** and **5** displayed in Figure 3.2. a and b. Control experiments using ketoprofen without any polymeric material present are shown in Figure 3.2.c. Two control experiments were performed to confirm the necessity of branched diblock copolymer during solvent evaporation. To start with, ketoprofen was directly added to water, the mixture stirred and left overnight, this resulted in a fine powder at the

water/ air interface. Secondly, ketoprofen was dissolved in ethanol, the solvent evaporated then water added, this afforded insoluble large crystals of ketoprofen at the water/ air interface.

3.3.3 Influence of drug to polymer ratio on particle size and nanoparticle yield

To determine the optimum drug to polymer ratio with respect to highest nanoparticle yield and influence on nanoparticle size polymer **5** and ketoprofen were evaporated from ethanol with varying drug to polymer ratios ranging from 0.2: 1 to 1: 1 (drug: polymer). For each experiment, the ethanol volume was kept constant to ensure the same evaporation rate. The premise was that this investigation might also elucidate the mechanism of drug nanoparticle formation. Table 3.3. shows the yield of suspended drug in water and resulting drug nanoparticle size and PDI. Figure 3.3.a displays the relationship between the yield of suspended ketoprofen with varying drug: polymer ratios from 0.2: 1 (17 wt % ketoprofen) to 1: 1 (50 wt % ketoprofen) and Figure 3.3. b displays the relationship between the drug nanoparticle sizes after suspension in water with varying drug: polymer ratios.

Table 3.3. Yield of suspended drug, hydrodynamic diameter (D_h) and PDI of drug nanoparticles prepared by evaporated from ethanol in the presence of polymer PEG_{135}-*b*-($PNIPAm_{50}$-*co*-$EDAm_{1.2}$)-*b*-PEG_{135} (**5**) branched diblock copolymer and subsequent re-dispersion in water with varying mass of ketoprofen.

Ketoprofen: polymer mass ratio	**ketoprofen**	**Z-Average D_h**	**PDI**	**Nanoparticle yield**
	wt%	**nm**	**-**	**%**
0.2: 1	17	211 ± 10	0.22	92 ±3
0.3: 1	23	210 ± 9	0.25	92 ±3
0.4: 1	29	222 ± 14	0.27	89 ±6
0.5: 1	33	205 ± 23	0.26	81 ±13
0.6: 1	28	277 ± 22	0.38	81 ±15
0.7: 1	41	259 ± 7	0.21	81 ±10
0.8: 1	44	263 ± 38	0.23	80 ±13
0.9: 1	47	239 ± 32	0.22	78 ±7
1: 1	50	273 ± 15	0.26	55 ±10

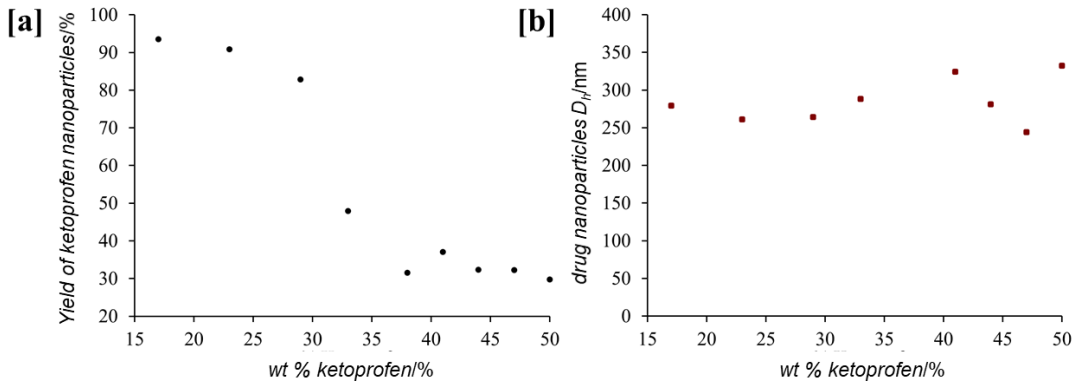

Figure 3.3. Plotted DLS data of a. initial total wt % of ketoprofen (relative to polymer) v yield of suspended drug in solution and b. initial total wt % of ketoprofen (relative to polymer) v drug nanoparticle size.

The yield of ketoprofen suspended clearly shows a dependence on the initial ratio of drug: polymer, and a point at which this ratio is optimal. Between 17 – 29 wt % of ketoprofen the yield of suspended drug is very high (92 – 89 %), when the wt % of ketoprofen reaches 33-48 wt % a slight decrease in drug yield to 80 % could be observed. The yield dropped significantly when the the wt % reaches ≥50. An approximate trend has been noticed that the yield deviations increase roughly with the increase of ketoprofen percentage. A similar trend was also observed for the size of the drug nanoparticles. This result would suggest that there is a minimum "cut-off" of polymer **5** required to successfully stabilise the ketoprofen drug nanoparticles during solvent evaporation and to disperse the resulting nanoparticles in water. It would appear that 70 – 85 wt % of branched diblock copolymer is required to facilitate the formation and dispersion of ketoprofen nanoparticles when the cross-linking density is 0.6 eq. Figure 3.3. b shows very consistent drug nanoparticle sizes (D_h = 200 – 220 nm) when the wt % of ketoprofen is 17 – 33 wt % (the range in which there is enough polymer to facilitate the process). However, when the initial wt % of ketoprofen increases significant variation in the size of drug nanoparticles (D_h = 200 – 300 nm) could be seen which could suggest that when the initial amount of polymer is lower (relative to the hydrophobic drug) the stabilization process is much more random and uncontrolled.

3.3.4 Cryo-TEM and PXRD characterisation of ketoprofen nanoparticles

Cryo-TEM analysis (Figure 3.4.) of ketoprofen drug nanoparticles prepared with polymer **4** with a drug: polymer ratio of 0.33: 1 was performed. This sample

was selected for Cryo-TEM analysis due to high yields of suspended drug after aqueous dispersion. Spherical particles of between 200-350 nm were observed. These sizes corresponded well to previous data obtained by DLS.

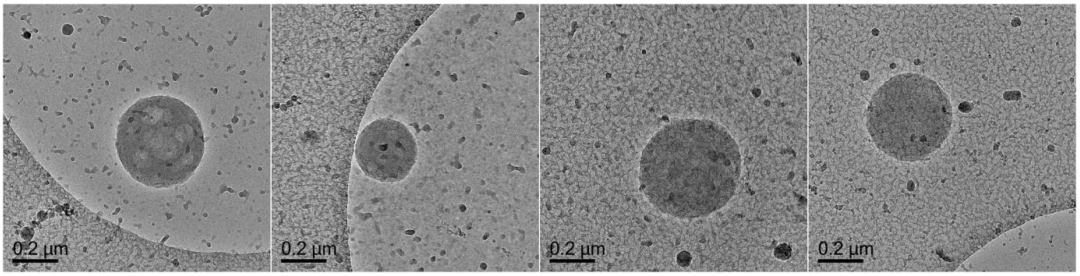

Figure 3.4. Cryo-TEM images of ketoprofen drug nanoparticles facilitated by the evaporation of ethanol in the presence of PEG_{135}-*b*-(PNIPAm$_{50}$-*co*-EDAm$_{0.6}$)-*b*-PEG_{135} (**4**) at a drug: polymer ratio of 0.33: 1.

Amorphous drug particle show better dissolution behaviour then their crystalline counterpart [27]. As such PXRD data was measured of the obtained nanoparticles to determine if the obtained nanoparticles are amorphous or crystalline. Figure 3.5. shows the obtained data.

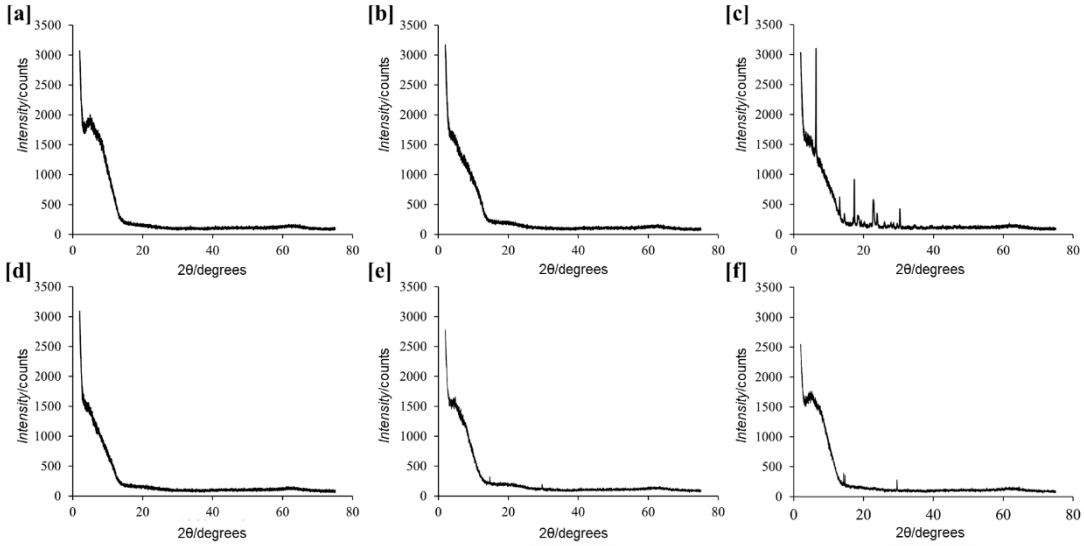

Figure 3.5. PXRD data of a) Ketoprofen nanoparticles stabilised by PEG_{135}-*b*-(PNIPAm$_{50}$-*co*-EDAm$_{0.6}$)-*b*-PEG_{135} (**4**) (ratio 0.33:1); b) Ketoprofen nanoparticles stabilised by PEG_{135}-*b*-(PNIPAm$_{50}$-*co*-EDAm$_{1.2}$)-*b*-PEG_{135} (**5**) (ratio 1:1); c) Ketoprofen evaporated without polymer present, d) Ketoprofen nanoparticles stabilised by PEG_{135}-*b*-(PNIPAm$_{50}$-*co*-EDAm$_{1.2}$)-*b*-PEG_{135} (**5**) (ratio 0.2:1), e) Ketoprofen nanoparticles stabilised by PEG_{135}-*b*-(PNIPAm$_{50}$-*co*-EDAm$_{1.2}$)-*b*-PEG_{135} (**5**) (ratio 0.9:1) and f) pure polymer.

After ethanol evaporation the solid material obtained showed amorphous character independent of polymer employed. This amorphous character was evident with drug: polymer ratios of 1: 1 (Figure 3.5. b) and 0.33: 1 (Figure 3.5. a) by the lack of diffraction peaks on the PXRD patterns. When the evaporation is performed without any polymer present the solid Ketoprofen obtained display crystalline character (Figure 3.5.c). The lack of diffraction patterns by PXRD measurement usually results from the low percentage of crystalline materials in a matrix or the low crystallinity of the materials. Due to the high content of ketoprofen in the measured samples, it can be reasonable concluded that ketoprofen nanoparticles showed an amorphous character. Polarised light microscope (PLM) may be additionally used to qualitatively identify the crystalline phase-based birefringence, by dispersing the samples in paraffin oil and subsequent imaging.[15,16] However, as PLM is mainly effective for micron particles,[17] it may be difficult to obtain convincing images. This data confirms that the application of branched diblock copolymers during solvent evaporation prevents the undesirable formation of crystalline ketoprofen.

From the obtained dynamic light scattering, Cryo-TEM and powder x-ray diffraction data the following mechanism (Scheme 3.1.) is proposed for the formation of drug nanoparticles. Initially, PEG-*b*-PNIPAm is fully solvated in ethanol and the drug compounds is dissolved at the molecular level. As the ethanol slowly evaporates the drug molecules diffuse into the branched diblock copolymer cores due to increasing drug concentration in solution, which prevents significant drug crystallisation. After ethanol evaporation the drug molecules are intimately distributed among the polymeric material, presumably small amounts of drug crystals or agglomerates will be present (during this stage cross-linking density plays a key role on the possible diffusion of drug molecules into branched diblock copolymers). After dispersion in water the solid material is broken up and spherical amorphous drug nanoparticles are formed.

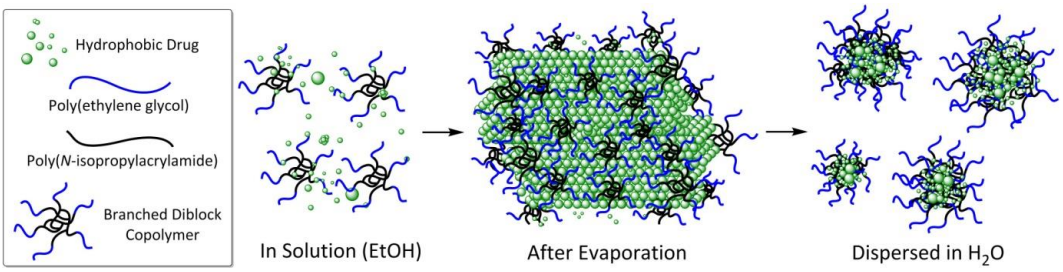

Scheme 3.1. Formation of drug nanoparticles facilitated by branched diblock copolymers via solvent evaporation.

3.3.5. Dissolution rates of ketoprofen nanoparticles

According to the Noyes-Whitney equation a decrease in size and subsequent increase in surface area is the reason why drug nanoparticles show an increase in dissolution rate compared to non-processed drugs.[18] Dissolution rates were measured for ketoprofen (control experiment) and drug nanoparticles of ketoprofen: **4** (0.33: 1). The measurements were done using a USP IV flow through apparatus, to assure that the nanoparticles were not able to leave the sample cell and only dissolved ketoprofen was measured. As small amounts of ketoprofen were measured to remain under sink conditions a closed loop set-up was chosen to minimise the measurement errors. Figure 3.7. shows the dissolution rates measured in the first 60 mins (crucial time scale in drug solubilisation).

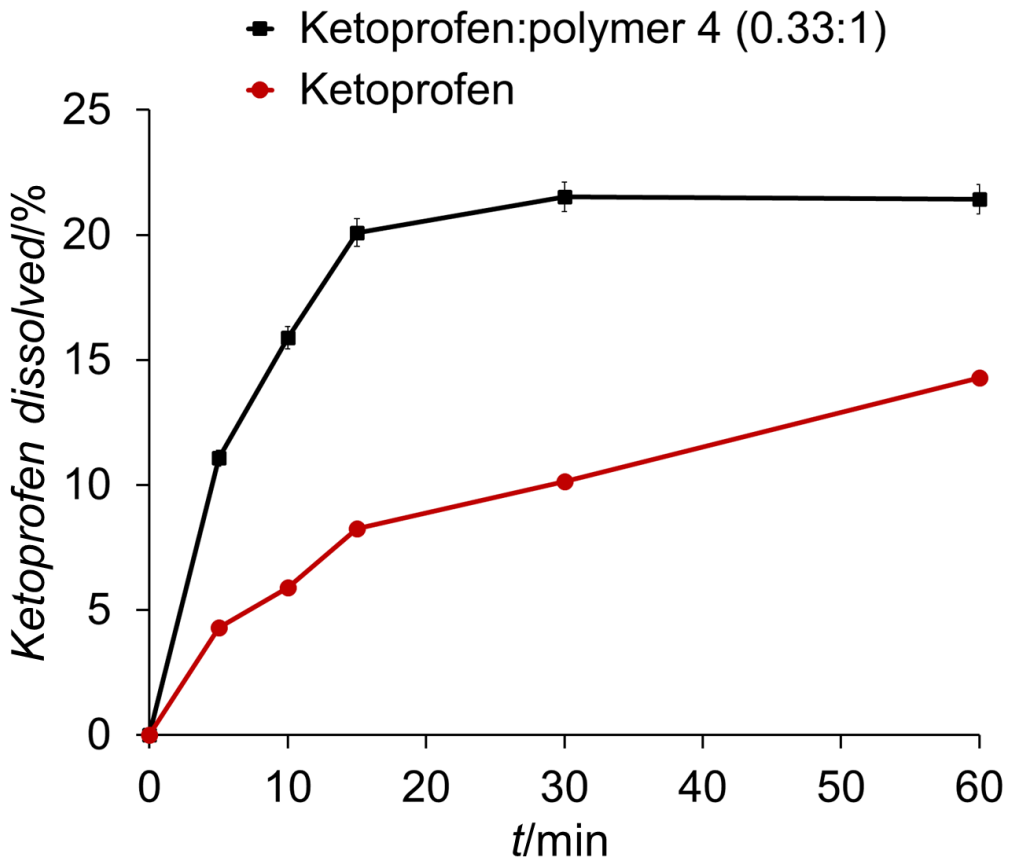

Figure 3.6. Dissolution rate of ketoprofen and ketoprofen: PEG_{135}-*b*-($PNIPAm_{50}$-*co*-$EDAm_{0.6}$)-*b*-PEG_{135} (**4**) (0.33: 1) nanoparticles in H_2O.

The percentage of ketoprofen that could be dissolved unfortunately did not reach a 100 % within this time limit. This was attributed to a significant amount of

the material (ketoprofen (control) as well as ketoprofen drug nanoparticles) being 'stuck' to the cell wall as well as to the glass beads. The glass beads were needed to ensure laminar flow and keep turbulences to a minimum. Furthermore, it has been shown for the USP IV that at a low velocity the experimental dissolution is inhibited,[19] however low velocity flow rates more closely resemble the situation that may be encountered in the intestines where inhomogeneous fluid 'pockets' of almost static flow rates can be found.[20] The commonly available devices measuring dissolution are usually for larger amounts of sample and larger sample sizes *i.e.* micron-range. Characterisation of dissolution rate of drug nanoparticles has been a significant challenge.[21] For example, our own efforts by using the light scattering approach[21] did not produce meaningful data. Although not completely convincing (because of the low percentage dissolved) the data obtained (Figure 3.6.) shows that ketoprofen drug nanoparticles of ketoprofen: **4** show a significant increase in dissolution compared to non-processed ketoprofen (control). The ketoprofen present in the drug nanoparticles was dissolved at a level of 22 % after 15 mins while at the same time only 8 % of ketoprofen could be dissolved from the control experiment.

3.3.6. Influence of temperature and pressure during evaporation

Table 3.4. The size and PDI of ketoprofen nanoparticles prepared by ketoprofen and polymer PEG_{135}-*b*-(PNIPAm$_{50}$-*co*-EDAm$_{0.6}$)-*b*-PEG_{135} (**4**) (0.33:1) evaporated from ethanol at different temperatures by open air evaporation and rotary evaporation. The data listed are for the as-prepared sample (t = 0 months) and stored in desiccator for 3 months. All the samples were freshly dissolved in water prior to DLS analysis. (r.t. means room temperature at 20 °C).

			t = 0 months		**t = 3 months**	
sample	**Method**	**T**	**Z-Average D_h**	**PDI**	**Z-Average D_h**	**PDI**
		°C	**nm**	**-**	**nm**	**-**
1	Evaporation	r.t.	208 ± 5	0.22	210 ± 4	0.22
2	Evaporation	50	193 ± 2	0.21	303 ± 10	0.37
3	Evaporation	80	213 ± 2	0.12	249 ± 3	0.21
4	Rotary evaporated	30	288 ± 4	0.27	219 ± 1	0.19
5	Rotary evaporated	50	204 ± 2	0.08	280 ± 4	0.35

The influence of variations in evaporation conditions on the resulting ketoprofen nanoparticles in the presence of **4** formed with a drug: polymer ratio of 0.33: 1 was further investigated. This branched diblock copolymer and drug: polymer ratio was selected due to its high yield of suspended drug after dispersion in water. The influence of evaporation temperatures (room temperature, 50 °C and 80 °C) and pressure (air evaporation and rotary evaporation at 30 °C or 50 °C) were studied. All of the obtained solid samples after solvent evaporation could be suspended completely in water to produce stable drug nanoparticle suspensions without any precipitates. A total of five samples (**1** – **5**) were prepared under various conditions, each sample was dispersed in water directly after solvent evaporation (time = 0 months). The dynamic light scattering profiles are displayed in Figure 3.7. a. To investigate stability during storage each sample was stored as a dry solid for three months before dispersion in water (time = 3 months), the dynamic light scattering data obtained is summarized in Table 3.4. Samples **1** – **3** displayed drug nanoparticles with similar sizes ($D_h \approx 200$ nm) after immediate dispersion (time = 0 months). This suggests that atmospheric evaporation is not significantly affected by temperature. After 3 months storage in solid form Samples **2** (50° C) and **3** (80° C) showed a minor increase in nanoparticle size and PDI after dispersion in water. Sample **1** (room temperature) showed a very consistent size and PDI after dispersion in water after 3 months of storage in solid form. These results clearly indicate that increasing the temperature during atmospheric evaporation does not impede nor improve the evaporation process. Samples **4** and **5** also displayed very promising nanoparticle sizes and PDIs. After dry storage for 3 months the drug nanoparticles readily dispersed in water without any significant increase in size. These results suggest that the obtained drug nanoparticles are suitably stabilised against aggregation by PEG-*b*-PNIPAm branched diblock copolymers. To further investigate the long-term storage potential, in solution, Sample **1** Ketoprofen nanoparticles dispersed in water after 0 days were left in water at room temperature and analysed by dynamic light scattering after 3 months ($D_h = 204 \pm 4$ nm, PDI = 0.20) and 9 months ($D_h = 225 \pm 1$ nm, PDI = 0.35) (Figure 3.7.b). No aggregation could be observed after 9 months, demonstrating the long-term stability of drug nanoparticles not only in solid state but also in aqueous suspension.

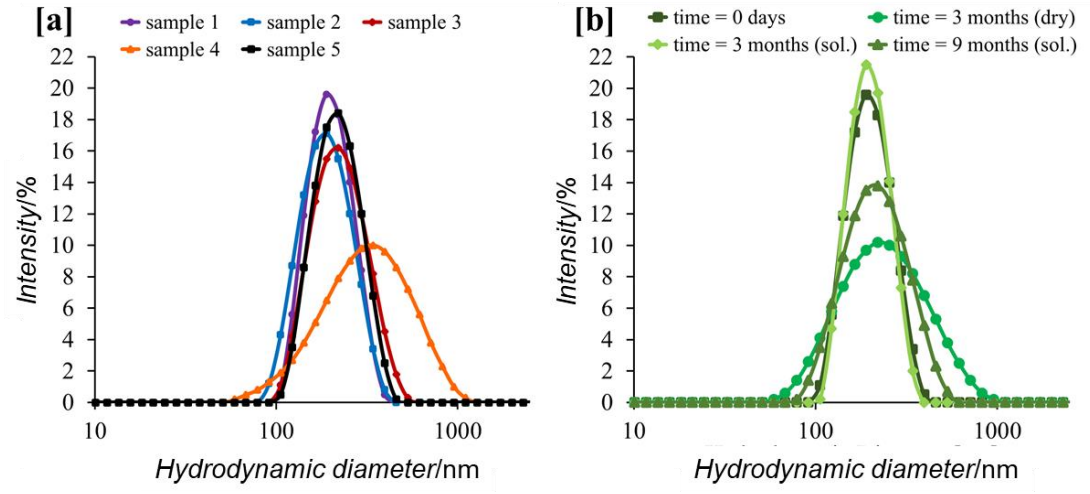

Figure 3.7. DLS profiles of ketoprofen nanoparticles in water prepared by evaporation of ketoprofen: polymer PEG_{135}-*b*-(PNIPAm$_{50}$-*co*-EDAm$_{0.6}$)-*b*-PEG_{135} (**4**) 0.33:1 from ethanol. a) evaporated at different temperatures and pressures and b) Evaporated from room temperature (sample **1**) and stored in solution or dry for 3 and 9 months.

3.4. Conclusion

In Chapter 2 it was observed that branched diblock copolymers of PEG-*b*-PNIPAm with longer PEG arms (M_w 6000 kDa) and lower cross-linkage (0.3 and 0.6 eq.) could stabilise nanoparticles slightly better than PEG-*b*-PNIPAm with shorter PEG (M_w 2000 kDa) and higher cross-linkage. Due to this they were subsequently used in this Chapter to form drug nanoparticles *via* a simple solvent evaporation technique. Initially different solvents were screened for their ability to facilitate the formation of drug/polymer nanoparticles. Favourable nanoparticles sizes and low PDI were obtained by evaporating ethanol. Due to the low toxicity and the non-hazardous pharmaceutical classification, ethanol was chosen for all further experiments. Hydrophobic actives (IMC, OR and ketoprofen) were screened to investigate the broadness of application of this approach. The screening process showed that all actives screened could be nanosized to particles of ~ 200 nm and higher yields could be achieved when less cross-linked branched polymers were used. This effect tended to be even more pronounced when the steric demand of the active increased *e.g.* Oil Red O. The best results were achieved using ketoprofen and ethanol (small particle sizes and high yields) regardless of branched block copolymers. However, decreasing the polymer to drug ratio and increasing the cross-linking, led to dramatically

reduced nanoparticles yields. To study the optimal loading ratio, *i.e.* least amount of polymer needed, ketoprofen and polymer **4** (0.6 cross-linked PEG-PNIPAm) were added in mass ratios of 0.1:1 to 1:1 to a constant amount of ethanol (to assure the same evaporation rate). DLS data obtained indicated no significant size changes across all ratios tested. UV/Vis data showed the optimal drug:polymer ratio (highest yield) to be 0.3:1. DLS, UV/Vis, Cryo-TEM and PXRD data was used to discern shape, sizes and the amorphous character of the drug nanoparticles. A mechanism for the formation of drug/polymer complexes could be proposed based on the measured data. Branched polymers are thought to arrest the crystal growth by 'anchoring' their hydrophobic core onto a growing crystal phase. The so formed film forms spherical particles spontaneously to stabilise the particles when water is added. Size and shape in the herein described evaporation technique is very much depended on evaporation rate of the solvent. Hence, we investigated the influence of changing the kinetics by temperature and pressure *i.e.* faster evaporation due to higher temperatures and lower pressure. No notable changes in size or size distribution was observed. Enhanced dissolution could be found for ketoprofen nanoparticles compared to non-processed ketoprofen.

In summary, it was possible to form nanoparticles of hydrophobic actives in high yields of up to 96 % with particles sizes around 200 nm by using branched block copolymers of PEG_{135}-*b*-($PNIPAm_{50}$-*co*-$EDAm_{2n}$)-*b*-PEG_{135} (n = 0.3 and 0.6) and a simple solvent evaporation technique. Due to the use of ethanol this technique uses only non-toxic materials and solvents and is highly cost efficient as well as energy efficient. The process could further be accelerated by increasing the temperature and reducing the pressure without significant changes to the particle sizes, PDIs or yields of the produced nanoparticles. The obtained dry films as well as redispersed nanosuspensions showed good storage stability over 3 months (dry) and up to 9 months (sol.) with no discernible size change. As such the herein presented method would be a cost-efficient and environmentally friendly alternative to conventional techniques used in the production of nanodrugs, such as media milling or spray drying.

3.5. References

1. J. J. Hu, W. K. Ng, Y. Dong, S. Shen and R. B. H. Tan, *Int. J. Pharm.*, 2011, **404**, 198-204.
2. P. Gassmann, M. List, A. Schweitzer and H. Sucker, *Eur. J. Pharm. Biopharm.*, 1994, **40**, 64-72.
3. B. C. Hancock and M. Parks, *Pharm. Res.*, 2000, **17**, 397-404.
4. N. Rodríguez-Hornedo and D. Murphy, *J. Pharm. Sci.*, 2004, **93**, 449-460.
5. N. Garti and H. Zour, *J. Cryst. Growth*, 1997, **172**, 486-498.
6. I. Weissbuch, L. Addadi, L. Leiserowitz and M. Lahav, *J. Am. Chem. Soc.*, 1988, **110**, 561-567.
7. S. L. Raghavan, A. Trividic, A. F. Davis and J. Hadgraft, *Int. J. Pharm.*, 2001, **212**, 213-221.
8. H. Konno and L. S. Taylor, *J. Pharm. Sci.*, 2006, **95**, 2692-2705.
9. G. Van den Mooter, M. Wuyts, N. Blaton, R. Busson, P. Grobet, P. Augustijns, and R. Kinget, *Eur. J. Pharm. Sci.*, 2001, **12**, 261-269.
10. R. Shi and H. M. Burt, *Int. J. Pharm.*, 2004, **271**, 167-179
11. B. Van Eerdenbrugh and L. S. Taylor, *Mol. Pharm.*, 2010, **7**, 1328-1337.
12. S. Xie, S. K. Poornachary, P. S. Chow and R. B. H. Tan, *Cryst. Growth Des.*, 2010, **10**, 3363-3371.
13. N. Rasenack and B. W. Müller, *Drug Dev. Ind. Pharm.*, 2002, **28**, 1077-1089.
14. ICH, Impurities: guideline for residual solvents Q3C (R5), http://www.ich.org/products/guidelines/quality/quality-single/article/impurities-guideline-for-residual-solvents.html, accessed: June, 2016.
15. S. Kumar, J. Shen and D. J. Burgess, *J. Control. Release*, 2014, **192**, 95-102.
16. C. Brough, D. A. Miller, J. M. Keen, S. A. Kuccera, D. Lubda and R. O. Williams III, *AAPS PharmSci. Tech.*,2016, **17**, 167-179.
17. R. A. Carlton, *Pharmaceutical Microscopy*, Springer, Berlin, 2011.
18. A. A. Noyes and W. R. Whitney, *J. Am. Chem. Soc.*, 1897, **19**, 930-934.
19. D. M. D'Arcy, B. Liu, G. Bradley, A. M. Healy and O. I. Corrigan, *Pharm. Res.*, 2010, **27**, 246-258.

20. C. Schiller, C. P. Fröhlich, T. Giessmann, W. Siegmund, H. Mönnikes, N. Hosten and W. Weitschies, *Aliment Pharmacol. Ther.*, 2005, **22**, 971-979.
21. K. Anhalt, S. Geissler, M. Harms, M. Weigandt and G. Fricker, *Pharm Res.*, 2012, **29**, 2887-2901.

Chapter 4

Solubilisation of hydrophobic drugs facilitated by thermorespon-sive hyperbranched polymers

This Chapter is based on the publication

J.-H. Liu, U. Wais, Y.-M. Zuo, Y. Xiang, Y.-H. Wang, A. W. Jackson, T. He and H. Zhang, "Unimolecular branched block copolymer nanoparticles in methanol for the preparation of poorly water-soluble drug nanoparticles" *J. Mater. Chem. B*, 2017, **5**, 423-427.

4.1. Introduction

Chapter 2 focused on the use of branched polymers to form a stabilising scaffold against agglomeration around drug nanoparticles, obtained *via* emulsions freeze-drying. Chapter 3 focused on using the same branched polymers to obtain drug nanoparticles by a simple solvent evaporation method. All polymers used were synthesised by conventional radical polymerisation and from linear PEG and were solids. Both techniques provided dry material, which could be re-dispersed in water to form nanosuspensions.

In this Chapter, branched polymers with non-linear PEG arms were synthesised to directly form nanosuspensions of hydrophobic actives without obtaining dried nanoparticles first. Considering that most biomedical and environmental application require aqueous formulations of water insoluble active, nanosuspensions could be a suitable solution and obtaining nanosuspensions directly with high yields would be beneficiary. The branched polymer poly(oligo(ethylene glycol) methyl ether methacrylate)-*b*-poly((butyl methacrylate)-*co*-(ethylene glycol dimethylacrylate)) (p(OEGMA-*b*-p(*n*BMA-*co*-EGDMA)) was synthesised in two different OEGMA:*n*BMA ratios of 36:60 (**DP 36/60**) and 36:40 (**DP 36/40**) with equal ratio of cross-linkage (0.9). The polymerisation technique was changed to ATRP, a living polymerisation technique, from conventional radical polymerisation and hence branched PEG, *i.e.* OEGMA, was used to obtain hydrophilic arms. By changing the polymerisation technique, it was assured that random chain growth is inhibited and as such a better control over the resulting architecture could be achieved.[1]

BMA was chosen as the core forming monomer due to its temperature sensitive behaviour. BMA exhibits upper critical solution temperature (UCST) behaviour in methanol. Although the UCST is not as well studied as the better-known phenomena of lower critical solution temperature (LCST) examples, especially in organic solvents or water/solvents mixtures, are known.[2-5] Quite a few of these examples are, unfortunately, often toxic. However, some non-hazardous examples have been shown which would be favourable for pharmacologic applications. An especially interesting focus lays hereby on polymers exhibiting UCST in water miscible solvents like methanol.[5]

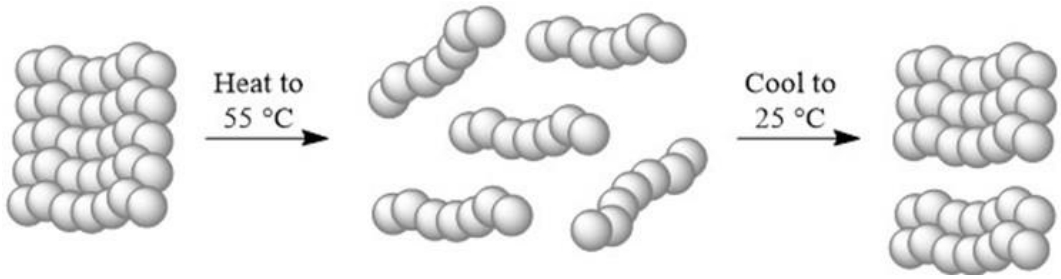

Figure 4.1. p(BMA) at different temperatures in MeOH; at 25 °C before heating (right); heated to 55 °C (middle) and cooled down to 25 °C again (left).

Polymers showing UCST behaviour become soluble above a specific temperature, in comparison to LCST where a polymer becomes insoluble above a specific temperature.[6] Although OEGMA itself also shows a UCST in methanol, it is at -10 °C and as such outside of the temperature range interesting for this study.[7] Figure 4.1. shows the temperature dependent transition of pBMA from insoluble to soluble back to insoluble. At 25 °C the linear PBMA strands are insoluble and stabilise by agglomeration. Heating to 55 °C leads to the linear PBMA strands becoming soluble and unimolecular polymer strands can be found in solution. PBMA turns insoluble again by cooling back down to 25 °C and agglomeration of the linear polymers can be observed.

^{1}H-NMR measurements of linear pBMA blocks in deuterated methanol at 25 °C and 60 °C show the reversible precipitation and solvation of the polymer (Figure 4.2. A). At 25 °C (Figure 4.2. A; spectrum ii and iii) no BMA signals can be detected. Heating to 60 °C (Figure 4.2. A; spectrum i) led to the solubilisation of linear block pBMA and NMR signals can be recorded. The shift of the H_2O signal at 25 °C is a direct consequence of polymer/water interactions due to solubilisation. The inlaid picture (Figure 4.2.B) shows that at 60 °C a clear methanolic polymer solution (i) can be obtained (linear block pBMA unimolecular dissolved), while at 25 °C pBMA precipitates out of solution as a white solid (ii and iii).[8]

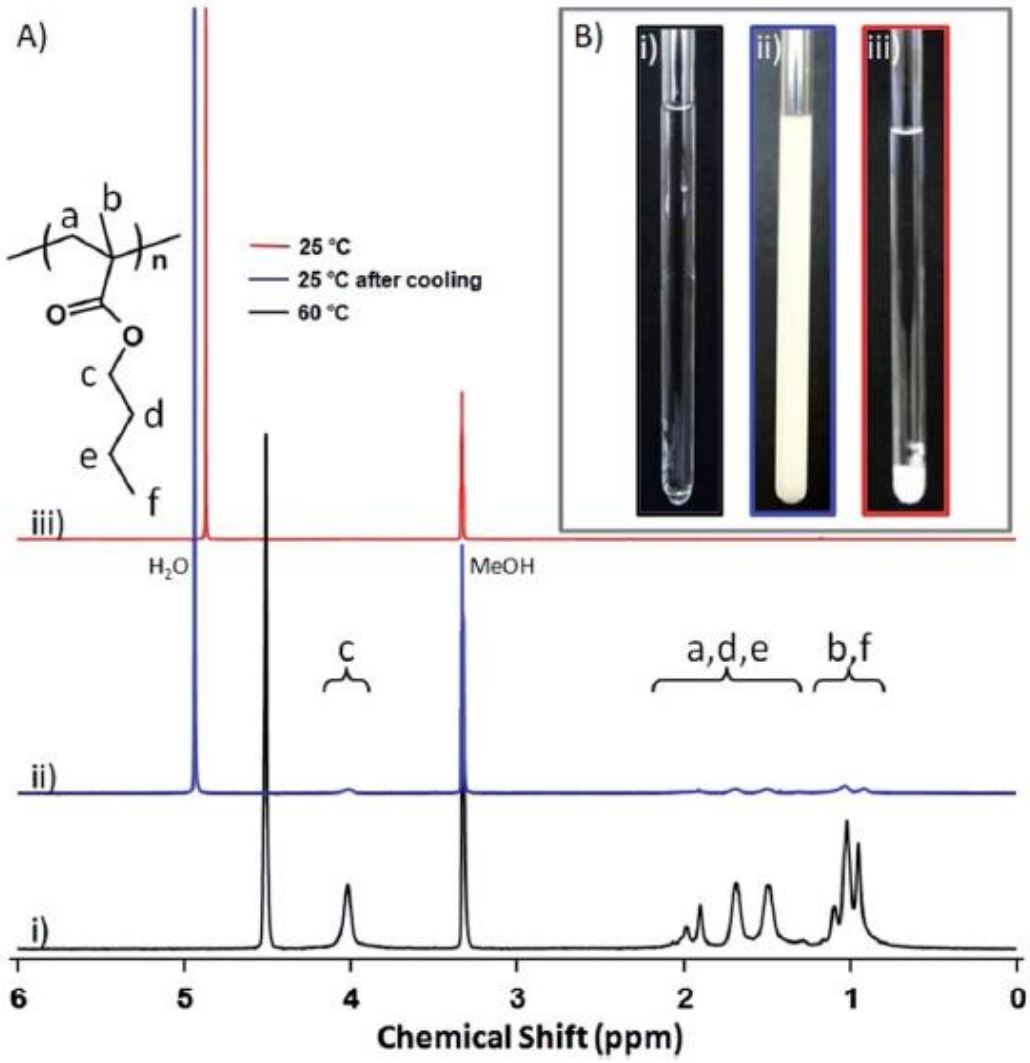

Figure 4.2. Studies of p(*n*BuMA) solubility in MeOH-d_4. (A) ^{1}H NMR spectra of (i) p(*n*BMA) heated to 60 °C, (ii) p(*n*BMA) after heating and cooling to 25 °C, (iii) p(*n*BMA) at 25 °C before heating; (B) photographs of p(*n*BMA) within the NMR tube at different temperatures – (i) 60 °C, (ii) after cooling to 25 °C, and (iii) at 25 °C prior to heating. Adapted with permission from Ref. 8 © 2014 Royal Society of Chemistry

In a branched copolymer like p(OEGMA-*b*-p(*n*BMA-*co*-EGDMA), OEGMA forms a hydrophilic shell at ambient temperature around the hydrophobic core of pBMA. When the solution is heated above the UCST the core becomes soluble. Micelles formed from such a diblock polymer would fall apart in this case. [9,10] However, branching leads to the retention of the core-shell structure. Heating and cooling through the UCST subsequently results in structural changes, *i.e.* collapse or shrinkage of one component, and size change due to agglomeration.[11] This behaviour could be used to form unimolecular polymer nanoparticle solutions in water by directly evaporating from the methanolic solution instead of the standard two-step, time consuming procedure of dialysing against water.[12,13]

In this Chapter, a thermoresponsive branched diblock copolymers of p(OEGMA)-*b*-(pBMA-*co*-pEGDMA) was synthesised by ATRP in two different ratios of hydrophilic to hydrophobic block. The thermoresponsive behaviour in methanol was used to incorporate hydrophobic actives *i.e.* ketoprofen and Oil Red (OR) and form drug nanoparticles in suspension.

4.2. Experimental

4.2.1. Chemicals and reagents

Deionized water was prepared using an AquaMAX-Basic 321 DI water purification system. Anthracene reagent grade, 97 %, ketoprofen ≥ 98 % (TLC) and Oil Red O (OR) dye content ≥ 75 % were purchased from Sigma-Aldrich and used as received. All other solvents were purchased from Sigma-Aldrich and used as received.

4.2.2. Characterization

The ^{1}H NMR spectra were recorded using a Brucker Avance III HD spectrometer at 500.13 MHz. Samples were analysed at 25 °C and 60 °C in MeOD. Particle sizes were measured by dynamic laser scattering (DLS) analysis on a Malvern Zetasizer Nanoseries at 25 °C from Malvern Instruments. Aqueous polymer solutions were obtained by dissolving branched diblock copolymers with a concentration of ~ 0.5 mg/ml in acetone under constant stirring. Water was added, and acetone was evaporated off in the fume cupboard. The obtained solution was directly used to measure DLS data. The measurements of aqueous drug nanosuspensions were performed with a concentration of ~ 0.2 mg/ml. Microparticles or aggregates were removed by centrifugation with an Eppendorf Centrifuge 5415 D at 3000 rpm for 3 minutes and one minute at 3600 rpm to ensure that larger particles precipitate.

*4.2.3. Synthesis of branched diblock copolymer p(OEGMA)-b-p(nBMA-co-EGDMA) (**DP 36/40** and **DP 36/60**) by ATRP*

Typically, synthesis of p(OEGMA)$_{36}$-*b*-p(*n*BMA$_{37}$-*co*-EGDMA$_{0.9}$) could be described as follows: into a Schlenk flask (50 ml) OEGMA (2.04 g, 6.8 mmol, 40 eq.), CuBr (24.5 mg, 0.17 mmol, 1 eq.), 2,2-bipyridine (bpy) (53.1 mg, 0.34 mmol, 2 eq.) and anisole (0.3 ml, for internal ^{1}H-NMR standard) were added to an isopropanol/water mixture (92.5:7.5 v/v, 4.2 ml) and degassed for an hour and a sample was taken

for NMR analyses, after which ethyl α-bromoisobutyrate (EBriB) (33.2 mg, 0.17 mmol, 1 eq.) were added using a microsyringe, and stirred under N_2 atmosphere at ambient temperature. In a second 50 ml Schlenk flask, CuCl (16.9 mg, 0.17 mmol, 1 eq.), bpy (53.1 mg, 0.34 mmol, 2 eq.), *n*BMA (0.965 g, 6.8 mmol, 40 eq.) and EGDMA (29.2 mg, 0.15 mmol, 0.9 eq.) were added to 5.8 ml of the same isopropanol/water mixture and degassed for an hour. After the conversion of OEGMA had reached 96 %, the mixture was added into the first flask rapidly using a syringe and taking care not to admit any air. A sample was taken immediately for NMR analysis. The reaction was carried out at ambient temperature under N_2. After the conversion had reached 94 % the reaction was stopped by adding THF to the mixture and exposing it to air. The mixture was passed through an Al_2O_3 column to remove the copper species. The branched diblock copolymer was obtained after precipitation three times into hexane and dried under vacuum.

4.2.4. Nanoparticle formulation by solvent evaporation

40 mg of POEGMA-b-*n*BMA (**DP 36/60** and **DP 36/40**) and 40 mg drug (ketoprofen, anthracene and OR) were stirred in 5 ml methanol for 20 min at room temperature (20 °C). The samples were then heated to 56℃ and stirred at 5000 rpm for further 20 min. After cooling to room temperature, 5 ml deionized water was added. It was noticed that the solution with POEGMA-b-*n*BMA (**DP 36/40**) turned opaque while the solution with POEGMA-b-*n*BMA (**DP 36/60**) was still clear. Another procedure was to directly process the methanol solution at room temperature. Methanol was evaporated off at room temperature in the fume cupboard. The endpoint of the evaporation was determined by visual examination. After evaporation of methanol, the samples with added water produced aqueous suspensions, which were analysed directly. The dry samples formed from methanol solution after evaporation were dissolved in 5 ml water to form suspensions for measurement.

4.2.5. Determination of Nanoparticle yield

After solvent evaporation the solid samples obtained were dispersed into water. Microparticles and aggregates were removed by centrifugation. The yield of suspended drug/dye in water was calculated as described below:

$$\mathbf{Yield} = \frac{\mathbf{m_{NP}}}{\mathbf{m_T}} \times \mathbf{100} = \frac{\mathbf{m_S}}{\mathbf{m_S + m_P}} \times \mathbf{100} \qquad (\mathbf{4.1.})$$

Where m_{NP} is the mass of drug/ dye suspended in water and m_T is the total initial mass of drug/ dye. m_S is the mass of drug/ dye in the suspension after centrifugation and m_P is the mass of precipitated drug/ dye after centrifugation. The centrifugation precipitant was re-dissolved in 3 mL ethanol and measured by UV/Vis. All samples were analysed in 1 to 1 (v/v) solutions of water/ethanol. Quantities of drug/ dye were determined against calibration curves of known concentrations in ethanol/water 1:1.

4.3. Results and discussion

4.3.1 Synthesis of temperature sensitive branched diblock copolymers

An amphiphilic A-B branched block copolymer was synthesised at ambient temperatures by a one-pot Cu(I)Br/2,2-bypiridine (bpy) catalysed, ATRP polymerisation in an isopropanol (IPA)/H_2O mixture using ethyl α-bromoisobutyrate (EBriB) initiator. Although pBMA is considered to be highly hydrophobic, the polar isopropanol is a good theta solvent for the polymer.[14] However, while isopropanol is a good solvent for BMA and p(BMA) and leads to the polymers acting like an ideal chain, p(OEGMA) is insoluble at room temperature in isopropanol, because of its UCST. The UCST for p(OEGMA) monopolymer chains of around the same molecular weight as were synthesised in the first step has been shown to be around 22 °C. However, at higher concentrations of the polymer the UCST increased dramatically. Adding water as a co-solvent led to dramatic decreases of the UCST in isopropanol, *i.e.* without water a UCST of 35.6 °C was measured for a linear monopolymer of 23000 g/mol, while in the presence of 4 vol % water the UCST decreased to -10 °C. This was attributed to the strong hydrogen bonding of water with p(OEGMA). Hence, the use of a isopropanol /water mixture was not just used to solubilise inorganic salts but also to ensure that p(OEGMA) was soluble at mild conditions and readily available for the second step of the polymerisation. The addition of hydrophobic polymers to the p(OEGMA) chain was found to be another factor that decreased the UCST. However, this was tested for the case of linear polymers and not branched polymers, where the hydrophobic cores might be more protected and as such have less influence.[15]

In the first step OEGMA (M_W = 300 g/mol) was polymerised to afford a linear block of p(OEGMA). A relatively low degree of polymerisation (DP) of 40 was aimed

for. The reaction was monitored by ^{1}H-NMR. To that end an internal standard of anisole was added before the reaction was started and an NMR spectrum was recorded. Figure 4.3. and Figure 4.4. show the ^{1}H-NMR spectra measured for **DP 36/40** throughout the reaction.

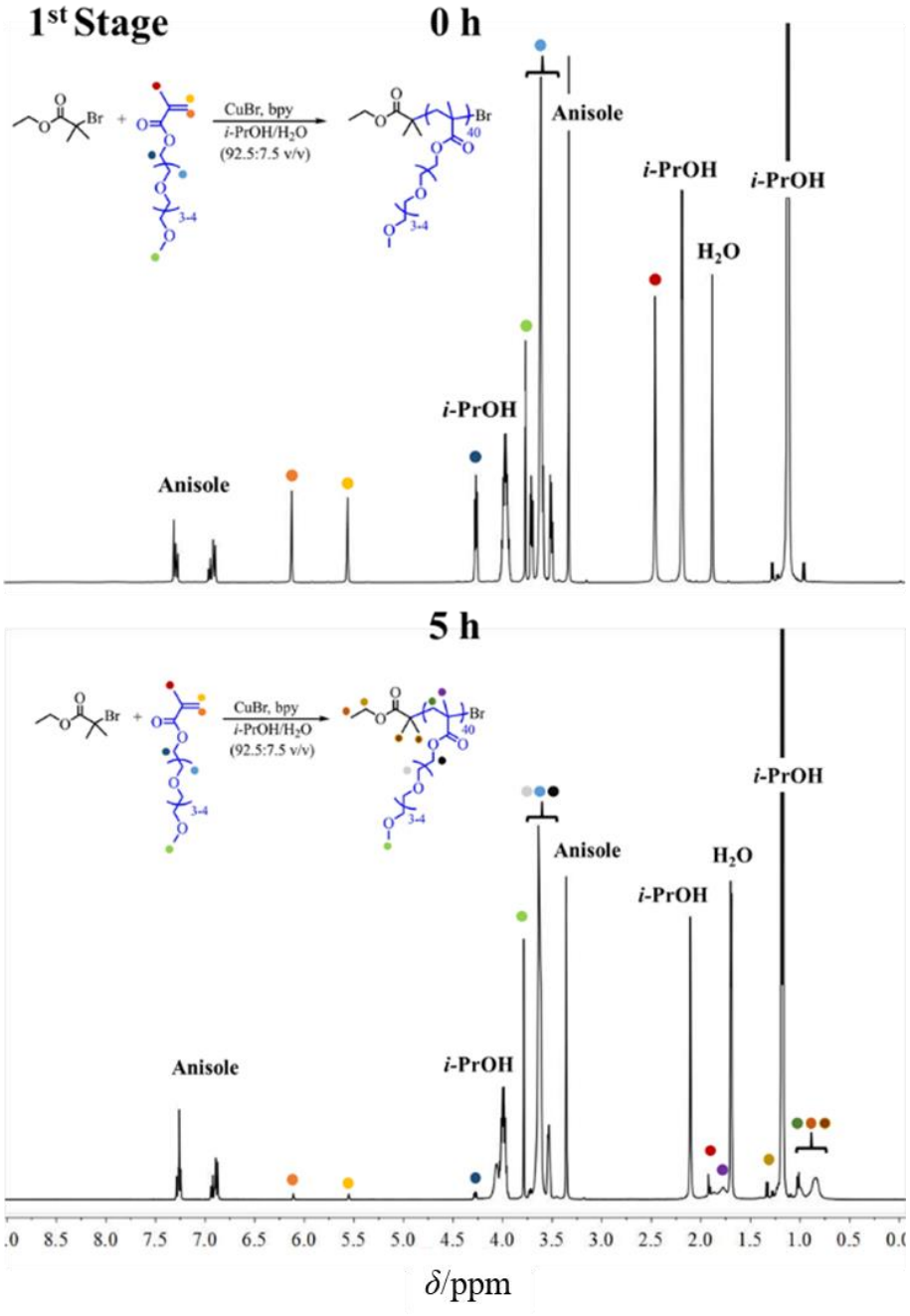

Figure 4.3. ^{1}H-NMR of the first-step of the one-pot synthesis of **DP 36/40**

Vinyl signals at 6.08 ppm (s, 1H, -C=CH<u>H</u>) and 5.31 ppm (s, 1H, -C=C<u>H</u>H) were integrated to 100 (%) the anisole signal at 6.86 ppm (s, 3H, -C-OC<u>H</u>$_3$) was inte-

grated subsequently and the obtained value was then used to check the reaction conversion. After 5 hours only 4 % of unreacted monomer remained (Figure 4.3.) and a mixture of *n*BMA and EGDMA was added. This allowed for the propagation of the hydrophobic block p(BMA) while simultaneously branching to other growing chains is occurring. The reaction conversion was followed as had been done in the first step. The reaction was stopped when 93 % conversion was reached (Figure 4.4.). The polymer was purified by precipitation into hexane.

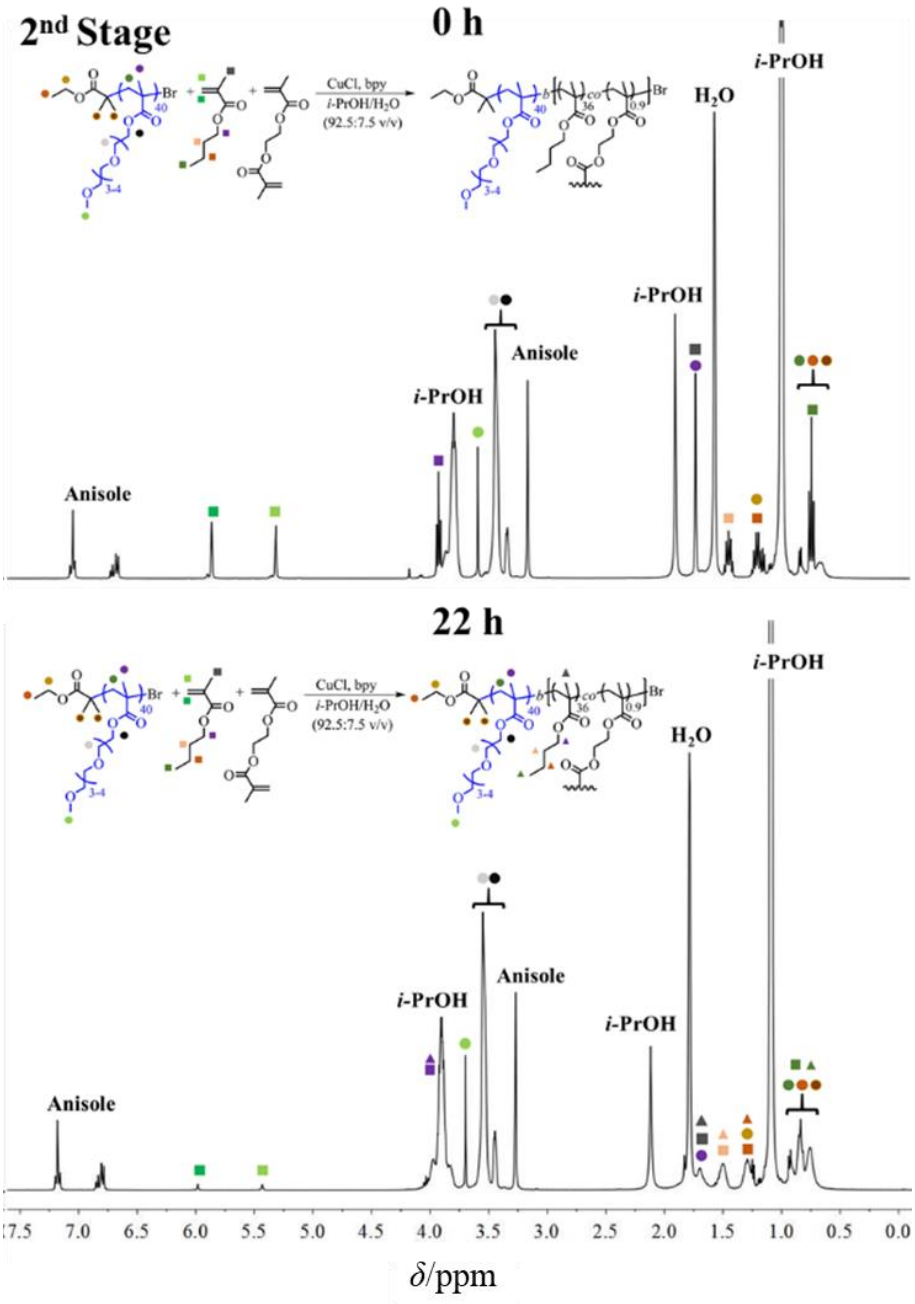

Figure 4.4. ^{1}H-NMR of the first-step of the one-pot synthesis of **DP 36/40**

Figure 4.5. shows the ^{1}H-NMR in $CDCl_3$ of **DP 36/40** after purification as an example. Integration of the CH_3 signal of OEGMA at 3.39 ppm (s, 3H, -CH_2)$_{3-4}$-O-C$\underline{H_3}$) to 108 (3H x 36 repeating units) gave 86 H atoms for the signal of *n*BMA at 1.41 ppm (3H, -CH_2-CH_2-C$\underline{H_3}$), which would mean that only 28 repeating units were added of *n*BMA. This unexpectedly low number might be a consequence of the cross-linking. Due to cross-linking some methyl groups of *n*BMA might be 'hidden' inside the core and as such some hydrogens might not be visible in the spectra. Hence, the degree of polymerisation was calculated using the NMR spectra recorded during the polymerisation

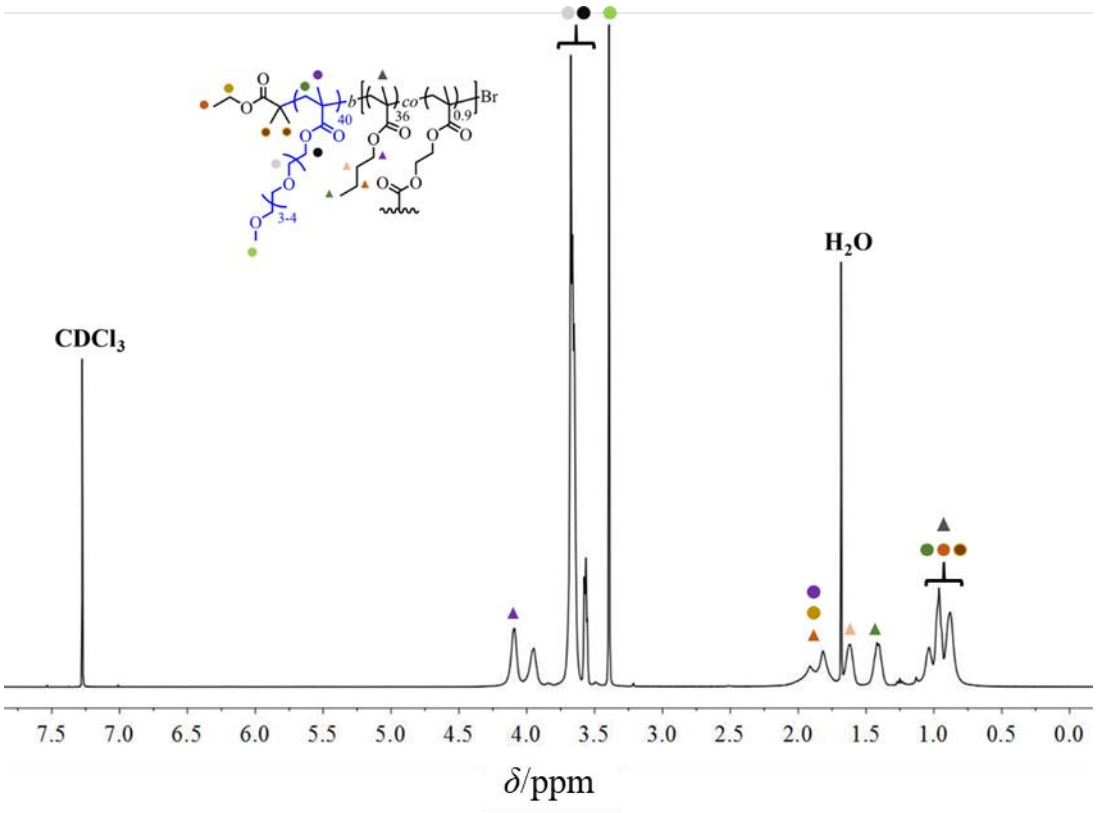

Figure 4.5. ^{1}H-NMR measured in $CDCl_3$ of **DP 36/40** after purification.

The synthesis of **DP 36/60** was followed in the same fashion. A solution of *n*BMA and EGDMA was added after a conversion of 90 % was reached. Table 4.1. shows the parameters used in both syntheses as well as the sizes obtained by measuring DLS in water. To assure that unimolecular nanoparticles were measured and not agglomerates, the polymers were dissolved in acetone and water was added dropwise. After acetone was evaporated off, DLS was measured in water. The measured sizes of 32 and 29 nm indicate the successful formation of branched polymers.

Table 4.1. Synthetic parameters for the synthesis of the branched diblock copolymers **DP 36/40** and **DP 36/60** as well as DLS size data.

Branched Block Copolymer	OEGMA	*n*BMA	EGDMA	Yield	size (D_h)
		eq.		%	nm
DP 36/40	40	40	0.9	60	32
DP 36/60	40	60	0.9	56	29

4.3.2. Characterisation

To compare the synthesised polymers, our collaborator Dr Tao He, synthesised the branched copolymer p(OEGMA)$_{36}$-*b*-(pBMA$_{20}$-*co*-pEGDMA$_{0.9}$) (**DP 36/20**) and the corresponding diblock p(OEGMA$_{36}$-*b*-BMA$_{54}$) (**DB DP 36/54**).

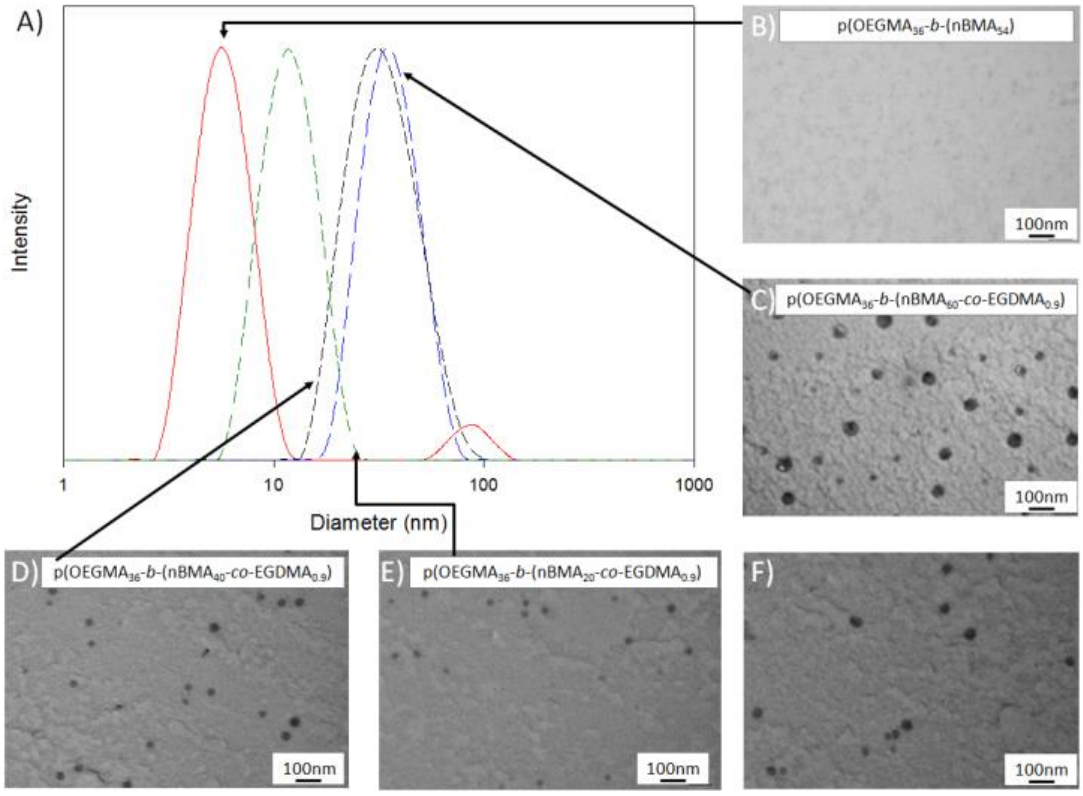

Figure 4.6. DLS data of p(OEGMA$_{36}$)-*b*-(*n*BMA-*co*-EGDMA$_{0.9}$) branched A-B block copolymer nanoparticles and the corresponding linear analogue after heating the solution through the UCST in methanol. (A) DLS data; blue dashed line **DP 36/60**; black dashed line **DP 36/40**; green dashed line **DP 36/20** and red line **DB DP 36/54**. And corresponding TEM images (B) linear **DB DP 36/54**; (C) branched **DP 36/60**; (D) branched **DP 36/40**; (E) branched **DP 36/20** and (F) branched nanoparticles of **DP 36/60** after heating through the UCST and dialysing into water (data recorded by Dr Tao He).

DLS data and TEM was measured in methanol and water at ambient temperatures to investigate if the method of thermal annealing is a viable alternative to dialysis. To that end the polymers were heated through the UCST and then cooled down to room temperature. Figure. 4.6. shows the obtained DLS data and TEM images.

In methanol, the Z-Average decreased from 37 nm to 33 nm to 25 nm with decreasing *n*BMA lengths (**DP 36/60** > **DP 36/40** > **DP36/20**) (Figure 4.6. A). The corresponding diblock **DB DP 36/54** showed sizes under 10 nm. This was assumed to be a single diblock copolymers solvated by p(OEGMA). This data showed that branched copolymers were obtained. The corresponding TEM images showed spherical nanoparticles with slightly larger sizes of 48 nm, 40 nm and 28 nm for **DP 36/60**, **DP 36/40** and **DP 36/20** respectively (Figure 4.6. C-E). The analogue diblock polymer **DB DP 54/60** formed an irregular film and no single nanoparticles could be detected (Figure 4.5. B). To demonstrate that the approach of heating through the UCSTs affords unimolecular, well dispersed nanoparticles, the same as dialysis against water, nanoparticles of **DP 36/60** were transferred from methanol to water by dialysis. The obtained TEM images (Figure 4.6.F) shows an average size of 45 nm and DLS Z-Average of 32 nm. The similar sizes indicate that the method of thermal annealing can be used as an alternative way to form nanoparticles more efficiently.

The stages of thermal annealing in methanol are shown in scheme 4.1. Dry polymer (**i**) is dissolved in methanol by heating through the UCST, whereby unimolecular polymer nanoparticles are obtained (**ii**). After cooling down to room temperature in methanol the *n*BMA core contracts but the polymer nanoparticles do not agglomerate (**iii**) addition of water and subsequent evaporation of MeOH at room temperature affords the same unimolecular nanoparticles (**iv**).

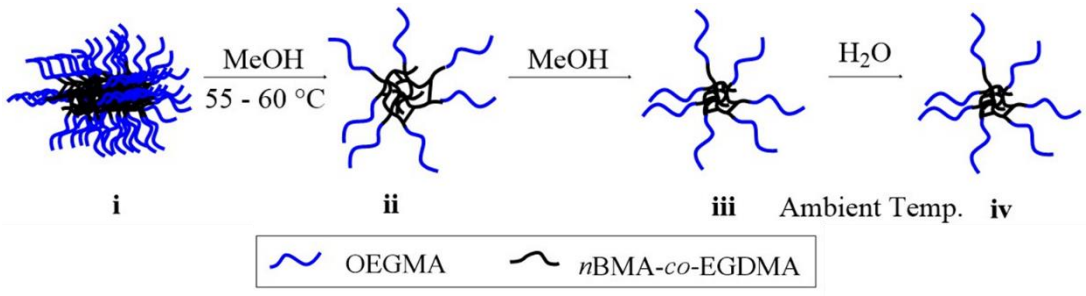

Scheme 4.1. Schematic representation of the thermal annealing process. i) dry polymer; ii) unimolecular branched polymer dissolved by heating through the UCST; iii) branched polymer at ambient Temperature in methanol and iv) branched polymer unimolecular dissolved in water.

The thermoresponsive behaviour was subsequetnly utilised to form drug nanoparticle. **DP 36/40** and **DP 36/60** were chosen for drug nanoparticle formation because of their bigger sizes and subsequent bigger core sizes. It was theorised that bigger core spaces would be able to stabilise hydrophobic nanoparticles better in aqueous solution.

4.3.3. Solvent evaporation at ambient temperature

A simple solvent evaporation procedure as that had been used in Chapter 3 was also applied to pOEGMA-*b*-p(*n*BMA-*co*-EGDMA) branched copolymers. The DLS data after resuspension in water is shown in Table 4.2.

Table 4.2. DLS data of of different hydrophobic actives evaporated from methanol and then re-dispersed into water. Drug:Polymer ratios were kept at 1:1.

Polymer	Drug	Z-Average	Number %	PDI
		nm		-
DP 40/60	Oil Red O	362 ± 4	52 ± 11	0.36
DP 40/60	Ketoprofen	-*	-*	-*
DP 36/40	Oil Red O	212 ± 3	-#	0.93
DP 36/40	Ketoprofen	80 ± 2	34 ± 5	0.38

* no measurement possible due to sample agglomerating; # high polydispersity and/or cumulant fit error high, no number % measurement possible

Independent of hydrophobic active used, no satisfactory results could be obtained. No nanoparticles were obtained for ketoprofen when **DP 40/60** was used, while the small size of around 80 nm of ketoprofen nanoparticles formed by **DP 40/40** hints at encapsulation of the active instead of the formation of drug nanoparticles. Both polymers used were able to form oil red nanoparticles. However, poor measurements as well as relatively high PDIs led us to believe that the formed nanoparticles were not stable in water. It was assumed that due to the change from linear PEG to non-linear PEG (OEGMA), which led to a physical change from a powder (PEG_{135}-*b*-(PNISOPROPANOLm_{25}-*co*-EDAm_{2n})-*b*-PEG_{135}) to a resin like morphology, the polymer could not be dissolved into water directly after methanol was evaporated. Hence drug nanoparticles could not be sufficiently stabilised and resuspended after

complete solvent evaporation. It was subsequently decided to evaporate into water to form drug nanosuspensions directly.

4.3.4. Solvent evaporation directly into water

When linear and block copolymers have been used before to produce drug nanosuspensions, the loading is usually done by solvent displacement or precipitation.[16] It is often difficult to load drugs into micelles in high yields and to obtain particles which are the right size to utilise the enhanced permeability and retention (EPR) effect. Herein, nanosuspensions of three hydrophobic actives, oil red, ketoprofen and anthracene were formed using **DP 36/40** and **DP 36/60** directly without redispersing a dry formulation. The evaporation yielded milky suspensions. The obtained DLS data and nanoparticle yield is presented in Table 4.3.

Table 4.3. DLS data of different hydrophobic actives evaporated from methanol into water. Drug: Polymer ratios were kept at 1:1.

Polymer	Drug	Z-Average	Number %	PDI	Yield
		nm		-	%
DP 36/60	Ketoprofen	198 ± 3	170 ± 9	0.03	100
DP 36/60	Oil Red O	109 ± 41	-[#]	0.17	34
DP 36/60	Anthracene	611 ± 8	459 ± 52	0.17	33
DP 36/40	Ketoprofen	214 ± 3	208 ± 3	0.02	100
DP 36/40	Oil Red O	66 ± 1	31 ± 2	0.15	17
DP 36/40	Anthracene	495 ± 6	399 ± 26	0.19	39

[#] high polydispersity and/or distribution fit error high, no number % measurement possible

Using **DP 36/60** afforded Ketoprofen particles of around 200 nm and no precipitant could be observed. Nanoparticles of anthracene, a highly hydrophobic dye could also be formed with sizes of around 600 nm and a nanoparticle yield of 33 %. DLS data could not be obtained in sufficiently good enough quality of oil red particles to confidently make a judgement about the particle size. When **DP 36/40** was used the DLS data obtained for oil red showed very small particles of around 66 nm. Consid-

ering the size of polymer nanoparticles measured without oil red (32 nm), nanoparticles might not have been formed, but rather branched particles with encapsulated oil red in their core comparable to a micelle. This would also explain the low particle yield. However, when anthracene or ketoprofen were used particles of 208 and 495 nm respectively could be obtained and in the case of ketoprofen a nanoparticle yield of 100 % was achieved. In all cases high loading was observed, considering that the initial concentration in water was 8 mg/ml. For anthracene a nanosuspension with concentrations of 3 mg/ml in water were obtained. Compared to the water solubility found in literature of 0.0013 mg/ml [17] this translates to an increase of 2000 %. Nanoparticle suspensions of ketoprofen could be obtained with a concentration of 8 mg/ml compared to unprocessed ketoprofen solutions of 0.05 mg/ml.[18] The DLS data for ketoprofen and oil red (**DP 36/40**) is shown in Figure 4.5.

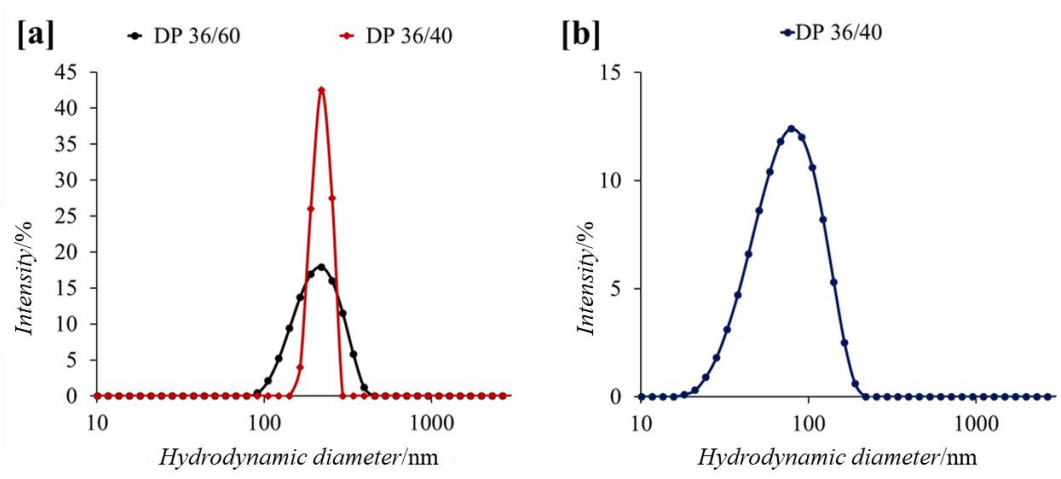

Figure 4.7. DLS data of a) ketoprofen nanosuspension using **DP 36/60** and **DP 36/40** and b) oil red nanosuspension using **DP 36/40** as stabilisers.

The branched diblock copolymers used in this work were synthesised by ATRP *via* the 'arm' first method. As such the longer the core forming chain can grow, the higher the statistical change that other polymer chains can be 'grabbed'. Hence intramolecular cross-linking increases, which in turn leads to the branched polymer being more spherical and ordered. It can be theorised that because the core region in **DP 36/40** is shorter it is also less protected/ordered and can interact better with drug molecules. **DP 36/60** on the other hand is slightly more ordered and as such the core is more protected by OEGMA arms and cannot interact as well with drug molecules.

This could be an explanation why, overall, using **DP 36/40** led to slightly better results with lower nanoparticle sizes and smaller PDIs.

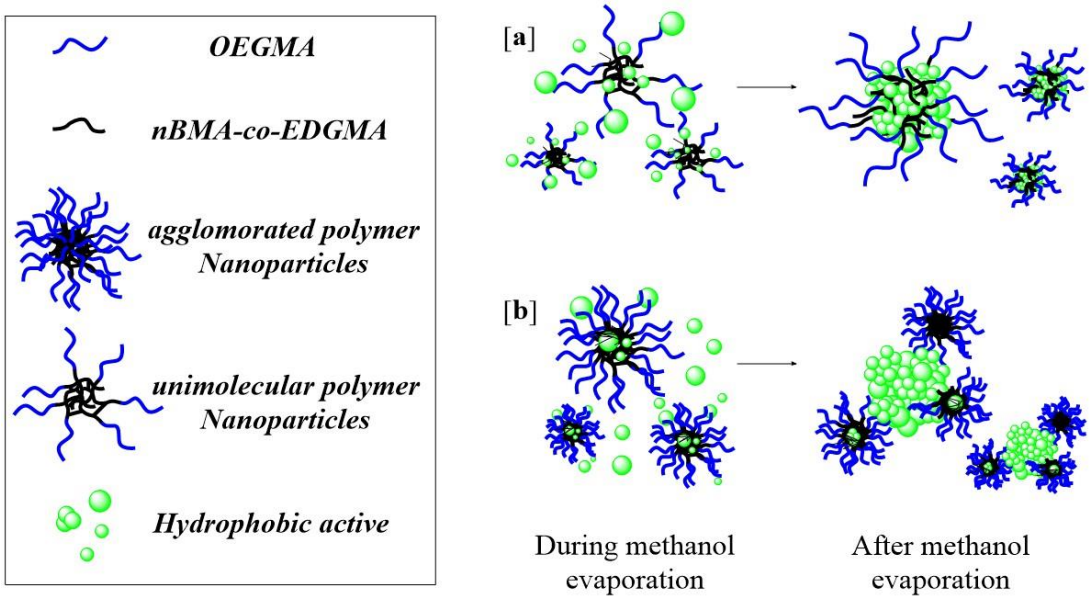

Scheme 4.2. Schematic representation of drug nanosuspension formation during and after methanol evaporation in the presence of a) unimolecular polymer nanoparticles and b) agglomerated polymer nanoparticles.

Nanosuspensions were formed by adding hydrophobic actives and polymers in a mass ratio of 1:1 to methanol and heating through the UCST to obtain a solution of well dispersed, unimolecular polymer nanoparticles and hydrophobic active. Water was added, and methanol was evaporated off at ambient temperatures. The addition of water should additionally lead to a decrease of the UCST temperature[19] and an increase in p(OEGMA) solubility, thus favouring the retainment of unimolecular polymer nanoparticles even at room temperature. The evaporation of methanol leads to the interaction of hydrophobic actives with the hydrophobic core of the branched polymer nanoparticles to protect against the increasingly hydrophilic environment. These particles then stabilise by agglomerating, *i.e.* the hydrophilic OEGMA arms cover the surface of a hydrophobic drug/pBMA complex. If the polymer nanoparticles would not be well dispersed as unimolecular nanoparticles as was achieved by using the thermal annealing process, but exist in solution as agglomerates, the interaction between drug and core would be complicated (Scheme 4.2.)

4.4. Conclusions

In this Chapter, branched diblock copolymer made from non-linear PEG arms and a thermoresponsive core of *n*BMA were synthesised *via* ATRP and used to directly form solutions of polymer nanoparticles by thermal annealing of a methanolic solution. The same polymer was then used to directly form nanosuspensions with very high drug content of up to 8 mg/ml and a nanoparticle yield of 100 %. While we focused in Chapter 3 on the stabilisation and growth inhibition ability of branched polymers in dependence on core cross-linkage, this Chapter focused on structural properties and core composition in relation to the ability to form nanoparticles. This was mainly possible because in comparison to the materials used in Chapter 3, which were synthesised by conventional radical polymerisation, the synthesis by ATRP afforded branched polymers of higher order due to better reaction control. Cryo-TEM images and DLS data confirmed, in comparison to an analogue diblock polymer, the successful synthesis of cross-linked branched polymer nanoparticles. The straightforward one-pot synthesis using isopropanol/water mixture at ambient temperatures would be favourable for industrial application. The thermal annealing behaviour could successfully be used to obtain methanolic solutions of unimolecular polymer nanoparticles without the need for a lengthy dialysis process. OEGMA as well as BMA exhibit thermo-responsive behaviour. OEGMA is known to have an LCST, while BMA exhibits UCST, both of which are of great interest to the pharmaceutical industry. The LCST and UCST are both greatly influenced by the type and lengths of the co-polymers as well as the lengths of the thermoresponsive block.[15,20,21]

After the initial characterisation, two polymers **DP 36/40** and **DP 36/60** were chosen for comparison of core composition dependent drug nanoparticle formation. To this end the UCST behaviour in methanol was initially used to obtain dried nanoparticles of ketoprofen and Oil Red O. This approach failed since the obtained materials could not be re-dispersed in water in a satisfactory manner. Consequently, drug nanosuspension were formed directly by dissolving the water insoluble drug and branched polymer in methanol, heating through the UCST to obtain unimolecular branched polymer nanoparticles and dissolved drug, followed by the addition of water and evaporation of methanol at ambient temperatures. With this approach nanosuspensions of ketoprofen, OR and anthracene in high yields were successfully obtained. Ketoprofen nanosuspensions with concentrations of 8 mg/ml with a drug to polymer

ratio of 1:1 mass ratio could be achieved, while for anthracene the nanosuspension concentration using the same ratios were at 3 mg/ml, which corresponds to 50 wt % and 25 wt % respectively. Both concentrations were unusual high compared what can normally be found in literature for diblock micelles *e.g.* 20-25 wt %.[22-24] Comparison of drug nanoparticle sizes and yields allowed to make conclusions about the stabilisation ability of the branched polymers in dependency of core composition and as such structural order. We observed that what we believed to be higher ordered structures *i.e.* more closely resembling dendrimers (**DP 36/60**) were less able to 'anchor' onto a crystal surface due to decreased hydrophobic interactions.

In summary we were able to successfully obtain nanosuspensions of highly water insoluble drugs with high yields, narrow PDIs and small particles sizes.

4.5. References

1. K. Matyjaszewski, *Macromolecules,* 2012, **45**, 4015-4039.
2. R. O. R. Costa and R. F. S. Freitas, *Polymer*, 2002, **43**, 5879-5885.
3. V. Boyko, Y. Lu, A. Richter and A. Pich, *Macromol. Chem. Phys.*, 2003, **204**, 2031-2039.
4. T. Gelbrich, M. Feyen, A. M. Schmidt, *Macromolecules,* 2006, **39**, 3469-3472.
5. R. Hoogenboom, H. M. L. Lambermont-Thijs, M. Jochems, S. Hoeppener, C. Guerlain, C. A. Fustin,J. F. Gohy and U. S. Schubert, *Soft Matter*, 2009, **5**, 3590-3592.
6. S. Glatzel, A. Laschewsky and J.-F. Lutz, *Macromolecules*, 2011, **44**, 413–415.
7. Y. Pei, K. Jarrett, M. Saunders, P. J. Roth, C. E. Buckley and A. B. Lowe, *Polym. Chem.*, 2016, **7**, 2740-2750.
8. A. B. Dwyer, P. Chambon, A. Town, T. He, A. Owen and S. P. Rannard, *Polym. Chem.*,2014, **5**, 3608-3616.
9. A. Fujihara, N. Shimada, A. Maruyama, K. Ishihara, K. Nakai, and S. I. Yusa, *Soft Matter*, 2015,**11**, 5204-5213.
10. G. Huang, H. Li, S. T. Feng, X. Li, G. Tong, J. Liu, C. Quan, Q. Jiang, C. Zhang and Z. Li, *Macromol. Chem. Phys*., 2015, **216**, 1014-1023.
11. P. J. Roth, T. P. Davis and A. B. Lowe, *Polym. Chem.*, 2012, **3**, 2228-2235.

12. T. He, D. J. Adams, M. F. Butler, C. T. Yeoh, A. I. Cooper and S. P. Rannard, *Angew. Chem. Int. Ed.*, 2007, **46**, 9243-9247.
13. T. He, D. J. Adams, M. F. Butler, A. I. Cooper and S. P. Rannard, *J. Am. Chem. Soc.*, 2009, **131**, 1495-1501.
14. S. McDonald and S. P. Rannard, *Macromolecules*, 2001, **34**, 8600-8602.
15. P. J. Roth, F. D. Jochum and P. Theato, *Soft Matter*, 2011, **7**, 2484-2492.
16. K. Letchford and H. Burt, *Eur. J. Pharm. Biopharm.*, 2007, **65**, 259-269.
17. K. Verschueren, *Handbook of Environmental Data on Organic Chemicals*, John Wiley & Sons, Hoboken, 2008.
18. S. Park, S.-E. Lee, J.-K. Lee, T.-H. Kim, W. S. Jang and J.-S. Park, *Int. J. Pharm. Investig.*, 2016, **46**, 487-493.
19. Q. Zhang and R. Hoogenboom, *Prog. Polym. Sci.*, 2015, **48**, 122-142.
20. C. R. Becer, S. Hahn, M. W. M. Fijten, H. M. L. Thijs, R. Hoogenboom and U. S. Schubert, *J. Polym. Sci. A*, 2008, **46**, 7138-7147.
21. Y. Koda, T. Terashima and M. Sawamoto, *ACS Macro Lett.*, 2015, **4**, 1366−1369.
22. N. Rapoport, *Prog. Polym. Sci.*, 2007, **32**, 962-990.
23. X. Shuai, H. Ai, N. Nasongkla, S. Kim and J. Gao, *J. Control. Release*, 2004, **98**, 415 – 426.
24. K. Kataoka, A. Harada and Y. Nagasaki, *Adv. Drug Deliv. Rev.*, 2001, **47**, 113-131.

Chapter 5

Solubilisation of hydrophobic drugs facilitated by pH-responsive hyperbranched polymers

This Chapter is based on the publication

U. Wais, H. Zhang and A. W. Jackson. "Star polymers possessing pH-responsive hyperbranched cores via RAFT polymerisation" *under preparation*

5.1. Introduction

Chapter 4 focused on the utilisation of ATRP to form branched amphiphilic polymers with a temperature responsive core. ATRP was chosen to impart good control over the resulting architecture than could be previously obtained using conventional free radical polymerisation as reported in Chapter 2 and 3.

Hyperbranched polymers (HBPs) are an interesting class of polymer architectures that have, in recent years, gained significant attention for biomedical application, due to their similarities to dendrimers. However, while dendrimers require a multistep synthesis and a laborious purification process, HBPs are synthetically easier to obtain while still maintaining many of the characteristics of dendrimers.[1] HBPs show enhanced solubility in a wide range of solvents due to lower chain entanglement, low melt and solution viscosity and a reduced hydrodynamic radius. Furthermore, they possess a large amount of chain ends for modification.[2]

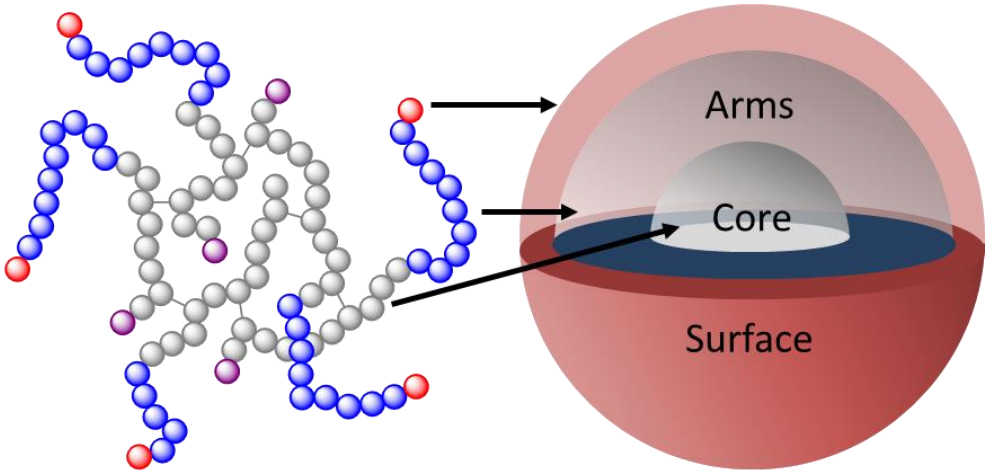

Figure 5.1. Schematic representation of a star hyperbranched polymer and its different regions *e.g.* core, arms and surface.

One of the most commonly used synthetic route to obtain HBPs is self-condensing vinyl polymerisation (SCVP). The combination of SCVP with reversible-deactivation radical polymerisation (RDRP) techniques such as ATRP and RAFT affords better control of branch lengths and variable functionalities [2] as well as the possibility for chain-extension of a second block to form star hyperbranched polymers (SHBP).[3,4] However, the combination of SCVP and RDRP requires the synthesis of an inimer to act as an initiator/monomer, which can be expensive and difficult to scale-up.[5] O'Brien *et. al.* [6] used conventional radical polymerisation in the presence of a vinyl monomer and a divinyl cross-linker to obtain hyperbranched polymers. Perrier

et. al. [7,8] extended this method by combining it with RAFT, which enables a straight forward, finely tunable and cost-effective route to form hyperbranched polymer that can easily be chain-extended to afford star polymers. The use of RAFT polymerisation makes it possible to tailor each part of a SHBP, *i.e.* core, arms and surface (Figure 5.1.) individually to suit specific needs, such as targeting or stimuli responsiveness.

The clinical application of polymers as drug nanocarriers and bioimaging tools is often hampered by the non-specific nature of polymers, instability in the blood stream, possible toxic decomposition products and short retention time.[9,10] The non-specific targeting can be addressed by modifying the polymer nanoparticle with small molecules which can act as antagonists for proteins on the surface of certain cells. Most polymers such as star-polymers, linear block polymers or bottle-brush polymers need to self-assemble to be able to encapsulate actives. However, these self-assembled structures fall apart and prematurely release their cargo when the concentration falls below the critical micelle concentration (CMC), which is often than not when injected into the bloodstream. On the other hand, three dimensional structures such as dendrimers and HBPs can encapsulate actives without self-assembly. This is because their branched cores already exhibit cavities which can be employed to encapsulate hosts. In addition, their chain ends can easily be used to afford nanocarriers with targeting moieties. Compared to their linear analogues increased sensitivity, specificity and circulation time could be observed when HBPs were used.[11]

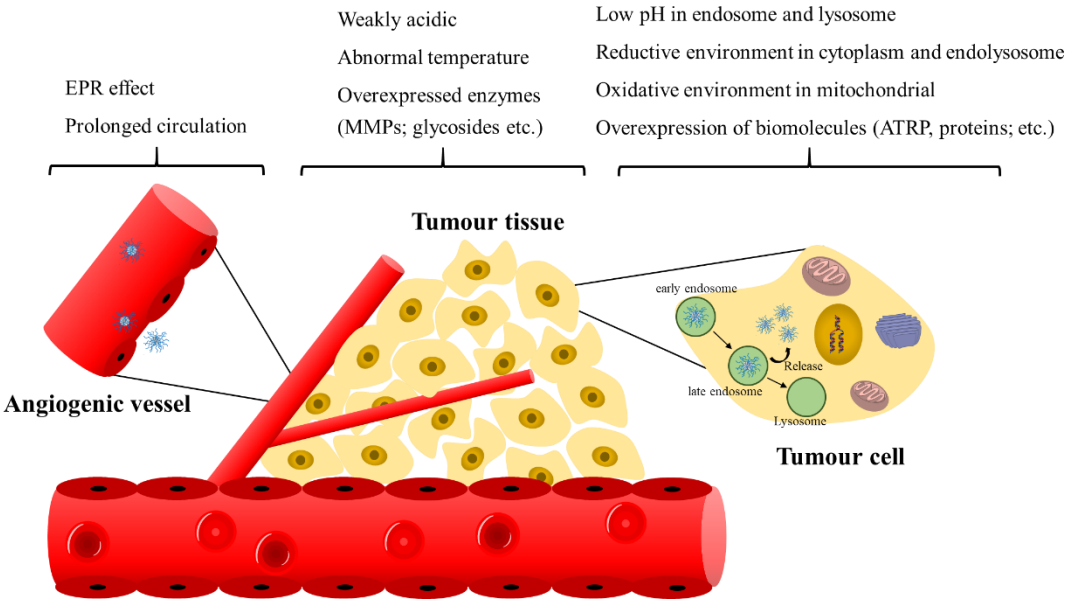

Figure 5. 2. Schematic representation of abnormal environment found in malignant tissue and cells used for active and passive targeting.

It has been shown that HBPs made from temperature sensitive monomers showed favourable behaviour for cell-targeting. Above the LCST the particles agglomerated into sub-micron particles and were able to enter the cells, while below the LCST, in the branched form, cells were excluded from entering.[12] Stimuli responsive polymers are especially interesting in cancer treatment, since cancer cells, and the malignant surrounding tissue, exhibit an abnormal environment compared to healthy tissue [13] (Figure 5.2.). Polymeric nanoparticles also have the additional benefit of being able to utilise the enhanced permeability and retention (EPR) effect.[14] To enhance the specificity of drug release at the target side pH or temperature responsive polymers are often chosen as carriers to facilitate the encapsulation and release at the pH or temperatures of malignant cells.[15] Polymers with pH responsiveness are particularly interesting because the cationic character of protonated polymers is known to facilitate the delivery into cells *e.g.* non-viral gene delivery.[2] Increased specificity can easily be afforded by using RAFT polymerisation and modifying the polymers with targeting moieties pre- or post-polymerisation.[16]

In this Chapter, a series of pH sensitive star hyperbranched polymers of the general constitution poly(ethylene glycol) methyl ether methacrylate-*b*-poly(2-(diethylamino)ethyl methacrylate-*co*-di(ethylene glycol) dimethacrylate) p(OEGMA)$_{80}$-*b*-p(DEAEMA$_x$-*co*-DEGDMA$_2$) with x = 25, 50, 100 and 200 as well as a diblock polymer p(OEGMA$_{80}$-*b*-DEAEMA$_{50}$) were synthesised *via* RAFT polymerisation. In order to study the influence of core composition on branching and pH sensitive behaviour, the hydrophilic arms and cross-linker equivalences were kept constant at 80 and 2, respectively. The series was then studied for pH responsive behaviour. OEGMA is known to exhibit a LCST. Hence, temperature was employed as a second stimulus and all polymers were tested for their behaviour at temperatures above and below the LCST and at low and high pH values. Subsequently the SHBP with the most favourable core-cross-linking was chosen to study pH responsive release of a hydrophobic drug, gelation behaviour and the surface modification with a fluorescent dye.

5.2. Experimental

5.2.1. Materials and Characterization

4-((((2-Carboxyethyl)thio)carbonothioyl)thio)-4-cyanopentanoic acid (BM1433) was purchased from Boron Molecular. Oligoethylene glycol methacrylate

monomethyl ether (OEGMA, $M_w \approx 300$ g/mol), 2-(diethylamino)ethyl methacrylate (DEAEMA) and di(ethylene glycol) dimethacrylate (DEGDMA) were passed through a basic alumina column to remove the inhibitor prior to use. ^{1}H NMR spectra were recorded on Bruker 400 Ultra Shield spectrometer. Size exclusion chromatography (SEC) was conducted on a Waters 717 plus autosampler equipped with a Waters 515 pump and a Waters 2414 refractive index (RI) detector. Three columns; Styragel HR0.5 (0-1,000), Styragel HR3 (500-30,000) and a Styragel HR5E (2,000-4,000,000) were applied in sequence for separation. Tetrahydrofuran was used as the eluent at 0.3 mL/min, molecular weights were determined against poly(styrene) standards. Static light scattering analysis was completed on a Viscotek Triple Detector Array (TDA) 302 equipped with a Refractive Index (RI) detector, Viscometer, Right Angle (90°) Light Scattering (RALS) and Low Angle (7°) Light Scattering (LALS). Separation was performed using two PLgel 5um Mixed-B columns connected in series. Samples were injected at a volume of 100 µL and eluted through the system at flow rate of 1 mL/min in THF. A temperature of 30 °C was maintained during separation and detection. Poly(styrene) 210 kDa was used as calibration for absolute molecular weight determination by Light Scattering. Deionized water was prepared using an Aqua-MAX-Basic 321 DI water purification system. Hydrodynamic diameter values were determined by dynamic light scattering (DLS) analysis on a Malvern Zetasizer Nanoseries from Malvern Instruments at 25 °C. The measurements were performed on aqueous nanoparticles solutions with concentrations of 3 mg/ml. UV/Vis analysis was performed on a Shimadzu UV-2700, Indomethacin concentrations were determined against a calibration curve of solutions of known concentration in EtOH.

*5.2.2. Synthesis of DEAEMA Hyperbranched Polymers (**HB1-HB4**)*

Hyperbranched polymers (**HB1-4**) were synthesised by the follow procedure. All experiments were conducted with constant monomer and solvent concentrations and varying amounts of RAFT chain transfer agent, radical initiator and cross-linker (Table 5.1). In a typical synthesis (**HB1**) the RAFT chain transfer agent 4-((((2-carboxyethyl)thio)carbonothioyl)thio)-4-cyanopentanoic acid (184 mg, 0.6 mmol, 1 eq), di(ethylene glycol) dimethacrylate (238 mg, 1.2 mmol, 2 eq), 2-(diethylamino)ethyl methacrylate (2.78 g, 15 mmol, 25 eq) and azobisisobutyronitrile (9.8 mg, 60 µmol, 0.1 eq) were transferred into a schlenk flask fitted with a magnetic stirrer bar and *N,N'*-dimethylformamide (3.0 g) added. The reaction mixture was degassed via three

freeze-pump-thaw cycles and backfilled with N_2. The reaction was heated to 70 °C and stirred at 500 rpm for 16 h after this time NMR analysis confirmed conversions of 90 – 99 %. The reaction was quenched by rapid cooling, and the polymer purified by three precipitations from THF into water. The polymer was dissolved into chloroform and dried over $MgSO_4$. The purified polymer was isolated as a yellow waxy solid. ^{1}H NMR ($CDCl_3$): δ 4.70 (br, C(O)O$\underline{CH_2}CH_2$O), 4.00 (br, C(O)O$\underline{CH_2}CH_2$N), 3.63 (br, C(O)OCH$_2\underline{CH_2}$O), 2.71 (br, CH$_2\underline{CH_2}$N), 2.58 (br, N($\underline{CH_2}CH_3)_2$), 1.84 (br, $\underline{CH_2}$C(CH$_3$)), 1.04 (br, N(CH$_2\underline{CH_3})_2$), 0.88 (br, CH$_2$C($\underline{CH_3}$)).

*5.2.3. Synthesis of OEGMA-b-DEAEMA Star Hyperbranched Polymers (**SHB1-4**)*

Star hyperbranched polymers (**SHB1-4**) were synthesised by the follow procedure. All experiments were conducted with constant concentrations of hyperbranched polymer precursor, monomer, solvent and radical initiator (Table 5.2). In a typical synthesis (**SHB1**) the hyperbranched polymer precursor (**HB1**, 0.68 g, 0.125 mmol, 1 eq), oligo(ethylene glycol) methyl ether methacrylate (3.0 g, 10 mmol, 80 eq) and azobisisobutyronitrile (2.1 mg, 12.5 µmol, 0.1 eq) were transferred into a schlenk flask fitted with a magnetic stirrer bar and *N,N'*-dimethylformamide (11 g) added. The reaction mixture was degassed via three freeze-pump-thaw cycles and backfilled with N_2. The reaction was heated to 70 °C and stirred at 500 rpm for 16 h after this time NMR analysis confirmed conversions of 90 – 99 %. The reaction was quenched by rapid cooling, and the polymer purified by three precipitations from THF into hexane. The purified polymer was isolated as a yellow oil. ^{1}H NMR ($CDCl_3$): δ 4.07 (br, C(O)O$\underline{CH_2}CH_2$N and C(O)O$\underline{CH_2}CH_2$O), 3.65 (br, ($\underline{CH_2CH_2}$O)$_n$), 3.54 (br, $\underline{CH_2}$OCH$_3$), 3.37 (br, CH$_2$O$\underline{CH_3}$), 2.95-2.65 (br, CH$_2\underline{CH_2}$N and N($\underline{CH_2}CH_3)_2$), 1.81 (br, $\underline{CH_2}$C(CH$_3$)), 1.14 (br, N(CH$_2\underline{CH_3})_2$), 0.87 (br, CH$_2$C($\underline{CH_3}$)).

*5.2.4. Synthesis of DEAEMA Linear Polymer (**LP1**)*

RAFT chain transfer agent 4-((((2-carboxyethyl)thio)carbonothioyl)thio)-4-cyanopentanoic acid (92 mg, 0.3 mmol, 1 eq), 2-(diethylamino)ethyl methacrylate (2.78 g, 15 mmol, 50 eq) and azobisisobutyronitrile (4.9 mg, 30 µmol, 0.1 eq) were transferred into a schlenk flask fitted with a magnetic stirrer bar and *N,N'*-dimethylformamide (3.0 g) added. The reaction mixture was degassed via three freeze-pump-thaw cycles and backfilled with N_2. The reaction was heated to 70 °C and stirred at 500 rpm for 16 h after this time NMR analysis confirmed a conversion of 99 %. The

reaction was quenched by rapid cooling, and the polymer purified by three precipitations from THF into hexane. The purified polymer was isolated as a yellow waxy solid. ^{1}H NMR ($CDCl_3$): δ 4.01 (br, C(O)O$\underline{CH_2}CH_2$N), 2.71 (br, $CH_2\underline{CH_2}$N), 2.59 (br, N($\underline{CH_2}CH_3)_2$), 1.84 (br, $\underline{CH_2}C(CH_3)$), 1.05 (br, N($CH_2\underline{CH_3})_2$), 0.89 (br, $CH_2C(\underline{CH_3})$).

*5.2.5. Synthesis of OEGMA-b-DEAEMA Linear Diblock Polymer (**DB1**)*

The linear polymer $DEAEMA_{50}$ (**LP1**, 1.16 g, 0.125 mmol, 1 eq), oligo(ethylene glycol) methyl ether methacrylate (3.0 g, 10 mmol, 80 eq) and azobisisobutyronitrile (2.1 mg, 12.5 µmol, 0.1 eq) were transferred into a schlenk flask fitted with a magnetic stirrer bar and *N,N'*-dimethylformamide (11 g) added. The reaction mixture was degassed via three freeze-pump-thaw cycles and backfilled with N_2. The reaction was heated to 70 °C and stirred at 500 rpm for 16 h after this time NMR analysis confirmed conversions of 92 %. The reaction was quenched by rapid cooling, and the polymer purified by three precipitations from THF into pentane. The purified polymer was isolated as a yellow oil. ^{1}H NMR ($CDCl_3$): δ 4.07 (br, C(O)O$\underline{CH_2}CH_2$N and C(O)O$\underline{CH_2}CH_2$O), 3.65 (br, ($CH_2\underline{CH_2}$O)n), 3.54 (br, $\underline{CH_2}OCH_3$), 3.37 (br, $CH_2O\underline{CH_3}$), 3.15-2.85 (br, $CH_2\underline{CH_2}$N and N($\underline{CH_2}CH_3)_2$), 1.83 (br, $\underline{CH_2}C(CH_3)$), 1.26 (br, N($CH_2\underline{CH_3})_2$), 0.93 (br, $CH_2C(\underline{CH_3})$).

*5.2.6. pH-Responsive Investigation (**SHB1-4** and **DB1**)*

Aqueous solutions of shell hyperbranched polymers (**SHB1-4**) and the linear diblock copolymer (**DB1**) were prepared by dissolving 30 mg polymer in 2 ml acetone, followed by the addition of 10 ml DI water at pH 5. Acetone was removed by evaporation at room temperature under constant stirring at 500 rpm. After acetone evaporation, 1M $HCl_{(aq)}$ and 1M $NaOH_{(aq)}$ were used to adjust the pH values from 5 to 9. Values were determined using a Mettler Toledo S220 pH probe. Measurements were performed in triplicate, by cycling between pH 5 and 9.

5.2.7. Indomethacin solubilisation and pH-Triggered Release

Typically, 200 mg of shell hyperbranched polymer **SHB1-4** (or linear diblock copolymer **DB1**) and 100 mg Indomethacin (IMC) were dissolved in 10 mL EtOH, and 10 mL DI water added slowly. EtOH was evaporated at room temperature under constant stirring at 500 rpm. The obtained solution was filtered to remove the excess IMC, UV-Vis was used to determine the % of IMC in solution. After the ethanol was

removed the pH of the obtained IMC/polymer solution was measured at pH 6.5. The 10 mL aqueous solution obtained was split into two stock solutions, one 5 mL solution was maintained at pH 6.5 and the second 5 mL solution adjusted to and maintained at pH 5.0. pH adjustments were made using small aliquots of 1M $HCl_{(aq)}$ and 1M $NaOH_{(aq)}$. At specific time points small samples were extracted and centrifuged to isolate the precipitated IMC from the IMC/polymer solution. 30 µL of the supernatant was taken out and dissolved in 2.97 mL EtOH for UV/Vis analysis, against a calibration curve of known IMC concentrations in EtOH, the remaining solution was replenished with 30 µL H_2O at pH 5 or 6.5 and added back to the respective IMC/polymer stock solutions.

5.2.8. Thiol Functionalisation of Star Hyperbranched Polymer via Aminolysis

The thiol chain end-functional star hyperbranched polymer (**SHB2-SH**) was synthesised by the following procedure. Trithiocarbonate chain end-functionalised star hyperbranched polymer (**SHB2**, 2.31 g, approx. 0.07 mmol of trithiocarbonate end-group, 1 eq) was dissolved in THF (10 mL) and transferred to a Schlenk flask fitted with a rubber septum. The solution was degassed via three freeze-pump-thaw cycles and backfilled with N_2. 3-Aminopropanol (0.26 g, 3.50 mmol, 50 eq) was added via syringe and the reaction was heated to 45 °C for 2 h. After this time the reaction was purified by two precipitations from THF into hexane. The polymer was isolated as a clear oil. Aminolysis was confirmed by UV-Vis (3 mg/ mL in THF) of **SHB2** compared with **SHB2-SH**. The process was performed under identical conditions with the linear diblock copolymer (**DB1**) to afford the thiol end-functionalised **DB1-SH**.

5.2.9. Gelation of Thiol Functional End-functionalised Star Hyperbranched Polymer

SHB2-SH (150 mg) was dissolved in the minimal amount of acetone required. H_2O (2 mL) was then added followed by H_2O (1 mL) containing 10 µl H_2O_2 (30 % w/w). The solution was left open for acetone to evaporate, the resulting polymer concentration is 5 wt %. Successful gelation was confirmed by the vial inversion test. The experiment was repeated using different polymer concentrations (1 and 10 wt %) and control experiments performed with **SHB2**, **DB1** and **DB1-SH**.

5.2.10. Conjugation of Fluorescein via Thiol-ene Click Chemistry

SHB2-SH (0.2 g, approx. 6.0 µmol of thiol end-group, 1 eq) and *N*-(5-Fluoresceinyl)maleimide (3.0 mg, 7.0 µmol, 1.2 eq) were dissolved in DMF (2 mL), the reaction was stirred for 20 h at room temperature in the dark. The polymer was purified by dialysis against H_2O in a 5 mL Float-A-Lyzer (M_w cut-off 8-10 kDa) for 24 h. After removal of water via freeze-drying, the desired polymer (**SHB2-Dye**) was obtained as a red oil. Successful dye conjugation was confirmed by UV-Vis (3 mg/ mL in H_2O) of **SHB2-Dye** compared with **SHB2** and **SHB2-SH**.

5.3. Results and discussion

5.3.1. Synthesis of p(OEGMA)$_{80}$-b-p(DEAEMA$_x$-co-DEGDMA$_2$)

A series of star hyperbranched polymers of the general structure pOEGMA$_{80}$-*b*-(DEAEMA$_x$-*co*-DEGDMA$_2$) with x = 25; 50; 100 and 200 as well as a linear diblock polymer p(OEGMA$_{80}$-*b*-DEAEMA$_{50}$) were synthesised by RAFT polymerisation *via* a 'core-first' approach. The polymers were named HB1-4 (hyperbranched polymer) and LP1 (linear polymer) before being grown out with OEGMA, after which they were denominated as SHB1-4 (star hyperbranched polymer) and DB1 (diblock polymer). In case of hyperbranched and star hyperbranched polymers the numbers 1-4 represent the degree of polymerisation of DEAEMA, *i.e.* HB1 = (DEAEMA$_{25}$-*co*-DEGDMA$_2$), SHB1 = pOEGMA$_{80}$-*b*-(DEAEMA$_{25}$-*co*-DEGDMA$_2$), HB2 = (DEAEMA$_{50}$-*co*-DEGDMA$_2$) and SHB2 = pOEGMA$_{80}$-*b*-(DEAEMA$_{50}$-*co*-DEGDMA$_2$) and so on. In case of the linear and diblock polymer only one polymer of the constitution p(DEAEMA$_{50}$) (LP1) and p(OEGMA$_{80}$-*b*-DEAEMA$_{50}$) (DB1) were synthesised. Scheme 5.1. shows a schematic presentation of the synthesis. Table 5.1 gives an overview of the synthetic parameters used for the hyperbranched cores (**HB1-6**) and linear polymer **LP1**. Table 5.2. shows the synthetic parameters used for the chain-extension to form star hyperbranched polymers (**SHB1-4**) and linear diblock **DB1** respectively.

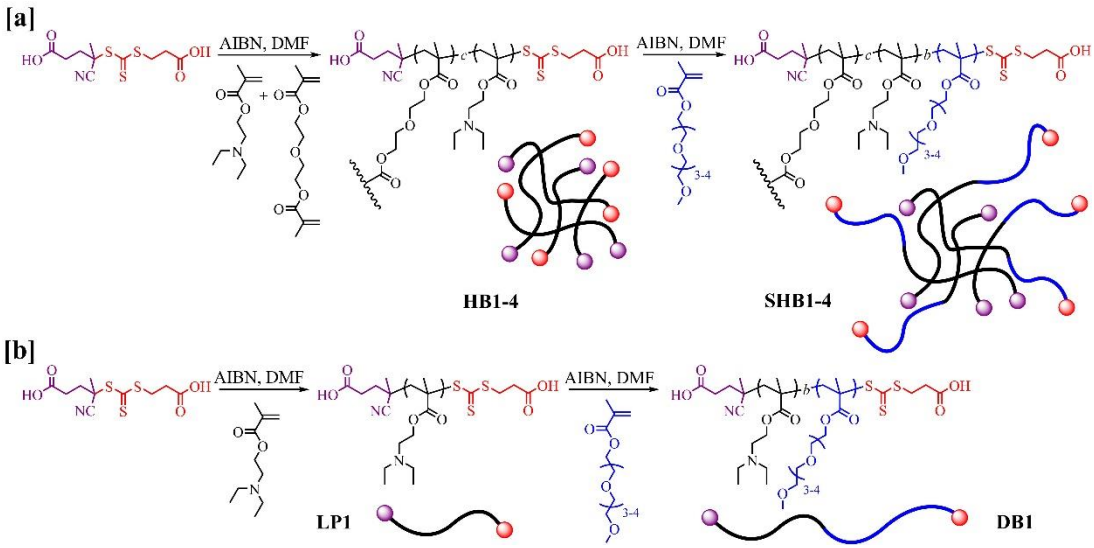

Scheme 5.1. Schematic presentation of the synthesis of a) hyperbranched cores **HB1-4** and extension to star hyperbranched polymers **SHB1-4** and b) linear polymer **LP1** and extension to diblock polymer **DB1** by RAFT polymerisation.

Initially, the pH responsive monomer DEAEMA was polymerised in the presence of a cross-linker (DEGDMA) and a RAFT chain transfer agent to afford hyperbranched polymers of DEAEMA-*co*-DEGDMA. This has been initially reported by Perrier *et. al.* using methyl methacrylate (MMA) and ethylene glycol dimethacrylate (EGDMA).[7] The copolymerisation of DEAEMA with the a relatively low equivalence of cross-linker (DEGDMA) by RAFT led to hyperbranched polymers. Table 5.1. shows the synthetic parameters used, as well as DLS data measured in THF, where the hyperbranched polymers are uniformly dissolved. Initially the cross-linker to CTA ratio was fixed at 2:1 and the monomer ratio was varied to 25, 50, 100 and 200 (**HB1-4**). Conversion was measured by ^{1}H-NMR. High conversions of over 90 percent were achieved for all polymers. The polymers were purified by precipitation twice into DI water.

After successfully obtaining polymers **HB1-4** the cross-linking to CTA equivalence was varied from 2:1 to 3:1, while keeping the ratio of cross-linker:DEAEMA at 1:25. However, when the crosslinking:CTA ratio exceeded 2 (**HB5** and **HB6**), the reaction gelled. Confirming what had previously been observed in the RAFT polymerisation of EGDMA and methyl methacrylate (MMA) by Perrier *et. al.* [7]

DLS data in THF showed that with increasing monomer units the size of the HB polymers increased from 14 nm to 33 nm from **HB1** to **HB4**. Linear polymer **LP1**

only show a size of 5 nm in THF, as expected for a linear polymer. Hence, branching was successfully achieved for **HB1-HB4**.

Table 5.1. Synthetic parameters for hyperbranched cores and linear block polymer **HB1-6** and **LP1,** DLS data in THF, DB = degree of branching and RB = average repeat units per branch (1/DB).

Name	[DEAEMA] : [CTA] : [DEGDMA] : [AIBN]	Conversion	Yield	D_h in THF	DB	RB
	-	%	%	nm	-	-
HB1	25 : 1 : 2 : 0.1	99	73	17	0.135	7.41
HB2	50 : 1 : 2 : 0.1	99	52	21	0.068	14.71
HB3	100 : 1 : 2 : 0.1	96	43	24	0.035	28.57
HB4	200 : 1 : 2 : 0.1	90	27	35	0.019	52.63
HB5	75 : 1 : 3 : 0.1	gelled	-	-	-	-
HB6	100 : 1 : 4 : 0.1	gelled	-	-	-	-
LP1	50 : 1 : 0 : 0.1	92	30	5	-	-

All experiments were performed in 50 wt % DMF at 70 °C for 20h

The degree of branching (DB), *i.e.* the fraction of branching units in each macromolecule, can be determined by analysing the ^{1}H-NMR spectra of **HB1-HB4**. Figure 5.3 shows an example of a NMR spectra of **HB2** (Figure 5.3.a and b) and **SHB2** (Figure 5.3.c) measured in $CDCl_3$. Equation 5.1 is used to calculate DB by relating the number of terminal (T), linear (L) and branching (B) units.[22] In RAFT polymerisation the terminal groups are equal with the chain transfer agent's R-group (R) and Z-group (Z). Equation (5.1) can be modified to yield equation (5.2). The Z-group used are not visible in ^{1}H-NMR spectroscopy. However, Z-groups and R-groups are approximately equal and so equation (5.3) can be obtained.[5] Linear (non-cross-linked) polymers have a DB close to zero, while perfectly branched structures have a DB of one.

$$DB = \frac{B + T}{B + T + L} \qquad (\mathbf{5.1})$$

$$DB = \frac{B + R + Z}{B + R + Z + L} \qquad (\mathbf{5.2})$$

$$DB = \frac{B + 2R}{B + 2R + L} \qquad (\mathbf{5.3})$$

When the integrals (Figure 5.3.b) of the terminal R-group protons (R) (-C$\underline{H_2}$COOH) at 2.33 ppm, the DEGDMA (B) protons (-CH$_2\underline{CH_2}$O-) at 3.63 ppm and the DEAEMA (L) protons (-$\underline{CH_2}$CH$_2$N-) at 4.00 ppm are inserted into equation 5.3, it is possible to obtain the degree of branching for each DEAEMA-*co*-DEGDMA hyperbranched polymer (Table 5.1.) and the average repeat units per branch (RB), which is equal to 1/DB. The degree of branching increased from 0.019 (**HB4**) to 0.135 (**HB1**) as the initial feed ratio of [DEAEMA]:[DEGDMA] increases from 100 to 12.5. The ratio of monomer to cross-linker is higher in **HB1** (12.5:1) than **HB4** (100:1), as such the statistically possibility to incorporate a second chain *via* a cross-linker is higher in **HB1**. Furthermore, shorter linear blocks should be more mobile and have less steric hindrance to 'grab' another growing polymer chain, favouring higher degrees of branching.

By using RAFT polymerisation, the prepared cores could easily be extended, even after prolonged storage at -20 °C, with OEGMA. Star hyperbranched polymers comprising of a hydrophobic hyperbranched core of DEAEMA and a linear hydrophilic exterior of OEGMA were obtained. OEGMA was chosen due to its known biocompatibility. Table 5.2. shows the synthetic parameters used for the extension of **HB1**-**HB4** and **LP1** to star hyperbranched and diblock polymer **SHB1**-**SHB4** and **DB1**, the size data measured in THF, as well as the number of arms.

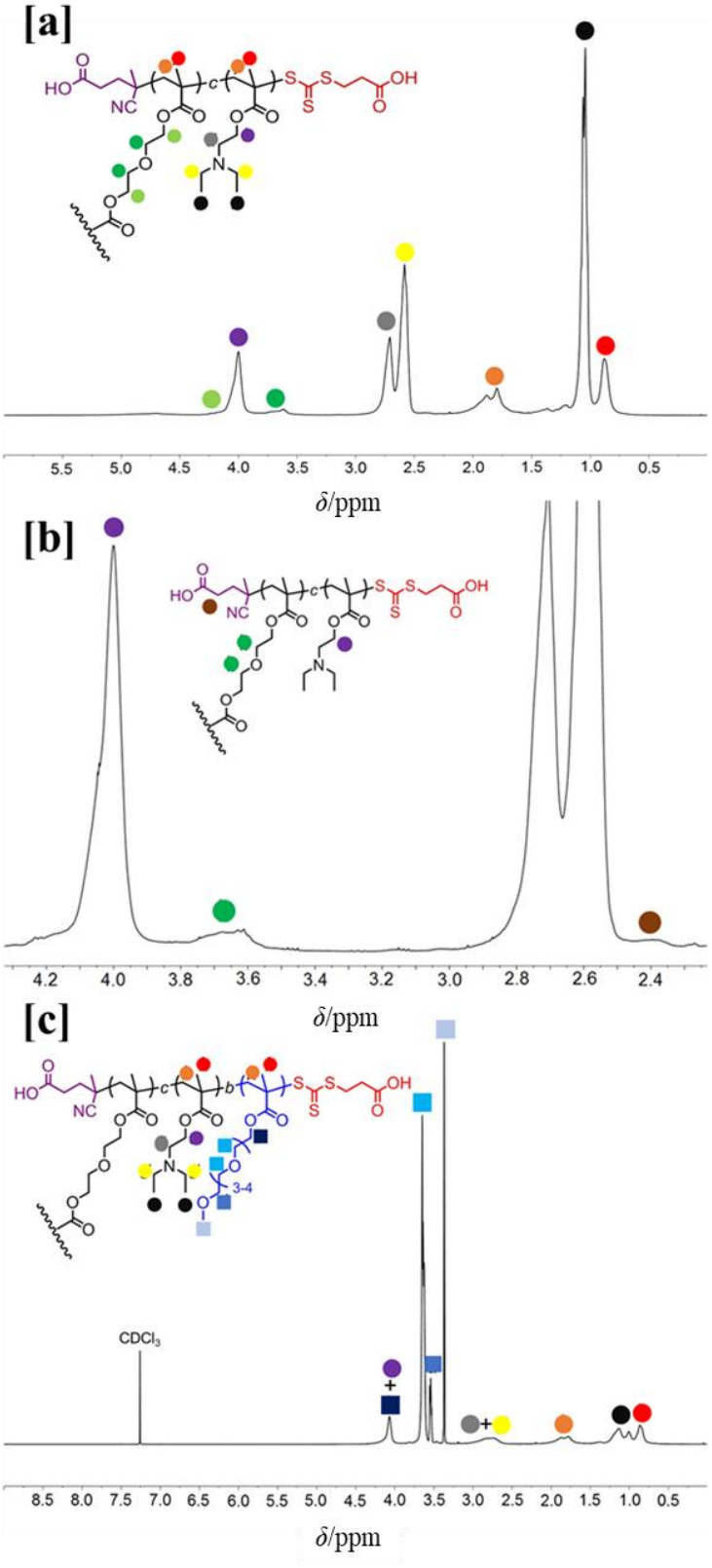

Figure 5.3. a) ^{1}H-NMR in $CDCl_3$ of **HB2**; b) Expansion of ^{1}H NMR ($CDCl_3$) spectra of **HB2** used to determine degree of branching (DB) and c) ^{1}H-NMR in $CDCl_3$ of **SHB2**.

All reactions reached conversions of over 90 %. Purification was done by precipitation into cold hexane three times. The size data measured in THF, where both blocks are soluble, shows an expected trend of decreasing sizes from **SHB1** to **SHB4** with a size dip for **SHB3**. The size decrease is a direct consequence of a decreasing degree of branching from **HB1** to **HB4**. Less chains are incorporated and hence grown out. The number of incorporated arms can be calculated as

$$no.of\ arms = \frac{M_n of\ SHB\ polymer - M_n of\ HB\ precursor}{M_n^{theo.}\ of\ poly(OEGMA)} \quad (\mathbf{5.4})$$

Where the number average molecular weight (M_n) of SHB polymer and HB polymer were obtained from static light scattering (SLS) measurements in THF (Table 5.3.) and the theoretical number average molecular weight of linear segments between branching points ($M_n^{theo.}$) of *poly*(OEGMA) was calculated according to the following equation

$$M_n^{theo.} = 80 \times M_W\ of\ OEGMA \times Conv. \quad (\mathbf{5.5})$$

With the mass average molar mass (M_w) taken from Table 5.3. and the conversion (Conv.) taken from Table 5.2. As had been observed in the size data in THF, the number of arms increased with increasing [DEAEMA]:[DEGDMA] feed ratio from 100 to 12.5, from 13.07 (**SHB1**) to 3.65 (**SHB4**).

Table 5.2. Synthetic parameters for star hyperbranched and diblock polymer **SHB1-4** and **DB1,** DLS data in THF and number of arms.

Name	[OEGMA] : [Macro-RAFT] : [AIBN]	Conversion	Yield	D_h in THF	No. of arms
	-	%	%	nm	-
SHB1	80 : 1 (**HB1**) : 0.1	95	98	65	13.07
SHB2	80 : 1 (**HB2**) : 0.1	96	71	66	9.59
SHB3	80 : 1 (**HB3**) : 0.1	96	67	36	4.08
SHB4	80 : 1 (**HB4**) : 0.1	96	37	52	3.65
DB1	80 : 1 (**LP1**) : 0.1	92	69	21	-

All experiments were carried out in 24 wt % DMF at 70 °C for 20h

Gel permeation chromatography (GPC) was recorded of **HB1**-**HB4**; **SHB1**-**SHB4**; **LP1** and **DB1** in THF. The results are presented in Table 5.3. All measured

molecular weights were off compared to what had been calculated from ^{1}H-NMR *e.g.* **HB1** was calculated to be M_n = 4900 g/mol and measured by GPC to be M_n = 5900 g/mol. This phenomenon has been described before for HB polymers.[1,19] GPC measures the hydrodynamic volume of a polymer and compares this to a linear standard of *poly*(styrene) of a known molecular weight. HBPs, due to their branched architecture, form coiled structures and as such the comparison to linear polymers is most likely unsuitable as a method. However, the obtained broad dispersity (PDI) values of 2.24-1.81 and 2.07-1.83 are indicative of cross-linked polymers obtained by copolymerisation with divinyls. Absolute M_n values obtained by online static light scattering displayed much high values confirming the preparation of cross-linking macromolecules. Theoretical Molecular weights for **HB1**-**HB4** and **LP1** were calculated using equation (5.6) with BM1433 being the chain transfer agent. Theoretical Molecular weights for **SHB1**-**SHB4** and **DP1** were calculated as

$$M_W^{theor.} = \left(\frac{[DEAEMA]}{[BM1433]} \times M_W\ of\ DEAEMA\ \times Conv.\right) + M_W\ of\ BM1433 \quad (\mathbf{5.6})$$

$$M_W^{theor.} = (M_W^{theor.}\ of\ HB1 - HB4(LP1)) + (n \times M_W\ of\ OEGMA \times Conv.) (\mathbf{5.7})$$

Table 5.3. Molecular weight calculated by NMR and GPC and DLS data for hyperbranched cores and star-hyperbranched polymers 1-4 as well as diblock polymer 1

Name	Conv.[a] [%]	$M_n^{theo.}$	M_n[b]	M_w[b]	PDI[b] (M_w/M_n)	M_n[c] SLS
	%		g/mol		-	g/mol
HB1	99	4,900	5,900	13,200	2.24	82,000
HB2	99	9,500	14,000	25,500	1.82	145,000
HB3	96	18,100	11,500	19,000	1.65	165,000
HB4	90	33,700	17,400	31,500	1.81	160,000
LP1	92	8,800	6,600	8,200	1.24	-
SHB1	95	27,700	31,500	65,100	2.07	380,000
SHB2	96	32,500	23,800	53,000	2.23	366,000
SHB3	96	41,100	21,300	43,200	2.03	259,000
SHB4	96	56,700	21,400	39,100	1.83	244,000
DB1	92	30,900	23,200	29,500	1.27	-

M_n^{theo} = theoretical number average molecular weight of linear segments between branching points; [a] Determined by ^{1}H NMR spectroscopy, [b] determined by SEC in THF against PS standards, [c] determined by SEC online static light scattering in THF

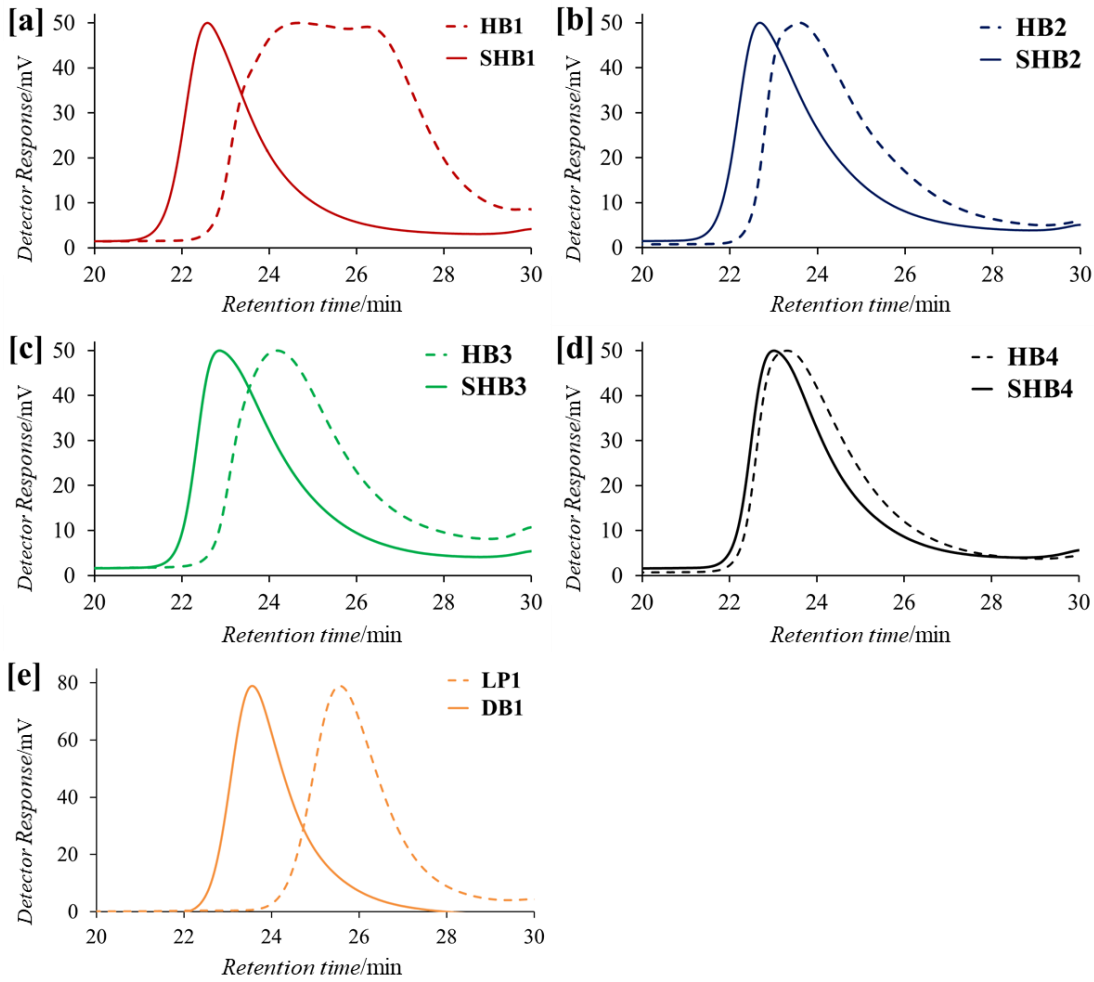

Figure 5.5. GPC graphs of hyperbranched cores (dotted line) and star hyperbranched polymers (solid line) as well as the linear analogue **LP1** and **DB1** in THF. a) **HB1** and **SHB1**; b) **HB2** and **SHB2**; c) **HB3** and **SHB3**; d) **HB4** and **SHB4** and e) **LP1** and **DB1**.

Comparison of the GPC curves of hyperbranched cores and star-hyperbranched polymers after extension (Figure 5.5.) showed the same effect as had already been observed in the DLS data in THF (Table 5.2) *i.e.* that with increasing DEAEMA units the branching decreases. In Figure 5.5 this can be observed through the increased difference in retention times between **HB1** and **SHB1** (Figure 5.5.a) compared to **HB4** and **SHB4** (Figure 5.5.d). Another indicator for branching is the broad dispersity (PDI). Perrier *et. al.* [8] found that a smaller dispersity (PDI) indicates less branching. Comparison between **LP1** (PDI = 1.26) and **HB1-HB4** (PDI ranging from 1.66 to 2.22) strongly suggests that the highest branching corresponds to **HB1**. In addition, **HB1** exhibits bimodal distribution (Figure 5.5.a) while **HB2-HB4** displayed monomodal distributions. In the next step star hyperbranched polymers **SHB1-SHB4** and diblock polymer **DB1** were tested for pH responsive behaviour.

5.3.2. pH responsive behaviour

Studies found that stimuli responsiveness of hyperbranched polymers is directly influenced by branching.[5, 20] Davis *et. al.* [20] found that with varying the degree of branching, they could directly influence the cloud point temperature of temperature responsive HBPs based on PEG-methacrylates. For this reason, it was decided to investigate the pH dependent behaviour in relation to core constitution and branching of a pH responsive star hyperbranched polymer. De *et. al.* [20] showed that a hyperbranched star polymer with pH responsive core of amino acid-based monomers showed interesting size changes with changing pH.[2] However, no systematic study was done on these polymers. Figure 5.6. shows the size changes of star hyperbranched polymers **SHB1**-**SHB4** in dependence of pH values. Table 5.4. gives an overview of the hydrodynamic radius at pH values under 5 and 7 and above 8.

Table 5.4. DLS data of **SHB1**-**SHB4** and **DB1** in H_2O at between pH values of 4 to 9.

Name	**D_h [nm] pH ≤ 5**	**D_h [nm] pH = 6-6.5**	**D_h [nm] pH ≥ 8**
		nm	
SHB1	54	52	66
SHB2	58	39	81
SHB3	44	47	64
SHB4	48	48	66
DB1	24	54	54

In Figure 5.6.a **SHB2** is compared to the analogues **DB1** polymer. As expected the diblock polymer showed a size of 24 nm at pH 4 till 6 and at higher pH (7) values the size increased to 54 nm. At low pH values the tertiary amine of DEAEMA is protonated and both blocks are soluble in water. Above a pH of 7 *i.e.* around the pK_a of DEAEMA of 7.3 [21] the DEAEMA block gets deprotonated and hence hydrophobic and the polymers assemble to micellar structures (Figure 5.6.a). **SHB2** exhibits sizes of around 58 nm below pH 5, where the DEAEMA core is fully protonated and as such swollen. Cross-linking leads to the retention of the branched polymer architecture (immobilization of linear DEAEMA blocks). The swelling of the DEAEMA core is then a direct consequence of the positive charges of the protonated nitrogen's repelling each other. Between pH 6 and 7 a decrease of the particles to sizes to 39 nm

could be observed (Table 5.4). In this pH range the DEAEMA core is partially protonated *i.e.* enough to stabilise unimolecular particles and not enough for swelling of the core. An increase in pH above 7 leads to the full deprotonation of the core. The DEAEMA units return to being completely hydrophobic. Large structures of around 81 nm were observed. This has been attributed to the formation of `Star-Hyperbranched'-Micelles *i.e.* at high pH the core is so hydrophobic that stabilisation is achieved by self-assembly of multiple star hyperbranched polymers. These structures had previously been observed by Summerlin *et. al.* in thermoresponsive polymers.[4] A schematic representation of this process is shown in the inlet in Figure 5.6.a. Comparison to **SHB1**, **SHB3** and **SHB4** (Figure 5.6.b and Table 5.4) showed that swelling and shrinkage between pH 5 and 7 could be observed in **SHB1** too. However, with a size change of 54 to 52 nm the effect was not very pronounced. This is probably a consequence of the denser crosslinking and smaller core. **SHB3** and **SHB4** exhibit no shrinking at pH 6. This was theorised to be due to the low crosslinking. Hence, **SHB3** and **SHB4** behaved more akin to a diblock.

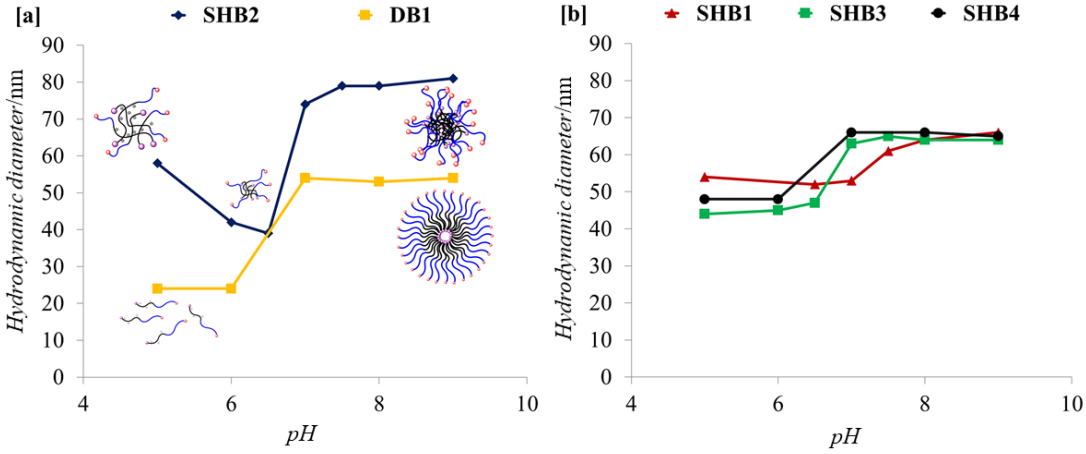

Figure 5.6. Changes in hydrodynamic diamter in dependences of pH of a) **SHB2** and **DB1** and b) **SHB1**, **SHB3** and **SHB4**.

5.3.3. Schizophrenic assembly in aqueous solutions

Poly(oligo (ethylene glycol mono-methyl ether) methacrylate (p(OEGMA)) is known to possess an LCST.[23,24] When both blocks of a polymer can be switched reversibly from hydrophobic to hydrophilic by different stimuli, schizophrenic assembly is a possibility. Schizophrenic micellization, describes the capability of a polymer to exist in aqueous medium in three different states, namely conventional micelles,

molecular dissolved chains and reverse micelles.[25,26] SHBs were tested for schizophrenic assembly by heating aqueous polymer solutions of **SHB1** – **SHB4** and **DB1** at pH 4 to 75 °C. NaOH was subsequently added to increase the pH to 9, while keeping the temperature at 75 °C, the solution was then cooled back to 25 °C. At constant temperature the pH was then decreased back to 5. The same was repeated in reserve to show the reversibility of the process. All sizes were recorded by DLS and the results are shown in Table 5.5 and Figure 5.7.

As had been observed before (Table 5.4 and Figure 5.6) unimolecular polymer nanoparticles were found at pH 4.5 and 25 °C, while star hyperbranched micelles were observed above pH 9 and 25 °C. When the aqueous solutions at pH 4.5 were heated above the LCST of p(OEGMA), *i.e.* 75 °C, structures between 474 nm (**SHB2**) and 135 nm (**SHB4)** were observed. These aggregates were stable even after prolonged time at 75 °C, while aggregates formed at pH 9 and 75 °C were significantly bigger and increased in size over time. This led us to believe that at pH 9, where both blocks are insoluble, aggregates of the polymer are formed which slowly precipitated out of solution. At pH 4.5 on the other hand, the DEAEMA core block is soluble and the formed aggregates can be stabilised in solution.

Table 5.5. DLS data of aqueous solutions **SHB1** – **SHB4** and **DB1** at different pH values and Temperatures.

Name	**D_h pH = 4.5 T = 25°C**	**D_h pH = 4.5 T = 75°C**	**D_h pH = 9 T = 25°C**	**D_h pH = 9 T = 75°C**
			nm	
SHB1	54	369	66	Insoluble
SHB2	58	474	81	Insoluble
SHB3	44	135	64	Insoluble
SHB4	48	196	66	Insoluble
DB1	24	356	54	Insoluble

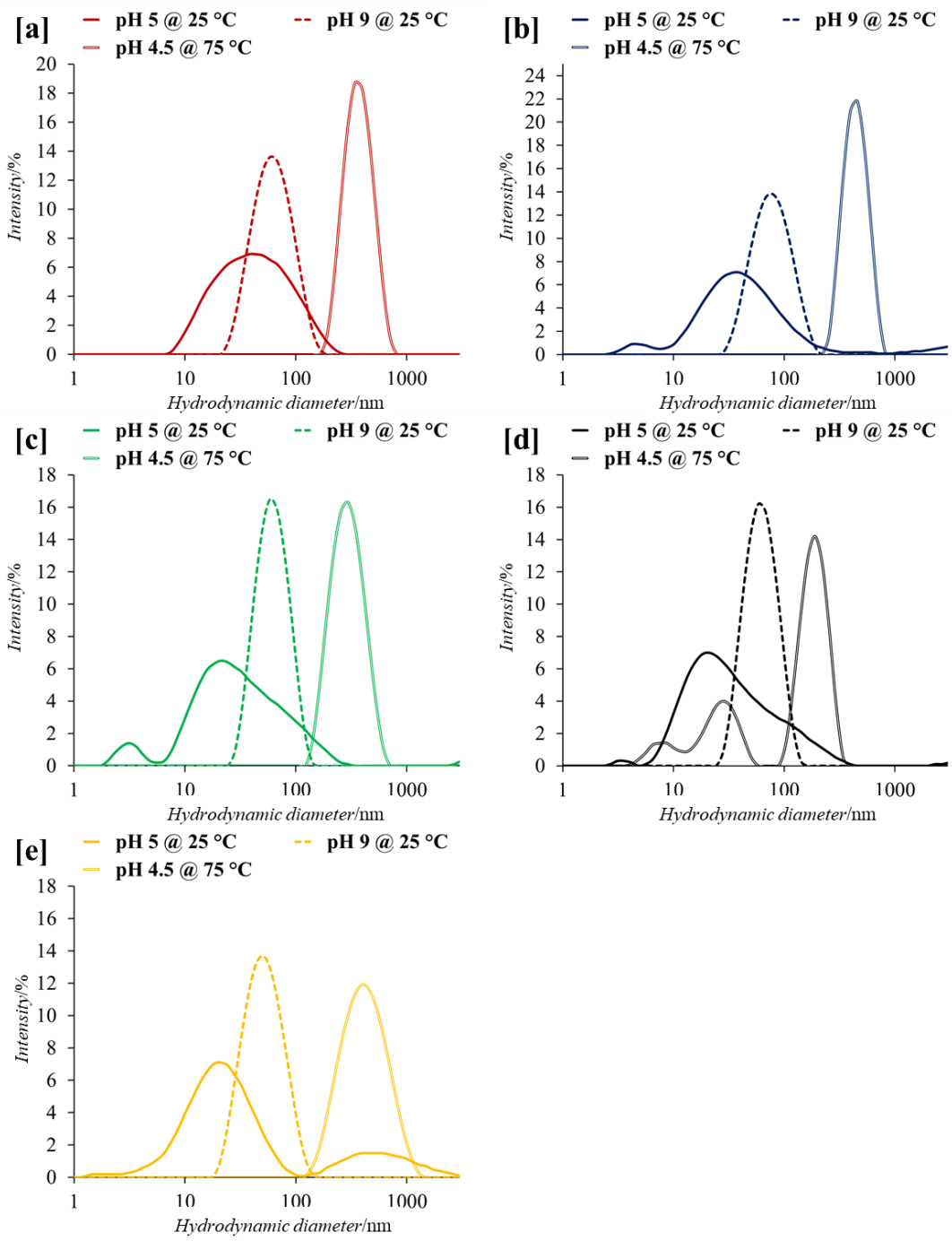

Figure 5.7. Plotted DLS data of a) **SHB1**; b) **SHB2**; c) **SHB3**; d) **SHB4** and e) **DB1** at pH 4.5 and 25 °C (bold line), pH 4.5 and 75 °C (double line) and pH 9 and 25 °C (dotted line).

Figure 5.8. shows the aqueous solutions of **SHB2** at pH 4.5 and pH 9 at 25 °C and 75 °C respectively. As expected for an unimolecular dissolved polymer, the solution was clear at pH 4.5 and 25 °C. At pH 9 and 25 °C the solution was opaque as is typical of a solution containing micelles. Heating the solution at pH 4.5 up to 75 °C turned the solution slightly less opaque and no precipitation could be observed. When

the solution at pH 9 was heated above the LCST, the whole solution turned milky white and precipitate could be seen.

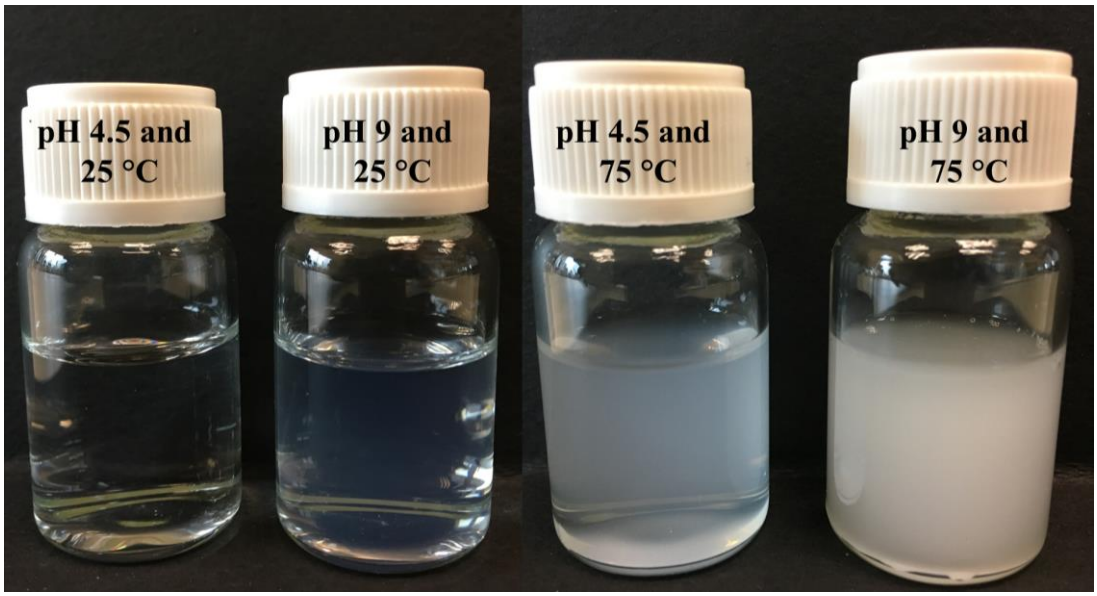

Figure 5.8. Aqueous solutions of **SHB2** at different Temperatures and pH values.

Armes *et. al.* [27] described the formation of different structures in block-selective solvents as a function of the inherent curvature of the molecule. The curvature can be estimated *via* the following equation

$$p = \frac{v}{a_0 l_c} \qquad (\mathbf{5.8})$$

with p = packing parameter, v = volume of hydrophobic chains, a_o = optimal area of head group and l_c = lengths of chains of hydrophobic tail.

They postulated that when $p \leq 1/3$ (High curvature) polymers self-assembled to micelles, between $1/3 \leq p \leq 1/2$ (medium curvature) cylindrical micelles were observed and between $1/2 \leq p \leq 1$ (low curvature) polymersomes were obtained.

Although this model best fits the behaviour of linear, amphiphilic diblock copolymers and does not account for crosslinking, it can still be used in this research to discuss possible structures for pH 9, 25 °C and pH 4, 75 °C. At pH 9 and 25 °C the hydrophobic core of the star hyperbranched polymers 'tightens'. Hence, v and l_c decrease, while at the same time the OEGMA block straightens and a_o increases. The curvature decreases to less than 1/3 and star hyperbranched-micelles form (Table 5.5.). At pH 4 and 75 °C the DEAEMA block becomes hydrophilic due to protonation, while OEGMA becomes insoluble, making DEAEMA the new head group. However, because of the low molecular weight, especially in **SHB1**, **SHB2** and **DB1**,

the area of the headgroup does not increase much in size. The OEGMA block, now the hydrophilic part, collapses above the LCST. Yet, it was theorised, on the basis of the size of the aggregates, that due to the relatively high molecular weight of the OEGMA block, steric hindrance keeps the block from folding tight enough to form inverse micelles. Unfortunately, because of the elevated temperatures needed, no Cryo-TEM images could be obtained. In **SHB3** and **SHB4** the observed structures at pH 4 and 75 °C were significantly smaller at 135 nm and 196 nm respectively. It was assumed that, because of the longer DEAEMA chain, the optimal area of the headgroup increased and the packing parameter decreased, which might have led to the formation of inverse micelles. From this data, the following structures for **SHB1**, **SHB2** and **DB1** were proposed (Figure 5.9).

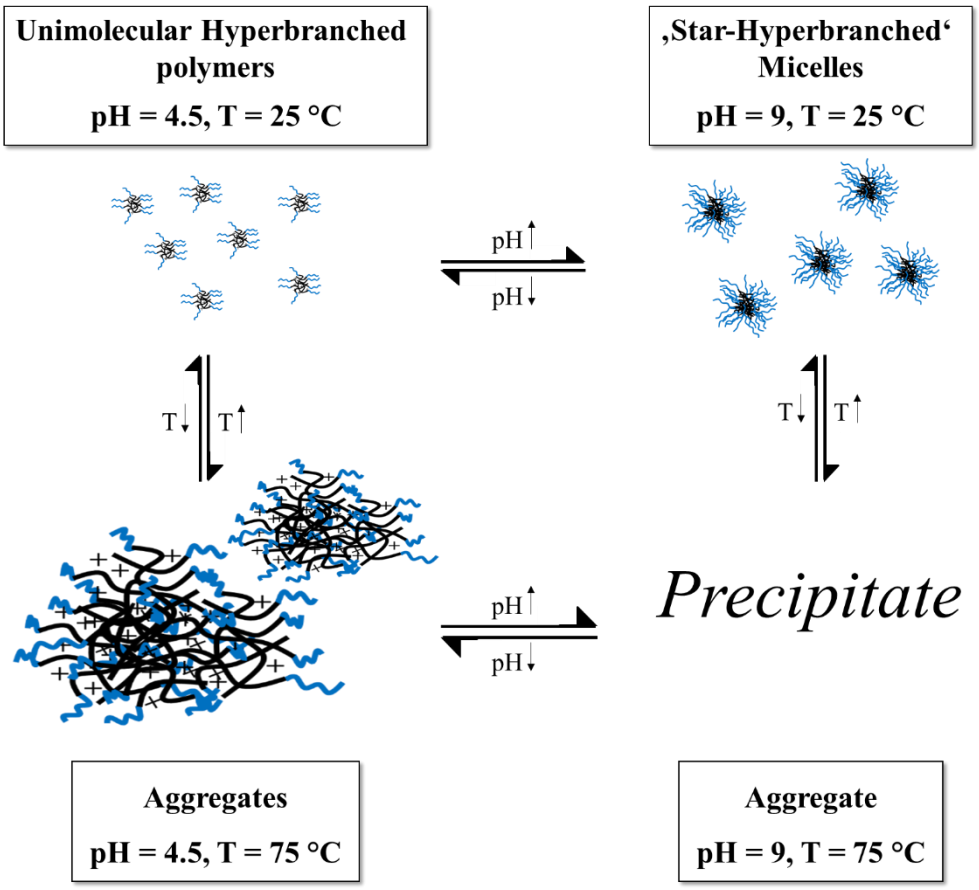

Figure 5.9. Different self-assembled structures of aqueous solutions of **SHB1**, **SHB2** and **DB1** at different pH values and temperatures.

Subsequently it was investigated if the varying core structures had any influence on the LCST. To that end DLS of aqueous samples of **SHB1**-**SHB4** and **DB1** at pH 4.5 were measured. These samples were heated stepwise and Z-average size data

and count rate was recorded every 0.2 °C. The results are shown in Figure 5.10. Table 5.6. lists the obtained LCSTs *i.e.* where the Z-Average as well as the count rate spike indicating the transition from hydrophilic to hydrophobic.

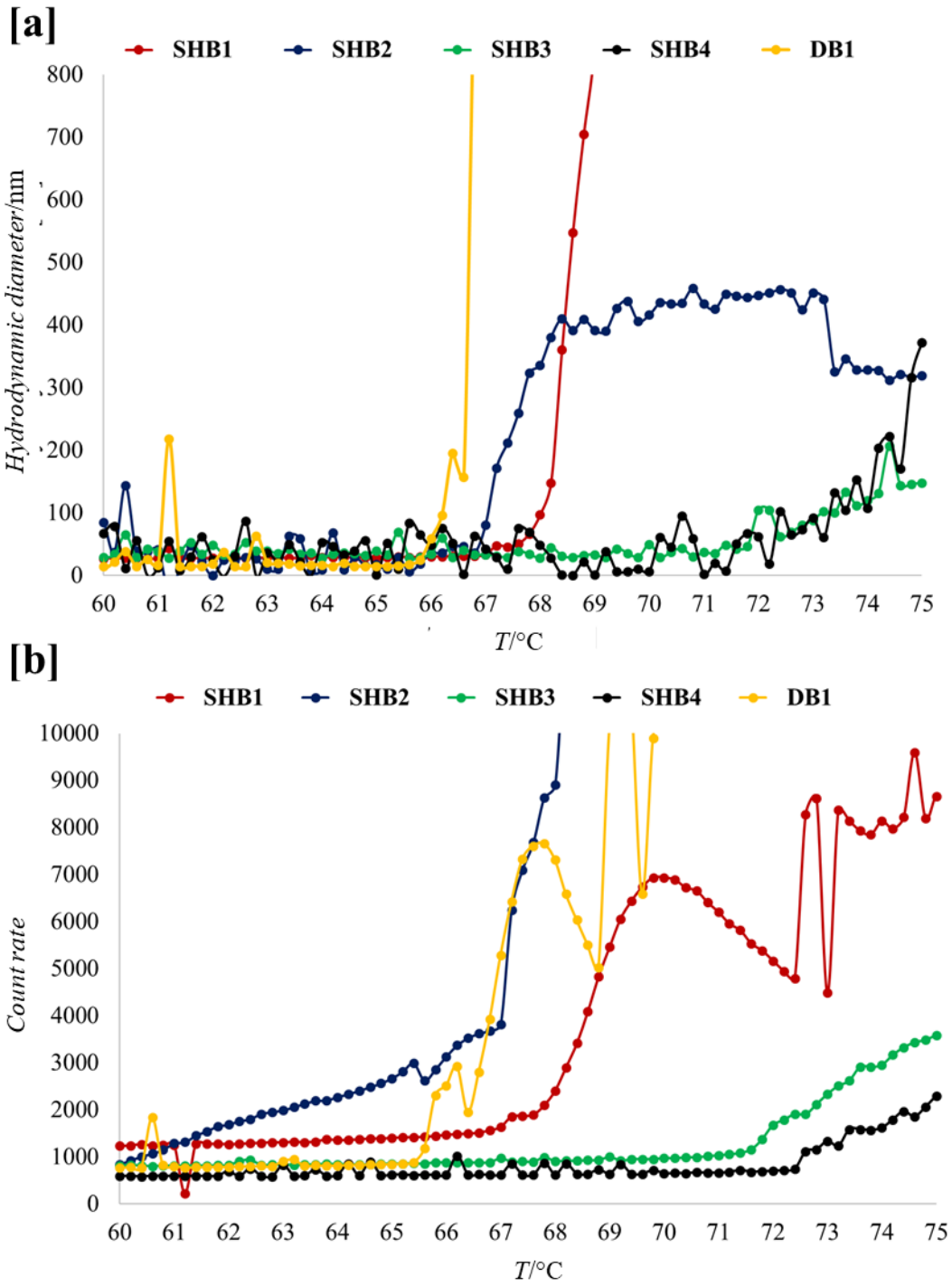

Figure 5.10. DLS data of a) Size against temperature at pH 4.5 and b) Count rate against temperature at pH 4.5.

Table 5.6. LCSTs of **SHB1-SHB4** and **DB1** at pH 4.5 derived from DLS data of Z-Average and count rate

Name	$LCST_{Z\text{-}Average}$	$LCST_{Count\ rate}$
	°C	
SHB1	68.0	68.0
SHB2	67.0	66.8
SHB3	72.0	72.0
SHB4	72.4	72.6
DB1	66.0	65.8

It was found that cross-linked polymers exhibited a slightly higher LCST than non-cross-linked structures *e.g.* **DB1** = 66 °C and **SHB2** = 67 °C, this is in direct contrast to what Davis *et. al.* [20] found when they studied a system of *poly*(di(ethylene glycol) methacrylate-*co*-oligo(ethylene glycol) methacrylate-*co*-ethylene glycol di-methacrylate) p(DEGMA-*co*-OEGMA-*co*-EGDMA). Their system however, did not possess a second, non-temperature sensitive block. **SHB3** and **SHB4** exhibited a substantially higher LCST of around 72 °C at which point the increase of count rate as well as Z-Average size was significantly lower than previously observed in **SHB1-SHB4** and **DB1**. This was attributed to the high molecular weight of the DEAEMA block increasing the hydrophilicity.

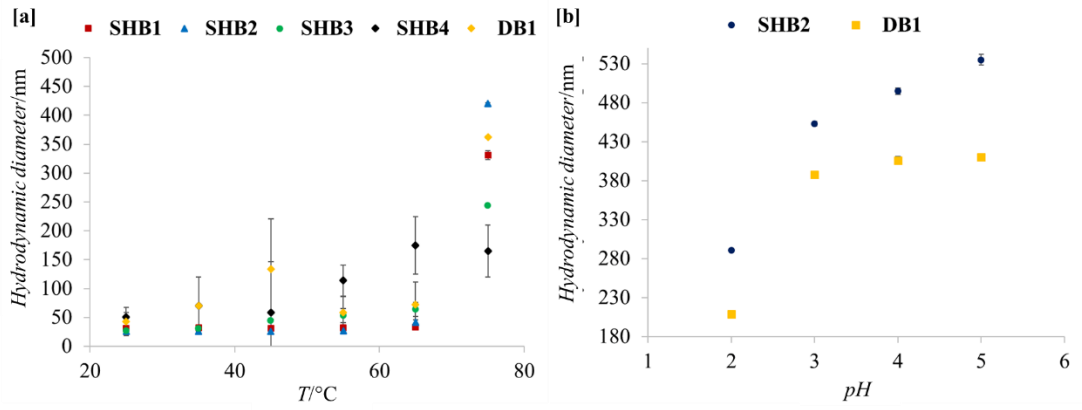

Figure 5.11. DLS data of a) **SHB1-SHB4** and **DB1** at 25, 35, 45, 55, 65 and 75 °C at pH 4.5 and b) **SHB2** and **DB1** at 75 °C and pH 5, 4, 3 and 2.

To ensure that the observed structures were stable over time at the recorded temperatures, aqueous solutions of **SHB1-SHB4** and **DB1** at pH 4.5 were heated from 25 to 75 °C in steps of 10 °C and kept at each temperature for 30 minutes after which

size data was recorded for another 30 minutes. The results are plotted in Figure 5.11. a.

The DLS data measured proved the previous observations. For **SHB1**, **SHB2** and **DB1** unimolecular structures were observed between 25 and 65 °C. After 75 °C the size increased dramatically to 350 – 450 nm, which correspondents well to previous observations in Figure 5.10. For **SHB3** and **SHB4** smaller sizes of 250 and 150 nm respectively could be detected. For **SHB3** the transition could be measured at 65 °C as had been shown before, while the size increase in **SHB4** started earlier at 55 °C.

As a further step, size changes as a function of pH was investigated. To that end, aqueous solutions of **SHB2** and **DB1** were measured at pH 2,3,4 and 5 and at 75 °C. The results are shown in Figure 5.12.b. It was found that for both polymers sizes were stable in between pH 5-3, with **DB1** being consistently smaller than **SHB2**. When the pH changed to pH 2, the sizes decreased from 380 to 200 nm for **DB1** and 450 to 280 nm for **SHB2**. A possible explanation is that a too acidic environment might have led to a disassembly of the structures.

After careful consideration of the presented data, **SHB2** was chosen to investigate drug encapsulation and release of a water insoluble drug, because of its favourable size changes in dependence of pH.

5.3.4. Drug encapsulation and triggered release

SHB2 and **DB1** were subsequently investigated for their encapsulation and pH dependent release profiles of indomethacin (IMC), a water insoluble drug. To that end indomethacin and polymer **SHB2** were dissolved into ethanol in a ratio of 1:2 and the same amount of DI water was added. After the ethanol was evaporated off, UV/Vis was measured of the aqueous solution to obtain the percentage of encapsulated drug. The results are shown in Figure 5.12. The inlet photo shows the control solution of **SHB2** in water, indomethacin evaporated into water without polymers, indomethacin and **SHB2** in a ratio of 1:2 in water at pH 6.5 and indomethacin and **SHB2** in a ratio

of 1:2 in water at pH 4.5.

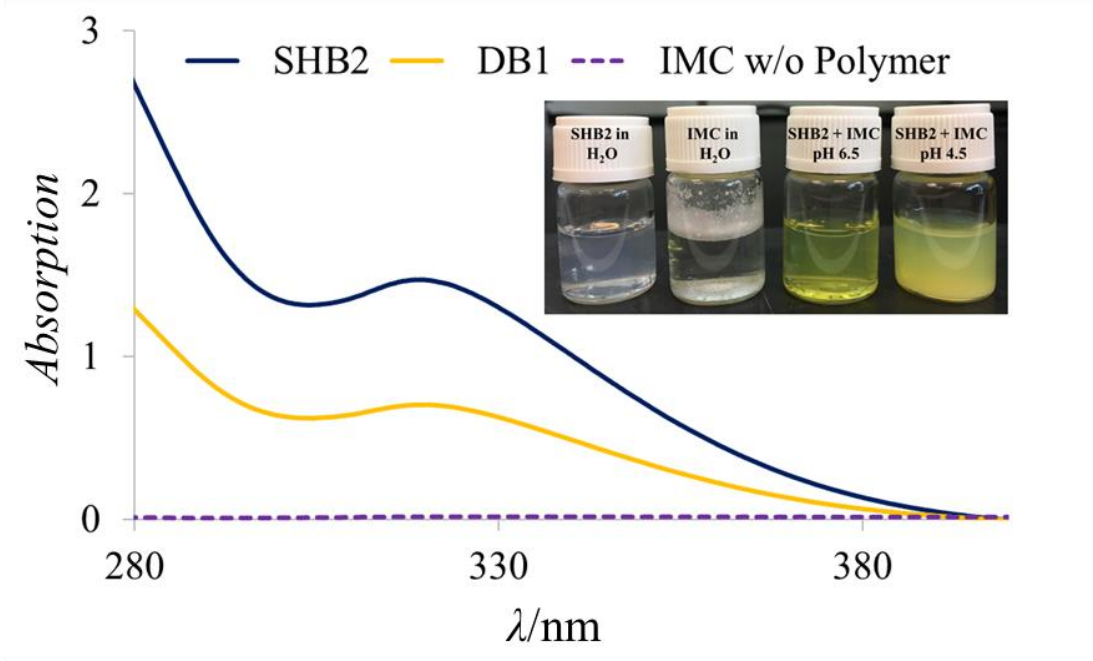

Figure 5.12. UV/Vis curves in DI water of **SHB2** and indomethacin (2:1) (blue line); **DB1** and indomethacin (2:1) (yellow line) and indomethacin without polymer (dotted line). The inlet shows the solutions of **SHB2** and indomethacin at different pH values and polymer and drug control solutions.

The UV/Vis data showed that without polymer present no indomethacin was dissolved in water. 100 % of IMC could be encapsulated into **SHB2**, while only 47 % of indomethacin had been encapsulated into **DB1**, which correspondents to 25 wt %, which is often found for micelles formed from linear polymers.[28-30] When the pH dropped to 4.5 precipitated indomethacin was observed (Inlet Figure 5.12). Next, indomethacin release from **SHB2** and **DB1** at pH 4.5 and pH 6.5 was measured. The plotted data is shown in Figure 5.13.

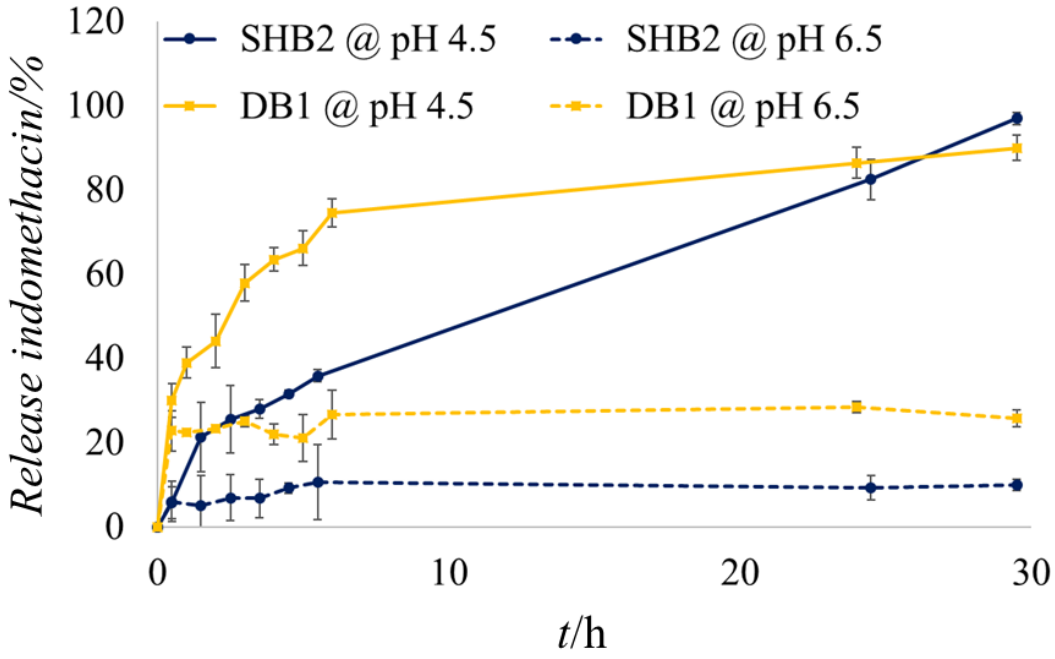

Figure 5.13. Release data of **SHB2** (blue) and **DB1** (yellow) at pH 4.5 (bold lines) and pH 6.5 (dotted line).

The release profiles of **SHB2** and **DB1** were measured over 30 hours at pH 4.5 and pH 6.5. At pH 4.5 an initial burst release of indomethacin of 5 % and 30 % in the first half hour for **SHB2** (blue bold line) and **DB1** (yellow bold line) respectively was observed. After another hour, 21 % indomethacin had been released from **SHB2** and 40 % from **DB1**. After 2 hours a slow, continues release of indomethacin from **SHB2** of 3-4% per hour was observed, until 97 % indomethacin had been released. The release profile for **DB1** on the other hand, showed that after 6 hours 75 % of the drug had already been released, after which the release significantly slowed down. At 30 hours only 90 % indomethacin could be detected in solution, while the rest remained encapsulated in **DB1**. The core of **SHB2** possesses cavities in which actives can be loaded at neutral pH. At low pH the core expands, and the indomethacin molecules slowly diffuse out. The result is a slow, continues, controlled release. Micelles formed from linear, non-cross-linked polymers (**DB1**) on the other hand, 'burst' apart when the pH decreases. The control experiments at pH 6.5 show an initial burst release of 6 % and 22 % for **SHB2** (dotted blue line) and **DB1** (yellow dotted line) respectively after pH adjustment. After 30 h, 10 % (**SHB2**) and 26 % (**DB1**) indomethacin had leached out, hence at pH 6.5 no significant release was detected. This data proved that the indomethacin release was triggered by lowering the pH.

The measured data showed that at lower pH, an encapsulated active could be released. This would be adventitious for a triggered release of cancer drugs into the cell, due to a lower pH in the endosome and lysosome. While it is possible for polymer nanoparticles to utilise the EPR effect to diffuse into a malignant cell, additional active targeting would be favourable. This can be achieved by functionalising the surface of the polymer nanoparticles.

5.3.5. End-group cleavage and functionalisation/ gelation

Using RAFT polymerisation, post-polymerisation modification is easily available by reducing the trithiocarbonate group of the Z-group to a thiol.[31] This enables the use of thiol-ene `click` chemistry. Different routes can be envisaged to obtain a thiol end-group, *e.g.* radical induced reduction, thermal elimination, reaction with a nucleophile.[32] In this work aminolysis was used to obtain a thiol end-group, following the example of Summerlin *et. al.* [33], because of the mild reaction conditions. Figure 5.14.a shows a scheme of the synthesis on the example of **SHB2**. The reaction was followed by UV/Vis.[34]

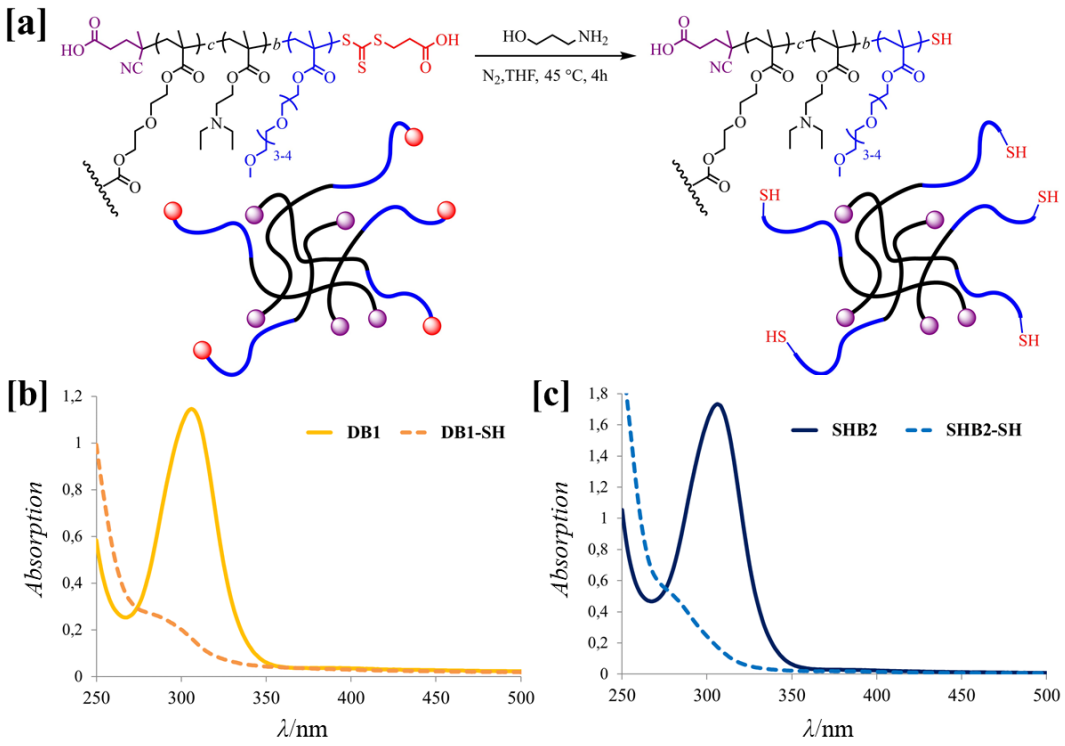

Figure 5.14. a) Schematic representation of the aminolysis reaction of **SHB2** to **SHB2-SH** and UV/Vis spectra pre- and post-aminolysis reaction of b) **DB1** and c) **SHB2** measured in THF.

Figure 5.14.b and c shows the measured UV/Vis spectra in THF pre- and post-aminolysis of **DB1** and **SHB2** respectively. Pre-reaction the UV/Vis spectra showed a strong signal at 310 nm. This was assigned to the trithiocarbonate group of the RAFT-transfer agent and can be found in both the spectra for **DB1** and **SHB2** pre-reaction. After the reaction the signal disappeared (yellow and blue dotted lines), due to the loss of the conjugated system. This proved that the reaction had been successful, and **SHB2-SH** and **DB1-SH** were obtained. To confirm that no disulphide bonds formed during the reaction, GPC was measured. No size change could be detected.

SHB2-SH was consequently reacted with *N*-(5-Fluoresceinyl)maleimide, a fluorescent dye, by thiol-ene 'click' chemistry. A fluorescent dye was chosen because it allowed the easy following of the reaction by UV/Vis as well as give a visual confirmation of a successful reaction. The reaction could be carried out at room temperature and non-inert conditions, under the exclusion of light. After stirring overnight, the product was purified by dialysis against DI water for 24 h. Freeze-drying afforded the product as a yellow powder. Figure 5.15.a shows a schematic representation of the thiol-ene 'click' reaction between **SHB2-SH** and *N*-(5-Fluoresceinyl)maleimide to afford **SHB2-dye**.

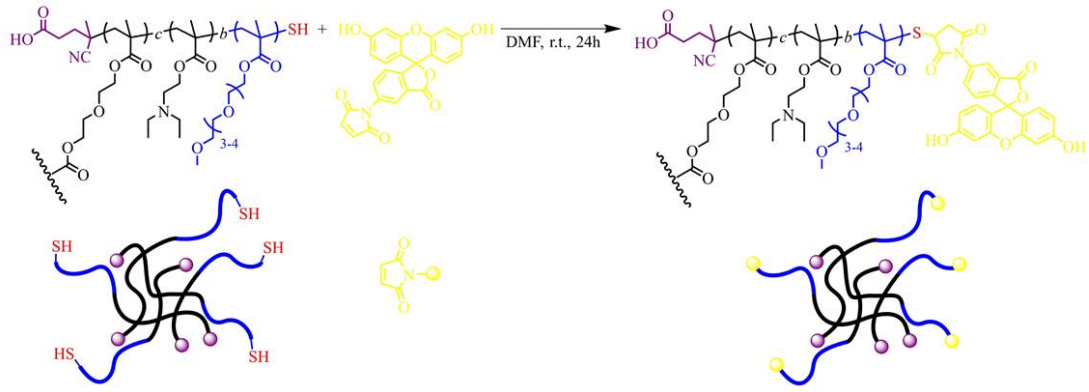

Figure 5.15. Schematic representation of the thiol-ene 'click' reaction between **SHB2-SH** and FM to afford **SHB2-dye**

Figure 5.16 shows the UV/Vis spectra of **SHB2-dye**, **SHB2** and **SHB2-SH** measured in water. Before aminolysis (bold line) a small shoulder at 310 nm indicates the presence of the trithiocarbonate group bond. After aminolysis the shoulder disappeared (dotted line), indicating the successful reduction to a thiol. The double line shows the product after the reaction with the fluorescent dye. A new sharp signal at

500 nm was clearly observed. The excitation wavelength for *N*-(5-Fluoresceinyl)maleimide has been stated as 490 nm in buffer solution (0.1 M Tris pH 8.0) by the vendor.[35] This corresponds well to the measurements in DI water and proves that the reaction had been successful, and this simple reaction could be used to obtain surface functionalized hyperbranched polymers.

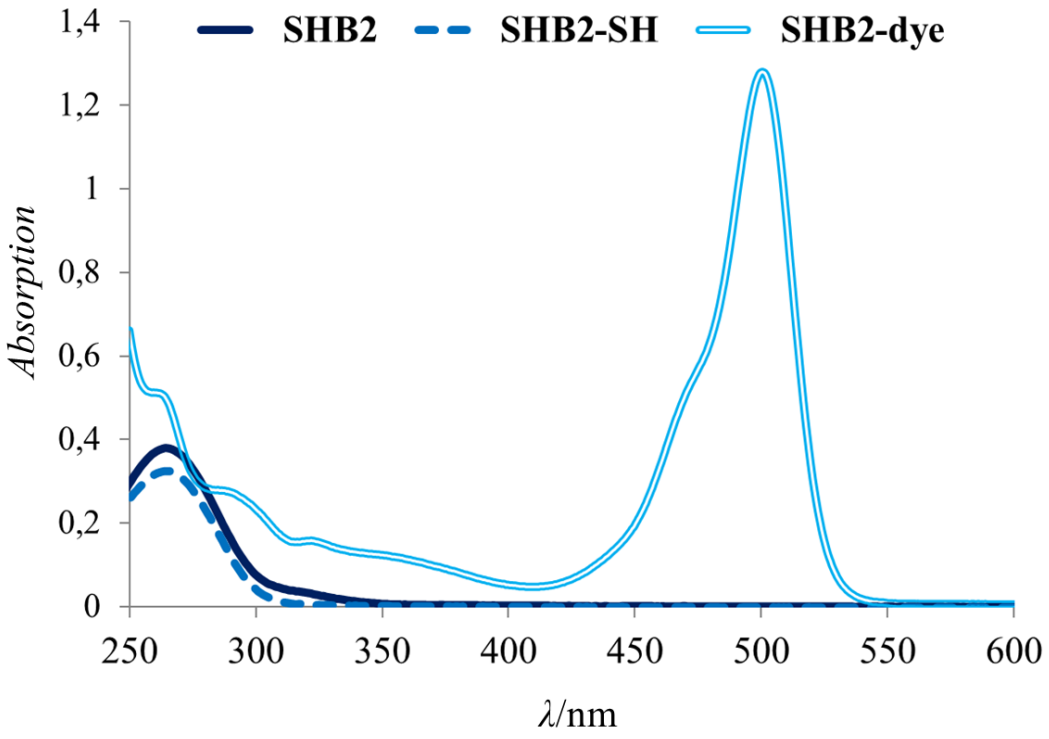

Figure 5.16. UV/Vis spectra of **SHB2** pre-aminolysis (bold line), **SHB2-SH** post-aminolysis (dotted line) and **SHB2-dye** after thiol-ene 'click' reaction (double line) in DI water.

Summerlin *et. al.* [33] described the synthesis of temperature sensitive, symmetrical triblock polymers by RAFT with a labile trithiocarbonate linkage in the midpoint of each chain. These polymers were able to form reversible hydrogels *i.e.* networks of polymer chains that are highly absorbent to water, by temperature changes. Cleavage of the trithiocarbonate bonds to thiols led to free-flowing micellar solution of diblock polymers above the LCST and the formation of gels under oxidative conditions. Hydrogels are highly interesting for pharmaceutical applications, due to their high porosity, which can easily be tuned by the cross-linking density and flexibility similar to natural tissue. Actives can be loaded into the gel matrix which are then able to diffuse out when the gel swells in water.[36,37]

The formation of hydrogels using **SHB2** was subsequently investigated. Figure 5.17.a shows a schematic representation of the gelation of **SHB2-SH** under oxidative conditions.

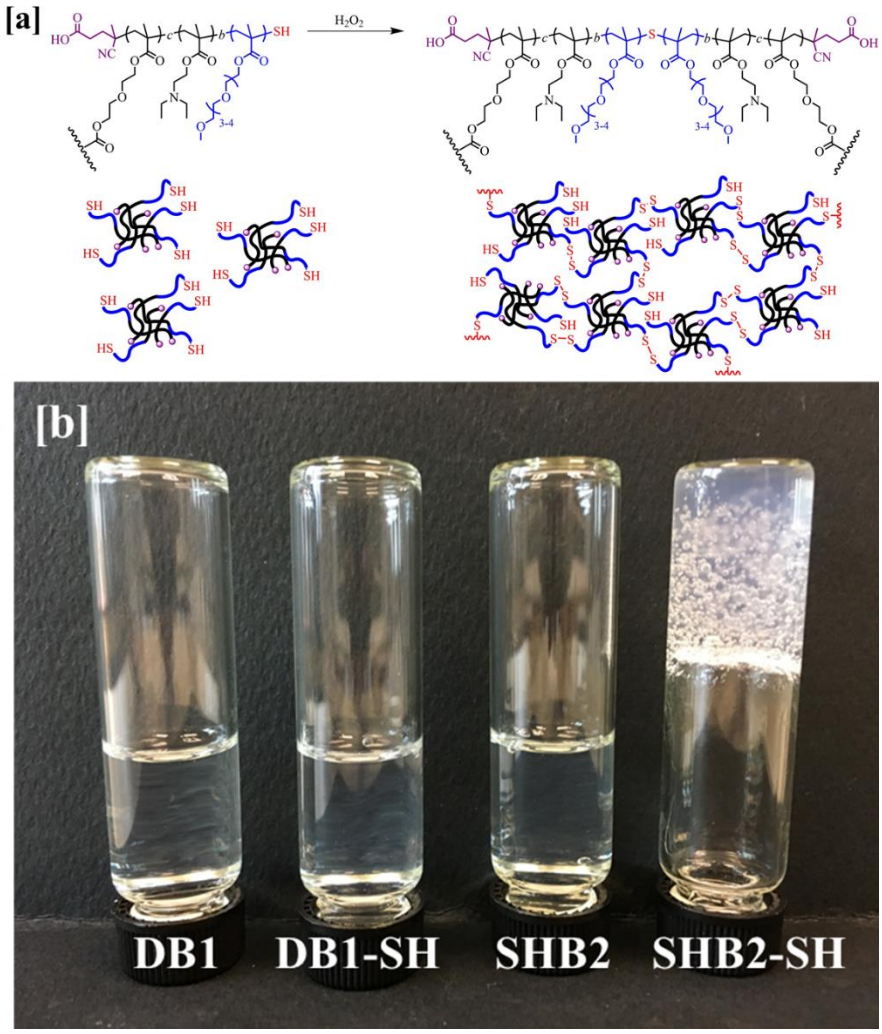

Figure 5.17. a) Schematic representation of the gelation of **SHB2-SH** under oxidative conditions and b) Vial inversion test of 5 wt % gels of **DB1**, **DB1-SH**, **SHB2** and **SHB2-SH** at pH 7.

Figure 5.17.b shows photographs of 5 wt % gels of **SHB2-SH** and **DB1-SH**, as well as the control experiments **SHB2** and **DB1** at pH 7. At 5 wt % gels could be formed of **SHB2-SH**, while even at a concentration of 10 wt % no gels could be formed using **DB1-SH**. This was attributed to the cross-linked nature of the hyperbranched polymers (Figure 5.17.a). Control experiments with **SHB2** and **DB1** showed that when the trithiocarbonate bond is still present no gel formation took place (Figure 5.17.b).

5.4. Conclusion

Up to this point we primarily focused on the formation of drug nanoparticles by bottom-up techniques. However, while the drug nanoparticles obtained in Chapter 2 and 3 showed prolonged storage ability in suspension and in solid form, the nano-suspensions obtained in Chapter 4 tended to agglomerate and precipitate after 24 hours. We theorised that this was mainly due to the changed polymer state from solid to viscous fluid. These types of polymers are, for that reason, more often used as nanocarriers for drug encapsulation and release, especially as an alternative to micellar carrier systems, which have been known to premature release their cargo in the bloodstream, due to the critical micelle concentration. Cross-linking circumvents this problem. Thus, this Chapter focused on the design and optimization of a hyperbranched polymer system for encapsulation and release of water insoluble actives.

DEAEMA was chosen as the core monomer to facilitate pH triggered structural changes, which can be used to trigger release at specific sites in the body.[13] A series of hyperbranched polymers with varying DEAEMA block lengths were successfully synthesised *via* RAFT polymerisation to avoid the use of heavy metals. Hyperbranched cores were chain-extended with OEGMA to form star hyperbranched polymers. A diblock polymer of the ratio DEAEMA:OEGMA 50:80 was synthesised to serve as a comparison. Increasing the ratio of DEAEMA:CTA, led to decreased branching and number of arms. This trend had a direct influence on the pH sensitive behaviour. Hyper star polymers with cores of 25 (**SHB1**) and 50 (**SHB2**) DEAEMA units showed core expansion below pH 6, after which the core contracted to form star hyperbranched micelles at high pH.

OEGMA possesses an LCST. Hence, star hyperbranched polymers were tested for 'schizophrenic' self-assembly. Polymers **SHB1**, **SHB2** and **DB1** showed interesting transitions to assembled structures around 500 nm at low pH and elevated temperature. **SHB2** was chosen for further studies because of its favourable behaviour at different pH values.

Initially, the encapsulation ability of hyperbranched star polymers compared to conventional diblock polymers was studied. A high drug loading ratio of 1:2 (drug:polymer) was chosen and it was observed that by using **SHB2** twice the amount of IMC could be encapsulated compared to a conventional diblock polymers. IMC release was recorded at pH 4.5 and 6.5 from **SHB2** and **DB1** over a period of 30 h.

DB1 showed a burst release at pH 4.5 in the first hour and fast release over a period of 7 h, after which the release slowed down. After 30 h no complete release had been observed. Release profiles of **SHB2** at pH 4.5 in comparison showed a small initial release of indomethacin, which was attributed to the change in pH. After the first hour a steady and slow release of indomethacin was observed that continued till, after 30 h, all active had been released. Release profiles at pH 6.5 both showed initial burst release after pH adjustment followed by drug 'leaching', confirming that the release is triggered at low pH values. Micellar drug carriers have been known to release their cargo in bursts after the external stimuli is applied. As such drug release often reaches 100% after a few hours.[39-41] While this might be desirable for some actives, prolonged, continues and slow drug release as was observed using HBPs, would be favourable for patients with chronic illnesses that require regular intake of drugs to decrease the daily intake and enhance patient comfort.

To increase the specificity of drug delivery, active targeting can be employed *i.e.* the surface of the polymer can be equipped with targeting ligands. The scope of surface modification was probed by modifying **SHB2** with a fluorescent dye. To that end the trithiocarbonate bond was reduced to a thiol bond *via* aminolysis. This thiol bond was then successfully used to 'click' on *N*-(5-Fluoresceinyl)maleimide, proving that star hyperbranched polymers could readily be surface modified by thiol-ene 'click' chemistry. This opens the possibility to use star hyperbranched polymers for active targeting in drug delivery or as a multifunctional platform for drug delivery and bioimaging.

Branched and star polymers have been used to form hydrogels for drug delivery. For this reason, star hyperbranched polymer **SHB2** was tested for the ability to form hydrogels. The obtained thiols were used to form disulphide bonds under oxidative conditions. It was possible to successfully form gels at 5 wt % concentration using **SHB2-SH**, while no gels could be formed using **DB1-SH** even at concentrations of 10 wt %.

In summary a versatile, easily synthesised polymer platform was obtained and systematically studied for drug encapsulation and release. Compared to conventional micelles, a favourable controlled and slow release could be measured. The investigated polymer platform is also promising for active targeting by simple surface modification.

5.6. References

1. R. M. England and S. Rimmer, *Polym. Chem*., 2010, **1**, 1533–1544.
2. S. G. Roy and P. De, *Polym. Chem*., 2014, **5**, 6365-6378.
3. J. A. Alfurhood, P. R. Bachler and B. S. Sumerlin, *Polym. Chem*., 2016, **7**, 3361-3369.
4. H. Sun, C. P. Kabb and B. S. Sumerlin, *Chem. Sci*., 2014, **5**, 4646-4655.
5. S. Pal, M. R. Hill and B. S. Sumerlin, *Polym. Chem*., 2015, **6**, 7871–7880.
6. N. O'Brien, A. McKee, D. C. Sherrington, A. T. Slark and A. Titterton, *Polymer*, 2000, **41**, 6027-6031.
7. B. Liu, A. Kazlauciunas, J. T. Guthrie and S. Perrier, *Macromolecules*, 2005, **38**, 2131-2136.
8. B. Liu, A. Kazlauciunas, J. T. Guthrie and S. Perrier, *Polymer*, 2005, **46**, 6293–6299.
9. I. L. Medintz, H. T. Uyeda, E. R. Goldman and H. Mattoussi, *Nat. Mater*., 2005, **4**, 435–446.
10. U. Resch-Genger, M. Grabolle, S. Cavaliere-Jaricot, R. Nitschke and T. Nann, *Nat. Methods*, 2008, **5**, 763–775.
11. Q. Zhu, F. Qiu, B. Zhu and X. Zhu, *RSC Advances*, 2013, **3**, 2071-2083.
12. S. Hopkins, S. Carter, L. Swanson, S. MacNeil and S. Rimmer, *J. Mater. Chem.*, 2007, **17**, 4022-4027.
13. Z. Ge and S. Liu, *Chem. Soc. Rev.*, 2013, **42**, 7289-7325.
14. J. Fang, H. Nakamura and H. Maeda, *Adv. Drug Del. Rev*., 2011, **63**, 136-151.
15. D. Schmaljohann, *Adv. Drug Del. Rev*., 2006, **58**, 1655–1670.
16. P. J. Roth, C. Boyer, A. B. Lowe and T. P. Davis, *Macromol. Rapid Commun.*, 2011, **32**, 1123-1143.
17. A. Blencowe, J. F. Tan, K. Goh and.G. G.Qiao, *Polymer*, 2009, **50**, 5-32
18. N. Y. Ahn and M. Seo, *RSC Adv.*, 2016, **6**, 47715-47722.
19. J. Han, S. Li, S. A. Tang and C. Gao, *Macromolecules*, 2012, **45**, 4966–4977.
20. M. Luzon, C. Boyer, C. Peinado, T. Corrales, M. Whittaker, L. Tao and T. P. Davis, *J. Polym. Sci., Part A: Polym. Chem.*, 2010, **48**, 2783–2792.
21. Z. Ge and S. Liu, *Chem. Soc. Rev.*, 2013, **42**, 7289–7325.
22. C. J. Hawker, R. Lee and J. M. J. Frechet, *J. Am. Chem. Soc.*, 1991, **113**, 4583-4588.

23. C. R. Becer, S. Hahn, M. W. M. Fijten, H. M. L. Thijs, R. Hoogenboom and U. S. Schubert, *J. Polym. Sci. A*, 2008, **46**, 7138-7147.
24. Y. Koda, T. Terashima and M. Sawamoto, *ACS Macro Lett.*, 2015, **4**, 1366−1369.
25. S. Liu, N. C. Billingham and S. P. Armes, *Angew. Chem. Int. Ed*. 2001, **40**, 2328-2331.
26. V. Bütün, N. C. Billingham and S. P. Armes, *J. Am. Chem. Soc.*, 1998, **120**, 11818-11819.
27. A. Blanazs, S. P. Armes and A. J. Ryan, *Macromol. Rapid Commun*., 2009, **30**, 267–277.
28. N. Rapoport, *Prog. Polym. Sci.*, 2007, **32**, 962-990.
29. X. Shuai, H. Ai, N. Nasongkla, S. Kim and J. Gao, *J. Control. Release*, 2004, **98**, 415 – 426.
30. K. Kataoka, A. Harada and Y. Nagasaki, *Adv. Drug Deliv. Rev.*, 2001, **47**, 113-131.
31. P. J. Roth, C. Boyer, A. B. Lowe and T. P. Davis, *Macromol. Rapid Commun.*, 2011, **32**, 1123-1143.
32. G. Moad, Y.K. Chong, A. Postma, E. Rizzardo and S. H. Thang, *Polymer*, 2005, **46**, 8458–8468.
33. A. P. Vogt and B. S. Sumerlin, *Soft Matter*, 2009, **5**, 2347-2351.
34. M. Li, P. De, S. R. Gondi and B. S. Sumerlin, *J. Polym. Sci. A*, 2008, **46**, 5093–5100.
35. Simga-Aldrich, http://www.sigmaaldrich.com/catalog/product/sigma/38132?lang=en&region=SG (accessed November 2017)
36. T. R. Hoare and D. S. Kohane, *Polymer*, 2008, **49**, 1993-2007.
37. M. Hamidi, A. Azadi and P. Rafiei, *Adv. Drug Deliv. Rev.*, 2008, **60**, 1638–1649.
38. K. Verschueren, *Handbook of Environmental Data on Organic Chemicals*, John Wiley & Sons, Hoboken, 2008.
39. W. Chen, F. Meng, F. Li, S.-J. Ji and Z. Zhong, *Biomacromolecules*, 2009, **10**, 1727–1735.
40. M. Nakayama, T. Okano, T. Miyazaki, F. Kohori, K. Sakai and M. Yokoyama, *J. Control. Release*, 2006, **115**, 46 – 56.

41. Y. Bae, N. Nishiyama, S. Fukushima, H. Koyama, M. Yasuhiro and K. Kataoka, *Bioconjugate Chem*., 2005, **16**, 122–130.

Chapter 6

Summary and Outlook

6.1. Summary

(Hyper)Branched polymers were investigated throughout this thesis for their potential to be employed in encapsulation and nanodrug formulation as favourable alternatives to established additives *i.e.* surfactants, liposomes and block copolymers which are currently used in the pharmaceutical industry.

In Chapters 2 and 3, we synthesised branched polymers of linear, low molecular weight PEG and varying core monomers, *i.e.* PNIPAm, BMA, and Styrene using conventional, radical polymerisation.

In Chapter 2, core-shell branched polymers were tested for their ability to stabilise emulsions, and for their use in emulsion freeze-drying, a novel bottom-up technique used to obtain nanoparticles of Indomethacin (IMC) and Oil Red O (OR). The branched polymers acted as a stabilising scaffold against agglomeration after the freeze-drying process. After successfully obtaining indomethacin and oil red nanoparticles *via* emulsion freeze-drying, the process was repeated on triclosan, an antimicrobial drug. The obtained triclosan nanoparticles were tested against *Candida albicans*, an opportunistic, pathogenic yeast, where a 6-fold increase in activity was found compared to non-processed triclosan.

In Chapter 3, drug nanoparticles were formed *via* a simple solvent evaporation technique using the lightly crosslinked polymer PEG_{135}-*b*-($PNIPAm_{50}$-*co*-$EDAm_{2n}$)-*b*-PEG_{135} (n = 0.3; 0.6). The influence of solvent, active, pressure and, temperature was investigated. Ethanol and ketoprofen were found to be the best combination of solvent and active for the process and were used for kinetic studies. Long-term stability, and the possibility to obtain small particle sizes, independent of pressure and temperature applied during the process was successfully demonstrated. PXRD, Cryo-TEM, and DLS data was subsequently used to propose a mechanism. Dissolution measurements indicated a clear increase in dissolution of the obtained ketoprofen nanoparticles compared to non-processed ketoprofen.

In Chapter 4, branched polymers of oligo(ethylene glycol) methyl ether methacrylate (OEGMA) and butyl methacrylate (BMA) with varying core compositions were synthesised by atom-transfer radical-polymerisation (ATRP) and tested for their ability to stabilise drug nanosuspension. ATRP was used to afford better polymerisation control compared to conventional polymerisation used in Chapter 2 and 3. BMA exhibits upper critical solution temperature (UCST) behaviour in meth-

anol and unimolecular polymer nanoparticle solutions could be obtained by heating through the UCST without the need for a dialysis process. The UCST was subsequently used to form drug nanosuspensions of water insoluble drugs. Nanosuspensions with high drug loading, *i.e.* up to 8 w/v %, small PDI and sizes below 460 nm were successfully obtained.

In Chapter 5, a polymer platform for encapsulation and targeted release was designed and optimised. A series of pH responsive star hyperbranched polymers of the composition p(OEGMA)$_{80}$-*b*-p(DEAEMA$_x$-*co*-DEGDMA$_2$) with increasing x was synthesised *via* reversible addition−fragmentation chain-transfer polymerisation (RAFT). The series was investigated for pH responsive behaviour in dependency of core composition *i.e.* shrinkage and expansion, and schizophrenic micellization. The polymer with the most favourable core composition was subsequently investigated and compared to a linear diblock copolymer analogue, for the encapsulation and pH triggered release of indomethacin. Increased encapsulation efficiency and prolonged, continuous release, instead of burst release, could be observed compared to the diblock analogue. The possibility of surface modification for active targeting was investigated. As a proof of concept, a fluorescent dye, *N*-(5-Fluoresceinyl)maleimide, was successfully 'clicked' on *via* thiol-ene click chemistry. Thiol end-group carrying polymers were successfully used to form gels of hyperbranched polymers *via* disulphide bond formation

In summary, different kinds of branched polymers were synthesised by conventional radical polymerisation, as well as RDRP, and their potential to be used in drug delivery of water insoluble drugs was studied.

It was demonstrated that by finely tuning the physical properties of the polymers, a plethora of applications are possible. Branched polymers could be used for the formation and stabilisation of solid drug nanoparticles by two different bottom-up techniques, *i.e.* emulsion freeze-drying, and solvent evaporation. Enhanced dissolution, bioavailability, and activity in-vitro compared to non-processed water insoluble drugs was successfully shown. Both bottom-up techniques using branched polymers investigated here, were shown to be good alternatives to current techniques applied in the pharmaceutical industry for producing drug nanoparticles. Using RDRP, a branched polymer platform was designed, in which every component, *i.e.* core, arms, and surface, can easily be modified. Due to the possibility to isolate and

store every step of the synthesis, batches of hyperbranched cores could be synthesised and 'grown' out with a wide variety of monomers to obtain a range of polymers with different physical and chemical characteristics. In this thesis, hyperbranched polymers with a cross-linked, pH responsive core were successfully used to release a cargo in acidic environments and presented a favourable alternative to micellar carrier to circumvent issues such as burst and premature release.

6.2. Outlook

Synthesising branched polymers by a 'core'-first method makes it possible to design every part of the branched polymer, *i.e.* core, arms, and surface to specifically fit certain needs. As such, further studies should be done using different core compositions to investigate the interactions of different water insoluble actives with the core to further optimise encapsulation and release as well as drug nanoparticle formation. Along with the investigation of the interaction between core and actives, stimuli responsive behaviour and release should be studied further. While a responsive core-forming monomer was used in this work to endow branched polymers with environmental responsiveness, *i.e.* core contraction and expansion, further studies on stimuli responsive cross-linkers, *e.g.* cross-linkers that possess disulphide bonds that would be reduced to thiols in a reductive environment, would be of interest for targeted drug delivery. Pre- or Post-modification of the Z-group of the RAFT-CTA to a reactive functionality can also be utilised to endow hyperbranched polymers with target specific ligands. These ligands can easily be chosen to fit specific proteins on maligned cells. Using this lock-key principle, it was shown to be possible to decrease the amount of drug needed in the treatment of cancer. Which in turn, would enhance patient comfort and toxic side effects of treatment. To demonstrate the dual ability of hyperbranched polymers for active targeting and stimuli responsive drug release, hyperbranched polymers should be endowed with targeting ligands and *in-vitro* studies should be conducted.

„Alles hat ein Ende nur die Wurst hat zwei"

German proverb